NORTHWESTERN UNIVERSITY

Coordination Complexes for the Development of Zn(II)-Activated MR Imaging Probes

A DISSERTATION

SUBMITTED TO THE GRADUATE SCHOOL

IN PARTIAL FULFILLMENT OF THE REQUIREMENTS

for the degree

DOCTOR OF PHILOSOPHY

Field of Chemistry

By

Jody L. Major

EVANSTON, ILLINOIS

June 2008

© Copyright by Jody L. Major 2008

All Rights Reserved

Abstract

Coordination Complexes for the Development of Zn(II)-Activated MR Imaging Probes

Jody L. Major

My thesis focuses on the design and synthesis of lanthanide coordination complexes as Zn(II)-responsive magnetic resonance imaging (MRI) contrast agents. These agents produce an increase in MR intensity upon binding of Zn(II) through water modulation to Gd(III) chelates. To this end, several Zn(II)-responsive contrast agents have been synthesized and studied in detail to investigate their ability to be activated in the presence of Zn(II), as well as their mechanism.

MRI has become a powerful tool for molecular imaging because of its ability to provide three-dimensional images of opaque organisms without the use of ionizing radiation. While intrinsic contrast between organs can be observed by using MRI, resolution and sensitivity improve greatly with the use of contrast agents such as Gd(III) chelates. Recently, a new class of biologically activated MR contrast agents has been developed in which a change in the relaxivity of the agent is observed upon a biological signal. The research presented in this thesis expands on this new class of agents.

I have designed the first example of a Gd(III)-based MRI contrast agent in which an increase in MR intensity is observed in the presence of Zn(II). In the absence of Zn(II), this agent creates a coordinatively saturated Gd(III) complex with no water access to produce a dark MR contrast. In the presence of Zn(II), a coordination change of the Gd(III) chelate occurs upon the binding of Zn(II), allowing access of water and hence a bright MR image. This agent is selective for Zn(II) as there is no change in relaxivity in the presence of Ca(II) or Mg(II) and it binds Zn(II) in concentrations relevant for the study of Zn(II) release from synaptic nerves.

Further investigation of this Zn(II)-activated agent included the synthesis of a series of agents with varied lengths of the carbon chain between the Zn(II)-binding groups and the Gd(III) chleate and with varied Zn(II)-binding groups. The relaxation enhancement of these agents as well as their mechanism of activation is presented. This work improves our understanding of biologically responsive MRI contrast agents and will allow for the development of a variety of ion-responsive contrast agents.

Acknowledgements

I would first like to thank my advisor, Professor Thomas J. Meade. Tom has been a constant source of support throughout my graduate career. His encouragement and patience have been unending. Thank you for providing me with the tools and guidance to become a research scientist and allowing me the freedom to pursue my own research path. The lessons you've taught me throughout the years have been invaluable and will not go forgotten as I pursue a career in academia.

Throughout my time here at Northwestern University, I have had the opportunity to work with a number of people who have been essential in the progression of my research. I would like to thank Professor Thomas O'Halloran for his helpful advice on my research and for proofreading my manuscript. Thanks to Professor Karl Scheidt for the many discussions to help me with the synthetic aspects of my research. I would also like to extend my gratitude to Dr. Yuyang Wu for all of the training and assistance with NMR spectroscopy.

To all of the members of the Meade group, both past and present, thank you! I have enjoyed working with all of you and sharing in our daily life challenges that we have all faced. To Frank Femia, Joe Duimstra, and Matthew Allen, thank you for all of the support and training you provided in the early years. I would not be the scientist I am today without the guidance and knowledge I received from each of you. Thanks to Rene Boiteau who has been an excellent undergraduate researcher and has helped in all aspects of this thesis. I would like to thank all of the biology students, especially Allison Harney, Keith Macrenaris, and Ellen Kohlmeir, who have provided to me a tremendous wealth of information and have helped me see my research through to the next step beyond chemistry. I would especially like to thank Kylie Barker, Elise Sikma, and Dave Ballweg for being the great people that you are. Every day you provide a work

environment that I am happy to go to. I look forward to seeing you each day and will miss the good times we've had. You have all been a tremendous help to me and have been the greatest of friends throughout my time here. I will miss you all greatly!

I would like to send a special thanks to my Preparing Future Faculty mentor, Dr. Pratibha Varma-Nelson, who provided me with more than just advice on the ins and outs of being a great teacher. She has been a great friend and confidant. Her mentorship throughout the years has been invaluable.

On a more personal note, I would like to extend my deepest gratitude to my family and friends for their endless support and encouragement. To Matt Kern, Mark Witschi, and especially Chris Graves who managed to be there for my Inorganic Seminar even after a night of celebrating his defense, thank you for friendship. I never would have imagined that I would meet lifelong friends during the first week of graduate school. Most importantly I would like to thank Aaron for being here through all of the good times and bad. His love and support has carried me through each day and I look forward to a lifelong of happiness with you.

Table of Contents

ABSTRACT **3**

ACKNOWLEDGEMENTS **5**

TABLE OF CONTENTS **7**

LIST OF FIGURES **10**

LIST OF SCHEMES **15**

LIST OF TABLES **15**

ABBREVIATIONS **16**

CHAPTER 1

INTRODUCTION **20**

1.1 INTRODUCTION 21

1.2 MAGNETIC RESONANCE IMAGING 23

1.2.1 Relaxation Theory 24

1.2.2 Factors affecting relaxivity 27

Hydration Number (q) 27

Water Exchange Rate ($1/\tau_m$) 29

Rotational Correlation Time (τ_R) 30

1.3 NEXT-GENERATION CONTRAST AGENTS 34

1.3.1 Biologically Responsive Contrast Agents 34

Ion-Responsive Contrast Agents 35

Enzyme-Activated Contrast Agents 39

pH-Responsive Contrast Agents 42

1.3.2 Cell-Permeable and Targeted Contrast Agents 42

Cell-Permeable Contrast Agents 43

Receptor-Targeted Contrast Agents 45

1.4 SCOPE OF THESIS 47

CHAPTER 2

THE DESIGN AND SYNTHESIS OF A Zn(II)-ACTIVATED MAGNETIC RESONANCE CONTRAST AGENT 50

2.1 INTRODUCTION 51

2.2 RESULTS AND DISCUSSION 55

2.2.1 Synthesis and Characterization 55

2.2.2 Relaxivity 60

2.2.3 Hydration Number (q) 64

2.2.4 Nuclear Magnetic Resonance Dispersion 67

2.2.5 Zinc Dissociation Constant 71

2.2.6 Stability Towards Transmetallation and Cytotoxicity 73

2.2.7 MR Images 75

2.3 CONCLUSIONS AND FUTURE ASPECTS 79

2.4 EXPERIMENTALS 80

CHAPTER 3

STRUCTURAL OPTIMIZATION OF Zn(II)-RESPONSIVE CONTRAST AGENTS 91

3.1 INTRODUCTION 92

3.2 RESULTS AND DISCUSSION 95

3.2.1 Synthesis and Characterization 95

3.2.2 Relaxivity 98

3.2.3 Hydration Number (q) 103

3.2.4 Mean Residence Lifetime of Water Protons (τ_m) 105

3.2.5 Zinc Dissociation Constants 110

3.2.6 Europium NMR 110

3.2.7 MR Images 115

3.3 CONCLUSIONS AND FUTURE ASPECTS 115

3.4 EXPERIMENTALS 118

CHAPTER 4

INVESTIGATING THE MECHANISM OF ACTIVATION OF Zn(II)-RESPONSIVE CONTRAST AGENTS 129

4.1 INTRODUCTION 130

4.2 RESULTS AND DISCUSSION 135

4.2.1 Synthesis and Characterization 135

4.2.2 Relaxivity 139

4.2.3 Hydration Number (q) 143

4.2.4 Zinc Dissociation Constants 145

4.2.5 Mean Residence Lifetime of Water Protons (τ_m) 145

4.2.6 Europium NMR 150

4.3 CONCLUSIONS AND FUTURE PERSPECTIVES 152

4.4 EXPERIMENTALS 154

APPENDIX

Zn(II)-RESPONSIVE MRI CONTRAST AGENTS FOR ATTACHMENT TO NANOPARTICLES 167

A.1 INTRODUCTION 168

A.2 RESULTS AND DISCUSSION 169

A.2.1 Synthesis, Characterization, and Relaxivity of Gd-DO3A SiNPs 169

A.2.2 Synthetic Approach to Modification of Gd-daa3 for Conjugation to SiNPs 176

A.3 CONCLUSIONS AND FUTURE ASPECTS 181

A.4 EXPERIMENTALS 182

REFERENCES 189

CURRICULUM VITA 202

LIST OF FIGURES

Figure 1.1. Clinically approved Gd(III)-based magnetic resonance contrast agents. **22**

Figure 1.2. Factors affecting relaxivity of Gd(III)-based MR contrast agents: the hydration number (q), the mean residence lifetime of bound water molecules (τ_m), and the rotational correlation time (τ_R). **28**

Figure 1.3. Structure of Gd-TREN-1-Me-3,2-HOPO, a $q = 2$ contrast agent. **31**

Figure 1.4. Structures of ligands with optimized τ_m. **31**

Figure 1.5. Schematic of polymer and dendrimer Gd(III) chelate constructs demonstrating internal rotation. **33**

Figure 1.6. A Ca(II)-activated MR contrast agents. **36**

Figure 1.7. A Zn(II)-responsive MR contrast agent. **38**

Figure 1.8. An MR contrast agent sensitive to β-galactosidase. **40**

Figure 1.9. An MR contrast agent activated by β-glucuronidase through a self-immolative linker. **40**

Figure 1.10. τ_m-modulated MRI contrast agents: (a) An MR contrast agent sensitive to alkaline phosphatase, and (b) an MR contrast agent sensitive to a human carboxypeptidase B, thrombin activatable fibrinolysis inhibitor (TAFI). **41**

Figure 1.11. Structures of intracellular contrast agents. Top: 8-amino acid polyarginine oligomer coupled to Gd(III)-DOTA; Bottom: 8-amino acid polyarginine oligomer coupled to Gd(III)-DTPA. **44**

Figure 1.12. A progesterone-conjugated MRI contrast agent. **46**

Figure 2.1. A Zn(II)-activated MRI contrast agent with proposed tetrahedral binding of Zn(II). **54**

Figure 2.2. Half of the Ca(II)-activated contrast agent (**Gd-DOPTA**) led to the design of complex **1** as a Zn(II)-activated agent. **56**

Figure 2.3. Overlay of analytical HPLC-MS traces of **Eu-1** at 0 (blue trace) and 72 hours (red trace) after preparatory HPLC purification. The desired product, **Eu-1**, is almost fully hydrolyzed after 72 hours. **59**

Figure 2.4. Relaxivity of **Gd-daa3** in the presence of $ZnCl_2$ at 60 MHz and 37 °C. **61**

Figure 2.5. Relaxivity of **Gd-daa3** in the presence of $CaCl_2$ and $MgCl_2$ at 60 MHz and 37 °C. **61**

Figure 2.6. Relaxivity of **Gd-daa3** with Zn(II) and Cu(II) at 60 MHz and 37 °C. **63**

Figure 2.7. Relaxivity of **Gd-daa3** in the presence of $ZnCl_2$ in HEPES buffer, human male serum, and 1% BSA in HEPES measured at 60 MHz and 37 °C. **63**

Figure 2.8. Energy level diagrams for Eu(III) and Tb(III). The two labeled emission transitions (solid line arrows) are the most intensive radiative transitions for each of the ions. Radiationless decay through coupling with O-H vibrations are labeled with dotted line arrows. **65**

Figure 2.9. Emission spectra of **Tb-daa3** with an excitation of 254 nm (inset). **66**

Figure 2.10. Nuclear magnetic resonance dispersion (NMRD) profiles of **Gd-daa3** in the absence of Zn(II) (solid symbols) and in the presence of Zn(II) (open symbols). **68**

Figure 2.11. The structure of FluoZin-1™, a commercially available Zn(II)-responsive fluorophore. **72**

Figure 2.12. Observed fluorescence curves of FluoZin-1 with 10 μM Zn(II) and varying concentrations of **Gd-daa3** measured in HEPES buffer at a pH of 7.4 followed by equations used to determine the dissociation constant of **Zn-Gd-daa3**. **74**

Figure 2.13. (A) Normal proliferation of NIH/3T3 cells is seen when they are incubated with 0.5 mM **Gd-daa3**. **(B)** **Gd-daa3** is taken up at a constant rate for up to 8 hours. **76**

Figure 2.14. T_1-weighted phantom MR images of a 1 mM solution of **Gd-daa3** in HEPES buffer. Sample **A**: HEPES buffer only; **B**: **Gd-daa3**; **C**: **Gd-daa3** with 1 mM $ZnCl_2$; **D**: **Gd-daa3** with 1 mM $MgCl_2$; and **E**: **Gd-daa3** with 1 mM $CaCl_2$. Images were obtained on a 4.7 T magnet with the following parameters: Repetition time (TR) = 100.0 ms; echo time (TE) = 14.3 ms, field of view (FOV) = 1.4/1.8 cm; and data matrix = 256 x 256. **77**

Figure 2.15. T_1-weighted phantom MR images of a 1 mM solution of **Gd-daa3** in HEPES buffer with various concentrations of $ZnCl_2$. **A**: 0 μM Zn; **B**: 50 μM Zn; **C**: 100 μM Zn; **D**: 500 μM Zn; and **E**: 1 mM Zn. Images were obtained on a 4.7 T magnet with the following parameters: Repetition time (TR) = 100.0 ms; echo time (TE) = 14.3 ms, field of view (FOV) = 1.4/1.8 cm; and data matrix = 256 x 256. **78**

Figure 3.1. Zn(II)-responsive MRI contrast agents with varying linker lengths between the Zn(II)-binding groups and the Gd(III) chelate. **94**

Figure 3.2. Relaxivity of **Gd-daa2** with the addition of $ZnCl_2$ in HEPES buffer measured at 37 °C and 60 MHz. **99**

Figure 3.3. Relaxivity of **Gd-daa4** in the presence of $ZnCl_2$ in HEPES buffer measured at 37 °C and 60 MHz. **99**

Figure 3.4. Relaxivity of **Gd-daa2** with Zn(II) and Cu(II) measured at 37 °C and 60 MHz in HEPES buffer. **101**

Figure 3.5. Relaxivity of **Gd-daa4** with Zn(II) and Cu(II) measured at 37 °C and 60 MHz in HEPES buffer. **101**

Figure 3.6. Relaxivity of **Gd-daa4** in the presence of $ZnCl_2$ in HEPES buffer and human male serum measured at 37 °C and 60 MHz. **102**

Figure 3.7. ^{17}O transverse relaxation rates with variable temperature for **Gd-daa2** at 54 MHz with and without Zn(II). A best-fit curve could not be fit to the experimental data due to the limited access of water to Gd(III). **107**

Figure 3.8. ^{17}O transverse relaxation rates with variable temperature for **Gd-daa3** at 54 MHz with and without Zn(II) showing the fit to the experimental data for **Gd-daa3 + Zn** (red line). The least squares fitting procedure gave [Gd] = 0.02 mM, τ_m = 112.0 ns, ΔH_M = 17.5 kJ/mol, T_{1e} = 20.2 ns, and q = 1. The hyperfine coupling constant was taken to be $A/\hbar = -3.8 \times 10^6$ rad s^{-1}. **108**

Figure 3.9. ^{17}O transverse relaxation rates with variable temperature for **Gd-daa4** at 54 MHz with and without Zn(II) showing the fit to the experimental data for **Gd-daa4 + Zn** (red line). The least squares fitting procedure gave [Gd] = 0.013 mM, τ_m = 24.9 ns, ΔH_M = 23.2 kJ/mol, T_{1e} = 77.0 ns, and q = 1. The hyperfine coupling constant was taken to be $A/\hbar = -3.8 \times 10^6$ rad s^{-1}. **109**

Figure 3.10. Observed titration curves of FluoZin-1 with Zn(II) at varying concentrations of **Gd-daa2** measuring the fluorescence at λ_{em} = 515 nm in HEPES buffer at a pH of 7.4. **111**

Figure 3.11. Observed titration curves of FluoZin-1 with Zn(II) at varying concentrations of **Gd-daa4** measuring the fluorescence at λ_{em} = 515 nm in HEPES buffer at a pH of 7.4. **111**

Figure 3.12. ^{1}H NMR spectrum (500 MHz) of **Eu-daa3** and assignment of the macrocyclic protons. M_{ax} = axial protons, M_{eq} = equatorial protons, M_{ac} = acyl protons, Ar = aromatic protons, and Me = methyl protons. **113**

Figure 3.13. EXSY spectrum (500 MHz) of **Eu-daa3** showing cross peaks between the axial and equatorial macrocyclic protons. **114**

Figure 3.14. T_1-weighted MR images of NIH/3T3 cells treated with **Gd-daa4** and/or Zn-pyrithione. **A:** Gd-daa4, **B:** control cells, **C:** Gd-daa4 + Zn-pyrithione, **D:** Zn-pyrithione. Images were obtained on a 4.7 T magnet with the following parameters: repetition time (TR) = 500.0 ms; echo time (TE) = 14.3 ms; field of view (FOV) = 3.0/3.0 cm; and data matrix = 256 x 256. **116**

Figure 4.1 Gd(III) complexes used as MRI contrast agents with a total coordination number of eight or nine. **131**

Figure 4.2. Three possible mechanisms for activation of the Zn(II)-responsive MRI contrast agent **Gd-daa3** and the resulting coordination environments. **A**. Closed structure has a coordination number of 9 and changes to a coordination number of 8 in the open structure. **B**. Both closed and open structures have a coordination number of 9. **C**. Both closed and open structures have a coordination number of 8. **133**

Figure 4.3. A series of Zn(II)-responsive contrast agents with varying Zn(II)-binding groups. **134**

Figure 4.4. Relaxivities of **1-4** at 60 MHz and 37 °C in the absence of Zn(II) in HEPES buffer. **140**

Figure 4.5. Relaxivities of **1-4** at 60 MHz and 37 °C before and after addition of $ZnCl_2$ in HEPES buffer. **142**

Figure 4.6. Relaxivities of **1-4** at 60 MHz and 37 °C in male human serum before and after addition of Zn(II). **142**

Figure 4.7. Observed titration curves of FluoZin-1 with Zn(II) at varying concentrations of **Gd-aa3** measuring the fluorescence at λ_{em} = 515 nm in HEPES buffer at a pH of 7.4. **146**

Figure 4.8. Observed titration curves of FluoZin-1 with Zn(II) at varying concentrations of **Gd-apa3** measuring the fluorescence at λ_{em} = 515 nm in HEPES buffer at a pH of 7.4. **146**

Figure 4.9. Observed titration curves of FluoZin-1 with Zn(II) at varying concentrations of **Gd-dpa3** measuring the fluorescence at λ_{em} = 515 nm in HEPES buffer at a pH of 7.4. **147**

Figure 4.10. ^{17}O transverse relaxation rates with variable temperature for **Gd-apa3** at 54 MHz with and without Zn(II) showing the fit to the experimental data for **Gd-apa3 + Zn** (red line). The least-squares fitting procedure[11] gave [Gd] = 0.02 mM, τ_m = 197 ns, ΔH_M = 45.5 kJ mol^{-1}, T_{1e} = 14.4 ns, and q = 1. The hyperfine coupling constant was taken to be A/h = -3.8 × 10^6 rad s^{-1}. **148**

Figure 4.11. ^{17}O transverse relaxation rates with variable temperature for **Gd-dpa3** at 54 MHz with and without Zn(II) showing the fit to the experimental data for both plots. For **Gd-dpa3 + Zn** the least-squares fitting procedure[11] gave [Gd] = 0.018 mM, τ_m = 10.8 ns, ΔH_M = 47.2 kJ mol^{-1}, T_{1e} = 4.7 ns, and q = 1.5 (red line). For **Gd-dpa3** without Zn(II) the fitting parameters gave [Gd] = 0.02 mM, τ_m = 6.2 ns, ΔH_M = 25.5 kJ mol^{-1}, T_{1e} = 11.5 ns, and q = 1.5 (blue line). The hyperfine coupling constant was taken to be A/h = -3.8 × 10^6 rad s^{-1} for both plots. **149**

Figure 4.12. ^{13}C NMR spectrum of **Eu-daa3** at 100 MHz. **151**

Figure 4.13. ^{13}C NMR spectrum of **Zn-Eu-daa3** at 100 MHz. **151**

Figure A.1. TEM images of (A) Si nanoparticles; (B) amine coated nanoparticles; and (C) Gd-DO3A-SiNPs. The images show that particle size and morphology is maintained throughout the synthesis of the nanoparticles, indicating that the particles are not affected by the reaction conditions. Scale bars for A and B are 20 nm and for C is 50 nm. **172**

Figure A.2. EDX spectra of final **Gd-DO3A-SiNPs**. **172**

Figure A.3. Possible sites for modification to **Gd-daa3** for attachment to SiNPs. **177**

LIST OF SCHEMES

Scheme 2.1. The synthesis of Zn(II)-activated contrast agents **1** and **2.** **57**

Scheme 3.1. The synthesis of **Gd-daa2 (1)**. **96**

Scheme 3.2. The synthesis of **Gd-daa4 (2)**. **97**

Scheme 4.1. The synthesis of **Gd-apa3 (3)** and **Gd-dpa3 (4)**. **137**

Scheme 4.2. The synthesis of the ^{13}C isotopically labeled **Eu-daa3** (* = ^{13}C). **138**

Scheme A.1. Synthetic scheme for conjugation of DO3A to silica nanoparticles. **170**

Scheme A.2. Synthesis of Gd-DO3A modified with triethyoxysilane. **175**

Scheme A.3. Synthesis of **Gd-daa3** with modifications to position A. **178**

Scheme A.4. Synthesis of **Gd-daa3** with modifications at position B. **180**

LIST OF TABLES

Table 2.1. Fluorescence lifetime decays in water and D_2O and the calculated hydration number. **66**

Table 2.2. Values of the parameters used to reproduce the relaxivity profiles of **Figure 2.10**. **69**

Table 2.3. T_1 measurements of the phantom samples imaged in **Figure 2.15** measured at 60 MHz and 37 ^{o}C. **78**

Table 3.1. Fluorescence decay lifetimes of **Tb-daa2, Tb-daa3,** and **Tb-daa4** in H_2O and D_2O and their calculated *q* values with an error of +/- 0.1. **104**

Table 3.2. T_1 measurements of the MR samples from **Figure 3.14** measured at 4.7 T. **116**

Table 4.1. Fluorescence decay lifetimes of **Tb-daa3, Tb-apa3,** and **Tb-dpa3** in H_2O and D_2O and their calculated *q* values with an error of +/- 0.1. **144**

Table 4.2. Zn(II)-dissociation constants calculated for **1-4**. **147**

Table A.1. Relaxivity values (60 MHz and 37 °C) and number of Gd(III) ions per particle. **173**

Abbreviations

Abbreviation	
Units	
C	Celsius
cm^{-1}	wavenumber
CN	coordination number
hr	hour
K	Kelvin
M	molar
MHz	megahertz
mM	millimolar
mmol	millimole
mol	mole
mL	milliliter
ms	millisecond
nm	nanometer
nM	nanomolar
ns	nanosecond
ppb	parts per billion
s	second
T	tesla
µM	micromolar
Chemicals	
APS	3-aminopropyltrimethoxy-silane
BAPTA	1,2-bis(*o*-aminophenoxy)ethane-*N,N,N',N'*-tetraacetic acid
BSA	bovine serum albumin
cyclen	1,4,7,10-tetraazacyclotetradecane
DMEM	Dulbecco's modified Eagles's medium
DMF	*N,N*-dimethylformamide

DNA	deoxyribonucleic acid
DO3A	*N,N',N''*-tricarboxymethylene cyclen
DOTA	*N,N',N'',N'''*-tetracarboxymethylene cyclen
DTPA	diethylenetriaminepentaacetic acid
EDC	1-ethyl-3-(3-dimethylaminopropyl)carbodiimide
Et_2O	diethyl ether
EtOAc	ethyl acetate
EtOH	ethanol
HEPES	N-(2-Hydroxyethyl)piperazine-N′-(2-ethanesulfonic acid)
HOPO	hydroxypyridinone
HSA	human serum albumin
Ln	lanthanide
MeCN	acetonitrile
MeOH	methanol
NBS	3-(N-morpholino)propanesulfonic acid
PBS	phosphate buffered saline
PPh_3	triphenylphosphine
TBAF	tetrabutylammonium fluoride
TBDMS	tetrabutyldimethylsilane
TFA	trifluoroacetic acid
THF	tetrahydrofuran
TIPS	triisopropylsilane
TPEN	*N,N,N',N'*-tetrakis(2-pyridylmethyl)ethylenediamine

General

EDX	energy dispersive x-ray spectroscopy
EPR	electron paramagnetic resonance
ESI-MS	electrospray ionization mass spectrometry
EXAFS	extended x-ray absorption fine structure
EXSY	exchange spectroscopy

FT	fourier transform
HPLC	high performance liquid chromatography
ICP-AES	inductively coupled plasma – atomic emission spectrometry
ICP-MS	inductively coupled plasma – mass spectrometry
LC-MS	liquid chromatography – mass spectrometry
MR	magnetic resonance
MRI	magnetic resonance imaging
NMR	nuclear magnetic resonance
NMRD	nuclear magnetic relaxation dispersion
RF	radio frequency
TEM	transmission electron microscopy
TLC	thin layer chromatography
UV/Vis	ultraviolet/visible spectroscopy
VT	variable temperature
ZFS	zero-field splitting

Symbols

Å	angstrom
br	broad
d	doublet
I	nuclear angular momentum quantum number
J	NMR coupling constant
K_d	dissociation constant
K_{sp}	solubility constant
m	multiplet
m/z	mass to charge ratio
P_m	mole fraction of contrast agent
q	hydration number
r_1	longitudinal relaxivity
R_{2p}	transverse relaxation rate

s	singlet
S	spin angular momentum quantum number
t	triplet
T	temperature
T_1	longitudinal nuclear relaxation time
T_{1e}	longitudinal electronic relaxation time
T_2	transverse nuclear relaxation time
ΔH	enthalpy of activation
$\Delta\nu_{1/2}$	line width at half peak height
$\hbar$	Dirac's constant
λ_{em}	wavelength emission
λ_{ex}	wavelength excitation
τ_c	correlation time
τ_m	mean water residency lifetime
τ_R	rotational correlation time

Chapter 1

Introduction

1.1 Introduction

Magnetic resonance imaging (MRI) is becoming increasingly popular in the medical field because of its ability to offer a non-invasive modality capable of producing three-dimensional representations of opaque organisms with temporal resolution. Although the sensitivity of MRI cannot compare to that of other imaging modalities such as positron emission tomography (PET), it does provide high-resolution images without the use of radiopharmaceuticals. In addition, MRI allows for the greatest spatial resolution of common imaging modalities with image resolution in the millimeter range for clinical applications and micrometer range for high-resolution MRI. Spatial resolution can be enhanced with the use of contrast agents. Roughly 50% of all MR scans use contrast agents.[1] With advances in chemistry and the subsequent synthesis of more efficient and specific contrast agents, MRI has moved into the forefront of molecular imaging.

Of the clinically relevant MR contrast agents available, most of them employ the paramagnetic metal Gd(III) (**Figure 1.1**). Although proton relaxivity is greatly enhanced with the use of paramagnetic ions, Gd(III) has emerged as the optimum choice due to its seven unpaired electrons, its high magnetic moment, and its long electron spin relaxation time (10^{-9} s).[2] However, Gd(III) itself is highly toxic as it has a similar ionic radius to Ca(II) and can disrupt Ca(II) signaling.[3] The safe administration of Gd(III) for MR imaging uses chelating agents that tightly bind Gd(III) to create thermodynamically stable complexes (log K_d ~ 21-25). The most commonly used chelating agents are macrocyclic (DOTA) and linear (DTPA) poly(amino-carboxylate) ligands that provide eight coordinating oxygen and nitrogen atoms to bind Gd(III). The ninth coordination position is occupied by water.

This chapter provides an introduction to magnetic resonance imaging and the theories of

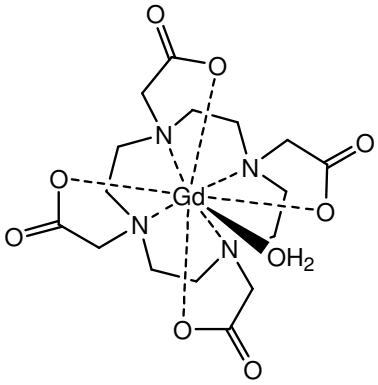

[(Gd(DOTA)(H$_2$O)]$^-$ (Dotarem^{TM})

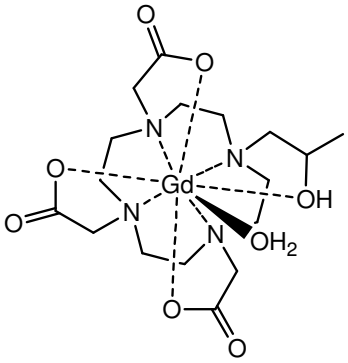

[(Gd(HP-DO3A)(H$_2$O)] (Prohance^{TM})

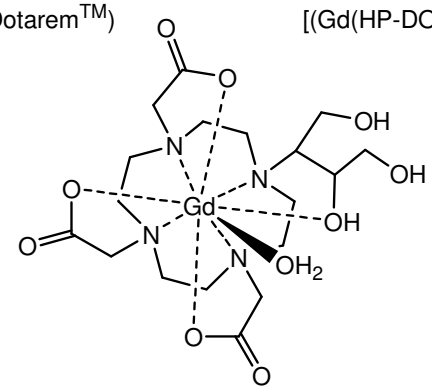

[(Gd(DO3A-butrol)(H$_2$O)] (Gadovist^{TM})

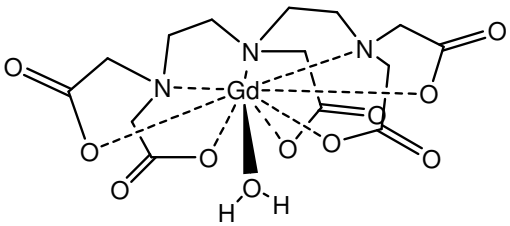

[Gd(DTPA)(H$_2$O)]$^{2-}$ (Magnevist^{TM})

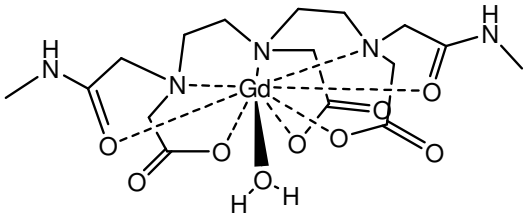

[Gd(DTPA-BMA)(H$_2$O)] (Omniscan^{TM})

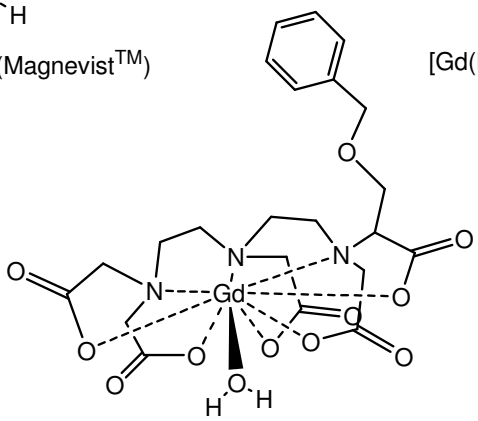

[Gd(BOPTA)(H$_2$O)]$^{2-}$ (MultiHance^{TM})

Figure 1.1. Clinically approved Gd(III)-based magnetic resonance contrast agents.

relaxation with respect to the use and optimization of Gd(III)-based contrast agents. In addition, second-generation contrast agents that are biologically responsive, cell-permeable, and targeted are considered.

1.2 Magnetic Resonance Imaging

Imaging with nuclear magnetic resonance (NMR) spectroscopy was first introduced by the pioneering work of Lauterbur in 1973.[4] Much like NMR spectroscopy, MRI exploits the differences in the relaxation rates of nuclear spins due to an applied magnetic field. MRI detects the electromagnetic radiation emitted from the transition of higher energy nuclei to a lower energy level. Although nuclei with a spin quantum number of $I = ½$ such as ^{1}H, ^{13}C, ^{19}F and ^{31}P can be used, most current MRI technology is based on ^{1}H nuclei. The NMR signal is relatively low compared to other spectroscopic methods, but due to the large number of atoms in a typical sample, it is still possible to detect a signal. Current technology uses magnetic field strengths up to 3 T for clinical imaging and up to 19 T for high-resolution imaging.[5]

MRI takes advantage of the most abundant molecule in biological tissues, water. It measures the proton NMR signal of water in which the signal intensity is proportional to the relaxation rates of the nuclear spins. In the presence of a magnetic field, the magnetic moments of the protons in water molecules orient themselves along the magnetic field, both in a parallel and antiparallel orientation. Due to the distribution of more nuclei in lower energy states, according to Boltzman's law, a net magnetic moment along the axial field is observed that precesses at the Larmor frequency. An applied radiofrequency pulse inverts the magnetization vector away from the axial field, and reorientation to the original magnetic field direction occurs through both longitudinal and transverse relaxation pathways. The process of realignment

characterized by T_1 is called longitudinal or spin-lattice relaxation, and it is the dominant factor in producing contrast in a T_1-weighted MR image.

Due to the heterogeneity of most MR samples, intrinsic contrast between organs can be observed from the varying water concentrations and local environments.[5, 6] Signal resolution and sensitivity can be greatly enhanced with the use of paramagnetic contrast agents. For T_1-weighted MR images, Gd(III)-based agents have emerged at the forefront due to the seven unpaired electrons of Gd(III) and its high magnetic moment. Since this thesis focuses on the development of lanthanide-based contrast agents for T_1 imaging, this chapter will focus on T_1 relaxation theories and current contrast agents.

1.2.1 Relaxation Theory

The theory of relaxation in the presence of paramagnetic ions is best described by the equations developed by Solomon, Bloembergen, and Morgan.[7, 8] Use of gadolinium complexes in MR imaging produces an increase in the T_1 relaxation rates and thus an increase in intensity. The observed relaxation rate of protons is the result of the sum of diamagnetic (d) and paramagnetic (p) contributions.

$$\frac{1}{T_{1,\,\mathrm{obs}}} = \frac{1}{T_{1,\,\mathrm{d}}} + \frac{1}{T_{1\,,\mathrm{p}}} \qquad \textbf{Equation 1.1}$$

The diamagnetic term arises from the relaxation rate of water proton nuclei in the absence of a paramagnetic ion. The paramagnetic term can be expressed as the relaxation rate enhancement induced by the paramagnetic species that is linearly proportional to its concentration (**Equation 1.2**). Therefore, the efficacy of Gd(III) complexes in decreasing T_1 of

local water protons is measured by its relaxivity value, r_1 ($mM^{-1}s^{-1}$), the slope of the line of $1/T_1$ versus [Gd].[5, 6]

$$\frac{1}{T_{1,\,\mathrm{obs}}} = \frac{1}{T_{1,\,\mathrm{d}}} + r_1[\mathrm{Gd}] \qquad \textbf{Equation 1.2}$$

The paramagnetic contribution is made up of both inner-sphere (IS) and outer-sphere (OS) contributions.

$$\frac{1}{T_{1,\,\mathrm{p}}} = \left(\frac{1}{T_{1,p}}\right)^{IS} + \left(\frac{1}{T_{1,p}}\right)^{OS} \qquad \textbf{Equation 1.3}$$

Inner-sphere relaxation is characterized by water molecules directly bound to the first coordination sphere of the metal ion. Relaxation effects from the paramagnetic ion arise from the dipole-dipole interactions between the nuclear spins and the local magnetic field of the unpaired electron spins. Therefore, water protons binding directly to the metal ion is important for the transmission of the paramagnetic effect to the bulk water solvent, since the bound water molecule exchanges with the bulk solvent. Outer-sphere contributions arise from the close proximity of water protons to the paramagnetic center, usually through hydrogen bonding to the ligand. Although both the inner-sphere and outer-sphere water protons contribute equally to the relaxation process, for the development of MR contrast agents, the inner-sphere term can easily be modified, and is therefore the major contribution to the overall proton relaxation rate.[5]

The inner-sphere relaxation mechanism arises from the chemical exchange of the water molecules bound to the first coordination sphere of the metal center to the bulk water solvent and can be expressed by **Equation 1.4**. P_M is the mole fraction of the gadolinium ion, q is the number of bound water molecules in the first coordination sphere, T_{1M} is the relaxation time of

the bound inner-sphere water protons, and τ_m is the mean residence lifetime of the bound water molecule.

$$\left(\frac{1}{T_{1,p}}\right)^{IS} = \frac{P_m q}{T_{1M} + \tau_m} \qquad \textbf{Equation 1.4}$$

Equation 1.4 states that if the water exchange is sufficiently fast, where $\tau_m << T_{1M}$, then inner-sphere relaxation is dependent on the relaxation enhancement of the bound water protons (T_{1M}), which is governed by both dipole-dipole (DD) and scalar (SC) mechanisms (**Equation 1.5**). The dipole-dipole mechanism involves the changes in the orientation of the electron spin and proton exchange to modulate the direction of the nuclear spin – electron vector. The scalar mechanism is independent of molecular orientation and involves the electron spin relaxation and water exchange only. Due to the highly ionic nature of Gd(III) bonds, the scalar coupling is considered to be relatively weak which causes dipole-dipole interactions to become the dominant factor in relaxation enhancement.

$$\frac{1}{T_{1,\mathrm{M}}} = \left(\frac{1}{T_1^{DD}}\right) + \left(\frac{1}{T_1^{SC}}\right) \qquad \textbf{Equation 1.5}$$

The correlation time that defines dipole-dipole relaxation is τ_c. This is determined by **equation 1.6**, where T_{1e} is the electron spin relaxation time, τ_m is the residence lifetime of bound water protons, and τ_R is the rotational correlation time.

$$\frac{1}{\tau_c} = \frac{1}{T_{1e}} + \frac{1}{\tau_m} + \frac{1}{\tau_R} \qquad \textbf{Equation 1.6}$$

Relaxivity is maximized when τ_c is equal to the inverse of the Larmor frequency.[5] Optimization of the parameters shows that τ_m should be decreased, but not such that it begins to limit T_{1M}.

1.2.2 Factors affecting relaxivity

The above equations demonstrate that proton relaxivity is influenced by a large number of parameters. To complicate matters, the parameters discussed are dependent on the magnetic field strength and termperature as well. Contrast agents currently used in clinical applications have relaxivity values around 4 $mM^{-1}s^{-1}$, far below the theoretical maximum near 100 $mM^{-1}s^{-1}$.[5] Due to the low relaxivity values of commercial contrast agents, they are only effective when used in concentrations greater than 0.1 mM.[9] In order to increase the relaxivity of current Gd(III)-based contrast agents, researchers have focused on optimizating the parameters that can most easily be modified, specifically the hydration number, the mean residence lifetime of bound water protons, and the rotational correlation time (**Figure 1.2**). The following section provides examples of Gd(III)-based agents designed to optimize each of these parameters.

Hydration Number (q)

Current clinical contrast agents utilize poly(amino-carboxylate) chelating ligands that bind Gd(III) with a coordination number of eight, leaving one available coordination site open for the binding of water. Efforts to increase the number of inner-sphere bound water molecules have been limited due to the need for a low Gd(III)-dissociation constant to reduce the effects of Gd(III) cytotoxicity. The loss of one coordinating group from the ligand can increase the Gd(III)-dissociation constant by three orders of magnitude.[6] However, as evidenced by **Equation 1.4**, doubling the number of bound water molecules would increase the relaxivity by a factor of two, providing a large increase in the observed intensity of an MR image.

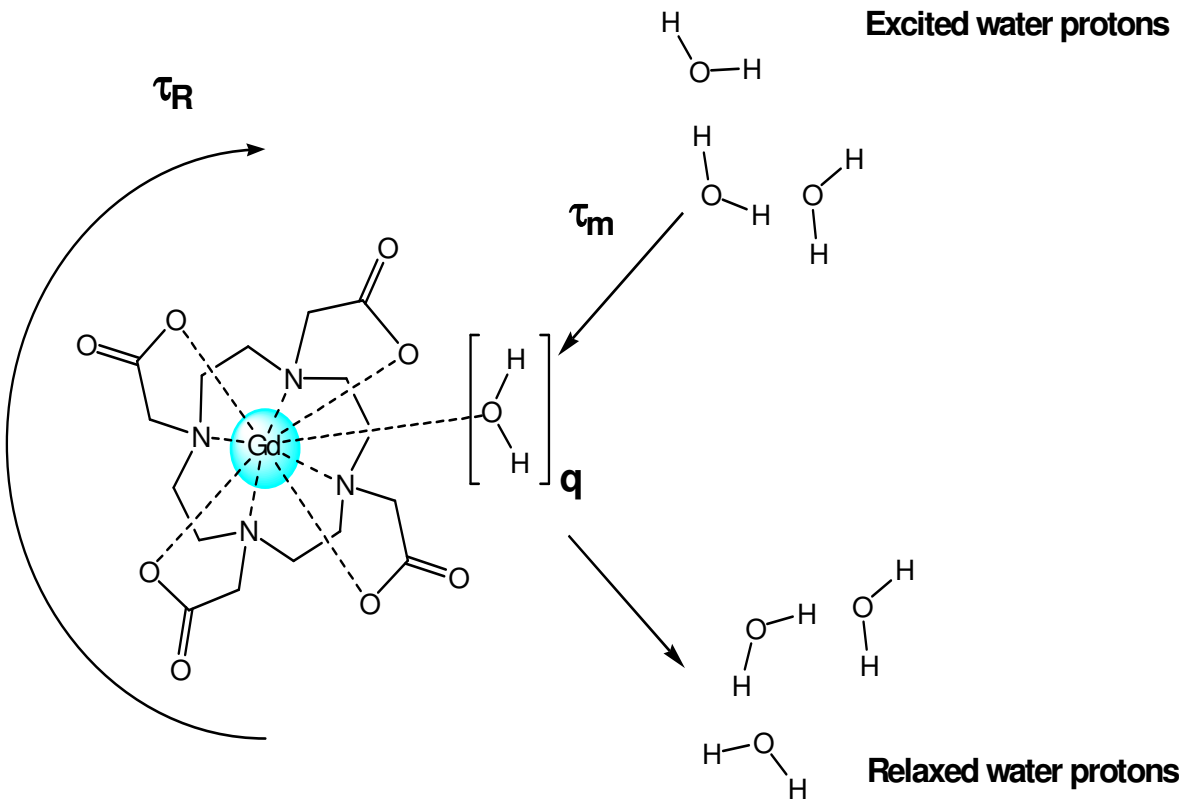

Figure 1.2. Factors affecting relaxivity of Gd(III)-based MR contrast agents: the hydration number (q), the mean residence lifetime of bound water molecules (τ_m), and the rotational correlation time (τ_R).

Ligands with a hydration number of two have recently been developed by Ken Raymond and coworkers. This new family of MRI contrast agents is comprised of all oxygen donors rather than traditional poly(amino-carboxylate) complexes and is based on hydroxypyridinone (HOPO) ligands.[1, 10, 11] The first such example, Gd-TREN-1-Me-3,2-HOPO (**Figure 1.3**), chelates Gd(III) through six oxygen atoms and provides two positions for water coordination without compromising thermodynamic stability.[12] The measured relaxivity of 10.5 $mM^{-1}s^{-1}$ at 20 MHz and 25 $^{\circ}C$ is more than double that of commercially available contrast agents. Efforts to increase water solubility of HOPO-based ligands continue because their use for *in vivo* studies remains limited due to poor aqueous solubility.

Water Exchange Rate ($1/\tau_m$)

The mean lifetime residence of inner-sphere water molecules contributes to proton relaxativity in two ways. First, it determines the chemical exchange rate of inner-sphere water protons with the bulk solvent (**Equation 1.4**). Secondly, it plays a role in the overall correlation time τ_c, which governs the dipole-dipole relaxation mechanisms (**Equation 1.6**). Typical nine-coordinate monohydrate contrast agents have a water exchange rate on the order of 10^6 s^{-1}, two orders of magnitude slower than the optimal exchange rate ($k_{ex} \sim 10^8$ s^{-1}).[13] The Gd-aqua ion has a much faster exchange rate ($k_{ex} \sim 10^9$ s^{-1}), indicating that the poly(amino-carboxylate) ligands greatly hinder water exchange.

Water exchange in lanthanide chelates can proceed through an associative or a dissociative mechanism. The mechanism of water exchange for the Gd-aqua ion is an associative pathway in which a nine-coordinate intermediate state is easily obtained. Conversely, the nine-coordinate monohydrate chelates must go through a dissociative

mechanism because there is no available site for a second water to bind. Therefore, an eight-coordinate intermediate state must be created for water exchange to occur; for most poly(amino-carboxylate) ligands this is a highly energetically unfavorable state, resulting in slow water exchange.[13, 14]

One way to alleviate the problem of slow water exchange has been to increase the steric compression about the water binding site to stabilize the unfavorable eight-coordinate intermediate.[15] Merbach and coworkers have shown that through modification of the poly(amino-carboxylate) backbones with additional methylene groups, steric crowding facilitated the release of the bound water molecule, leading to near-optimized chemical exchange rates via an increase of two orders of magnitude (**Figure 1.4**). This approach has been demonstrated in both macrocyclic and linear poly(amino-carboxylate) ligands.[13] Unfortunately, these modifications slightly reduce the thermodynamic stability of both the poly(amino-carboxylate) ligands, potentially limiting their possible use in clinical applications.

Rotational Correlation Time (τ_R)

A third major parameter in the development of improved contrast agents is the rotational correlation time (τ_R) that contributes to the overall correlation time (τ_c) (**Equation 1.6**). Molecular tumbling is dependent on both the molecular size and rigidity of the agent. There are two main methods for optimization of τ_R. The first involves the development of contrast agents to create large molecular weight dendrimers agents,[16-19] polymer scaffolds,[20] and lipid-based vesicles.[21, 22] The second involves non-covalent attachment to macromolecules such as proteins

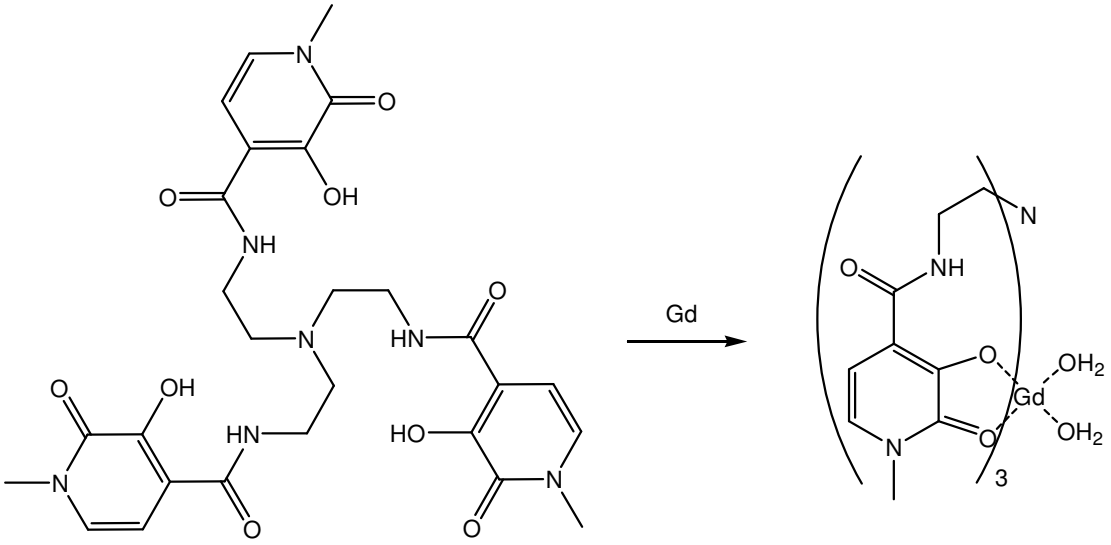

Figure 1.3. Structure of Gd-TREN-1-Me-3,2-HOPO, a q = 2 contrast agent.[12]

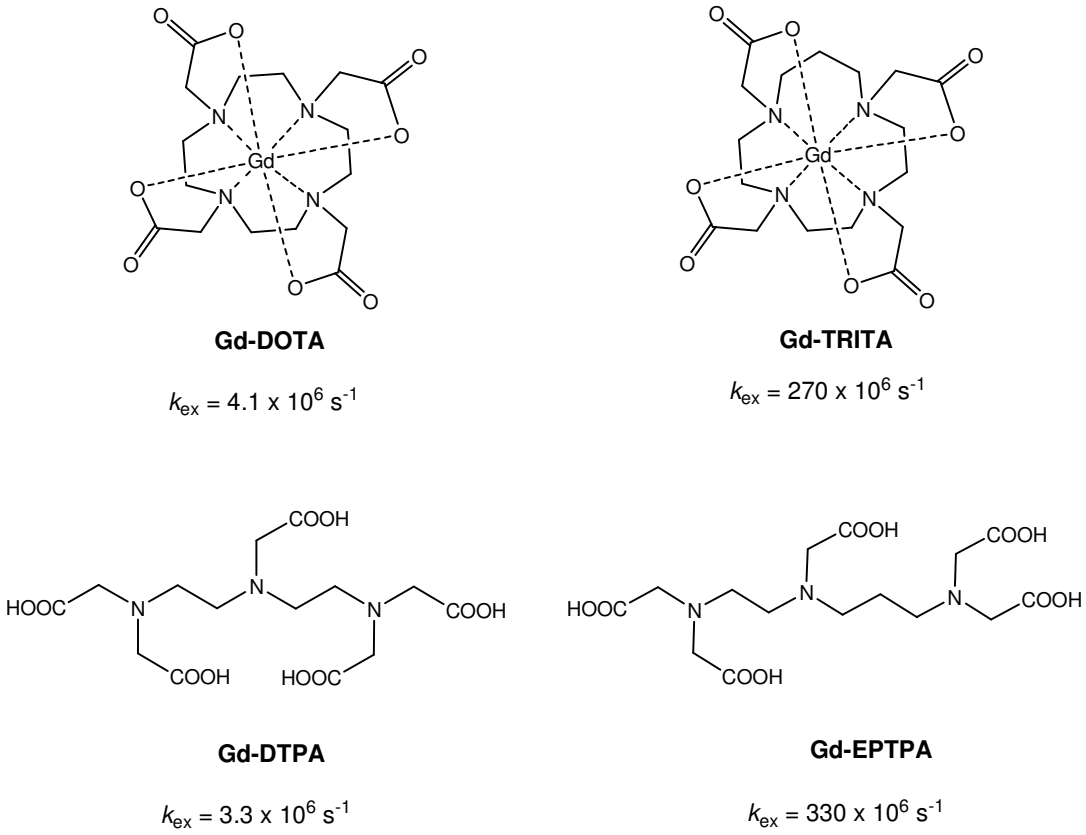

Figure 1.4. Structures of ligands with optimized τ_m.[13]

and DNA, more commonly known as receptor-induced magnetization enhancement (RIME).[23, 24] Both of these methods increase the rotational correlation time and thus enhance water proton relaxivity.

When designing contrast agents with reduced rotation of the Gd(III) chelate due to conjugation with dendrimers or polymers there are two rotational parameters to be considered. The first is the overall tumbling rate of the entire macromolecule which generally increases due to the large molecular weight of the complex. The second parameter involves the local rotational time of each Gd(III) chelate. Due to the flexibility of the dendrimers and polymers, internal rotation about the Gd(III) ion is still possible, limiting the optimization of τ_m (**Figure 1.5**). Several efforts to increase the rotational correlation time of the local environment of the Gd(III) chelate have been developed through conjugation to rigid backbones to limit internal rotation.[25] One such example uses a metal-templated self-assembly approach in which two Gd(III)-DTPA chelates are appended to a bipyridyl ligand that chelates Fe(II) creating a high relaxivity complex.[26]

Increasing the rotational correlation time through non-covalent attachment to proteins poses its own drawbacks. While the large increase in molecular weight contributes to the increased proton relaxivity, a reduction in the chemical exchange rate of water protons limits the effects of the reduced tumbling time. This phenomenon has been demonstrated by the use of MS-325, a DTPA-based agent designed to bind to serum albumin with high affinity.[24] An almost 50% reduction of the water exchange rate is seen upon binding to albumin through electrostatic or hydrophobic interactions.[24] These findings demonstrate the complexity of creating high relaxivity contrast agents and the subtle interplay between each of the parameters affecting relaxivity that has limited the development of brighter contrast agents.

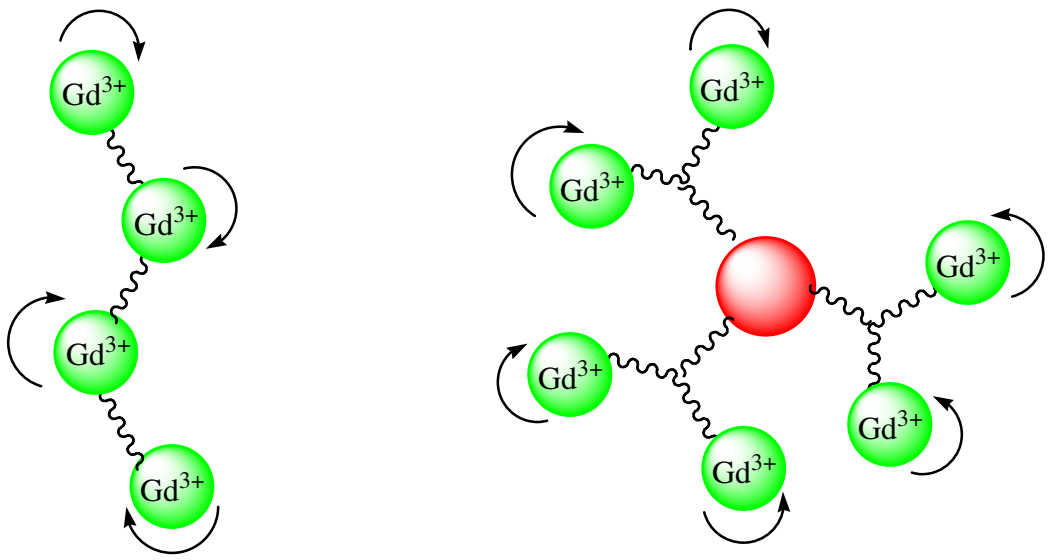

Figure 1.5. Schematic of polymer and dendrimer Gd(III) chelate constructs demonstrating internal rotation. (Adapted from Ref. 9)

1.3 Next-Generation Contrast Agents

Despite efforts in improving the proton relaxation rates of Gd(III)-chelates, as discussed above, these agents are limited to the blood pool and are constitutively active. This limits their ability to report on anatomical features rather than on physiological properties. The Meade group has pioneered the development of contrast agents whose relaxivities are responsive to changes in the biological environment and this provides a means to non-invasively illustrate physiological properties such as a change in ion concentrations or an increase in enzyme activation. This work has inspired the development of "smart" or "activated" contrast agents from other groups to include agents that are responsive to pH changes and changes in the partial pressure of oxygen. There are several comprehensive reviews on activated MR contrast agents, and only a select few will be discussed in further detail in this chapter.[27-29]

Another obstacle for current MR contrast agents is their restriction to the extracellular environment. With advancements in MR imaging techniques for cellular resolution, a great deal of research has been devoted to the the development of cell-permeable contrast agents.[25] The employment of activated MR contrast agents is greatly dependent on the ability of these agents to cross cell membranes, as most physiological responses take place in the intracellular environment. The Meade group has developed several novel contrast agents that have improved cellular permeability and are receptor-targeted which will be further discussed below.

1.3.1 Biologically Responsive Contrast Agents

The concept of activated contrast agents involves modulation of one or several parameters affecting relaxivity to produce distinct relaxation states before and after activation. Most commonly these contrast agents modulate the access of water through changes in the

coordination environment surrounding Gd(III). An ideal "smart" contrast agent will produce a low relaxation state ($q = 0$) before activation and a high relaxation state ($q = 1$) after activation to produce an increase in MR signal intensity upon activation. Several examples are discussed further.

Ion-Responsive Contrast Agents

The development of ion-responsive contrast agents has been inspired by ion-activated fluorescent reporters. Unlike light-based microscopy, MRI can provide deep-tissue penetration without the drawbacks of light-scattering and photobleaching.[5, 6] The first of such systems was designed by Li et al. to report on fluctuations in Ca(II) concentrations for imaging signal-transduction events.[30, 31] The design of this agent incorporated a well-known Ca(II)-binding motif, BAPTA (1,2-bis(*o*-aminophenoxy)ethane-*N,N,N',N'*-tetraacetic acid), appended to two Gd-DOTA chelates (**Figure 1.6**). In the absence of Ca(II), the four aminoacetate arms from the Ca(II)-binding moiety bind to Gd(III) creating a closed $q = 0$ complex with the low relaxivity of 3.3 $mM^{-1}s^{-1}$ at 500 MHz and 25 °C. Upon the addition of Ca(II), a 75% increase in relaxivity is observed due to a conformational change in which the aminoacetate arms selectively bind Ca(II) allowing access of water to Gd(III). This agent is responsive to the presence of Ca(II) ions in the range of 0.1 to 10 μM, physiologically relevant concentrations for intracellular Ca(II) signaling. New calcium-activated contrast agents have recently been reported in which activation occurs at concentrations in the millimolar range to report on changes in the extracellular environments.[32, 33] However, the relaxation enhancement of these agents is reported to be only about 15%, an increase that may not be sufficient for visualization with MRI.

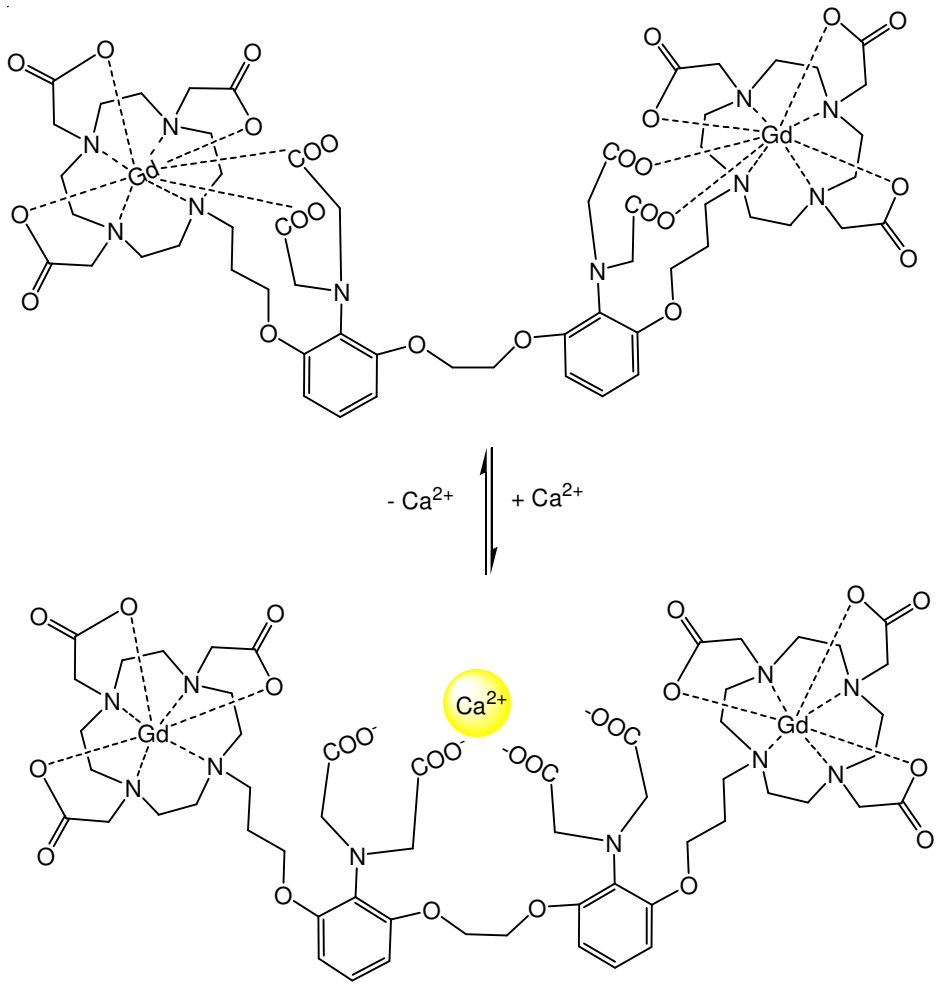

Figure 1.6. A Ca(II)-activated MR contrast agents.[30]

Another important metal ion that has received much attention in molecular imaging is Zn(II). Nagano and coworkers have developed several DTPA derivatives incorporating pyridyl Zn(II)-binding groups.[34, 35] These agents, however, provide a decrease in image intensity upon Zn(II)-activation. In the unactivated state, an open structure is observed in which water access to Gd(III) is allowed creating a high relaxation and therefore a bright image (**Figure 1.7**). Addition of Zn(II) closes the structure, thus inhibiting access of water to Gd(III) creating a low-relaxivity state. As Zn(II) concentrations are increased, a re-opening of the agent is observed in which the original relaxation state is restored. This agent thereby produces a change only when Zn(II) concentrations are equal to the concentration of the contrast agent. Although a measurable change in proton relaxivity is observed, the decrease in relaxivity upon activation is not ideal. A negative feedback-probe provides inconclusive results, as the decrease in intensity can be attributed to the addition of Zn(II) or to the diffusion of the agent.

More recently, Lippard and coworkers reported a Zn(II)-responsive agent that employs a Mn(III)-porphyrin agent with both MR and fluorescent capabilities.[36] In the absence of Mn(III), the agent acts as fluorescent reporter that is activated by Zn(II). Addition of Mn(III) to the porphyrin provides MRI functionality through modulation of water access to Mn(III) due to the presence of Zn(II). *In vitro* studies demonstrate a decrease in relaxivity enhancement with the addition of Zn(II) while *in vivo* experiments show an increase in T_1 relaxivity. Further investigation will be needed to understand the observed relaxation dynamics.

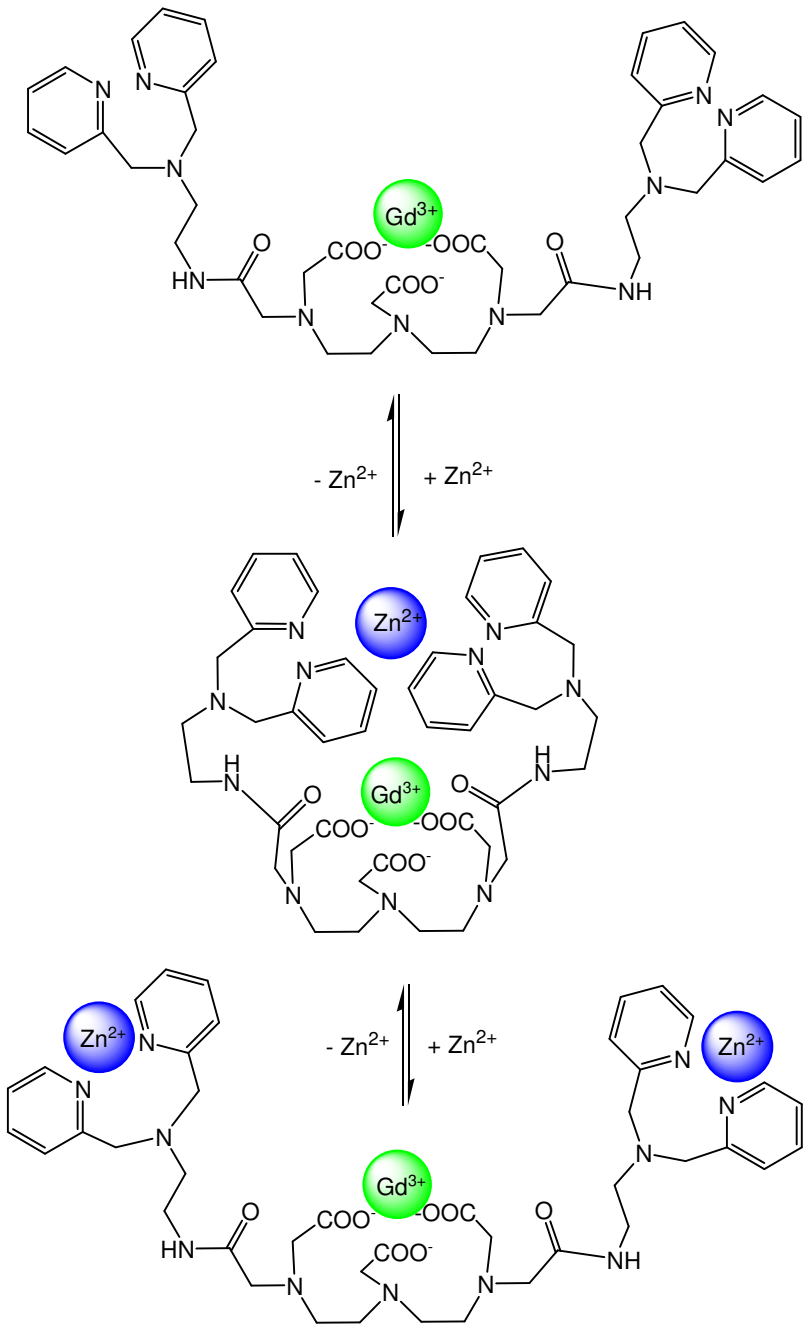

Figure 1.7. A Zn(II)-responsive MR contrast agent.[35]

Enzyme-Activated Contrast Agents

A second class of biologically responsive MR contrast agents includes those that respond to an increase in enzyme activity. The most significant of these agents, EGadMe, developed in the Meade laboratory, contains a β-galactose sugar moiety appended onto a Gd-DOTA chelate.[37-39] Before activation, a $q = 0$ complex is observed due to the binding of endogenous carbonate to Gd(III) (**Figure 1.8**). Cleavage of the sugar by the enzyme β-galactosidase leaves an available hydroxyl group that can then kick out the carbonate and bind Gd(III). Since the carbonate binds in a bidentate fashion and the hydroxyl group binds in a monodentate fashion, a coordination space is freed for water access to create a $q = 1$ complex. This agent presents a novel method for imaging gene expression as the β-galactosidase enzyme is commonly used as a reporter gene in microbiology.

Building on this concept of blocking water access with enzyme substrates, a second enzyme-activated agent was developed by Duimstra et al.[40] This agent reports on the activity of the oncologically relevant β-glucuronidase enzyme. In this design, the enzyme substrate β-glucuronic acid is attached to a Gd-DOTA chelate through a self-immolative linker. Hydrolysis of β-glucuronic acid triggers a cascade reaction that releases the Gd(III) chelate, carbon dioxide, and the bridging arm (**Figure 1.9**).

Another approach to the design of enzyme activated contrast agents modulates τ_m rather than changing the hydration number. These agents rely on hydrophobic moieties with high affinities for human serum albumin to effect the non-covalent interaction of the agent with HSA, producing a large increase in τ_m. The first agent utilizes a phosphate group that can be cleaved by alkaline phosphatase to generate the hydrophobic aryl residue with a high affinity for HSA (**Figure 1.10a**). The second agent contains a tris- lysine peptide chain that is cleaved by a

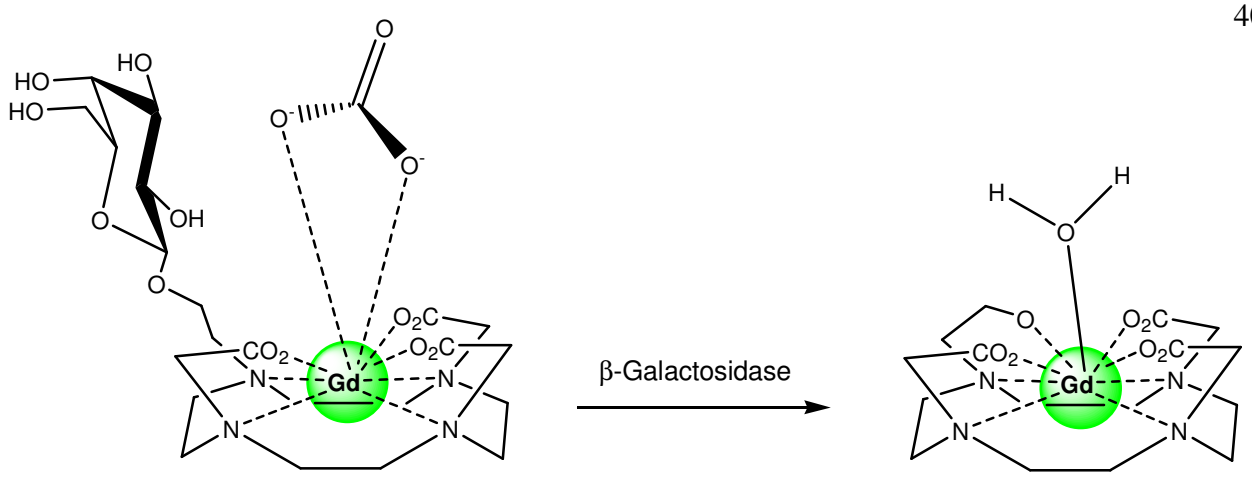

Figure 1.8. An MR contrast agent sensitive to β-galactosidase.[39]

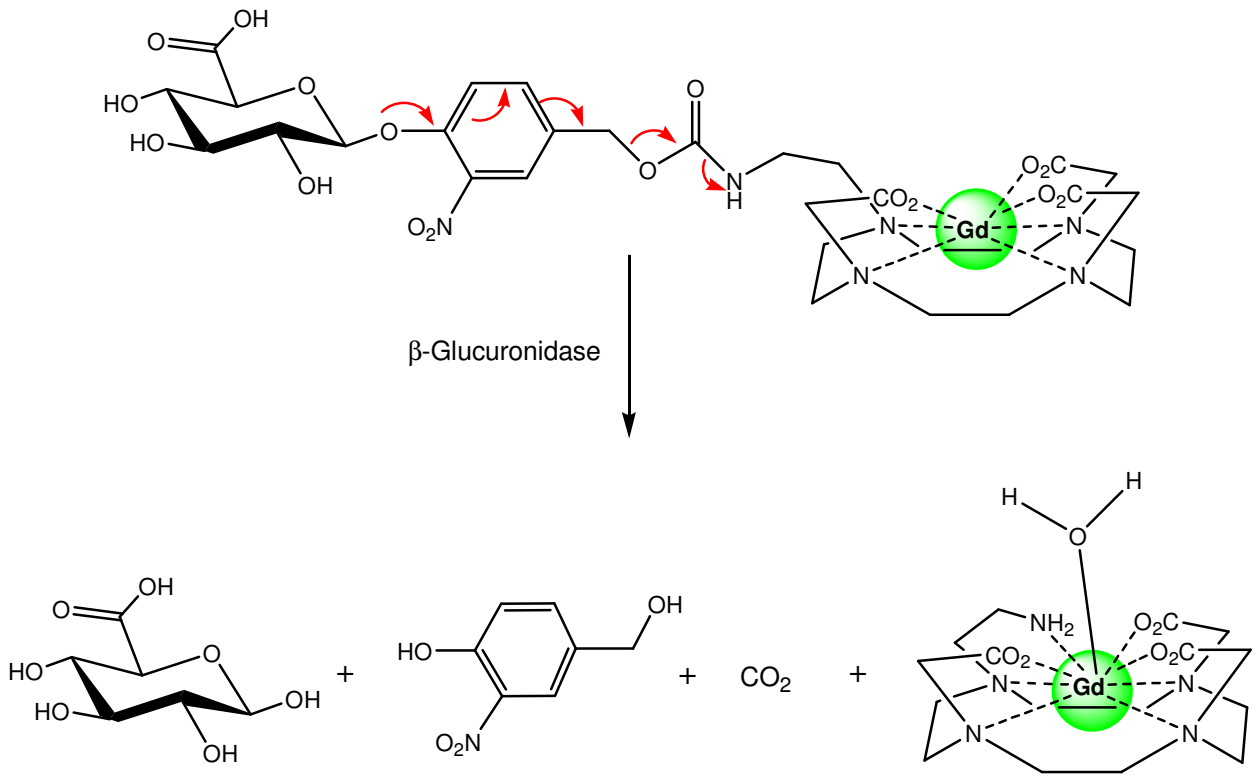

Figure 1.9. An MR contrast agent activated by β-glucuronidase through a self-immolative linker.[40]

(a)

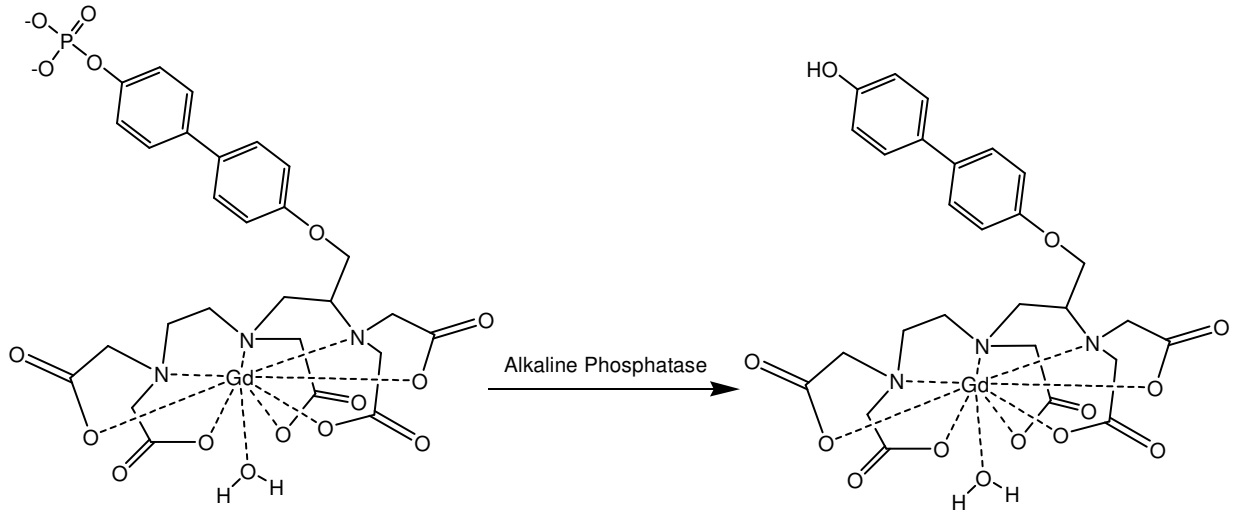

(b)

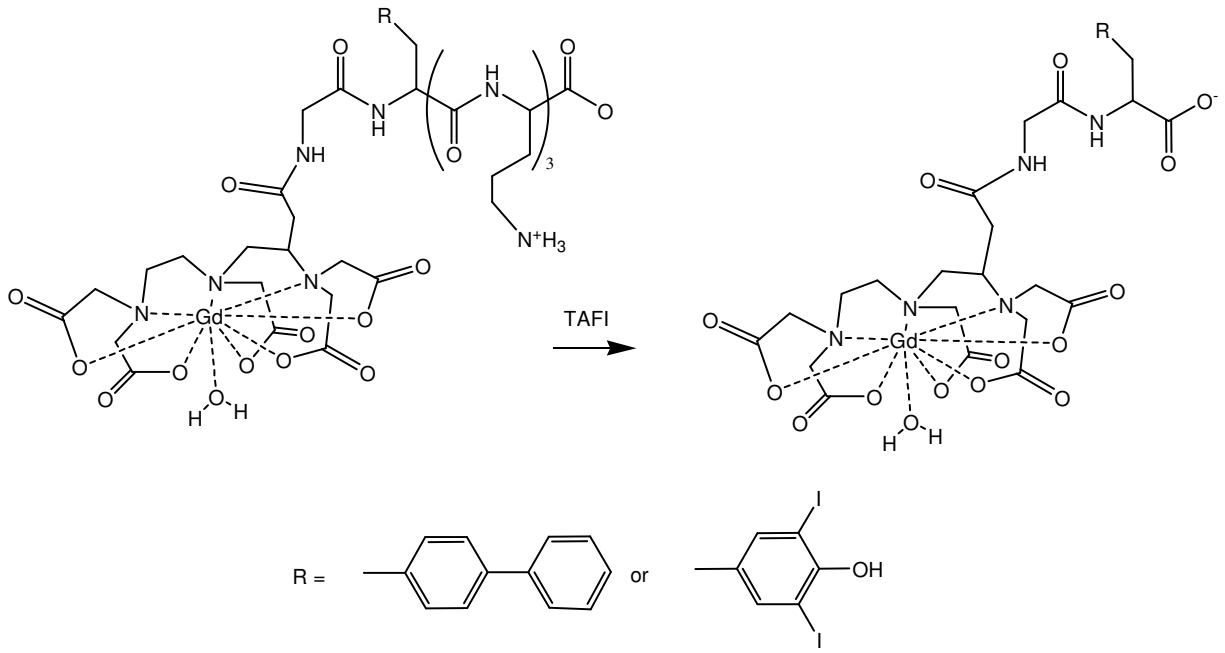

Figure 1.10. τ_m-modulated MRI contrast agents: (a) An MR contrast agent sensitive to alkaline phosphatase, and (b) an MR contrast agent sensitive to a human carboxypeptidase B, thrombin activatable fibrinolysis inhibitor (TAFI).[41]

human carboxypeptidase B, thrombin-activatable fibrinolysis inhibitor (TAFI).[41] Removal of the charged lysine groups by TAFI leaves a hydrophobic diphenylalanine or a 3,5-diiodotyrosine group, both with a high binding affinity for HSA (**Figure 1.10b**).

pH-Responsive Contrast Agents

Due to the changes in pH environments of tumor tissue, pH-responsive contrast agents can provide a novel method for diagnosing and evaluating the progression of cancerous tumors. There are several examples of pH-responsive MRI contrast agents in the literature,[42, 43] however, one such agent developed by Zhang et al. is unusual in that the pendant arms of the Gd(III) chelate can be modified to provide a range of pH dependencies through modulation of τ_m.[44] Changes in the pH produce varying protonation states on the non-coordinating phosphonate arms and either inhibit the exchange of coordinated waters or catalyze their exchange. With further development of pendant arms, a series of contrast agents with varying pH sensitivities can be envisioned.

1.3.2 Cell-Permeable and Targeted Contrast Agents

Although tremendous strides have been made in the development of activated contrast agents, their full potential has yet to be realized due to their inability to penetrate the cell membrane. The low sensitivity of MRI and the low relaxivity values of current contrast agents require the use of large doses of contrast agents (0.1 – 0.3 mmol/kg). Improvement in the targeting of contrast agents will help to accumulate agents in specified locations, possibly reducing necessary dosages required. In this section some examples of work leading to the design of cell-permeable and targeted contrast agents are discussed.

Cell-Permeable Contrast Agents

Transport of contrast agents across cellular membranes has been achieved with a variety of cell-penetrating peptides and transduction domains. The human immunodeficiency virus (HIV) trans activating protein (Tat) has been conjugated to both T_1 and T_2 MR contrast agents to achieve high cellular uptake of the agents and internalization into the nucleus.[45, 46] The relaxivity of the Tat-DOTA conjugate before addition to cells was 4.1 $mM^{-1}s^{-1}$. After cell internalization a relaxivity of 2.2 $mM^{-1}s^{-1}$ was measured due to the limited water diffusion inside cells. With a decrease in the observed relaxivity it is evident that large amounts of contrast agent will be needed for MR imaging within cells. While the 13-mer domain can be synthesized on an automatic peptide synthesizer, strategies to synthesize cell-transducing contrast agents in large-scale (several grams) quantities is required.

Arginine-rich peptides, such as the HIV-Tat peptide, have been well documented as membrane-permeable peptides capable of intracellular protein and drug delivery.[47, 48] Studies have shown that a minimum of eight arginines within the peptide are needed for sufficient transport.[48] With this understanding the Meade group has developed a strategy to conjugate an arginine octamer to Gd(III)-DOTA and Gd(III)-DTPA contrast agents (**Figure 1.11**).[49-51] The arginine octamer could be made using standard peptide synthesis techniques on solid-phase resins allowing for a facile method to synthesize large quantities of the peptide. Cellular uptake of the conjugates with three cell lines showed sufficient labeling to be visualized by MRI. The Meade group is currently investigating the use of the arginine octamer as a cellular transduction domain for biologically responsive contrast agents to image intracellular protein activation.

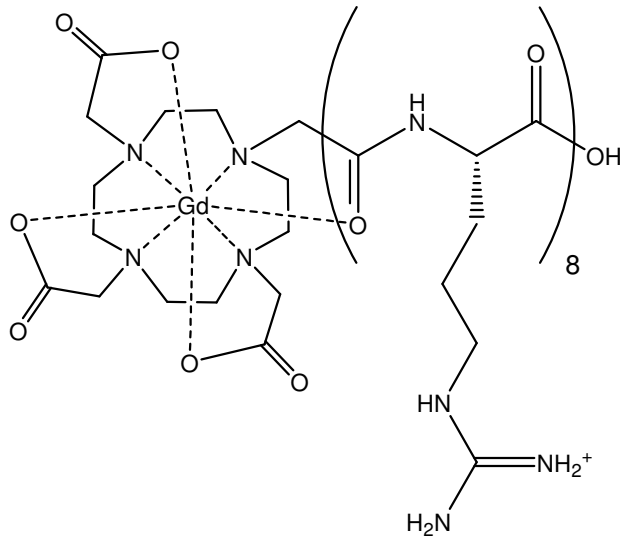

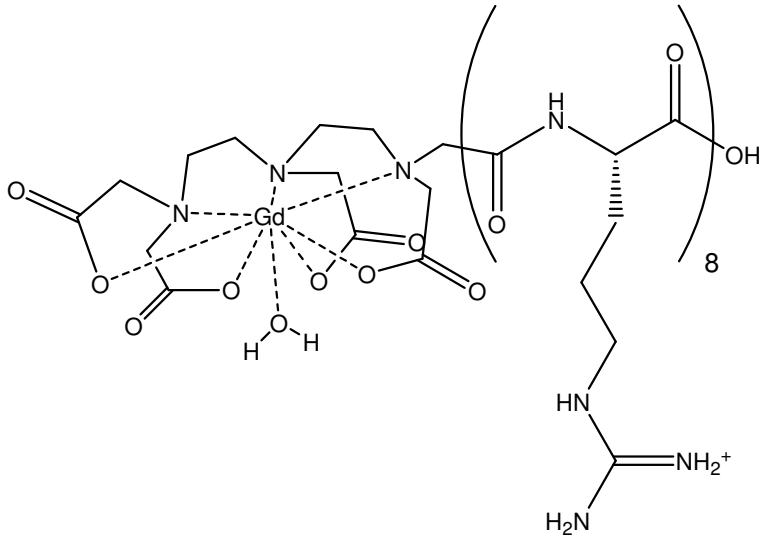

Figure 1.11. Structures of intracellular contrast agents. Top: 8-amino acid polyarginine oligomer coupled to Gd(III)-DOTA; Bottom: 8-amino acid polyarginine oligomer coupled to Gd(III)-DTPA.[50, 51]

Receptor-Targeted Contrast Agents

An efficient method for specific delivery of contrast agents involves their conjugation to molecular targeting platforms such as monoclonal antibodies[52] and cell receptors.[53-55] An early example of the development of receptor-targeted contrast agents involves the use of DNA as a molecular scaffold that electrostatically binds poly-lysine conjugated to Gd(III)-DTPA chelates or transferrin, an iron delivery protein.[56] DNA is first incubated with transferrin-modified poly-lysine and then with the Gd(III)-DTPA-modified poly-lysine to create a DNA-polycation complex. Treatment of cells displaying the transferrin receptor with the DNA complexes showed high levels of uptake with an accumulation of about 1500 Gd(III) ions per cell. For receptor-targeted contrast agents to become clinically relevant, methods need to be developed where full characterization of the final contrast agent can be achieved. The poly-lysine complex can only provide a range of Gd(III) chelates that can be conjugated. Synthetic strategies to remedy this are being developed to make small-molecule chelates modified with specific sites for attachment of receptor molecules.

The Meade laboratory has developed several successful targeted small-molecule steroid-conjugated Gd(III) chelates specific for hormone-receptor positive cells.[57, 58] The expression of progesterone receptor (PR) is a critical component in the diagnosis of human breast cancers and is typically measured by tissue biopsy or radioisotope injection. The recent development of progesterone-modified MRI contrast agents provides a non-invasive diagnostic tool to determine PR levels (**Figure 1.12**). *In vitro* results show that progesterone contrast agents interact favorably with progesterone receptors, accumulate in breast cancer cells, and enhance MRI contrast intensity. With the success of these *in vitro* results, research is currently underway for use of these agents *in vivo*.

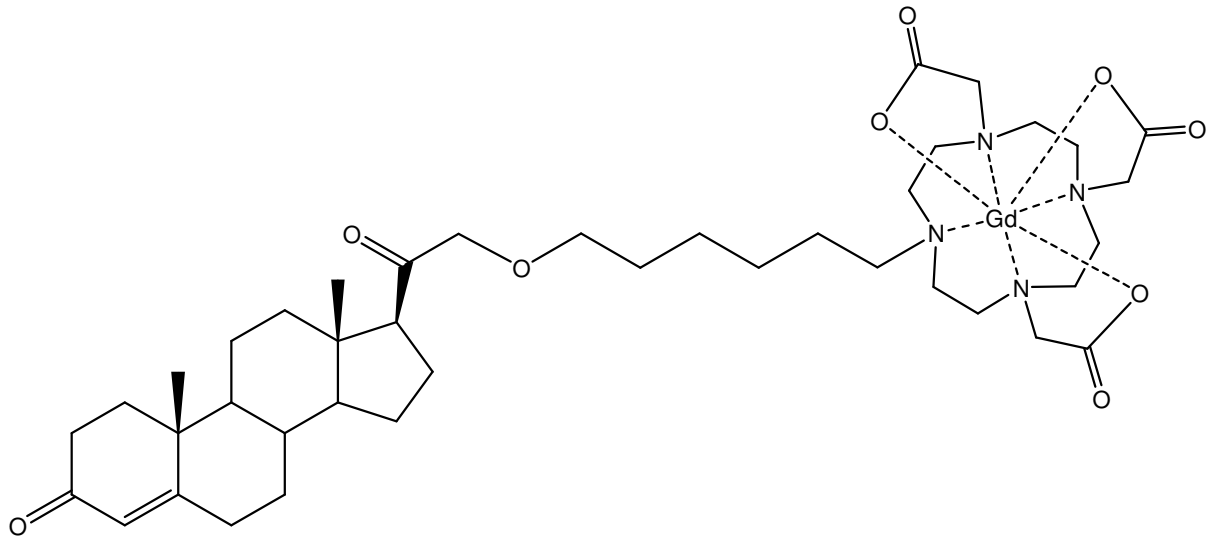

Figure 1.12. A progesterone-conjugated MRI contrast agent.[58]

1.4 Scope of Thesis

This thesis focuses on the investigation of water modulation to lanthanide chelates with the goal of developing responsive MRI contrast agents. This first chapter provided an overview of the mechanism of proton T_1 relaxation in the presence of a paramagnetic ion and presented the parameters affecting T_1 relaxation rates. Further discussion explored their manipulation to improve the efficacy of Gd(III) chelates used as MRI contrast agents. In addition, this chapter introduced progress made in the development of second-generation contrast agents including activated contrast agents, cell-permeable agents, and receptor-targeted agents. The activated agents are designed to report on physiological properties such as fluctuating ion concentrations and enzyme activity. The cell-permeable and receptor-targeted agents are designed to improve specificity for increased accumulation of agents to their intended area.

The second chapter introduces the design, synthesis, and investigation of a Zn(II)-responsive contrast agent. To understand the specific functions of Zn(II), research has focused on the development of Zn(II) fluorescent probes that have greatly increased our knowledge of the biological function of this ion in cell and tissue culture experiments. Since fluorescent microscopy will always be limited by its inability to penetrate deep tissue and its photobleaching properties, the development of a Zn(II)-activated MRI contrast agent provides an alternative method to study Zn(II) in biological systems. Although there are several Zn(II)-responsive MR contrast agents, Chapter 2 introduces the first example of a Gd(III)-based MRI contrast agent in which an increase in relaxivity is observed in the presence of Zn(II). A detailed investigation of the agents relaxivity, hydration number, and Zn(II)-binding affinity will be presented.

In an effort to improve the relaxivity enhancement of the agent presented in Chapter 2, the length of the carbon linker between the Gd(III)-chelate and the Zn(II) binding arms was

varied. In Chapter 3, the synthesis and evaluation of these complexes as Zn(II)-responsive contrast agents is presented. Although the original agent presented in Chapter 2 provides an increase in relaxivity, the addition of one methylene unit to the carbon linker yielded a greater increase in relaxivity upon the binding of Zn(II). A detailed examination of the structural properties of these agents through NMR spectroscopy provides insight into the observed change in relaxivity. This examination includes relaxivity, hydration number, Zn(II)-dissociation constants and ^{17}O NMR to determine τ_m.

Chapter 4 investigates the activation mechanism of Zn(II)-responsive contrast agents. In order to develop more sensitive Zn(II)-responsive agents and other ion-responsive contrast agents, it is important to understand the mechanism by which the agents work. The mechanism of activation of the class of Zn(II)-responsive probes presented in Chapters 2 and 3 is examined through the study of a series of contrast agents with varied Zn(II)-binding groups. The design, synthesis, and evaluation of three new agents with various Zn(II)-binding groups is introduced. The relaxation enhancement effects of these new agents, along with hydration numbers and Zn(II)-dissociation constants are evaluated. In addition, the synthesis of the ^{13}C isotopically labeled Eu(III) version of the original Zn(II)-responsive agent from Chapter 2 is presented to provide a means of studying the Zn(II)-binding groups upon activation. NMR studies confirm that the mechanism of activation takes place due to a change in coordination geometry about the paramagnetic center upon Zn(II)-binding.

The appendix introduces a means of amplifying the signal upon activation by conjugating a *q*-modulated Zn(II)-responsive agent to nanoparticles. The development of MRI contrast agents has been progressing toward the use of polymer and dendrimer scaffolds to increase relaxivity. This design is twofold. First, it increases the number of gadolinium chelates and,

secondly, it effectively increases the rotational correlation time. The use of nanoparticles for this purpose has been investigated to a lesser extent. In these cases Gd(III) is often doped into a nanoparticle core or loaded into micelles for contrast agent delivery. While a large increase in relaxivity is observed, the possibility of Gd(III) leakage remains due to the absence of a chelating group. An alternate approach using nanoparticles would covalently attach T_1 contrast agents to the outside of the particle. To date, there has been no investigation of the use of activated contrast agents attached to particles. In this work, modification of the original Zn(II)-responsive agent synthesis is presented for its covalent attachment to either silica nanoparticles or iron oxide particles.

Chapter 2

The Design and Synthesis of a Zn(II)-Activated Magnetic Resonance Contrast Agent

Adapted from:

Major, J. L., Parigi, G., Luchinat, C., Meade, T. J. "The synthesis and *in vitro* testing of a zinc-activated MRI contrast agent." *Proc. Nat. Acad. Sci., USA.* **2007**, *104(35)*, 13881-13886.

2.1 Introduction

Zinc(II) plays a critical role in cellular physiology and is involved in structural stability, catalytic activity, and signal transduction pathways.[1-3] While a great deal is known about the biochemistry of Zn(II) in metalloproteins, far less is understood about its specific mechanisms of cellular physiology and distribution, as well as its pathology.[4] Zinc is the second most abundant transition metal in the body behind iron; however, most of it is tightly regulated and bound to metalloproteins under physiological conditions. Free Zn(II) concentrations in the extracellular brain tissue are about 150 nM[2, 3] while cellular zinc concentrations can be as high as 1 mM within synaptic nerves.[5] Under abnormal stress such as a stroke or an epileptic seizure, roughly 100-300 μM Zn(II) is released from the synaptic nerve into the somatic tissue resulting in a thousand-fold increase in free Zn(II) concentrations. While still under debate, evidence suggests that these large sudden increases in Zn(II) concentrations have been linked to the precipitation of amyloid plaques in Alzheimer's disease.[6-8]

To study zinc in biological systems, chemists and biologists have had to create systems to visualize zinc due to its inherent spectroscopically "silent" properties. Its d^{10} electronic configuration leaves no available d-d transitions for standard absorption spectroscopy techniques. It is diamagnetic, eliminating EPR spectroscopy techniques and because its main isotope has a nuclear spin of zero, NMR is rendered ineffective. Even with these limitations there are advantages to having a d^{10} configuration. Zinc forms an extremely stable ion (Zn(II)) that does not undergo oxidation-reduction reactions readily. Additionally, Zn(II) has a flexible coordination geometry because it is not subject to ligand-field stabilization effects allowing for Zn(II) to have the unique ability to bind to a variety of metal binding groups in the body.[9]

Most of our knowledge of zinc's structural properties has come from X-ray crystallography and EXAFS.[9] Isomorphous substitution with metals that have electronic or magnetic properties such as cobalt has proven to be valuable as well. These techniques allow the study of bound Zn(II) ions while the study of free Zn(II) ions has been more elusive. In the last couple of decades fluorescent Zn(II)-sensors have become a powerful tool in tracking free Zn(II) in the body.[10, 11] Progress in fluorescent zinc probes has led to sensors that are extremely sensitive to Zn(II), detecting concentrations in the picomolar range. Even with such sensitivity, fluorescent microscopy will always be limited by its inability to penetrate deep tissue and its photobleaching properties. In addition, most fluorescent probes need to be excited in the UV range causing damage to the cells being studied.

Magnetic resonance imaging (MRI) provides an alternative means to study Zn(II) in biological systems. Unlike light-based microscopy, MRI can provide non-invasive three-dimensional imaging without the limitations of light-scattering and photobleaching. Lippard and coworkers recently reported on a Mn(III)-porphyrin Zn(II) imaging agent with both MR and fluorescent capabilities.[12] Gadolinium-based MR contrast agents sensitive to Zn(II) concentrations have been reported based on the binding of Zn(II) to *N, N, N', N'*-tetrakis(2-pyridylmethyl)ethylenediamine (TPEN) (**Figure 1.7**).[13, 14] These agents show a decrease in relaxivity upon binding of Zn(II), corresponding to a bright-to-dark signal upon Zn(II) binding. A negative feedback probe can mean that there is zinc present but the signal could alternatively be decreasing in brightness due to diffusion of the agent and thereby giving inconclusive results. The contrast agent presented in this chapter provides positive feedback, a dark-to-bright signal. Any observed changes in MR signal intensity would only be from the activation of the agent via Zn(II)-binding.

In this chapter, a gadolinium-based MRI contrast agent with diaminoacetate Zn(II)-binding groups is introduced (**Figure 2.1**). Based on our previously published Ca(II)-activated contrast agent,[15, 16] this complex was designed with two N-acetic acid groups that will selectively bind Zn(II) to effectively open the contrast agent for water access to the gadolinium. **Gd-daa3** (**dia**mino**a**cetate with **3** methylene carbons) is the first gadolinium-based MRI contrast agent that shows an increase in relaxivity in the presence of Zn(II).

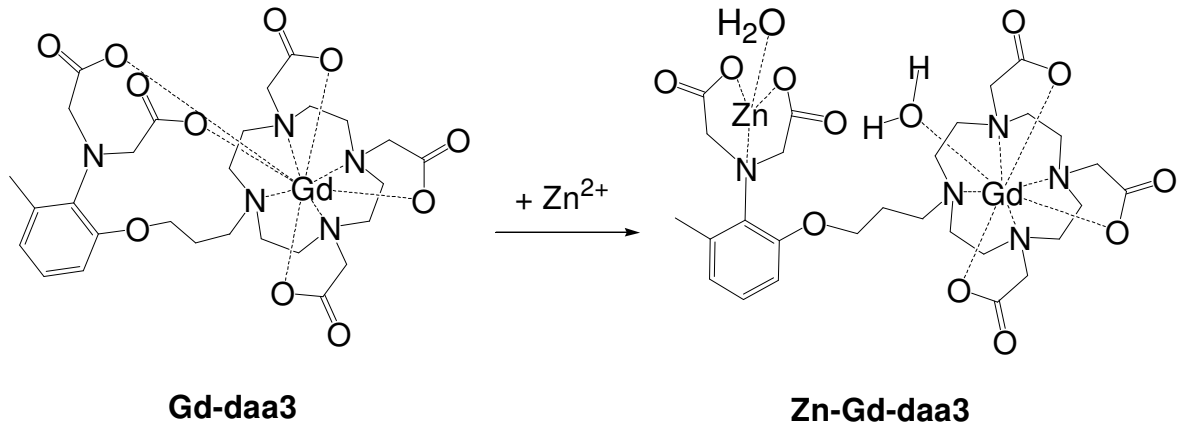

Figure 2.1. A Zn(II)-activated MRI contrast agent with proposed tetrahedral binding of Zn(II).

2.2 Results and Discussion

2.2.1 Synthesis and Characterization

The design of **Gd-daa3** began with the study of our previously reported Ca(II)-activated MR contrast agent. Gd-DOPTA has four aminoacetate arms to chelate Ca(II), however, because of zinc's greater electron density, an agent specific for zinc activation could be envisioned by looking at half of the Gd-DOPTA molecule having only two aminoacetate chelating arms. The higher charge density and electrostatic potential of Zn(II) makes it a good electrophile, seeking neutralization by complexation. Larger ions such as Na(I), Ca(II), and Mg(II) have a smaller charge density and are commonly seen as charge carriers or ion triggers in biological functions and therefore are not easily complexed.[17]

Efforts were first focused on the synthesis of **1** as seen in **Figure 2.2** and **Scheme 2.1**. The synthesis of **1** begins with the alkylation of 2-nitrophenol with (3-bromopropoxy)-*tert*-buytldimethyl silane to yield the protected alcohol **3**. Previous efforts with the addition of 1,3-dibromopropane or 3-bromopropanol to 2-nitrophenol led to the unexpected cyclization of a six-membered ring after reduction of the nitro group. This was circumvented by use of a TBDMS protecting group which could be removed by mild acidic conditions with a fluoride source. After addition of the protected alcohol (**3**), the nitro group was then reduced under standard palladium-catalyzed hydrogenation conditions and reacted immediately with *tert*-butylbromoacetate under basic conditions to yield **5**. Reaction with tetrabutylammonium fluoride to remove the TBDMS group was followed by bromination of the alcohol to give intermediate **9**. DO3A-tris-*tert*-butyl ester was synthesized following literature procedure[18] and combined with **9** to yield the fully protected ligand **11**.

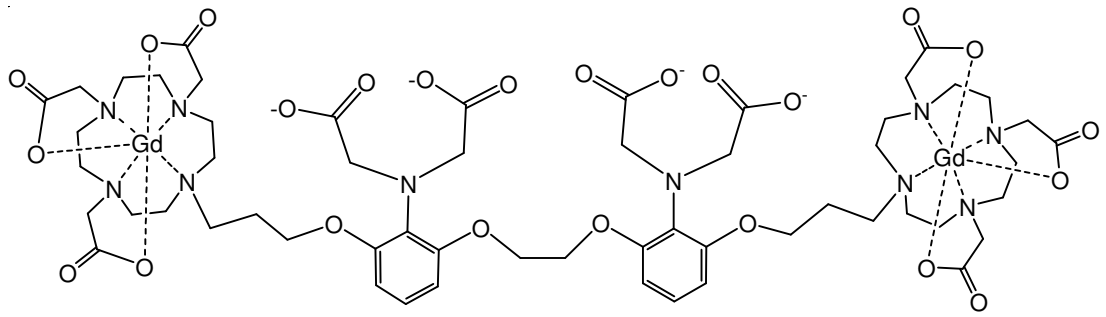

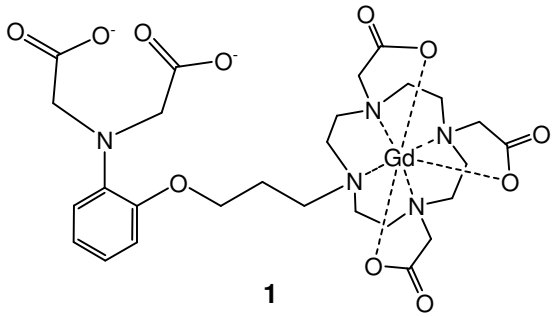

Figure 2.2. Half of the Ca(II)-activated contrast agent (**Gd-DOPTA**) led to the design of complex **1** as a Zn(II)-activated agent.

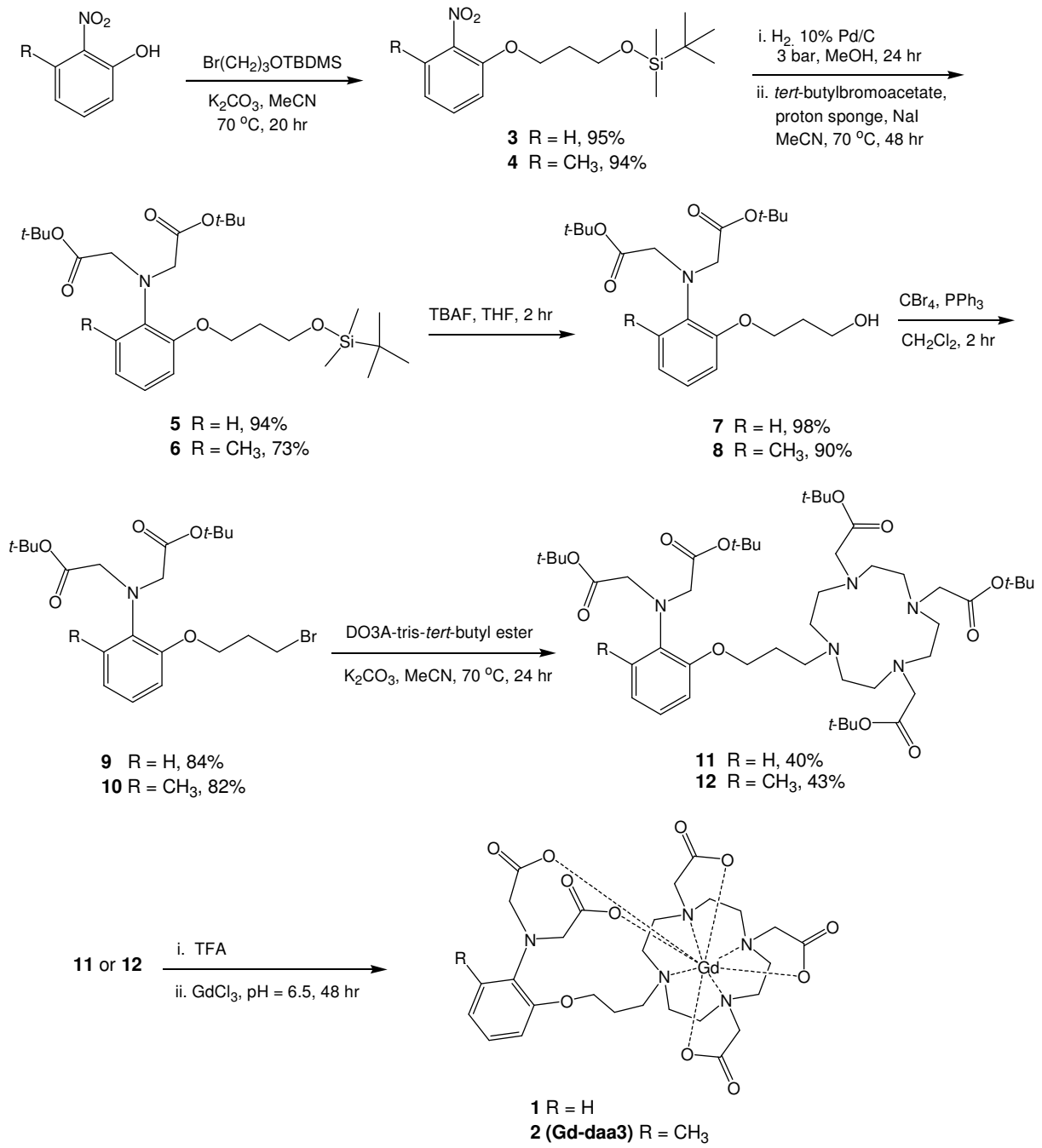

Scheme 2.1. The synthesis of Zn(II)-activated contrast agents **1** and **2.**

The protected ligand was then deprotected with a 10 mL solution of trifluoroacetic acid : triisopropylsilane : H_2O (95:2.5:2.5) overnight. The acid is blown off under air and product is precipitated with the addition of diethyl ether. After centrifugation, the ether is decanted and the pellett is washed several more times then brought up in water and freeze-dried. To make the final metal complexes, the deprotected ligand is dissolved in 5 mL deionized water and the pH is adjusted to 7 with 1 M NaOH. A slight excess of MCl_3 (M = Gd, Eu, or Tb) is dissolved in 3 mL deionized water and added to the ligand in 0.5 mL increments with continual adjustment of the pH to ~6.5. The reaction is left stirring for up to twenty-four hours at room temperature. The pH is raised to 10 to precipitate any unreacted M^{3+} (M = Gd, Eu, or Tb) as $M(OH)_3$ and centrifuged. The supernatant is collected and adjusted to a pH of 7 with 0.5 M HCl. After freeze-drying, the crude product is purified by reverse phase column chromatography on semi-preparatory HPLC and fractions are then analyzed for purity via analytical LC-MS and elemental analysis.

While the fully protected ligand **11** could be synthesized, purification of the metal complexes posed problems due to the hydrolysis of the aminoacetate arms in aqueous media. Figure **2.3** shows an overlay of the analytical HPLC traces of the same sample of the europium analog of **1** at 0 and 72 hours after purification via semi-preparatory HPLC. After three days, the HPLC trace clearly shows a more prominent peak of the hydrolyzed product with m/z = 701 $[(M - 60)]^+$. Due to the instability of **1** in aqueous media, a more robust ligand was required.

In this case, we envisioned that addition of an electron donating group to the aromatic ring would help stabilize the compound and slow down the hydrolysis of the aminoacetates. To do this, ligand **12** was made from the starting material of 3-methyl-2-nitrophenol to create the gadolinium compound **Gd-daa3** in acceptable yields (**Scheme 2.1**). Evidence of the hydrolysis

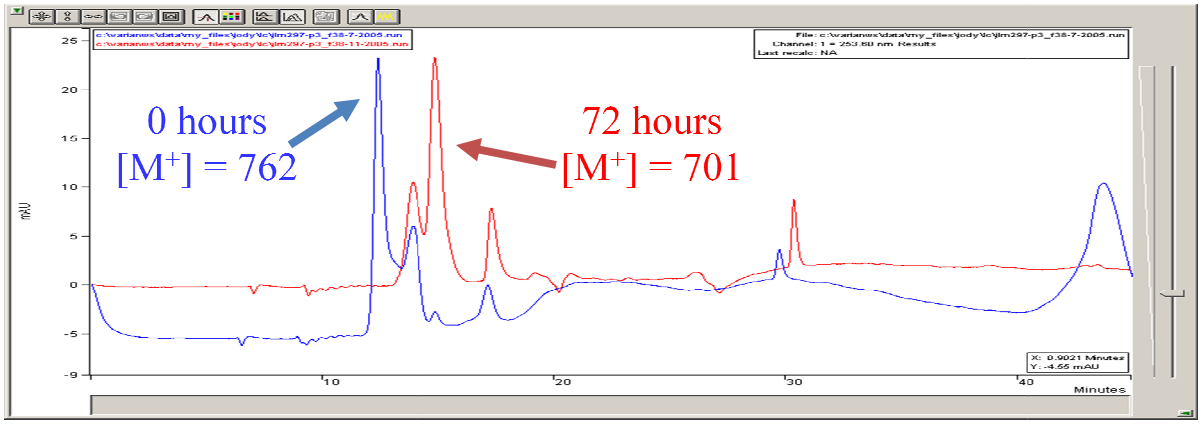

Figure 2.3. Overlay of analytical HPLC-MS traces of **Eu-1** at 0 (blue trace) and 72 hours (red trace) after preparatory HPLC purification. The desired product, **Eu-1**, is almost fully hydrolyzed after 72 hours.

side-product was only seen when **12** was subjected to acidic conditions during addition of the metal and the impurity could be separated via HPLC purification. No other degradation was seen after purification of the desired product, **Gd-daa3**.

2.2.2 Relaxivity

The efficacy of **Gd-daa3** for use as an MRI contrast agent is measured by its relaxivity value, the slope of the line of the reciprocal of T_1 versus the concentration of gadolinium. The relaxivity of **Gd-daa3** was first evaluated in the presence and absence of Zn(II) in a non-coordinating HEPES buffer at 60 MHz and 37 °C (**Figure 2.4**). The relaxivity of **Gd-daa3** in the absence of Zn(II) was 2.3 $mM^{-1}s^{-1}$, consistent with a Gd-complex having no coordinating waters. As $ZnCl_2$ was titrated with aliquots of 0.5 equivalents intervals, an increase in relaxivity was observed with a value 5.1 $mM^{-1}s^{-1}$ measured for the addition of one equivalence of Zn(II). This doubling of the relaxivity in the presence of Zn(II) can be explained by the change in the coordination environment surrounding the Gd(III) to allow for the access of one water molecule as depicted in **Figure 2.1**. The clinically used agent Gd-DTPA has a relaxivity of 3.8 $mM^{-1}s^{-1}$ at 60 MHz and 37 °C.[19] In the presence of Zn(II) **Gd-daa3** has a 34% higher relaxivity than Gd-DTPA. In addition, it has a 39% lower relaxivity in the absence of Zn(II) than Gd-DTPA providing a darker image in its "off" state. The difference between "on" and "off" states are more visible than would be seen for the steady state of clinical agents.

Similar relaxivity studies were conducted with $MgCl_2$ and $CaCl_2$ to test the selectivity of **Gd-daa3** for Zn(II) over other biologically relevant cations known to have higher cellular concentrations. There is no significant change in relaxivity for either Mg(II) or Ca(II) even when density and therefore high electrostatic potential, Ca(II) and Mg(II) are larger ions with a smaller

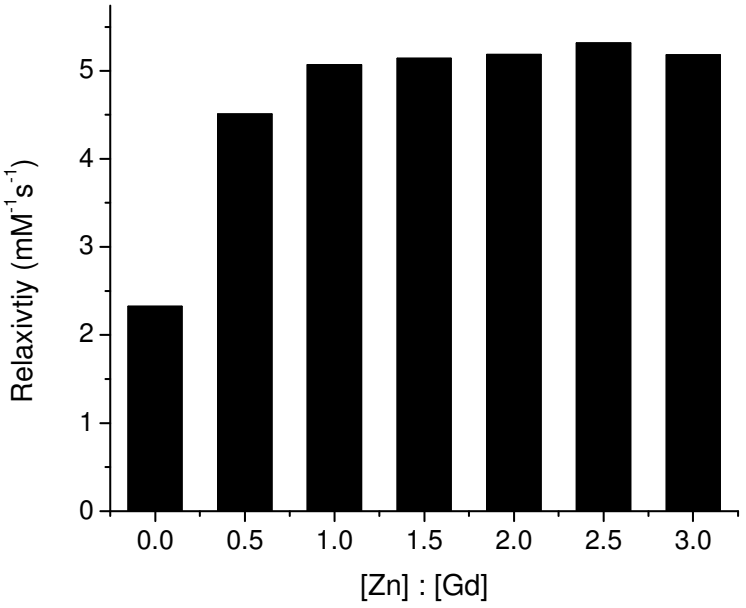

Figure 2.4. Relaxivity of **Gd-daa3** in the presence of $ZnCl_2$ at 60 MHz and 37 °C.

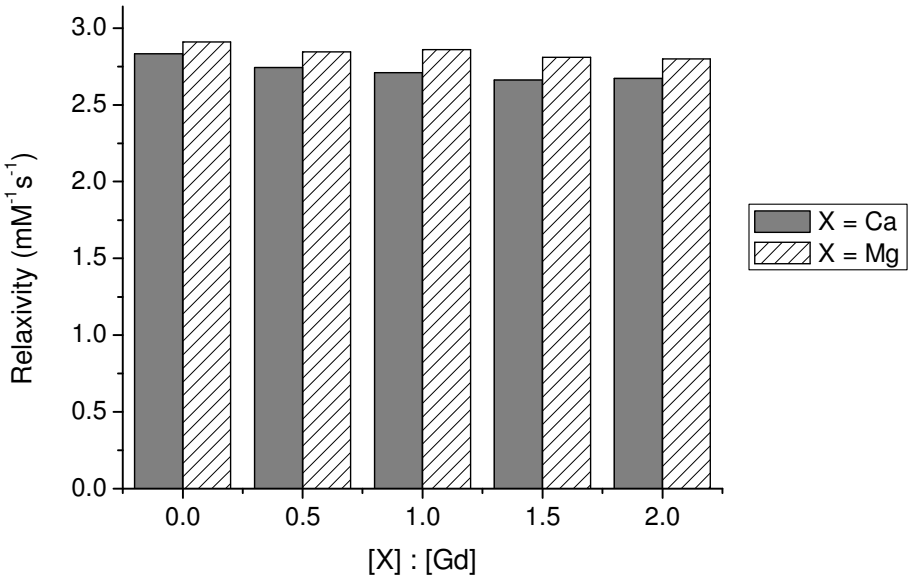

Figure 2.5. Relaxivity of **Gd-daa3** in the presence of $CaCl_2$ and $MgCl_2$ at 60 MHz and 37 °C.

an excess of these dications is present **(Figure 2.5).** Unlike Zn(II) which has a high charge charge density leading to a lower affinity for chelation. Generally, Ca(II) and Mg(II) are used as charge carriers or ion triggers and are not commonly seen chelated in the body. Similar to fluorescent Zn(II) sensors,[20] the loss of acetic acid groups improves the selectivity for Zn(II) by greatly reducing the ability of Ca(II) to bind.

Binding with Cu(II) was studied as well due to its ability to be chelated by oxygen donors. The relaxivity of **Gd-daa3** shows that Cu(II) does bind and increase relaxivity but to a lesser extent than Zn(II) (**Figure 2.6**). An increase in relaxivity from 2.2 $mM^{-1}s^{-1}$ to 4.2 $mM^{-1}s^{-1}$ is observed with one equivalence of $CuCl_2$ in HEPES buffer. In neurotransmission, where there is considerable interest in studying free Zn(II), Cu(II) concentrations are ten-fold less than Zn(II). Estimates of Cu(II) concentrations are only about 30 μM while Zn(II) is expected to be at least 300 μM.[21] At these concentrations, activation by Cu(II) would not interfere with the activation of the contrast agent by Zn(II) and would therefore not contribute to the change in the MR signal intensity.

To further test the viability of this increase in relaxivity for *in vivo* studies, measurements with Zn(II) were conducted in male human serum. Results show a significant reduction in the percent increase in relaxivity observed compared to measurements made in HEPES buffer, only 21% increase in serum versus 114% increase of in HEPES buffer (**Figure 2.7**). Nonetheless, there is still a considerable increase in relaxivity upon Zn(II) binding indicating that these agents could be detected under normal physiological conditions. In addition, the relaxivity in human serum is higher than in HEPES. This result is most likely due to τ_R effects from non-specific binding to proteins such as albumin which makes up about half of the total protein concentration

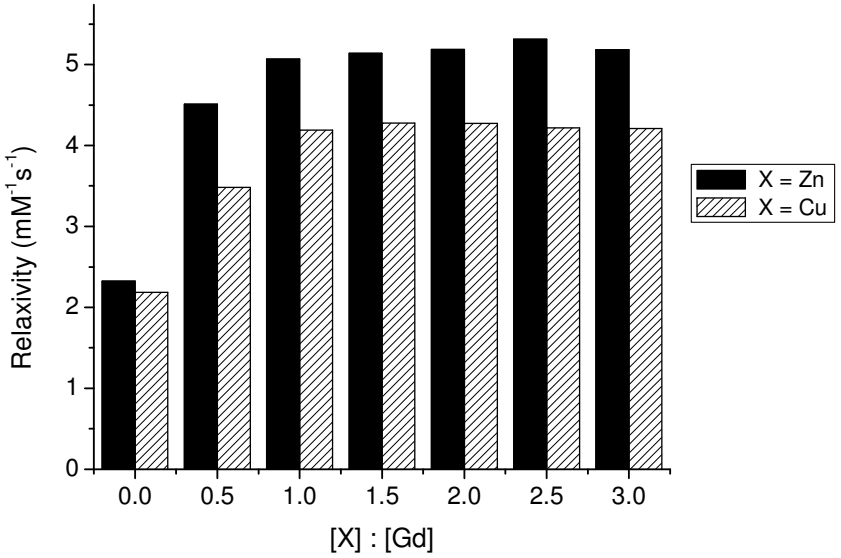

Figure 2.6. Relaxivity of **Gd-daa3** with Zn(II) and Cu(II) at 60 MHz and 37 °C.

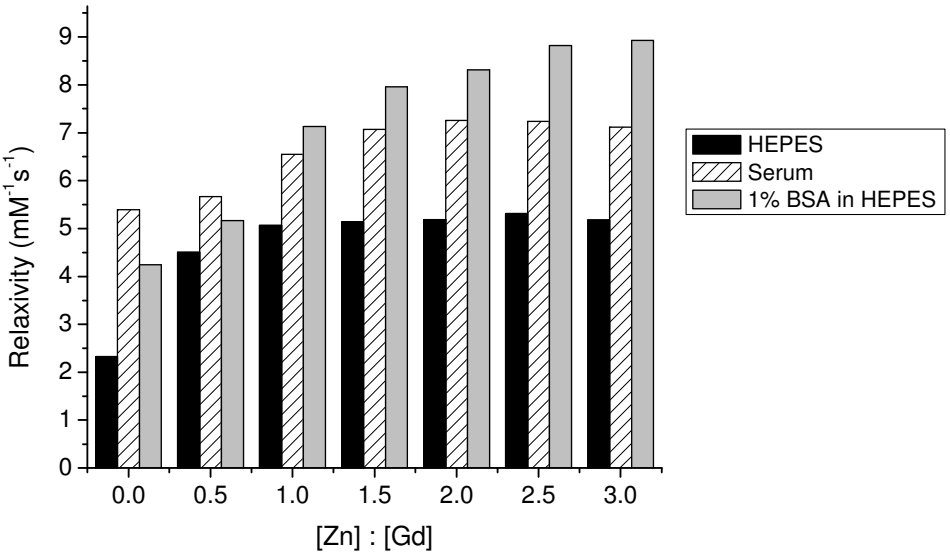

Figure 2.7. Relaxivity of **Gd-daa3** in the presence of $ZnCl_2$ in HEPES buffer, human male serum, and 1% BSA in HEPES measured at 60 MHz and 37 °C.

in serum.[22] To test the validity of this argument, relaxivity measurements were performed in HEPES buffer with added bovine serum albumin (BSA). In a HEPES solution with 1% BSA, the relaxivity of **Gd-daa3** with one equivalent of Zn(II) was 7.1 $mM^{-1}s^{-1}$, compared to a relaxivity of 6.5 $mM^{-1}s^{-1}$ when in serum.

2.2.3 Hydration Number (q)

The relaxivity measurements of **Gd-daa3** with Zn(II) are consistent with what would be expected for small molecules going from a closed conformation with no inner-sphere waters to one that has access to one inner-sphere water. To determine if this was the case, values of *q* were found by preparing the terbium analogs and acquiring time-based fluorescence microscopy measurements. For rare-earth ions, the dominant mode of radiationless deactivation is through the loss of electronic excitation energy through high-frequency vibrations. In particular, the O-H oscillators provide an efficient non-radiative decay pathway for aqueous solutions of the $^5D_0$ excited state of Tb(III) while lower energy vibrations such as O-D oscillators do not (**Figure 2.8**).[23, 24]

Horrocks and Sudnick showed the ratio of fluorescence lifetimes in H_2O and D_2O is proportional to the hydration number (*q*) for Eu(III) and Tb(III) complexes.[25] By comparing complexes with known values of *q* determined from their crystal structure to the difference in their luminescence lifetimes in H_2O and D_2O, they were able to determine an equation for the linear correlation that is observed. The fluorescence lifetime decay times were determined for **Tb-daa3** in the absence and presence of Zn(II) monitoring the emission at 544 nm with an excitation at 254 nm (**Figure 2.9**). Using the most recent equation developed for Tb(III)

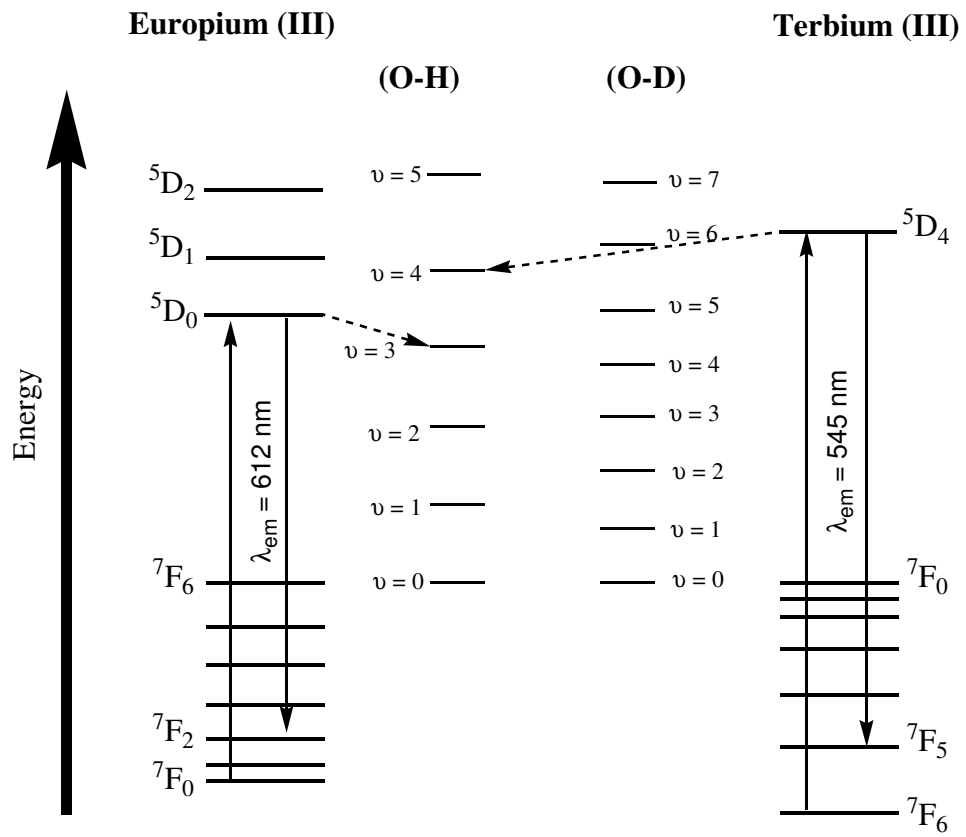

Figure 2.8. Energy level diagrams for Eu(III) and Tb(III). The two labeled emission transitions (solid line arrows) are the most intensive radiative transitions for each of the ions. Radiationless decay through coupling with O-H vibrations are labeled with dotted line arrows. (Figure adapted from Ref. 23)

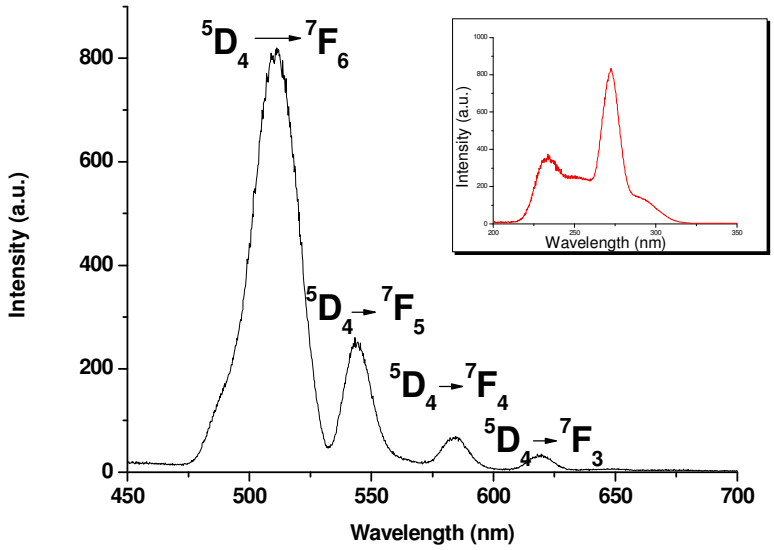

Figure 2.9. Emission spectra of **Tb-daa3** with an excitation of 254 nm (inset).

Table 2.1. Fluorescence lifetime decays in water and D_2O and the calculated hydration number.

	t_1 H_2O (ms)	t_1 D_2O (ms)	q (± 0.1)
Tb-daa3	1.97	2.71	0.3
Zn-Tb-daa3	1.46	2.65	1.0

complexes (q = 4.2 ms[(1/t_{H2O}) - (1/t_{D2O}) - 0.06])[26], q was determined for **Tb-daa3** with and without Zn(II) with an uncertainty of ±0.1 (**Table 2.1**). These results confirm that one inner-sphere water is present when in the presence of Zn(II) for **Gd-daa3** supporting the proposed method of activation shown in **Figure 2.1**.

2.2.4 Nuclear Magnetic Resonance Dispersion

The measurement of relaxation rates as a function of magnetic field through nuclear magnetic resonance dispersion (NMRD) is widely used for characterizing magnetic resonance contrast agents and can be used to provide evidence for q-modulation.[19] The observed bulk water proton relaxivity is provided by the sum of i) the outer-sphere contribution, due to the dipolar interaction between unpaired electrons and protons of freely diffusing water molecules, and ii) the inner-sphere contribution. The latter is due to the dipolar interaction between unpaired electrons and protons of water molecules coordinated to the paramagnetic ion (first sphere) or anchored at a fixed distance r from the metal ion (second-sphere) in exchange with bulk water protons. When such exchange is fast (i.e. the exchange rate is faster than the relaxation rate of the protons of bound water molecules), the observed bulk water proton relaxivity is a good reporter of the presence of water molecules coordinated to the metal ion. A slow exchange regime, on the other hand, is characterized by an increase in relaxivity with increasing temperature, as the exchange rate increases with temperature.

The NMRD profiles of **Gd-daa3** and their fittings, measured in the presence and absence of Zn(II) at 292, 298 and 310 K, are reported in Figure **2.10** and **Table 2.2**. An overall increase in relaxivity is observed at all fields in the Zn(II)-containing sample. Such an increase is in agreement with a larger hydration of the gadolinium site. The decrease in relaxivity with

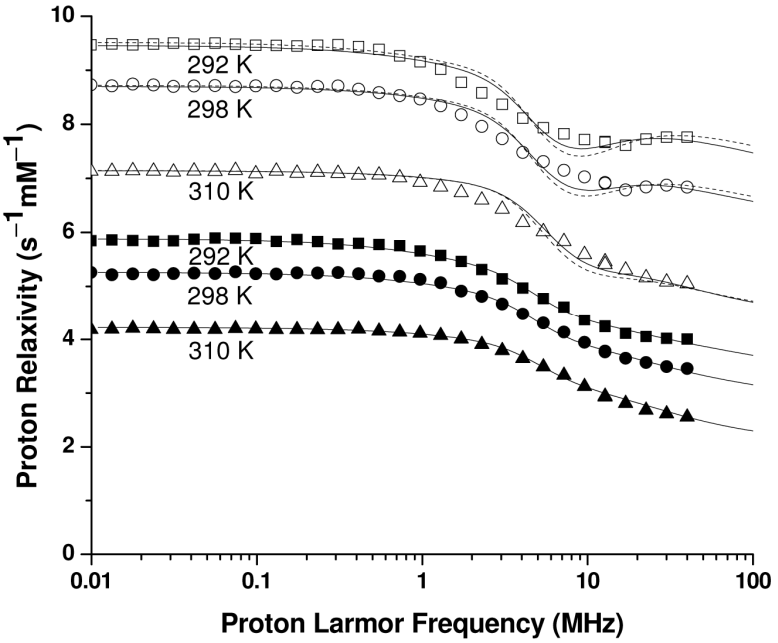

Figure 2.10. Nuclear magnetic resonance dispersion (NMRD) profiles of **Gd-daa3** in the absence of Zn(II) (solid symbols) and in the presence of Zn(II) (open symbols).

Table 2.2. Values of the parameters used to reproduce the relaxivity profiles of **Figure 2.10**.

[a]corresponding to two water protons at 3.7 Å from the gadolinium ion.

	T (K)	Δ_t (cm^{-1})	τ_v (ps)	τ_R (ps)	D (cm^2s^{-1})	d (Å)	q	τ_M (μs)	D_{ZFS}, (cm^{-1})
Gd-daa3	292	0.035	25.5	140	1.9	3.8	0.35[a]		
	298	0.035	25	130	2.5	3.8	0.35[a]		
	310	0.035	24	100	3.8	3.8	0.35[a]		
Gd-daa3+Zn	292	0.036	25.7	185	1.9	3.5	1.35[b]	2.9	
	298	0.037	24	160	2.5	3.5	1.35[b]	2.7	
	310	0.039	22.2	100	3.8	3.5	1.35[b]	2.5	
	292	0.034	26	175	1.9	3.5	1		0.012
	298	0.0343	25	160	2.5	3.5	1		0.012
	310	0.037	23	110	3.8	3.5	1		0.012

[b]fixed assuming the presence of one additional water molecule. Fits are also possible for q values from 0.8 to 1.5.

T: temperature
Δ_t: transient zero-field splitting (ZFS)
τ_v: correlation time for electron relaxation
τ_R: reorientational time
D: diffusion coefficient
d: distance of closest approach of outer-sphere water molecules
q: number of water molecules with protons at 3.1 Å from the metal ion
τ_M: water proton lifetime in the coordination shell
D_{ZFS}: static ZFS

increasing temperature actually indicates the occurrence of a fast exchange regime for the inner-sphere relaxation. Outer-sphere relaxation is always expected to decrease with increasing temperature. One dispersion profile is present, from about 2-10 MHz, as expected for both the outer-sphere relaxation and the inner-sphere relaxation for complexes with reorientational times of the order of 100 ps, in agreement with the molecular weight of the present system, and electron relaxation times typical of gadolinium complexes.[27, 28] The increase in relaxivity at high frequencies, observed for the profiles of the Zn(II)-containing sample acquired at the lower temperatures, indicates the field dependence of the electron relaxation time.

The analysis performed according to current theories[27] confirms that in the absence of Zn(II), the outer-sphere contribution is dominant, setting an upper limit for the possible fraction of coordinated water $q = 0.3 \pm 0.2$, calculated for water protons at a typical distance for the first-coordination sphere of Gd(III) (~ 3.1 Å). The relaxation rates can be very well reproduced using the Freed model[28] and the Solomon-Bloembergen-Morgan (SBM) theory[29, 30] by the simultaneous contributions of outer-sphere relaxation and second-sphere relaxation (solid lines in **Figure 2.10**). The latter is due to the presence of two water protons at 3.7 Å from the metal ion with a field dependence for the electron relaxation rates similar to what is obtained for Gd-DTPA.[27, 31]

The overall increase in the relaxation rate values obtained for the Zn(II)-coordinated complex (open symbols in **Figure 2.10**) can be reproduced with SBM theory considering the presence of an additional regularly coordinated water molecule: a $q = 1.2 \pm 0.3$ is in fact obtained. The best fit profiles (solid lines in **Figure 2.10**) are satisfactory although not always in perfect agreement with the experimental data, probably due to the presence of both static and transient zero field splitting (ZFS), as expected for Gd(III) complexes. Presently, available

fitting programs cannot properly account for their simultaneous presence in fast rotating systems. The SBM theory in fact neglects the presence of static ZFS. Data were also analyzed using a slow rotation program including ZFS.[30, 32] Even in such a model, the data are consistent with the presence of a regularly coordinated water molecule (dotted lines in **Figure 2.10**). These results indicate that a water molecule in fast exchange is regularly coordinated to the Gd(III) ion in the presence of Zn(II), whereas it is not detected in the absence of Zn(II), in agreement with the scheme depicted in **Figure 2.1**.

2.2.5 Zinc Dissociation Constant

A primary goal of this research is to prepare a series of MR agents with a range of Zn(II)-binding constants for *in vitro* and *in vivo* studies. This will allow us to employ the appropriate contrast agent depending on the specific levels of Zn(II) expected to be present. A contrast agent with a binding constant in the 10^4 M^{-1} range will be optimal in imaging released zinc from synaptic nerve clefts. A more appropriate contrast agent for imaging Zn(II) released from pancreatic β-islets would be one with a binding constant on the order of 10^7 M^{-1}. To evaluate the effectiveness of **Gd-daa3** as a potential in vivo probe, a competitive binding assay with the commercially available fluorophore FluoZin-1 (**Figure 2.11**) is used to calculate the zinc dissociation constant. The published dissociation constant for Zn-FluoZin-1 (8.6×10^{-6} M)[20] is expected to be close to the dissociation constants of **Gd-daa3** due to its similar Zn(II)-binding groups.

A sample of 10 μM $ZnCl_2$ in HEPES buffer is titrated with aliquots of FluoZin-1 until the fluorescence reaches a maximum to determine the F_{max}. Competition studies are then done with

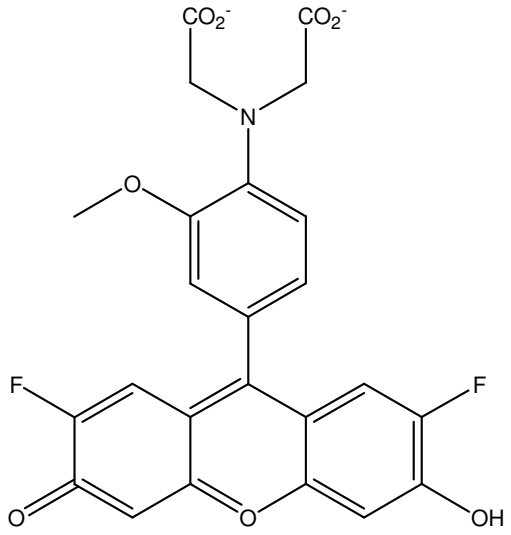

Figure 2.11. The structure of FluoZin-1™, a commercially available Zn(II)-responsive fluorophore.

Gd-daa3 at varying concentrations**.** The equilibrium constant can be calculated as shown in **Figure 2.12**. Using the same concentration of $ZnCl_2$, an excess concentration of contrast agent is added and allowed to reach equilibrium to form the Zn-Gd complex. Aliquots of FluoZin-1 are added to establish equilibrium between Zn-FluoZin-1 and the Zn-Gd complex. The fluorescence intensity of the Zn-FluoZin-1 complex is then measured at λ_{em} = 515 nm with an excitation of λ_{ex} = 495 nm to determine the concentration of Zn-FluoZin-1 complex that has been formed. With a known amount of fluorophore present and known amounts of Zn-FluoZin-1 complex formed, the amount of non-complexed fluorophore remaining can be then be calculated. This assay assumes because there is a limited supply of Zn(II) present, at equilibrium, all of the Zn(II) ions are either bound to the dye or the contrast agent. This allows for the calculation of the concentration of the Zn-Gd complex. The remaining **Gd-daa3** in the system is then assumed to not be complexed with Zn(II). Using the dissociation constant of Zn-FluoZin-1, the dissociation constant of the Zn-Gd-daa3 complex was found to be 2 x 10^{-4} M, a range that would be optimal for imaging Zn(II) released in the brain. These results provide a rough estimate of the Zn(II)-binding ability of **Gd-daa3**.

2.2.6 Stability Towards Transmetallation and Cytotoxicity

Gd-daa3 was monitored for 24 hours in a 0.1 M phosphate buffer to determine its stability in solution. Due to the low solubility of Gd_3PO_4 (K_{sp} = $10^{-22.26}$ mol^2/L^2)[33] any dissociation of gadolinium from Gd-daa3 will precipitate causing a subsequent decrease in relaxivity which was not seen. A more accurate measurement of the amount of gadolinium dissociation can be made from centrifuging the samples and collecting aliquots of the supernatant for evaluation of gadolinium concentration via ICP. This was done at various time-

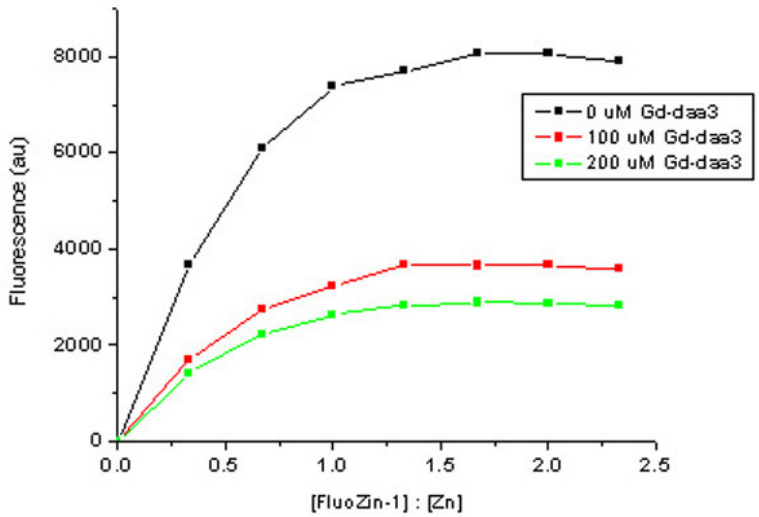

$$\text{ZnGddaa3} + \text{FluoZin1} \rightleftharpoons \text{ZnFluoZinl} + \text{Gddaa3}$$

$$K_{eq} = \frac{[\text{ZnFluoZin1}][\text{Gddaa3}]}{[\text{ZnGddaa3}][\text{FluoZin1}]} = K_{f(ZnFluoZin)} K_{d(ZnGddaa3)} = \frac{K_{d(ZnGddaa3)}}{K_{d(ZbFluoZin)}}$$

$$f = (\text{F} - \text{F}_0)/(\text{F}_{max} - \text{F}_0)$$

$$[\text{ZnFluoZinl}] = f * [\text{FluoZin1}]_T$$

$$[\text{FluoZin1}] = [\text{FluoZin1}]_T - [\text{ZnFluoZinl}]$$

$$[\text{ZnGddaa3}] = [\text{Zn}]_T - [\text{ZnFluoZin1}]$$

$$[\text{Gddaa3}] = [\text{Gddaa3}]_T - [\text{ZnGddaa3}]$$

Figure 2.12. Observed fluorescence curves of FluoZin-1 with 10 μM Zn(II) and varying concentrations of **Gd-daa3** measured in HEPES buffer at a pH of 7.4 followed by equations used to determine the dissociation constant of **Zn-Gd-daa3**.

points up to 24 hours and it was found that there was no significant change in [Gd] indicating no loss of gadolinium from the **Gd-daa3** complex. This suggests a dissociation constant for **Gd-daa3** on the order of that seen for Gd-DO3A (log K_d = 21) and its derivatives.

Treatment of NIH/3T3 cells with 0.5 mM **Gd-daa3** for up to 24 hours shows no observable cell death as visualized by trypan blue staining. Cells proliferated exponentially at the expected rate indicating low toxicity from the agent (**Figure 2.13A**). The cell doubling time for NIH/3T3 cells is approximately 16 hours, and there are over twice as many cells at 24 hours than at 8 hours as would be expected, implying greater than 99% cell viability. **Gd-daa3** was effectively taken up by NIH/3T3 cells at a constant rate for the first 8 hours of treatment. The maximal intracellular concentration of **Gd-daa3** of approximately 10^{-14} mol Gd/cell is achieved at 8 hours and maintained up to 24 hours (**Figure 2.13B**). These results provide support for potential in vivo studies in the future.

2.2.7 MR Images

To provide evidence for use of **Gd-daa3** as a responsive MR contrast agent, in vitro MR images were obtained on a 4.7 T magnet. An increase in intensity for **Gd-daa3** is observed in the presence of Zn(II) while there is no discernible difference with Ca(II) or Mg(II) (**Figure 2.14**). More importantly, phantom images of various Zn(II) concentrations shows that we can easily visualize the difference between 100 μM and 500 μM zinc concentrations (**Figure 2.15**). To confirm there was a measurable difference between zinc concentrations, T_1 was measured on these same samples on a 1.4 T (60 MHz) magnet at 37 °C (**Table 2.3**).

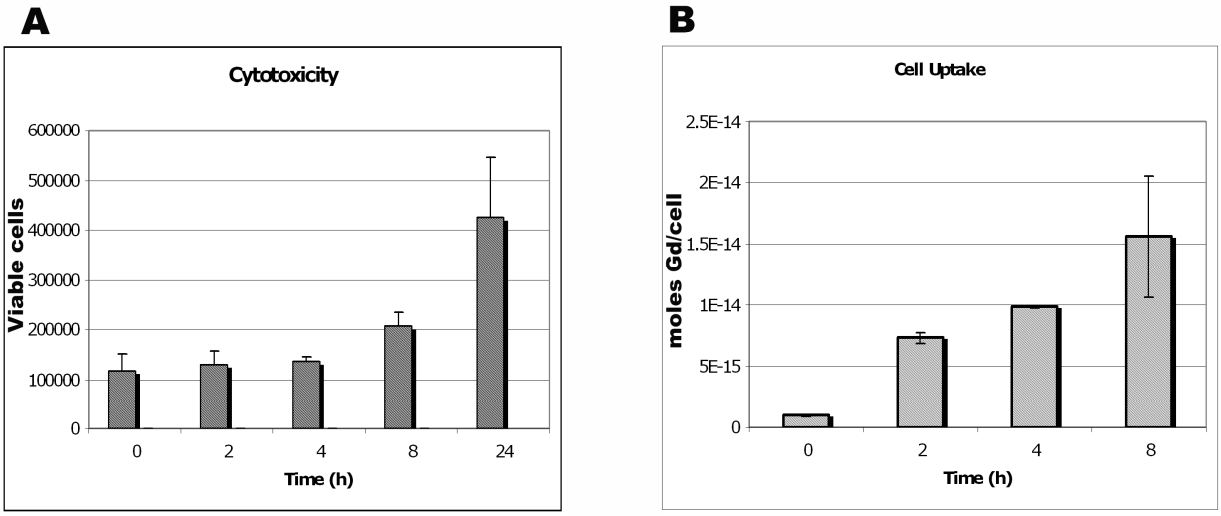

Figure 2.13. (A) Normal proliferation of NIH/3T3 cells is seen when they are incubated with 0.5 mM **Gd-daa3**. **(B) Gd-daa3** is taken up at a constant rate for up to 8 hours.

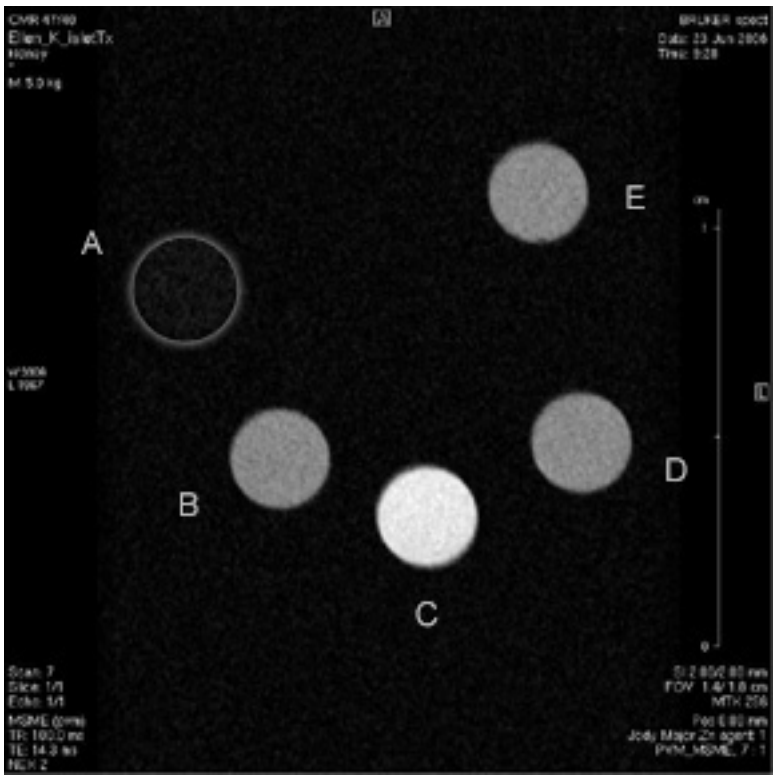

Figure 2.14. T_1-weighted phantom MR images of a 1 mM solution of **Gd-daa3** in HEPES buffer. Sample **A**: HEPES buffer only; **B**: **Gd-daa3**; **C**: **Gd-daa3** with 1 mM $ZnCl_2$; **D**: **Gd-daa3** with 1 mM $MgCl_2$; and **E**: **Gd-daa3** with 1 mM $CaCl_2$. Images were obtained on a 4.7 T magnet with the following parameters: Repetition time (TR) = 100.0 ms; echo time (TE) = 14.3 ms, field of view (FOV) = 1.4/1.8 cm; and data matrix = 256 x 256.

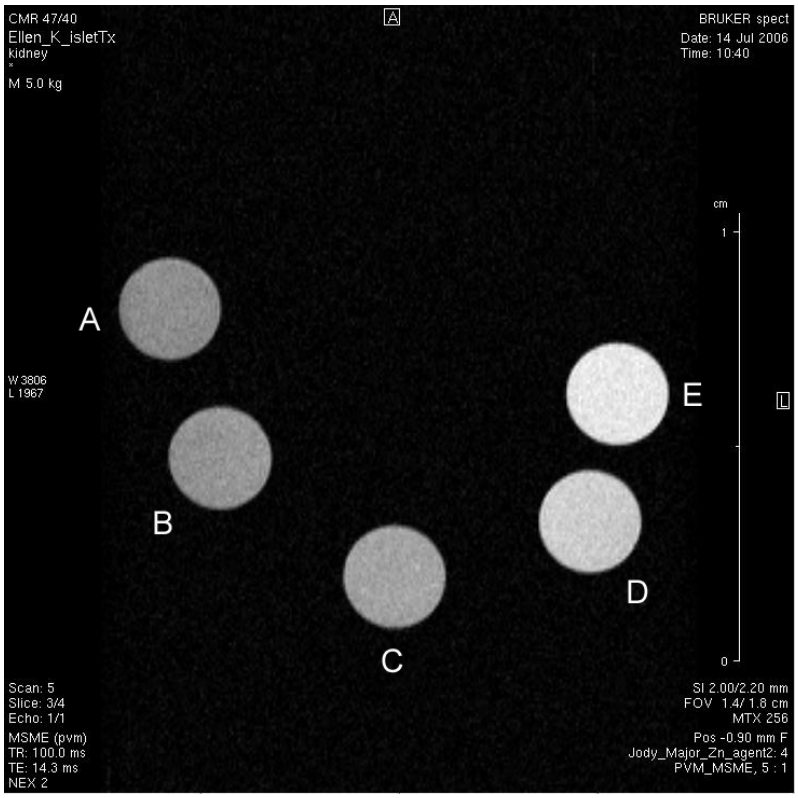

Figure 2.15. T_1-weighted phantom MR images of a 1 mM solution of **Gd-daa3** in HEPES buffer with various concentrations of $ZnCl_2$. **A**: 0 µM Zn; **B**: 50 µM Zn; **C**: 100 µM Zn; **D**: 500 µM Zn; and **E**: 1 mM Zn. Images were obtained on a 4.7 T magnet with the following parameters: Repetition time (TR) = 100.0 ms; echo time (TE) = 14.3 ms, field of view (FOV) = 1.4/1.8 cm; and data matrix = 256 x 256.

Table 2.3. T_1 measurements of the phantom samples imaged in **Figure 2.15** measured at 60 MHz and 37 °C.

[Zn] uM	T_1 (ms)
0	353
50	309
100	282
500	185
1000	159

2.3 Conclusions and Future Aspects

In summary, this chapter presents the first example of a Zn(II)-responsive MR contrast agent that exhibits an increase in relaxivity upon the addition of Zn(II). The design of **Gd-daa3** was inspired by Gd-DOPTA, a *q*-modulated Ca(II)-activated MR contrast agent. Due to the higher electron affinity of Zn(II), a selective Zn(II)-binding agent was envisioned exploiting half of the Gd-DOPTA complex. Attempts at utilizing **1** as a Zn(II)-activated agent were unsuccessful due to the hydrolysis of the aminoacetate arms used as the zinc-binding group. Although this agent has been reported as a Cu(II)-sensitive MR agent[34] its use would be limited due to its aqueous instability. Through addition of an electron donating group to the aromatic ring a stable Zn(II)-responsive agent was successfully synthesized.

Gd-daa3 exhibits strong selectivity towards Zn(II) over other prevalent biological messengers such as Ca(II) and Mg(II) with a greater than 100% increase in relaxivity upon Zn(II) binding. Although an increase in relaxivity can be observed with the addition of Cu(II), the concentrations of biologically available Cu(II) is ten-fold less than that of free Zn(II). Relaxivity studies conducted in human blood serum prove the capability of translation into *in vivo* experiments. More importantly, the zinc-dissociation constant calculated from a fluorescent competitive binding assay reveal that **Gd-daa3** is responsive towards physiologically relevant Zn(II) concentrations released into the brain. Phantom MR images of **Gd-daa3** with varying concentrations of Zn(II) confirm these results.

This is the first generation of Zn(II)-activated MR contrast agents with an increase in relaxivity. While the zinc-dissociation constant calculated is useful for the study of Zn(II) release from synaptic nerve vessels in the brain, this agent would not be sensitive enough for the study of Zn(II) release from pancreatic β-islet cells. An agent that was responsive to Zn(II)

concentrations in the nanomolar range would be useful for the imaging the activity of transplanted β-islet cells for the treatment of Type II diabetes. Efforts will continue to focus on the development of Zn(II)-activated MR contrast agents with a higher sensitivity towards Zn(II) for use in biological systems where Zn(II) concentrations are minimal.

2.4 Experimentals

General Methods. $GdCl_3 \cdot 6H_2O$, $TbCl_3 \cdot 6H_2O$ and 1,4,7,10-Tetraazacyclododecane (cyclen) were purchased from Strem Chemicals (Newburyport, MA). FluoZin™-1 was purchased from Invitrogen. Male human blood serum was obtained from Sigma (St. Louis, MO) (catalog no. H1388). All other chemicals were purchased and used as is from Sigma Aldrich. CH_2Cl_2, THF, and MeCN were dried using a solvent system purchased from Glass Contour (San Diego, CA). Water was purified using a Millipore Milli-Q synthesis water system. Nuclear magnetic resonance spectra were recorded on either Varian Mercury 400 MHz or Varian Inova 500 MHz using deuterated chloroform as the solvent. All spectra were referenced to an internal TMS standard. Electrospray mass spectra were obtained on a Varian 1200L single quadrupole mass spectrometer. Elemental analysis was performed by Desert Analytics Laboratory (Tucson, AZ). All samples were prepared in a 100 mM KCl/100 mM HEPES buffer at a pH of 7.4 unless otherwise noted. DO3A-tris-*tert*-butyl ester was prepared following literature procedures.[18]

***tert*-Butyl-dimethyl-[3-(2-nitro-phenoxy)-propoxy]-silane (3).** 2-nitrophenol (3.0 g, 21.6 mmol) was dissolved in 80 mL dry acetonitrile. Anhyrdrous potassium carbonate (14.9 g, 108 mmol) was added and allowed to react for 10 minutes before the addition of 3-bromopropoxy-*tert*-butyldimethyl silane (10.9 g, 43.1 mmol). The reaction was refluxed for 24 hours then

cooled to room temperature and filtered. After rotary evaporation of the solvents, **3** was purified via silica gel chromatography with 5% ethyl acetate in hexanes producing a bright yellow oil in 95% yield. ^{1}H NMR (500 MHz, $CDCl_3$) δ = 7.83 (d, *J* = 8 Hz, 1H), 7.52 (t, *J* = 8.5 Hz, 1H), 7.12 (d, *J* = 8.5 Hz, 1H), 7.01 (t, *J* = 8 Hz, 1H), 4.22 (t, *J* = 5.5 Hz, 2H), 3.84 (t, *J* = 5.5 Hz, 2H), 2.03 (m, 2H), 0.88 (s, 9H), 0.04 (s, 6H). ^{13}C NMR (126 MHz, $CDCl_3$) 152.7, 140.1, 134.3, 125.7, 120.2, 114.5, 66.1, 59.2, 32.2, 26.1, 18.4, -5.3. MS (ESI-positive) *m/z* Calcd for (M + Na^+): 334.1, Found: 334.2.

***tert*-Butyl-dimethyl-[3-(3-methyl-2-nitro-phenoxy)-propoxy]-silane (4).** To a solution of 3-methyl-2-nitrophenol (5.0 g, 32.6 mmol) in dry acetonitrile (300 mL) under nitrogen was added K_2CO_3 (11.26 g, 81.5 mmol). After the reaction had turned a bright red color due to the deprotonated state of the phenol after about 10 minutes, 3-bromopropoxy-*tert*-butyldimethyl silane (9.04 mL, 39.2 mmol) was added. The reaction was refluxed at 70 °C until it was a pale yellow color (several days), cooled to RT and filtered. After rotary evaporation of the solvent, the filtrate was brought up in 100 mL ethyl acetate and washed once with an aqueous saturated sodium bicarbonate solution and once with brine. The organic layer was dried over Na_2SO_4 and concentrated *in vacuo*. The residue was purified on a silica gel column eluting with 1% ethyl acetate in hexanes yielding **4** as light yellow crystals (10.11 g, 94% yield). ^{1}H NMR (500 MHz, $CDCl_3$) δ = 7.27 (t, *J* = 8 Hz, 1H), 6.89 (d, *J* = 8.5 Hz, 1H), 6.84 (d, *J* = 8 Hz, 1H), 4.15 (t, *J* = 6 Hz, 2H), 3.75 (t, *J* = 6 Hz, 2H), 2.30 (s, 3H), 1.96 (m, *J* = 5.5 Hz, 2H), 0.88 (s, 9H), 0.04 (s, 6H). ^{13}C NMR (126 MHz, $CDCl_3$) δ = 150.44, 142.43, 131.06, 130.76, 122.54, 111.01, 65.89, 59.15, 32.23, 26.11, 18.49, 17.17, -5.13, -5.41. MS (ESI-positive) *m/z* Calcd for (M + H^+): 325.2, Found: 326.2; Calcd for 348.1 (M + Na^+): 348.2, Found: 348.1.

(*tert*-Butoxycarbonylmethyl-amino)-acetic acid *tert*-butyl ester (5). To a preloaded reaction flask containing 10% Pd on C in catalytic amounts was added a solution of **3** (3.0 g, 9.6 mmol) in 50 mL methanol. The reaction was set up on a hydrogen reactor for 24 hours with a hydrogen pressure of 2.5 bar. The palladium was removed by filtering over celite then the product was concentrated via rotary evaporation. Complete reduction of the nitro group to an amine was confirmed by MS [(ESI-positive) *m/z* = 282.2 ($M + H^+$) and 304.3 ($M + Na^+$)]. The reduced product was brought up in 40 mL dry acetonitrile. To this was added 4.7 g Proton Sponge (21.2 mmol) and 3.08 mL (20.9 mmol) *tert*-butylbromoacetate followed by the addition of 3.13 g (20.9 mmol) sodium iodide. The reaction was refluxed for 5 days then cooled to room temperature and filtered. Crude product was absorbed onto silica then purified via column chromatography eluting with 2% ethyl acetate in hexanes. **5** was obtained in 87% yield (4.25 g). ^{1}H NMR (400 MHz, $CDCl_3$) δ = 6.85 (m, 4H), 4.09 (t, *J* = 6.8 Hz, 2H), 4.05 (s, 4H), 3.80 (t, *J* = 6 Hz, 2H), 2.02 (m, 2H), 1.45 (s, 18H), 0.90 (s, 9H), 0.05 (s, 6H). ^{13}C NMR (100 MHz, $CDCl_3$) δ = 171.1, 151.2, 139.6, 122.4, 121.2, 119.5, 113.5 81.5, 65.9, 60.4, 54.8, 33.1, 28.7, 26.5, 18.9, -4.8. MS (ESI-positive) *m/z* Calcd for ($M + Na^+$): 532.3, Found: 532.2. Anal Calcd for $C_{15}H_{47}NO_6Si$: C, 63.62; H, 9.29; N, 2.75. Found C, 63.73; H, 9.06; N, 2.77.

(*tert*-Butoxycarbonylmethyl-{2-[3-(*tert*-butyl-dimethyl-silanyloxy)-propoxy]-6-methyl-phenyl}-amino)-acetic acid *tert*-butyl ester (6). **4** (4.0 g, 12.3 mmol) dissolved in 100 mL methanol was added to a flask preloaded with 10% Pd on carbon in catalytic conditions. The reaction was set up on hydrogen reactor at 2.5 bar for 24 hours. Upon completion of hydrogenation, the reaction was filtered over celite. The celite was rinsed several times with 50

mL methanol and the filtrate was concentrated via rotary evaporation of the solvent. Half of the reduced product (6.32 mmol) was then transferred to a 250 mL round bottom flask and dissolved in dry acetonitrile (60 mL). Approximately 2 equivalent of proton sponge (2.39 g, 11.2 mmol) was completely dissolved in reaction before adding 11.2 mmol of *tert*-butyl bromoacetate followed by NaI (1.6 g, 10.6 mmol). After 5 days at refluxing temperatures, TLC (1:20; EtOAc:hexanes) showed two UV active spots closely running together representing the addition of one and two *tert*-butyl acetates respectively. The crude product was absorbed onto silica and purified on a silica gel column eluting with a slow gradient of 2% ethyl acetate in hexanes to 5% to separate both products. The desired product **6** with two *tert*-butyl acetates was collected in 73% yield (4.7 g) as a light yellow oil. ^{1}H NMR (400 MHz, $CDCl_3$) δ = 6.98 (t, J = 8 Hz, 1H), 6.77 (d, J = 7.2 Hz, 1H), 6.70 (d, J = 8 Hz, 1H), 4.03 (t, J = 6 Hz, 2H), 3.84 (t, J = 5.6 Hz, 2H), 3.73 (s, 4H), 2.46 (s, 3H), 2.03 (m, J = 6.4 Hz, 2H), 1.39 (s, 18H), 0.89 (s, 9H), 0.06 (s, 6H). ^{13}C NMR (100 MHz, $CDCl_3$): 170.83, 156.98, 139.34, 137.98, 126.01, 122.77, 109.66, 80.45, 64.72, 60.1, 57.73, 32.89, 28.69, 28.25, 18.85. MS (ESI-positive) *m/z* Calcd for (M + Na^+): 546.3, Found: 546.3.

{*tert*-Butoxycarbonylmethyl-[2-(3-hydroxy-propoxy)-phenyl]amino}-acetic acid *tert*-butyl ester (7). In 80 mL of dry THF was added **5** (4.5 g, 8.8 mmol) and tetrabutylammonium fluoride (5.78 g, 22.1 mmol). The reaction was stirred for two hours at room temperature. After rotary evaporation of THF, the crude product was brought up in ~50 mL ethyl acetate and washed once with water then brine. The organic layer was dried over Na_2SO_4 then filtered and concentrated via rotary evaporation. The resultant oil was purified through a silica plug eluting with 33% ethyl acetate in hexanes yielding **7** as a yellow oil in quantitative yield. ^{1}H NMR (500 MHz,

$CDCl_3$) δ = 6.89 (m, 4H), 4.17 (t, *J* = 4.5 Hz, 2H), 4.02 (s, 4H), 3.84 (t, *J* = 4 Hz, 2H), 2.02 (m, 2H), 1.42 (s, 18H). ^{13}C NMR (126 MHz, $CDCl_3$) δ = 170.8, 151.2, 139.6, 122.7, 121.4, 120.2, 114.1, 81.4, 67.1, 60.5, 54.8, 31.4, 28.3. MS (ESI-positive) *m/z* Calcd for (M + Na^+): 418.2, Found: 418.2.

***{tert*-Butoxycarbonylmethyl-[2-(3-hydroxy-propoxy)-6-methyl-phenyl]-amino}-acetic acid *tert*-butyl ester (8)**. To a solution of **6** (2.4 g, 4.58 mmol) in THF (50 mL) was added tetrabutylammonium fluoride (2.99 g, 11.45 mmol). After two hours at room temperature the deprotection was complete as observed by TLC (1:3 EtOAc:hexanes). THF was removed via rotary evaporation. The crude product was brought up in ethyl acetate and washed once with water and then brine. The organic layer was dried over sodium sulfate, filtered, concentrated, and purified through a silica plug eluting with 25% ethyl acetate in hexanes yielding 1.69 g of **8** (90.1% yield). ^1H NMR (400 MHz, $CDCl_3$) δ = 6.98 (t, *J* = 8.4 Hz, 1H), 6.79 (d, *J* = 7.2 Hz, 1H), 6.74 (d, *J* = 8 Hz, 1H), 4.11 (t, *J* = 6 Hz, 2H), 3.92 (t, *J* = 5.2 Hz, 2H), 3.82 (s, 4H), 2.44 (s, 3H), 2.07 (m, *J* = 5.2 Hz, 2H), 1.38 (s, 18H). ^{13}C NMR (100 MHz, $CDCl_3$) 171.24, 156.45, 138.53, 137.41, 125.65, 123.25, 110.16, 80.91, 65.60, 56.88, 32.31, 28.68, 28.21, 18.99. MS (ESI-positive) *m/z* Calcd for (M + H^+): 409.2, Found: 410.2; Calcd for (M + Na^+): 432.2. Found: 432.2.

{[2-(3-Bromo-propoxy)phenyl]-*tert*-butoxycarbonylmethyl-amino}-acetic acid *tert*-butyl ester (9). In 80 mL of dry dichloromethane was dissolved 8.8 mmol of **7**. To this was added 3.65 g (11 mmol) carbon tetrabromide and 3.46 g (13.2 mmol) triphenylphosphine. After two hours at room temperature the reaction was washed once with water then brine and the organics

were dried over Na_2SO_4 and filtered. After rotary evaporation of the solvents the crude product was absorbed onto silica for column purification eluting with 5% ethyl acetate in hexanes. The product was collected as a light yellow oil in 84% yield (3.38 g). ^{1}H NMR (500 MHz, $CDCl_3$) δ = 6.87 (m, 4H), 4.14 (t, *J* = 6 Hz, 2H), 4.03 (s, 4H), 3.61 (t, *J* = 6.5 Hz, 2H), 2.33 (m, 2H), 1.44 (s, 18H). ^{13}C NMR (126 MHz, $CDCl_3$) δ = 170.5, 150.3, 139.3, 122.0, 121.3, 119.3, 113.8, 81.1, 66.5, 54.3, 32.4, 30.3, 28.1.

{[2-(3-Bromo-propoxy)-6-methyl-phenyl]-*tert*-butoxycarbonylmethyl-amino}-acetic acid *tert*-butyl ester (10). To a solution of **8** (1.65 g, 4.05 mmol) in methylene chloride (40 mL) was added carbon tetrabromide (1.68 g, 5.06 mmol) followed by slow addition of triphenylphosphine (1.59 g, 6.07 mmol). After two hours at room temperature the reaction was washed with water and brine, dried over sodium sulfate, filtered and concentrated. The crude product was purified on a silica gel column eluting with 5% ethyl acetate in hexanes giving **10** in 82% yield (1.57 g). ^{1}H NMR (400 MHz, $CDCl_3$) δ = 6.99 (t, *J* = 8 Hz, 1H), 6.81 (d, *J* = 7.2 Hz, 1H), 6.72 (d, *J* = 8 Hz, 1H), 4.09 (t, *J* = 4.8 Hz, 2H), 3.76 (s, 4H), 3.69 (t, *J* = 6 Hz, 2H), 2.45 (s, 3H), 2.34 (m, *J* = 6.8 Hz, 2H), 1.39 (s, 18H). ^{13}C NMR (100 MHz, $CDCl_3$) δ = 170.81, 156.51, 139.25, 137.8, 125.91, 123.27, 109.85, 80.64, 65.61, 57.3, 32.7, 30.63, 28.23, 27.31, 18.89. MS (ESI-positive) *m/z* Calcd for ($M + Na^+$): 494.1, Found: 496.1.

(tert-Butoxycarbonylmethyl-{2-[3-(4,7,10-tris-tert-butoxycarbonylmethyl-1,4,7,10-tetraaza-cyclododec-1-yl)-propoxy]-phenyl}-amino)-acetic acid tert-butyl ester (11). To a solution of **9** (1.4 g, 3.2 mmol) in 35 mL of dry acetonitrile was added 0.7 g (4.9 mmol) anhydrous potassium carbonate and 0.8 g (1.6 mmol) DO3A-tris-*tert*-butyl ester. The reaction was refluxed

for 48 hours then cooled to room temperature and filtered rinsing with methanol. The crude product was absorbed onto silica and purified via silica gel column chromatography eluting with 2% methanol in dichloromethane. **11** was collected in 36% yield (0.51 g) as an orange oil. ^{1}H NMR (500 MHz, $CDCl_3$) δ = 6.85 (m, 4H), 4.21 (t, *J* = 5.5 Hz, 2H), 4.00 (s, 2H), 3.97 (s, 2H), 3.62 (t, *J* = 9 Hz, 2H), 3.49 -2.26 (broad, 22H), 1.95 (m, 2H), 1.43 (s, 45H). ^{13}C NMR (126 MHz, $CDCl_3$) δ = 173.1, 170.6, 170.3, 150.8, 139.6, 122.8, 121.6, 120.1, 114.3, 82.9, 82.5, 82.0, 81.9, 81.4, 67.6, 56.9, 56.0, 54.8, 54.7, 53.2, 50.5, 28.4, 28.1. MS (ESI-positive) *m/z* Calcd for ($M + H^+$): 891.6, Found: 892.6; Calcd for ($M + Na^+$): 914.6, Found: 915.6.

(*tert*-Butoxycarbonylmethyl-{2-methyl-6-[3-(4,7,10-tris-*tert*-butoxycarbonylmethyl-1,4,7,10-tetraaza-cyclododec-1-yl)-propoxy]-phenyl}-amino)-acetic acid *tert*-butyl ester (12). To a solution of DO3A-tris-*tert*-butyl ester (0.87 g, 1.69 mmol) in 5 mL of dry acetonitrile was added K_2CO_3. After five minutes, a solution of **10** (0.80 g, 1.69 mmol) in 5 mL of dry acetonitrile was added to the reaction and the mixture was refluxed overnight. The reaction was cooled and filtered rinsing with acetonitrile and methanol. After the solvents were removed by rotary evaporation, the crude product was purified on a silica gel column eluting with 2% MeOH in CH_2Cl_2 to yield **12** in 43% yield (0.66 g). After trituration with diethyl ether several times a pale yellow solid was obtained. ^{1}H NMR (500 MHz, $CDCl_3$) δ = 6.95 (t, *J* = 8 Hz, 1H), 6.78 (d, *J* = 7 Hz, 1H), 6.66 (d, *J* = 8 Hz, 1H), 4.10 (t, *J* = 5 Hz, 2H), 3.94 (t, *J* = 6 Hz, 2H), 3.79 (s, 2H), 3.73 (s, 4H), 3.52 (s, 2H), 3.36 (s, 4H), 3.14-2.2 (broad, 16H), 2.43 (s, 3H), 1.99 (m, *J* = 6 Hz, 2H), 1.46 (s, 9H), 1.44 (18H), 1.39 (s, 9H), 1.37 (s, 9H). MS (ESI-positive) *m/z* Calcd for (M^+): 905.6, Found: 906.6; Calcd for ($M + Na^+$): 928.6, Found: 928.6.

General metallation procedure. A TFA solution, 95 : 2.5 : 2.5 (TFA : H_2O : triisopropylsilane) was added to the protected ligands **11** and **12** for several hours. After the TFA was removed by purging the solution with air, ~15 mL of diethyl ether was added. The precipitate was centrifuged and decanted. The diethyl ether wash was repeated two more times with the final pellet being brought up in H_2O and the pH adjusted to 6.5 with 1 M NaOH. A small excess (1.2 equivalents) of $GdCl_3 \cdot 6H2O$ was then added and stirred at room temperature for several days. Unreacted Gd(III) precipitated as $Gd(OH)_3$ after the addition of 1 M NaOH and the crude mixture was purified by semi-preprative HPLC on a reverse phase column eluting with acetonitrile and water using an isocratic ramp from 0% to 100% acetonitrile in 35 minutes. Analytical HPLC-MS was used to confirm the purity and identity of the collected fractions. Pure fractions were then freeze-dried and stored in a dessicator. The same procedure is followed with $EuCl_3 \cdot 6H_2O$ and $TbCl_3 \cdot 6H_2O$ to obtain the Eu(III) and Tb(III) metal complexes.

Gadolinium(III)-(Carboxymethyl-{2-methyl-6-[3-(4,7,10-tris-carboxymethyl-1,4,7,10-tetraaza-cyclododec-1-yl)-propoxy]-phenyl}-amino)-acetic acid (2, Gd-daa3). Analytical LC-MS showed a single peak with *m/z* (ESI-positive) Calcd for ($M + H^+$): 778.2, Found: 781.2. Anal. Calcd for $C_{28}H_{38}GdN_5O_{11} \cdot 2H_2O \cdot 2Na$: C 39.11, H 4.93, N 8.14. Found: C 39.33, H 4.93, N 7.84.

Tb-daa3. Analytical LC-MS showed a single peak with *m/z* (ESI-positive) Calcd for ($M + H^+$): 779.2, Found: 779.2; Calcd for and ($M + Na^+$): 802.2, Found: 801.2.

Relaxivity measurements. A 1 mM solution of the gadolinium complex was made up in buffer containing 100 mM KCl/100 mM HEPES at pH = 7.4 or in human blood serum. These solutions

were serially diluted four times to give 500 μL of five different sample concentrations at a [Gd]:[Zn] ratio of 1:0. Aliquots of a 5.0 mM $ZnCl_2$ solution in HEPES was added to each of the samples to give a [Gd]:[Zn] ratio of 1 : 0.5. After 30 minutes of incubation at 37 °C, T_1 measurements were performed on a Bruker mq60 Minispec relaxometer with an inversion recovery pulse sequence with the appropriate recycle delays. This titration was repeated until a 1:3 ([Gd]:[Zn]) ratio was reached. Similar titration experiments were done with $CaCl_2$, $MgCl_2$, and $CuCl_2$ to test the effects of competing cations.

Luminescence Lifetime Measurements. The fluorescence decay rates of the terbium analogs of **2** in buffered H_2O and D_2O were measured on a Hitachi F4500 fluorimeter monitoring the emission at 544 nm with an excitation of 254 nm. Aliquots of HEPES buffer and $ZnCl_2$ in HEPES were freeze dried before bringing up in D_2O to assure there was no water present. A 200 μM solution of the terbium complex in HEPES buffer was measured in the presence of 300 μM $ZnCl_2$ and without $ZnCl_2$. Twenty-five scans were averaged and fit to a mono-exponential decay with an r^2 value of 0.99.

Nuclear Magnetic Relaxation Dispersion. Longitudinal water proton relaxation rates were measured with a Stelar Spinmaster FFC-2000-1T fast field cycling relaxometer in the 0.01 – 40 MHz proton Larmor frequency range, using the standard field cycling protocol. R_1 values were obtained with an error smaller than 1%. Proton nuclear magnetic relaxation dispersion (NMRD) profiles were thus obtained by plotting proton relaxation rates as a function of applied magnetic field. The NMRD data, subtracted from the diamagnetic contribution of buffer alone and normalized to 1 mM Gd(III) concentration, were then analyzed in terms of inner-sphere and

outer-sphere effects. Gd(III) complexes are expected to have both static and transient zero field splitting (ZFS). Presently, available fitting programs cannot properly account for their simultaneous presence in fast rotating systems. Therefore, the data was analyzed using either SBM theory (no static ZFS) or slow rotation programs including ZFS.

Calculation of Zinc-Dissociation Constants. To a 10 μM sample of $ZnCl_2$ in HEPES buffer are titrated 100 μL aliquots of 0.1 mM FluoZin-1 until saturation of fluorescence was reached. Between aliquots, 30 minutes was allowed for the reaction to reach equilibrium. A series of **Gd-daa3** at various concentrations in 10 μM $ZnCl_2$ were then titrated with FluoZin-1 in the same manner. The equilibrium established assumes a 1:1 (Gd:Zn) complex is formed. After each aliquot of fluorophore was added, the percent saturation of fluorescence ($f = (F - F_0)/(F - F_{max})$), where F_0 is the minimum fluorescence without zinc and F_{max} is the fluorescence when saturated with zinc, was calculated to determine the amount of Zn(II) bound to the dye. With known amounts of Zn(II), FluoZin-1, and Gd-daa3 added to the system, the equilibrium constant was determined.

Magnetic Resonance Imaging. In vitro phantom MR images were obtained of **Gd-daa3** in HEPES buffer with 1 mM Zn(II), Mg(II), and Ca(II) ions loaded in 3 mm NMR tubes. Images were obtained on a 4.7 T horizontal bore Bruker biospec using a multispin multiecho sequence. The phantom samples were prepared one hour in advance of image acquisition. A second set of phantom images of 1 mM **Gd-daa3** in HEPES buffer with Zn(II) concentrations of 0 μM, 50 μM, 100 μM, 500 μM, and 1 mM were imaged. The following parameters were used for both

phantom sets: TR = 100.0 ms, TE = 14.3 ms, FOV = 2.5/2.0 cm, data matrix = 256 x 256 (TR = repetition time; TE = echo time; FOV = field of view).

Cytotoxicity. NIH/3T3 cells were seeded at 10^5 cells per well in 24-well tissue culture plates with Dulbecco's modified Eagle's medium (DMEM) containing 10% bovine calf serum and incubated overnight in a 5% CO_2 incubator at 37 °C. The media was then changed and **Gd-daa3** added at a concentration of 500 μM. After 2, 4, 8, and 24 hours, cells were washed three times with 1 x PBS and exposed to 250 μL of 0.25% trypsin and harvested. Cells were diluted with an equal volume of 0.4% trypan blue and counted on a hemacytometer. For quantification of cellular uptake of **Gd-daa3** into cells, the concentration of Gd(III) was then determined using inductively coupled plasma mass spectrometry (ICP-MS). Cells were incubated with concentrated nitric acid at 70 °C for 3 hours. The dissolved cells were diluted into a 5 mL solution with 3% nitric acid and 5 ppb of an indium internal standard.

Chapter 3

Structural Optimization of Zn(II)-Responsive Contrast Agents

3.1 Introduction

The development of Zn(II)-responsive MRI contrast agents offers the ability to acquire three-dimensional images of variations in Zn(II) concentrations in a non-invasive time-resolved manner. Zinc is the second most abundant transition metal in the body behind iron; however, most of it is tightly regulated and bound to metalloproteins under physiological conditions. Disruption of Zn(II) homeostasis has been implicated in a variety of neurological disorders.[1, 2] The release of free Zn(II) from synaptic nerves in the brain has been implicated in the precipitation of amyloid plaques in Alzheimer's disease.[3-5] Despite the need to be able to visualize free Zn(II) concentrations, the ability to report on Zn(II) concentrations *in vivo* has been a challenge for biologist and chemists due to its inherent spectroscopically "silent" properties. Although the development of fluorescent probes for Zn(II) has provided much insight into the physiology of biological zinc,[6, 7] light-based microscopy is limited to due to its inability to penetrate deep tissue and its photobleaching properties. MRI can offer an alternative means to image Zn(II) with the development of Zn(II)-responsive contrast agents.

In Chapter 2, the first Zn(II)-activated MRI contrast agent in which an increase in relaxivity is observed with increasing Zn(II) concentrations was introduced. **Gd-daa3** provided a greater than 100% increase in relaxivity upon Zn(II) binding resulting in a bright MR image. In addition, **Gd-daa3** displays selectivity for Zn(II) over other biologically relevant dications such as Ca(II) and Mg(II). The Zn(II)-dissociation constant calculated for **Gd-daa3** shows that it can bind Zn(II) in the hundreds of micromolar range, concentrations expected to for the release of Zn(II) from synaptic nerves in the brain.[8, 9]

In an effort to increase the relaxation enhancement of Zn(II)-responsive contrast agents, two new agents have been synthesized with varied carbon chain lengths between the Zn(II)-

binding groups and the Gd(III) chelate. In this chapter, the synthesis and evaluation of **Gd-daa2** (**dia**mino**a**cetate with **2** methylene carbons) and **Gd-daa4** (**dia**mino**a**cetate with **4** methylene carbons) are introduced (**Figure 3.1**). Their T_1 relaxation, hydration numbers, and Zn(II)-binding dissociation constants are investigated and discussed in relation to the original agent **Gd-daa3**. The results from these studies show that **Gd-daa4** provides a greater than 200% increase in relaxivity upon Zn(II)-binding, a significant improvement over **Gd-daa3**. Investigation of the ^{17}O NMR transverse relaxtion rates shows that the slight structural variation of an added methylene carbon displays an optimized proton chemical exchange rate and therefore an optimized relaxivity in the presence of Zn(II).

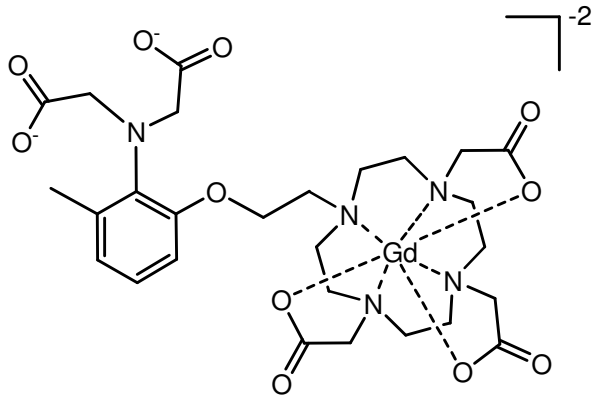

Gd-daa2 (1)

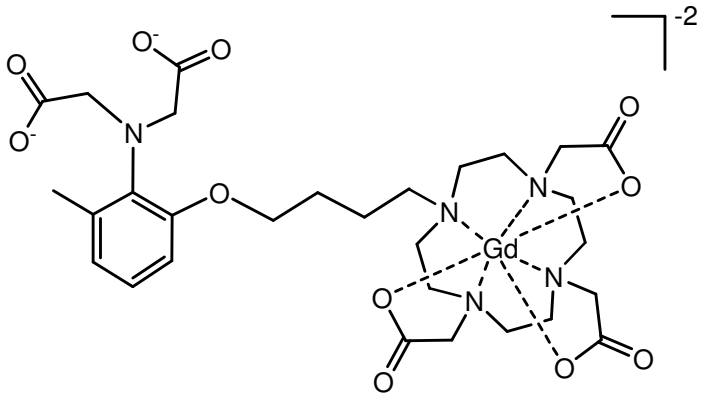

Gd-daa4 (2)

Figure 3.1. Zn(II)-responsive MRI contrast agents with varying linker lengths between the Zn(II)-binding groups and the Gd(III) chelate.

3.2 Results and Discussion

3.2.1 Synthesis and Characterization

Following the synthetic procedure of **Gd-daa3**, **Gd-daa2** was synthesized in a similar manner (**Scheme 3.1**). To the commercially available 3-methyl-2-nitrophenol, (2-bromoethoxy)-*tert*-butyldimethyl silane was added using anhydrous potassium carbonate in acetonitrile to yield the protected alcohol **3**. The nitro group was reduced to the amine under standard palladium-catalyzed hydrogenation conditions and reacted immediately with *tert*-butylbromoacetate to give **4**. Deprotection of the TBDMS group was afforded by reaction with tetrabutylammonium fluoride in tetrahydrofuran to yield **5**. Bromination of the alcohol to give **6** was achieved with carbon tetrabromide and triphenylphosphine in dichloromethane. DO3A-tris-*tert*-butyl ester was synthesized following literature procedure[10] and added to **6** under basic conditions to yield the fully protected ligand **7**.

The synthesis of **Gd-daa4** (**Scheme 3.2**) begins with alkylation of 3-methyl-2-nitrophenol with 4-bromobutyl acetate to give **8**. Because the acetate protecting group can be cleaved under basic conditions, it was reprotected with the acid cleavable TBDMS protecting group which is stable to the conditions used to add the *tert*-butylbromoacetate arms to the amine. This was achieved through deprotection of the acetate group in a 10% solution of sodium hydroxide in water and reprotection with *tert*-butyldimethylsilyl chloride in DMF with imidazole following literature procedures.[11] The fully protected ligand **14** could then be synthesized using the same reaction procedures outlined for **Gd-daa2**.

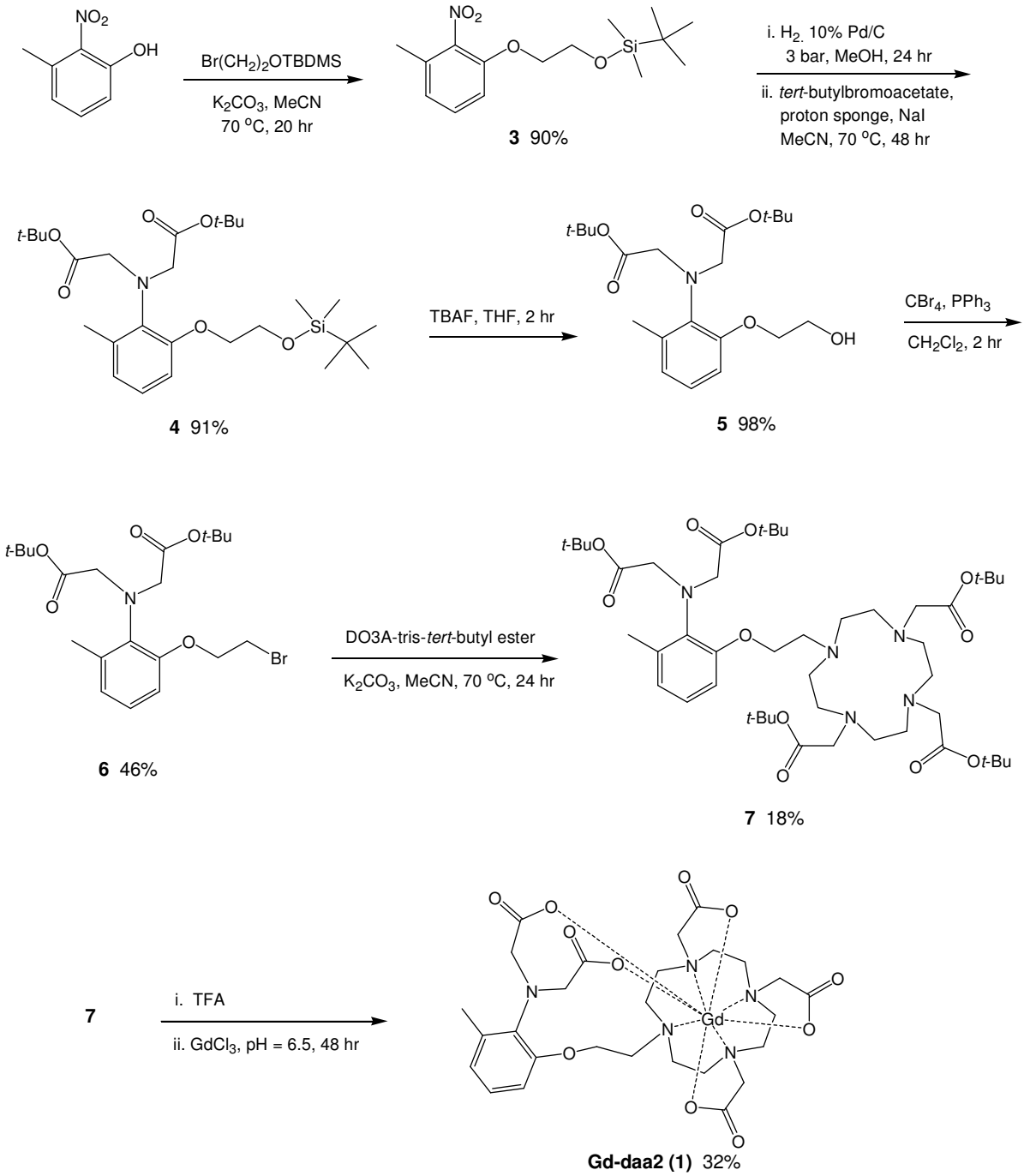

Scheme 3.1. The synthesis of **Gd-daa2 (1)**.

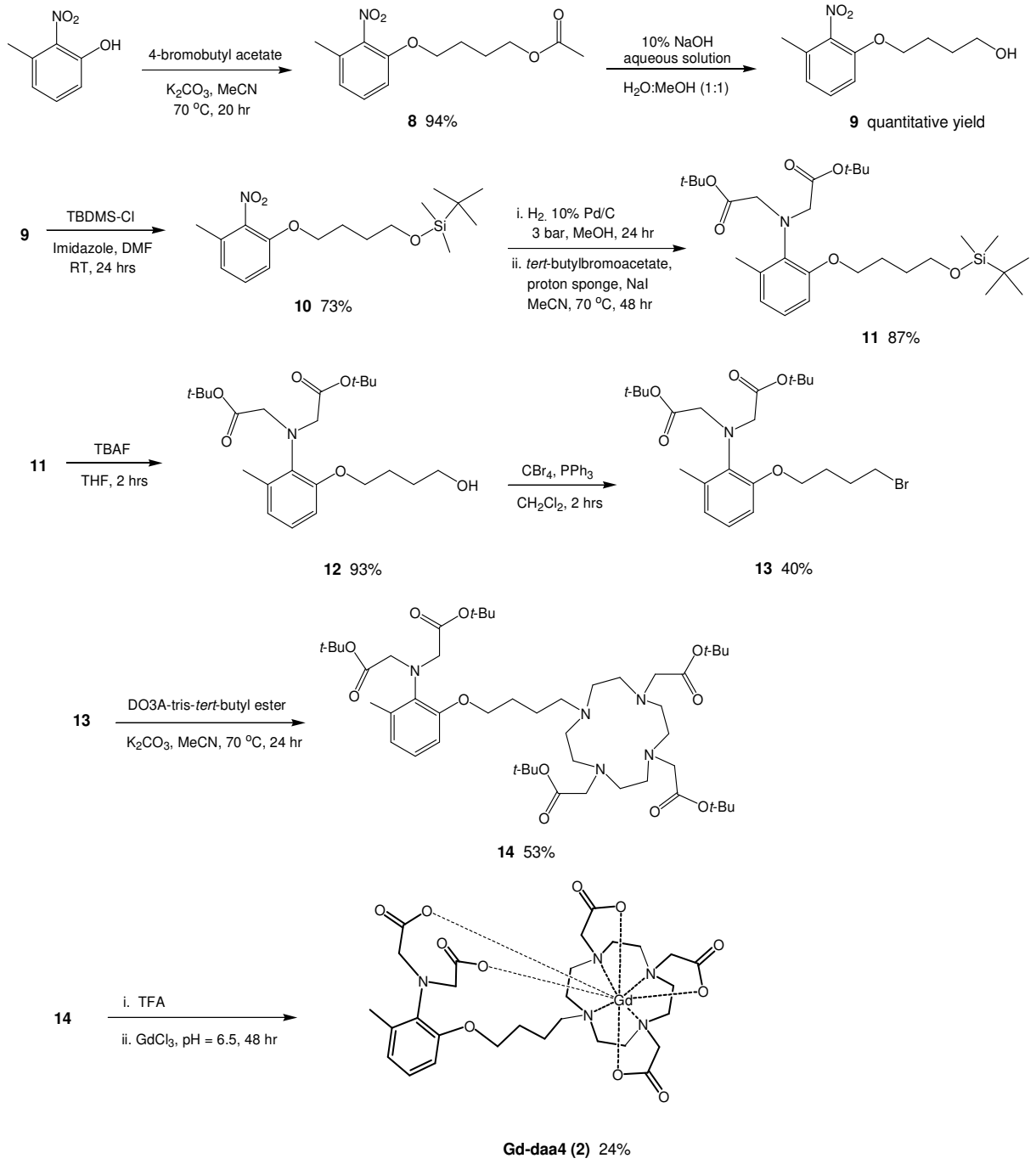

Scheme 3.2. The synthesis of **Gd-daa4 (2)**.

The protected ligands **7** and **14** are then deprotected with a solution of trifluoroacetic acid with triisopropylsilane in water. The acid is blown off under air and the deprotected product is precipitated with the addition of diethyl ether. After centrifugation, the ether is decanted and the product is washed several more times with diethyl ether and then brought up in water and freeze-dried. The final metal complexes were synthesized through reaction of the deprotected ligands with MCl_3 (M = Gd, Eu, or Tb) at a pH of ~6.5 for up to 24 hours at room temperature. Unreacted metal is precipitated as $M(OH)_3$ with 1 M NaOH and pelleted through centrifugation. The supernatant is collected and adjusted to a pH of 7 with 0.5 M HCl. After freeze-drying, the crude product is purified by reverse phase column chromatography on semi-preparatory HPLC and fractions were then analyzed for purity via analytical LC-MS and elemental analysis.

3.2.2 Relaxivity

To evaluate **Gd-daa2** and **Gd-daa4** as potential Zn(II)-responsive contrast agents, their relaxivities were first evaluated in the presence and absence of Zn(II) in a non-coordinating HEPES buffer at 60 MHz and 37 °C (**Figures 3.2** and **3.3** respectively). Before the addition of Zn(II), both agents exhibit low relaxivity values as expected for a closed $q = 0$ complex. Upon addition of Zn(II) an increase in relaxivity is observed for both **Gd-daa2** and **Gd-daa4**. However, the increase measured in the presence of Zn(II) for **Gd-daa2** is only 21% compared to the increase of over 100% observed when there are three methylene carbons present. For **Gd-daa4**, an increase from 2.1 $mM^{-1}s^{-1}$ with no Zn(II) present to 6.5 $mM^{-1}s^{-1}$ with one equivalent of Zn(II) is observed representing a greater than 200% increase in relaxivity. This data demonstrates a trend in which as the carbon chain length increases between the Zn(II)-binding

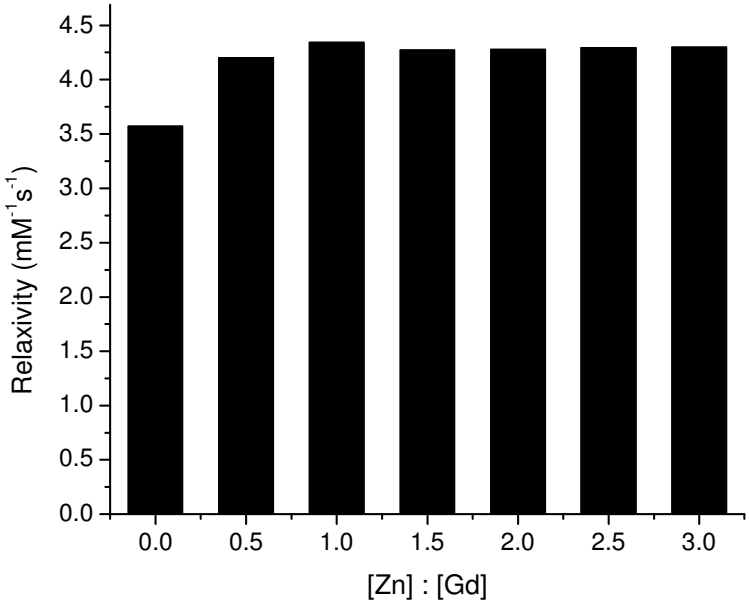

Figure 3.2. Relaxivity of **Gd-daa2** with the addition of $ZnCl_2$ in HEPES buffer measured at 37 °C and 60 MHz.

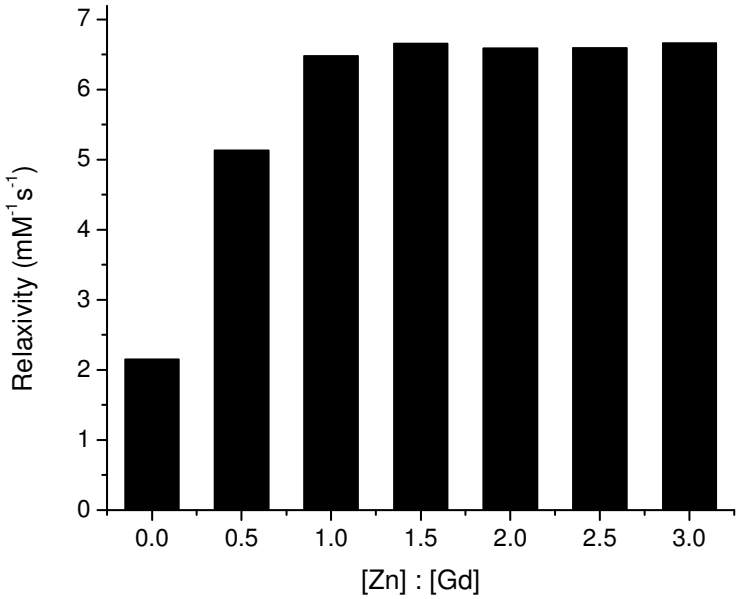

Figure 3.3. Relaxivity of **Gd-daa4** in the presence of $ZnCl_2$ in HEPES buffer measured at 37 °C and 60 MHz.

groups and the Gd(III) chelate, a greater increase in relaxivity is achievable upon the addition of Zn(II). This could be due to either a larger *q* value or from an increase in the water exchange rate in the open structure as the aminoacetates are moved further away from the Gd(III) chelate.

To test the selectivity of these agents for Zn(II) over other prevalent biological dications, their relaxivities were measured in the presence of Ca(II), Mg(II), and Cu(II). As observed with the original Zn(II)-responsive agent, **Gd-daa3**, there was no observable change in relaxivity for **Gd-daa2** and **Gd-daa4** in the presence of Ca(II) or Mg(II). In the case of Cu(II), there is a significant increase in relaxivity observed for both agents (**Figures 3.4** and **3.5**). However, the concentrations of Cu(II) are ten-fold less than Zn(II) during neurotransmission, estimated to be about 30 μM.[12] At these low concentrations, there is expected to be little interference from Cu(II) in the relaxivity enhancement due to the presence of Zn(II).

To further test the viability of these relaxivity increases for *in vivo* studies, measurements were conducted in male human serum with Zn(II). Results with **Gd-daa2** show only a 3% relaxation enhancement in the presence of Zn(II) indicating that this agent would not be viable for further biological testing. The increase observed for **Gd-daa4** with Zn(II) in serum shows a 21% relaxation enhancement as compared to the 200% increase observed in HEPES buffer (**Figure 3.6**). This was similar to the relaxivity measured for **Gd-daa3** in Chapter 2 and is indicative of non-specific binding to human serum albumin which makes up about half of the total protein concentration in serum.[13] Nonetheless, the relaxation enhancement observed is still considerable enough for detection of Zn(II) under normal physiological conditions.

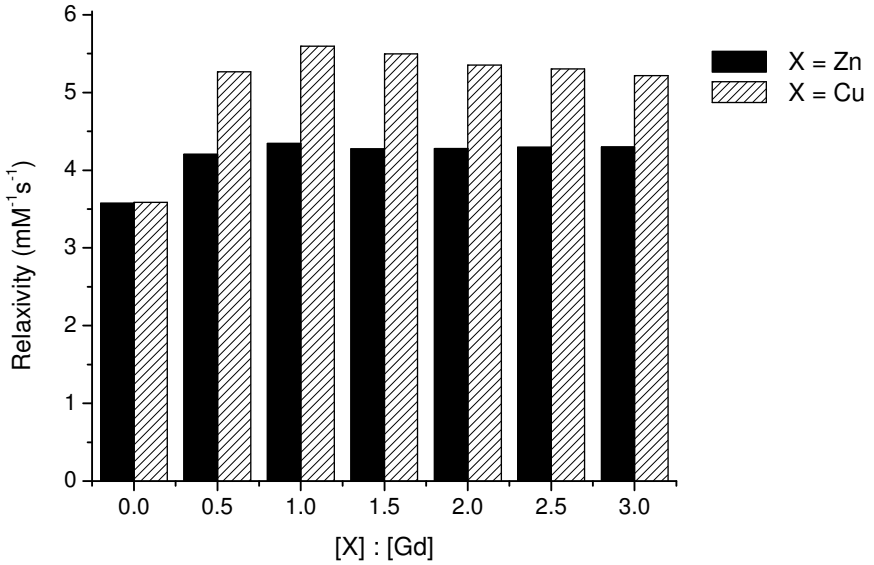

Figure 3.4. Relaxivity of **Gd-daa2** with Zn(II) and Cu(II) measured at 37 °C and 60 MHz in HEPES buffer.

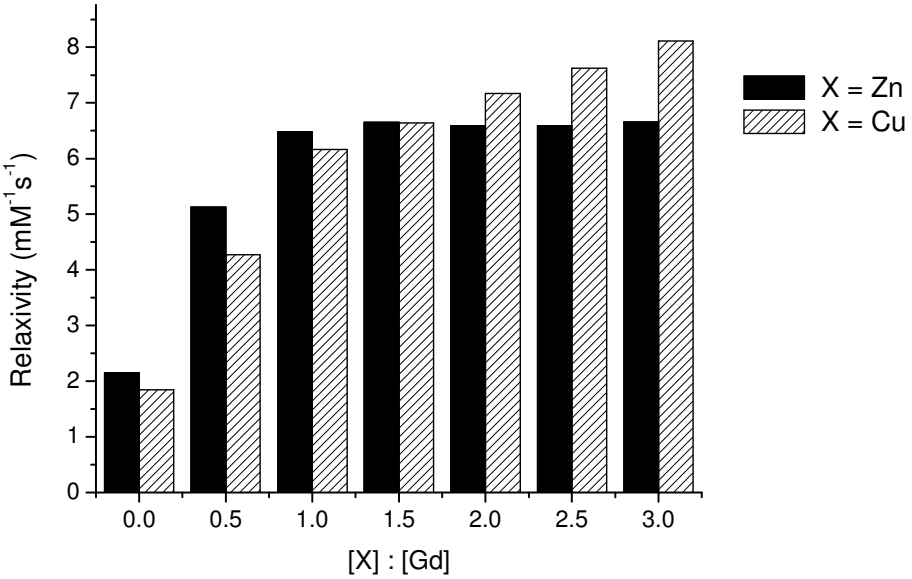

Figure 3.5. Relaxivity of **Gd-daa4** with Zn(II) and Cu(II) measured at 37 °C and 60 MHz in HEPES buffer.

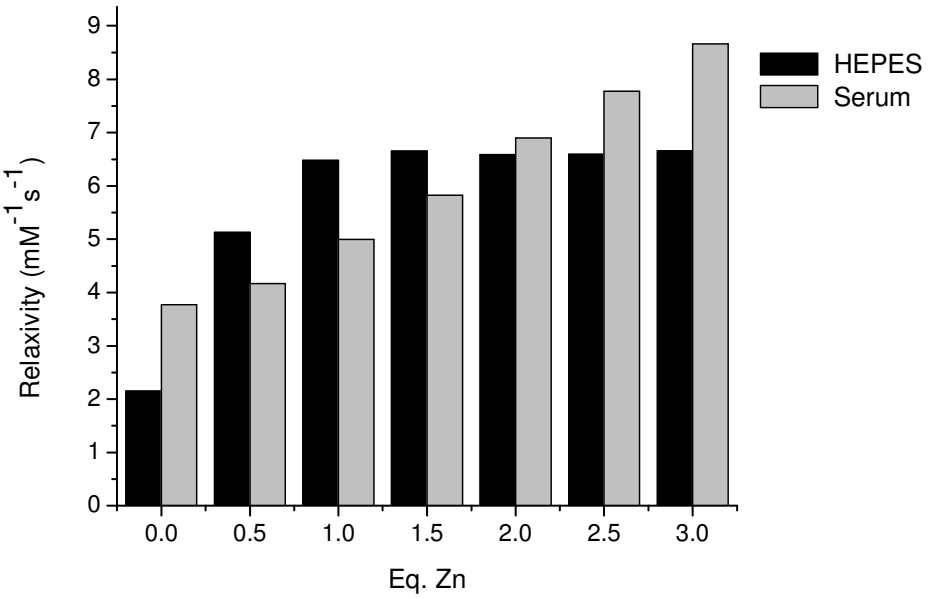

Figure 3.6. Relaxivity of **Gd-daa4** in the presence of $ZnCl_2$ in HEPES buffer and human male serum measured at 37 °C and 60 MHz.

3.2.3 Hydration Number (q)

To confirm that there is a conformation change of the contrast agents upon Zn(II)-binding, allowing increased access of water to Gd(III), the Tb(III) analogs of each of the agents was synthesized (**Tb-daa2** and **Tb-daa3**). Values of q were determined through time-based fluorescence microscopy measurements. For rare-earth ions such as Tb(III), the dominant mode of radiationless deactivation is through the loss of electronic excitation energy through high-frequency vibrations. Due to more efficient vibronic coupling of the Tb(III) excited state to the O-H oscillators than to the O-D oscillators, a shorter luminescence lifetime is observed in H_2O than in D_2O.[14, 15] The fluorescence decay rates of the Tb(III) analogs in water and D_2O both with and without Zn(II) were measured and used to calculate q using **Equation 3.1**.[16]

$$q = 4.2\ \text{ms}\left[\left(\frac{1}{\tau_{H2O}}\right) - \left(\frac{1}{\tau_{D2O}}\right) - 0.06\right] \qquad \textbf{Equation 3.1}$$

The fluorescence lifetimes and calculated q values are summarized in **Table 3.1**. These measurements confirm that a coordinatively saturated Gd(III) complex with a hydration number of zero is found when there is no Zn(II) present. In the presence of Zn(II), **Tb-daa2** has a hydration number of 0.4, indicating that there is very little access of water to Gd(III). This would explain the low increase in relaxivity observed for **Gd-daa2**. The calculated q value for **Tb-daa4** in the presence of Zn(II) gives a hydration number of 1.0. This confirms that the large increase in relaxivity observed for **Gd-daa4** is partially due to the increase in hydration number. However, the results of **Gd-daa3** have a hydration number of one as well but only displays an increase in relaxivity of just over 100% while **Gd-daa4** has a 200% increase in relaxivity. Therefore, this large increase cannot be explained solely by the increase in hydration number.

Table 3.1. Fluorescence decay lifetimes of **Tb-daa2, Tb-daa3,** and **Tb-daa4** in H_2O and D_2O and their calculated *q* values with an error of +/- 0.1.

	τ H_2O (ms)	**τ D_2O (ms)**	***q***	**τ H_2O (ms) + Zn(II)**	**τ H_2O (ms) + Zn(II)**	***q* + Zn(II)**
Tb-daa2	2.16	2.76	0.2	1.95	2.76	0.4
Tb-daa3	1.97	2.71	0.3	1.46	2.65	1.0
Tb-daa4	2.32	2.63	0.0	1.53	2.85	1.0

3.2.4 Mean Residence Lifetime of Water Protons (τ_m)

A water molecule coordinated to the metal center is in constant exchange with bulk water. As discussed in Chapter 1, an increase in the water exchange rate effectively increases the relaxation enhancement observed. The large increase in relaxivity for **Gd-daa4** over **Gd-daa3** could not be accounted for by measuring the hydration number, as they both increased from a q = 0 complex in the closed state to a q = 1 complex in the presence of Zn(II). It was postulated then, that this relaxation enhancement could arise from an increase in the water proton exchange rate. To investigate the reasons for this large increase, variable temperature ^{17}O NMR measurements were done to calculate the water exchange rates of **Gd-daa2**, **Gd-daa3**, and **Gd-daa4**.

The water exchange rate can be determined directly from variable temperature ^{17}O NMR measurements. The transverse ^{17}O relaxation rate can be determined through measurement of the line width of the ^{17}O NMR signal. For each complex, the line width at half peak height were measured both with and without Zn(II) at temperatures ranging from 5 ^{o}C to 75 ^{o}C. R_{2p} at each temperature is then calculated using $R_{2p} = \Delta\nu_{1/2}*\pi$ and plotted against temperature. The experimental data was fit to the Swift-Connick theory using **Equation 3.2**,[17]

$$\frac{1}{T_{2\mathrm{m}}} \cong \frac{\mathrm{S(S+1)}}{3}\left(\frac{\mathrm{A}}{\hbar}\right)^2 (T_{1\mathrm{e}}^{-1} + \tau_{\mathrm{m}}^{-1})^{-1} \qquad \textbf{Equation 3.2}$$

where S is the electron spin quantum number (7/2 for Gd(III)), $A/\hbar$ is the hyperfine coupling constant between the Gd(III) ion and the oxygen nucleus, T_{1e} is the electronic relaxation time, and τ_m is the mean residence lifetime of the coordinated water molecule. The temperature dependence of T_{1e} and τ_m can be described by the Eyring equations (**Equations 3.3** and **3.4),**

$$\frac{1}{T_{1e}} \cong \frac{1}{T_{1e}^{298}} \exp\left(\frac{\Delta E_{T1e}}{R}\left(\frac{1}{T} - \frac{1}{298K}\right)\right) \qquad \textbf{Equation 3.3}$$

$$\frac{1}{\tau_m} \cong \frac{1}{\tau_m^{298}} \frac{T}{298\ K} \exp\left(\frac{\Delta H}{R}\left(\frac{1}{298\ K} - \frac{1}{T}\right)\right) \qquad \textbf{Equation 3.4}$$

where ΔE_{T1e} and ΔH are the energy and enthalpy of activation, respectively, for the exchange process.[18]

A typical profile of the plot of R_{2p} versus temperature shows two regions. The first is the slow kinetic region which is observed at low temperatures where the transverse relaxation rate increases with temperature. The second region is the fast exchange region where a decrease in transverse relaxation rate is seen with increasing temperature.[18] The plots of R_{2p} for **Gd-daa2**, **Gd-daa3**, and **Gd-daa4** both with and without Zn(II) are presented in **Figures 3.7**, **3.8**, and **3.9** respectively. The plots for **Gd-daa3** and **Gd-daa4** in the absence of Zn(II) could not produce a best-fit curve[19] due to the limited access of water to Gd(III) in the closed structure. This was the case for **Gd-daa2** as well both with and without Zn(II).

The water residence lifetimes calculated for the best-fit curves of **Gd-daa3** and **Gd-daa4** in the presence of Zn(II) provide a τ_m equal to 112 ns for **Gd-daa3** and 29 ns for **Gd-daa4**. These are with the range of 10-1000 ns commonly seen for DOTA derivatives.[19] The order of magnitude lower τ_m measured for **Gd-daa4** compared to **Gd-daa3** explains the larger relaxivity enhancement observed for **Gd-daa4** in the presence of Zn(II). The addition of a methylene carbon between the Gd(III) chelate and the Zn(II)-binding groups provides more space for the exchange of water to Gd(III). This would facilitate a faster exchange rate of water protons and therefore a higher relaxivity as observed. Further investigation with variable pressure NMR to

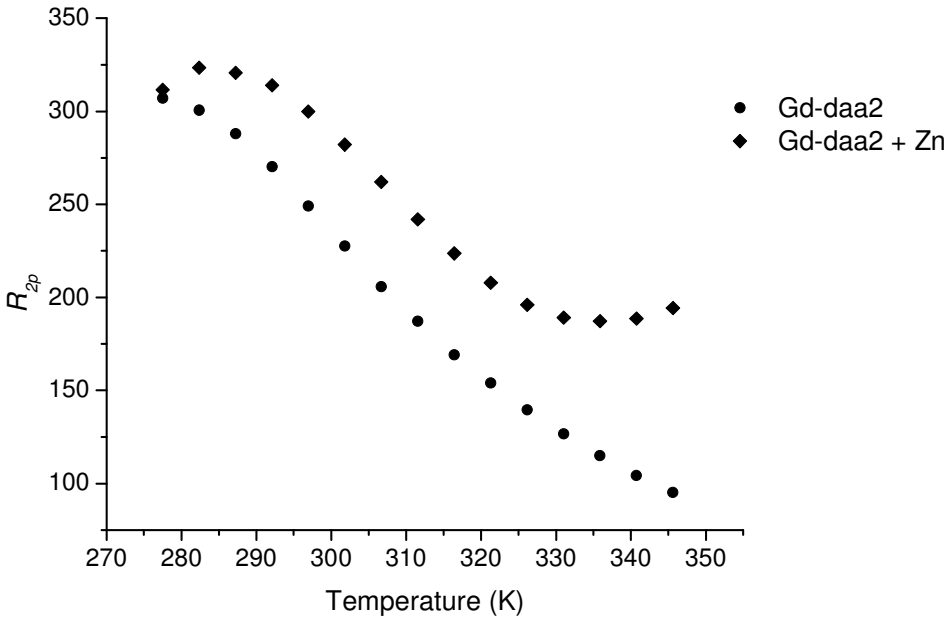

Figure 3.7. ^{17}O transverse relaxation rates with variable temperature for **Gd-daa2** at 54 MHz with and without Zn(II). A best-fit curve could not be fit to the experimental data due to the limited access of water to Gd(III).

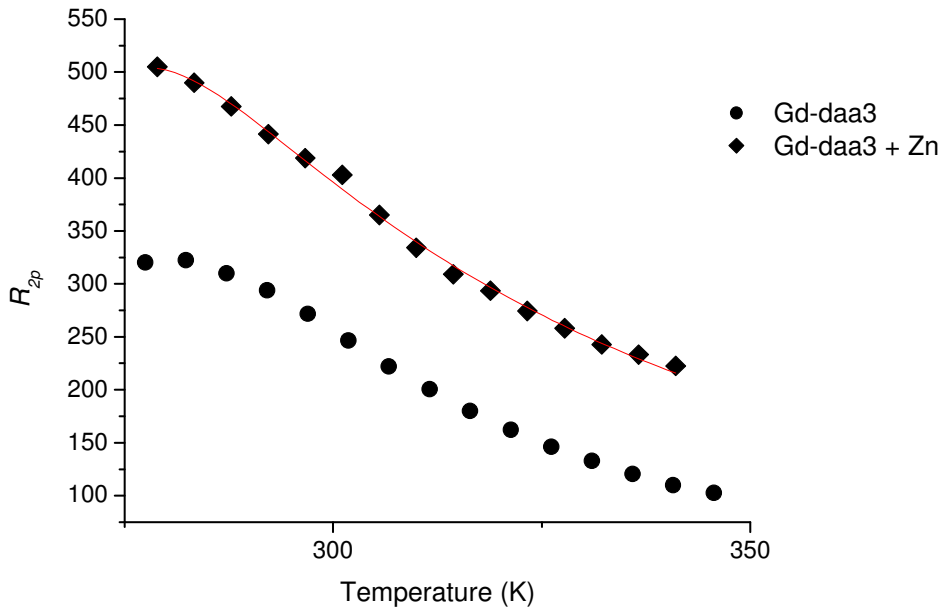

Figure 3.8. ^{17}O transverse relaxation rates with variable temperature for **Gd-daa3** at 54 MHz with and without Zn(II) showing the fit to the experimental data for **Gd-daa3 + Zn** (red line). The least squares fitting procedure gave [Gd] = 0.02 mM, τ_m = 112.0 ns, ΔH_M = 17.5 kJ/mol, T_{1e} = 20.2 ns, and q = 1. The hyperfine coupling constant was taken to be A/ħ = -3.8 x 10^6 rad s^{-1}.

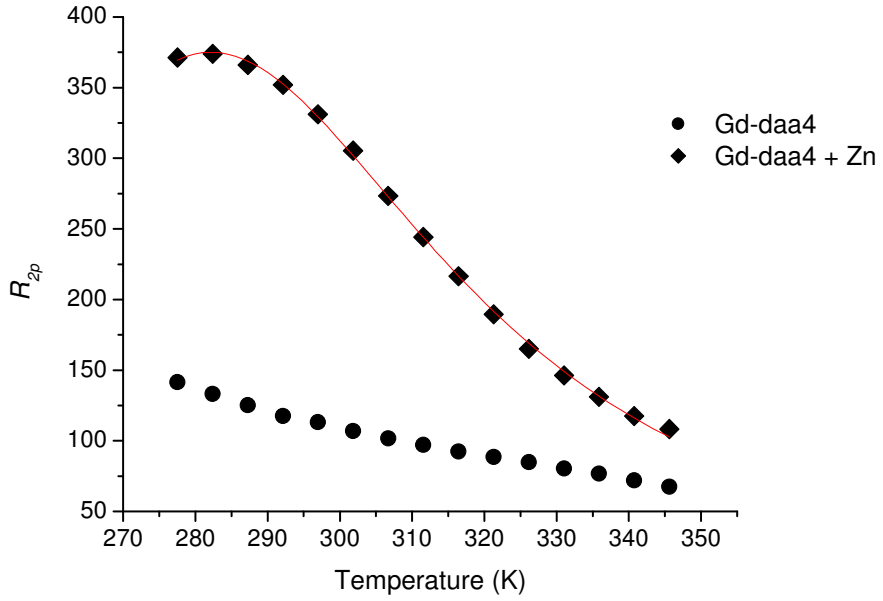

Figure 3.9. ^{17}O transverse relaxation rates with variable temperature for **Gd-daa4** at 54 MHz with and without Zn(II) showing the fit to the experimental data for **Gd-daa4 + Zn** (red line). The least squares fitting procedure gave [Gd] = 0.013 mM, τ_m = 24.9 ns, ΔH_M = 23.2 kJ/mol, T_{1e} = 77.0 ns, and q = 1. The hyperfine coupling constant was taken to be A/ħ = -3.8 x 10^6 rad s^{-1}.

determine the volume of activation of the water binding site would determine if this was the case. In addition, because the profile of **Gd-daa3** with Zn(II) shows little curvature at low temperatures, to get a more accurate value of τ_m, ^{17}O relaxation rates should be measured at variable fields.

3.2.5 Zinc Dissociation Constants

To evaluate the effectiveness of these agents to bind Zn(II), a competitive binding assay with the Zn(II)-binding fluorophore FluoZin-1 was used. FluoZin-1 binds Zn(II) through two aminoacetate arms with a Zn(II)-dissociation constant of 8.6 x 10^{-6} M.[20] The Zn(II)-dissociation constants for **Gd-daa2** and **Gd-daa4** were found following procedures outlined in Chapter 2. The fluorescence titration curves for **Gd-daa2** and **Gd-daa4** are shown in **Figures 3.10** and **3.11** respectively. Similar to **Gd-daa3** discussed in Chapter 2, both of these agents bind Zn(II) in the hundreds of micromolar range, K_d = 3 x 10^{-4} M for **Zn-Gd-daa2** and K_d = 8 x 10^{-5} M for **Zn-Gd-daa4**. Due to having the same Zn(II)-binding groups presents, the dissociation constants were not expected to be significantly different as observed. These contrast agents exhibit optimal binding constants for the imaging of Zn(II) released from synaptic nerve clefts during ischemia.[2]

3.2.6 Europium NMR

From the above studies, it is evident that variation of the structure by addition of a methylene group between the Zn(II)-binding groups and the Gd(III) chelate has a profound difference on the relaxation enhancements of these agents in response to Zn(II). In an effort to provide further understanding of the structural differences, the Eu(III) analogs of **Gd-daa2**, **Gd-**

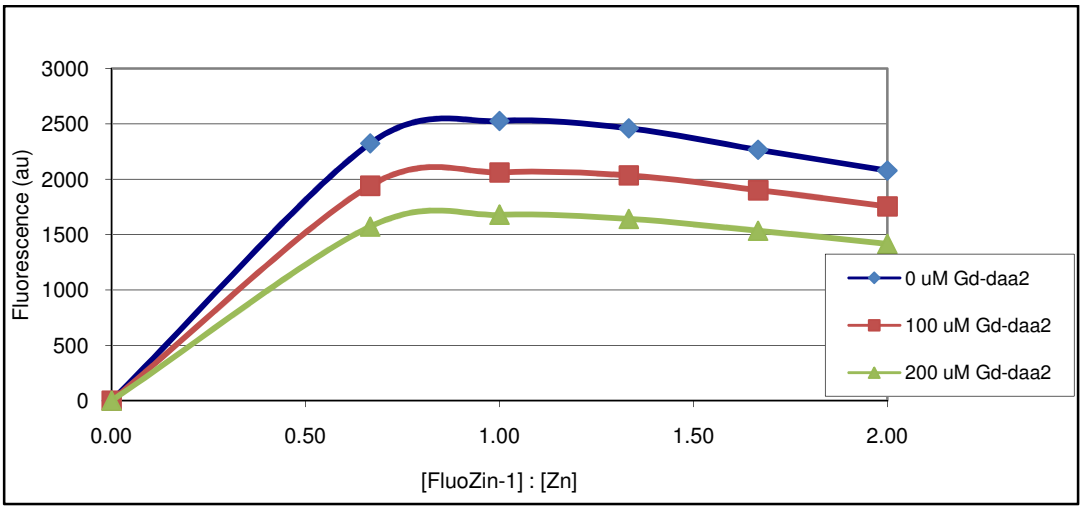

Figure 3.10. Observed titration curves of FluoZin-1 with Zn(II) at varying concentrations of **Gd-daa2** measuring the fluorescence at λ_{em} = 515 nm in HEPES buffer at a pH of 7.4.

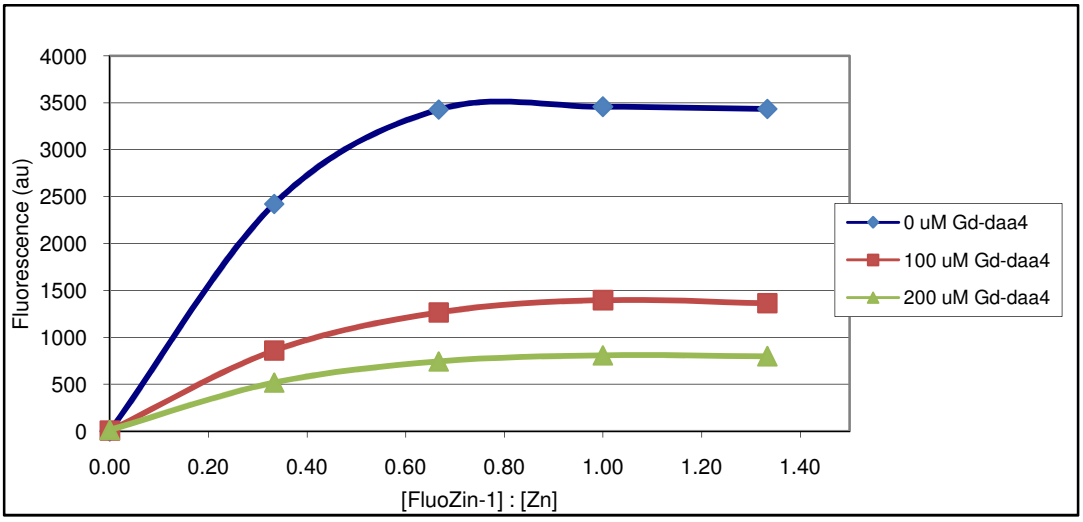

Figure 3.11. Observed titration curves of FluoZin-1 with Zn(II) at varying concentrations of **Gd-daa4** measuring the fluorescence at λ_{em} = 515 nm in HEPES buffer at a pH of 7.4.

daa3, and **Gd-daa4** were synthesized for investigation of their solution structures through NMR spectroscopy. It is known from the literature that lanthanide complexes containing DOTA derivatives are present in two isomer conformations, square antiprism (SAM) and twisted square antiprism (TSAP).[18] These isomers can interconvert through ring inversion or through rotation of the acetate arms.[21, 22] Since the interconversion between isomers is slow, the two coordination isomers can usually be distinguished by ^{1}H NMR spectroscopy. The chemical shifts that are most shifted on the macrocyclic ring due to the paramagnetic Eu(III) metal are the axial protons. Examination of their shifts allows assignment of the two coordination isomers.[21]

The three Eu(III) complexes examined by ^{1}H NMR spectroscopy show similar chemical shifts and therefore provide no evidence in their structural differences. However, thorough examination of **Eu-daa3** allowed for the assignment of the coordination isomer in the absence of Zn(II). The proton NMR spectrum of **Eu-daa3** is presented in **Figure 3.12**. The chemical shifts of the axial protons between 20 and 35 ppm correspond to the more compact SAM isomer. There are no peaks observed between 10 and 20 ppm, characteristic peak shifts observed for the TSAP isomer, indicating that only one isomer is present. Further investigation with two-dimensional exchange spectroscopy (EXSY) (**Figure 3.13**) allowed complete assignment of the macrocyclic protons following literature precedence.[21]

The presence of the SAM isomer in the Eu(III) complexes when there is no Zn(II) present indicates that a compact complex is formed with the binding of the aminoacetate arms to the metal center. It was expected that in the presence of Zn(II), chemical shifts from the TSAP isomer would be observed due to the opening of the structure. The TSAP isomer is typically observed when there is fast water exchange.[22] Unfortunately, due to the insolubility of the

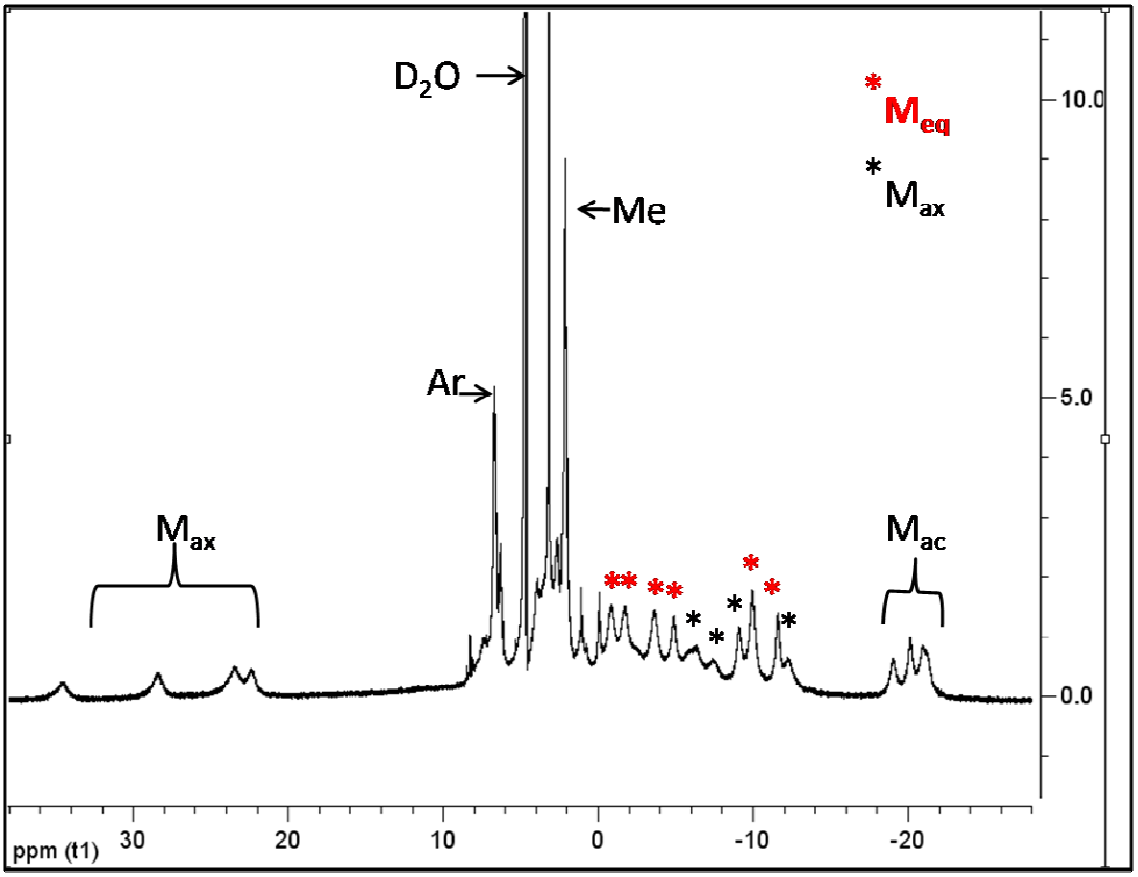

Figure 3.12. ^{1}H NMR spectrum (500 MHz) of **Eu-daa3** and assignment of the macrocyclic protons. M_{ax} = axial protons, M_{eq} = equatorial protons, M_{ac} = acyl protons, Ar = aromatic protons, and Me = methyl protons.

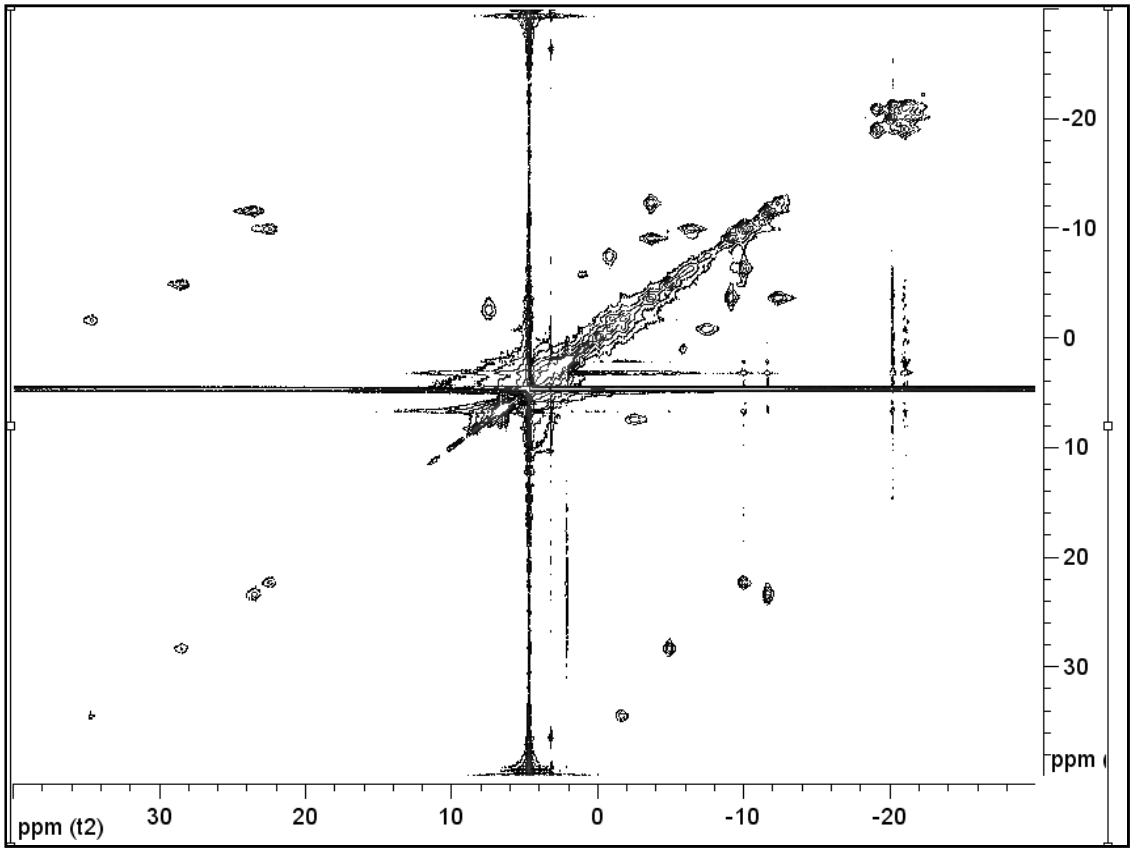

Figure 3.13. EXSY spectrum (500 MHz) of **Eu-daa3** showing cross peaks between the axial and equatorial macrocyclic protons.

Zn(II)-Eu-daa3 complex in D_2O, efforts to obtain clear NMR spectra of the Zn(II)-complexes was not possible.

3.2.7 MR Images

Gd-daa4 has been shown to provide the greatest relaxation enhancement in the presence of $ZnCl_2$ and was therefore chosen for cellular imaging of Zn(II). NIH/3T3 cells were treated with 0.5 mM **Gd-daa4** for 24 hours then washed three times with 1X PBS to remove any agent that was not taken up by cells. After washes, the cells were split into two groups to have a control where no Zn(II) was added while the second half were treated with the Zn(II) ionophore pyrithione in a 1:1 ratio at 1 mM Zn(II) concentrations for 10 min. A second batch of NIH/3T3 cells were either treated with Zn-pyrithione or left alone to serve as controls as well. Cell suspensions were then pelleted and imaged on a 4.7 T magnet (**Figure 3.14**). Results show that a change in T_1 relaxation due to intracellular Zn(II) can be imaged via MR. To confirm that this was a significant change when Zn(II) and **Gd-daa4** were both used, T_1 was measured on the 4.7 T magnet (**Table 3.2**).

3.3 Conclusions and Future Aspects

This chapter presents the synthesis and evaluation of two new Zn(II)-responsive MRI contrast agents with varying carbon chain lengths between the Zn(II)-binding groups and the Gd(III) chelate. When compared to the original Zn(II)-responsive agent presented in Chapter 2, **Gd-daa3**, it was shown that addition of a methylene carbon to make **Gd-daa4** improved the proton relaxation enhancement due to Zn(II)-binding. **Gd-daa4** produces a 200% increase in relaxivity in the presence of Zn(II) and is selective for Zn(II) over other dications such as Ca(II)

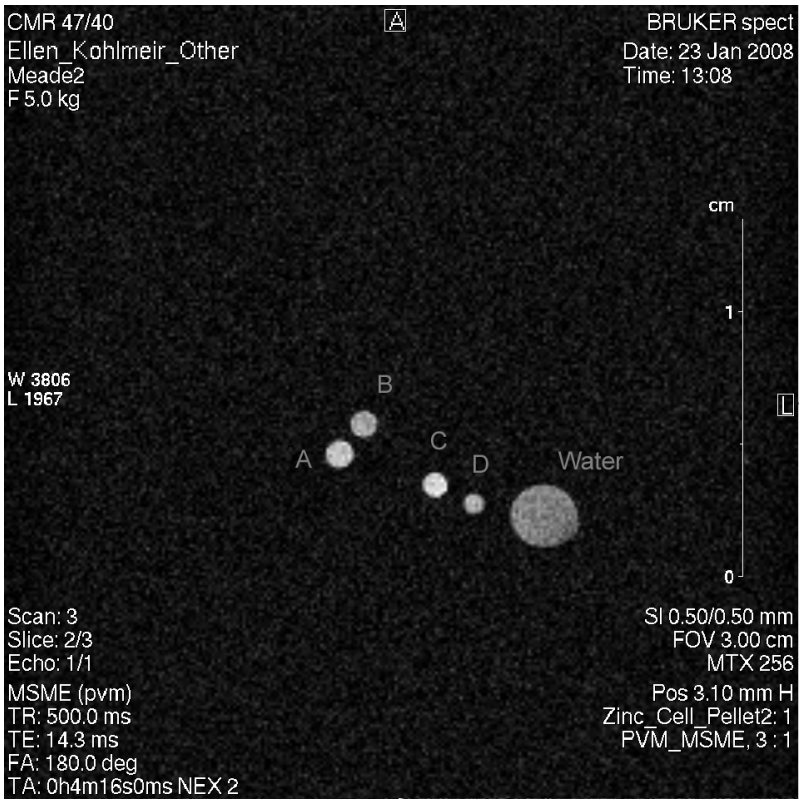

Figure 3.14. T_1-weighted MR images of NIH/3T3 cells treated with **Gd-daa4** and/or Zn-pyrithione. **A:** Gd-daa4, **B:** control cells, **C:** Gd-daa4 + Zn-pyrithione, **D:** Zn-pyrithione. Images were obtained on a 4.7 T magnet with the following parameters: repetition time (TR) = 500.0 ms; echo time (TE) = 14.3 ms; field of view (FOV) = 3.0/3.0 cm; and data matrix = 256 x 256.

Table 3.2. T_1 measurements of the MR samples from **Figure 3.14** measured at 4.7 T.

	Sample	**T_1 (ms)**
A	Gd-daa4	2370
B	Control Cells	2699
C	**Gd-daa4 + Zn**	**1705**
D	Zn	2384
	H_2O	3146

and Mg(II), physiological relevant neurological secondary messengers. Results indicate that this agent increases from a $q = 0$ complex in the closed structure before the addition of Zn(II) to a $q = 1$ complex after addition of Zn(II). While **Gd-daa3** exhibits the same increase in the hydration number upon Zn(II) binding, it was found that the greater relaxation enhancement provided by **Gd-daa4** is a result of a faster water exchange rate.

Removal of a methylene carbon to make **Gd-daa2** provided no significant enhancement of proton relaxivity upon Zn(II)-binding. Results from fluorescence lifetime decay measurements of the Tb(III) analog show that the hydration number of **Gd-daa2** shows little change in the presence of Zn(II). While Zn(II)-binding was confirmed through a fluorescence competition binding assay, it is speculated that removal of a methylene carbon between the Zn(II)-binding groups and the Gd(III) chelate does not allow for an open structure in the presence of Zn(II) for easy access of water to Gd(III).

Efforts to try and understand the structural differences of these agents with ^{1}H NMR spectroscopy were not successful. The closed structure of the Eu(III) analogs of the three agents have very similar chemical shifts in the ^{1}H NMR spectrum. However, upon closer evaluation of **Eu-daa3** using two-dimensional ^{1}H NMR exchange spectroscopy, the square antiprism isomer was determined to be the dominant coordination isomer. Evaluation of the **Zn-Eu-daa3** complex by NMR has been unsuccessful so far due to the insolubility of Zn(II) in D_2O.

Further evaluation of the systematic variation of the carbon chain length should be investigated using molecular modeling calculations. Unfortunately, current modeling techniques do not allow for the use of lanthanide metals. The closest approximation available is with the use of Y(III). However, the coordination number of Y(III) is at best seven and the complexes that are being investigated have a coordination number of nine. Current work in the Meade lab

in collaboration with Professor Ratner is on the development of molecular modeling programs that can account for Gd(III). As progress is made with this program, these agents will be looked at further using computational modeling to provide insight into the structural differences present through modification of the carbon chain length between the Zn(II)-binding groups and the Gd(III) chelate.

The use of **Gd-daa4** for imaging intracellular Zn(II) was demonstrated in NIH/3T3 cells using the Zn(II) ionophore pyrithione to deliver Zn(II). A greater than 50% decrease in T_1 relaxation times was observed when **Gd-daa4** was incubated with Zn-pyrithione as compared to control cells. Combined results with HEPES buffer, human serum, and cellular imaging prove that **Gd-daa4** displays a relaxivity increase in the presence of Zn(II) in each of the systems indicating that this agent is a successful candidate for *in vivo* studies. Further evaluation of **Gd-daa4** for imaging Zn(II) will be continued in collaboration with Dr. Drobyshevsky and Dr. Tan at Evanston Northwestern Healthcare Research Institute. Efforts will focus on the use of **Gd-daa4** for imaging Zn(II) release in mouse brain slices after ischemia.

3.4 Experimentals

General Methods. $GdCl_3 \cdot 6H_2O$, $TbCl_3 \cdot 6H_2O$, $EuCl_3 \cdot 6H_2O$ and 1,4,7,10-tetraazacyclododecane (cyclen) were purchased from Strem Chemicals. FluoZin™-1 was purchased from Invitrogen. Isotopically labeled $^{17}OH_2$ was purchased from Cambridge Isotope Laboratories, Inc. (Andover, MA). Male human blood serum was obtained from Sigma (St. Louis, MO) (catalog no. H1388). All other chemicals were purchased and used as is from Sigma Aldrich. CH_2Cl_2, THF, DMF and MeCN were dried using a solvent system purchased from Glass Contour, San Diego, CA. Water was purified using a Millipore Milli-Q synthesis water system. Nuclear magnetic resonance

spectra were recorded on either Varian Mercury 400 MHz or Varian Inova 500 MHz using deuterated chloroform as the solvent. All spectra were referenced to an internal TMS standard. Electrospray mass spectra were obtained on a Varian 1200L single quadrupole mass spectrometer. Elemental analysis was performed by Desert Analytics Laboratory (Tucson, AZ). All samples were prepared in a 100 mM KCl/100 mM HEPES buffer at a pH of 7.4 unless otherwise noted. DO3A-tris-*tert*-butyl ester was prepared following literature procedures.[10]

***tert*-Butyl-dimethyl-[2-(3-methyl-2-nitro-phenoxy)-ethoxy]-silane (3).** To a solution of 3-methyl-2-nitrophenol (4.0 g, 26.1 mmol) in dry acetonitrile (300 mL) under nitrogen was added K_2CO_3 (9.02 g, 65.25 mmol). After the reaction turned a bright red color due to the deprotonated state of the phenol in about ten minutes, (2-bromo-ethoxy)-*tert*-butyldimethylsilane (6.68 mL, 31.32 mmol) was added. The reaction was refluxed at 70 °C until a pale yellow color was produced (several days), cooled to room temperature and filtered. After rotary evaporation of the solvent, the oil was brought up in 100 mL ethyl acetate and washed once with an aqueous saturated sodium bicarbonate solution and once with brine. The organic layer was then dried over Na_2SO_4 and concentrated in *vacuo*. The crude residue was purified on a silica gel column eluting with 3% ethyl acetate in hexanes, yielding **3** as light yellow crystals (7.33 g, 90% yield). ^{1}H NMR (500 MHz, $CDCl_3$) δ = 7.23 (t, J = 8.5 Hz, 1H), 6.88 (d, J = 9 Hz, 1H), 6.81 (d, J = 8 Hz, 1H), 4.08 (t, J = 5.5 Hz, 2H), 3.90 (t, J = 5 Hz, 2H), 2.25 (s, 3H), 0.86 (s, 9H), 0.04 (s, 6H). ^{13}C NMR (126 MHz, $CDCl_3$) δ = 150.4, 142.5, 130.9, 130.6, 122.8, 111.5, 70.9, 61.8, 26.0, 18.4, 17.0, -5.3. MS (ESI-positive) *m/z* Calcd for ($M + H^+$): 311.1, Found: 312.1.

(*tert*-Butoxycarbonylmethyl-{2-[2-(tert-butyl-dimethyl-silanyloxy)-ethoxy]-6-methyl-phenyl}-amino)-acetic acid tert-butyl ester (4). **3** (2.0 g, 6.43 mmol) dissolved in 30 mL methanol was added to a flask preloaded with 10% Pd on carbon in catalytic amounts. The reaction was set up on a hydrogen reactor at 2.5 bar for 24 hours. Upon completion of hydrogenation as determined by TLC (1:20; EtOAc:hexanes), the reaction mixture was filtered over celite and rinsed several times with methanol and concentrated via rotary evaporation of the solvent. The reduced product was then transferred to a 250 mL round bottom flask and dissolved in dry acetonitrile (60 mL). Approximately 2 equivalent of proton sponge (3.03 g, 14.15 mmol) was completely dissolved in the reaction before adding 14.15 mmol of *tert*-butyl bromoacetate followed by NaI (2.12 g, 14 mmol). After 5 days of reacting at refluxing temperatures, TLC (1:20; EtOAc:hexanes) showed two UV active spots closely running together representing the addition of one and two *tert*-butyl acetates respectively. The crude product was absorbed onto silica and purified on a silica gel column eluting with a slow gradient of 2% ethyl acetate in hexanes to 5% ethyl acetate to separate both products. The desired product **4** was isolated in 91% yield (3.0 g, 5.8 mmol). ^{1}H NMR (100 MHz, $CDCl_3$) δ = 6.97 (t, J = 8.4 Hz, 1H), 6.80 (d, J = 7.6 Hz, 1H), 6.71 (d, J = 8 Hz, 1H), 4.01 (m, 4H), 3.76 (s, 4H), 2.45 (s, 3H), 1.40 (s, 18H), 0.92 (s, 9H), 0.12 (s, 6H). ^{13}C NMR (400 MHz, $CDCl_3$) δ = 170.6, 156.6, 139.1, 137.8, 125.6, 122.7, 109.7, 80.1, 69.2, 61.7, 57.3, 27.5, 25.8, 18.5, 18.2, -5.4. MS (ESI-positive) *m/z* Calcd for ($M + H^+$): 509.3, Found: 510.2; Calcd for ($M + Na^+$): 532.3, Found: 532.2.

{*tert*-Butoxycarbonylmethyl-[2-(2-hydroxy-ethoxy)-6-methyl-phenyl]-amino}-acetic acid tert-butyl ester (5). To a solution of **4** (2.9 g, 5.59 mmol) in THF (50 mL) was added tetrabutylammonium fluoride (3.65 g, 13.98 mmol). After two hours at room temperature the

deprotection was complete as observed by TLC (1:3 EtOAc:hexanes). THF was removed via rotary evaporation. The crude product was brought up in ethyl acetate and washed once with water and then brine. The organic layer was dried over sodium sulfate, filtered, concentrated, and purified through a silica plug eluting with 25% ethyl acetate in hexanes yielding 2.17g of **5** (98.2% yield). ^{1}H NMR (400 MHz, $CDCl_3$) δ = 6.95 (t, *J* = 7.2 Hz, 1H), 6.77 (d, *J* = 7.2 Hz, 1H), 6.64 (d, *J* = 8 Hz, 1H), 4.03 (t, 2H), 3.95 (t, 2H), 3.86 (s, 4H), 2.38 (s, 3H), 1.36 (s, 18H). ^{13}C NMR (100 MHz, $CDCl_3$) δ = 172.2, 156.1, 138.3, 137.6, 125.8, 123.5, 109.7, 81.5, 67.0, 61.8, 55.8, 28.5, 19.0. MS (ESI-positive) *m/z* Calcd for (M + Na^+): 418.2, Found: 418.1.

{[2-(2-Bromo-ethoxy)-6-methyl-phenyl]-tert-butoxycarbonylmethyl-amino}-acetic acid *tert*-butyl ester (6). To a solution of **5** (2.17 g, 5.49 mmol) in anhydrous methylene chloride (55 mL) was added carbon tetrabromide (2.28 g, 6.86 mmol) followed by slow addition of triphenylphosphine (3.60 g, 13.73 mmol). After two hours at room temperature the reaction was washed with water and brine. The organic layer was dried over sodium sulfate, filtered and concentrated. The crude product was purified on a silica gel column eluting with 3% ethyl acetate in hexanes giving **6** in 46% yield (1.2 g, 2.5 mmol). ^{1}H NMR (400 MHz, $CDCl_3$) δ = 6.99 (t, *J* = 7.2 Hz, 1H), 6.83 (d, *J* = 7.2 Hz, 1H), 6.66 (d, *J* = 8 Hz, 1H), 4.28 (t, *J* = 6.8 Hz, 2H), 3.79 (s, 4H), 3.70 (d, *J* = 5.6 Hz, 2H), 2.45 (s, 3H), 1.39 (s, 18H). ^{13}C NMR (100 MHz, $CDCl_3$) δ = 171.2, 156.4, 139.9, 138.4, 126.3, 124.1, 110.4, 80.9, 68.4, 57.8, 29.9, 28.6, 19.2. MS (ESI-positive) *m/z* Calcd for (M + Na^+): 480.1, Found: 481.9.

(*tert*-Butoxycarbonylmethyl-{2-methyl-6-[2-(4,7,10-tris-tert-butoxycarbonylmethyl-1,4,7,10-tetraaza-cyclododec-1-yl)-ethoxy]-phenyl}-amino)-acetic acid tert-butyl ester (7).

To a solution of DO3A-tris-*tert*-butyl ester (1.08 g, 2.10 mmol) in 25 mL of dry acetonitrile was added K_2CO_3 (0.87 g, 6.30 mmol). After five minutes, a solution of **6** (1.16 g, 2.53 mmol) in 5 mL of dry acetonitrile was added to the reaction and the mixture was refluxed overnight. The reaction was cooled and filtered rinsing with acetonitrile and methanol. After the solvents were removed by rotary evaporation, the crude product was purified on a silica gel column eluting with 2% MeOH in CH_2Cl_2 to produce **7** in 18% yield (0.34 g, 0.4 mmol). After trituration with diethyl ether several times a pale yellow solid was obtained. ^{1}H NMR (400 MHz, $CDCl_3$) δ = 6.92 (t, J = 4.8 Hz, 1H), 6.77 (d, J = 7.6 Hz, 1H), 6.69 (d, J = 8.8 Hz, 1H), 4.11 (t, broad, 2H), 3.79 (s, 4H), 3.74 (s, 2H), 3.64 (s, 4H), 3.49-2.86 (broad, 16H), 2.18 (s, 3H), 1.44 (s, 18H), 1.39 (s, 27H). MS (ESI-positive) *m/z* Calcd for (M + Na^+): 914.6, Found: 914.4.

Acetic acid 4-(3-methyl-2-nitro-phenoxy)-butyl ester (8). In a two-neck 250 mL round bottom flask, 3-methyl-2-nitrophenol (2.0 g, 13.06 mmol) was dissolved in 100 mL dry acetonitrile. Addition of potassium carbonate (4.5 g, 32.65 mmol) results in an instant color change from yellow to red upon deprotonation of the phenol in about ten minutes. After deprotonation of the starting material, 4-bromobutyl acetate (2.27 mL, 15.67 mmol) is added and left to reflux overnight or until reaction is complete as seen by color change back to a light yellow solution. The reaction is then cooled to room temperature and filtered. After rotary evaporation of the solvent, the mixture is brought up in 100 mL ethyl acetate and washed once with an aqueous saturated sodium bicarbonate solution and once with brine. The organic layer is then dried over Na_2SO_4 and concentrated *in vacuo*. The crude mixture is purified on a silica gel column eluting with 10% EtOAc in hexanes yielding **8** as a pale yellow oil in 93% yield (3.5 g, 12.1 mmol). ^{1}H NMR (500 MHz, $CDCl_3$) δ = 7.25 (t, J = 8 Hz, 1H), 6.84 (d, J = 9 Hz, 1H),

6.82 (d, J = 8 Hz, 1H), 4.07 (t, J = 6.5 Hz, 2H), 4.04 (t, J = 6.5 Hz, 2H), 2.26 (s, 3H), 2.02 (s, 3H), 1.81 (m, 2H), 1.76 (m, 2H). ^{13}C NMR (126 MHz, $CDCl_3$) δ = 171.3, 150.3, 142.5, 131.1, 130.8, 122.8, 111.1, 68.9, 64.0, 25.8, 25.3, 21.1, 17.1. MS (ESI-positive) *m/z* Calcd for (M + Na^+): 290.1, Found: 290.0.

4-(3-Methyl-2-nitro-phenoxy)-butan-1-ol (9). Deprotection of the acetate group of **8** is achieved after an hour of stirring in 50 mL of 10% NaOH in a 1:1 (methanol:water) solution. After deprotection as observed by TLC, the reaction was neutralized with 20 mL of 0.5 M HCl. The organics were then extracted twice with diethyl ether and dried over sodium sulfated. Pure product is obtained after rotary evaporation of the solvent in quantitative yield. ^{1}H NMR (500 MHz, $CDCl_3$) δ = 7.27 (t, J = 8.5 Hz, 1H), 6.87 (d, J = 8.5 Hz, 1H), 6.83 (d, J = 8 Hz, 1H), 4.07 (t, J = 6.5 Hz, 2H), 3.66 (t, J = 6 Hz, 2H), 2.28 (s, 3H), 1.84 (m, 2H), 1.69 (m, 2H). ^{13}C NMR (126 MHz, $CDCl_3$) δ = 150.2, 142.7, 130.9, 130.7, 122.5, 111.1, 69.2, 62.2, 29.1, 25.5, 16.9. MS (ESI-positive) *m/z* Calcd for (M + Na^+): 248.1, Found: 247.9.

***tert*-Butyl-dimethyl-[4-(3-methyl-2-nitro-phenoxy)-butoxy]-silane (10).** To a solution of **9** (2.7 g, 12 mmol) in dry DMF (2 mL/g of starting alcohol) was added *tert*-butyldimethylsilyl chloride (2.17 g, 14.4 mmol) followed by imidazole (2.04 g, 30 mmol). The reaction was stirred at room temperature for 15 hours then quenched with 20 mL of water and extracted twice with ethyl acetate. The organic layers were combined and dried over sodium sulfate and filtered. After concentration *in vacuo*, the crude product was purified via silica gel chromatography eluting with 2% ethyl acetate in hexanes in 73% yield (2.9 g, 8.7 mmol). ^{1}H NMR (500 MHz, $CDCl_3$) δ = 7.27 (t, J = 8 Hz, 1H), 6.87 (d, J = 8 Hz, 1H), 6.84 (d, J = 8 Hz, 1H), 4.08 (t, J = 6

Hz, 2H), 3.66 (t, *J* = 6.5 Hz, 2H), 2.31 (s, 3H), 1.85 (m, 2H), 1.66 (m, 2H), 0.90 (s, 9H), 0.06 (s, 6H). ^{13}C NMR (126 MHz, $CDCl_3$) δ = 150.5, 131.1, 130.8, 122.6, 111.2, 99.9, 69.5, 62.8, 29.3, 26.2, 25.9, 18.5, 17.2, -5.1. MS (ESI-positive) *m/z* Calcd for (M + Na^+): 362.2, Found: 362.1.

(*tert*-Butoxycarbonylmethyl-{2-[4-(*tert*-butyl-dimethyl-silanyloxy)-butoxy]-6-methyl-phenyl}-amino)-acetic acid *tert*-butyl ester (11). **11** was synthesized following the same procedure used for **4** in 87% yield. ^{1}H NMR (500 MHz, $CDCl_3$) δ = 6.99 (t, *J* = 8 Hz, 1H), 6.79 (d, *J* = 7.5 Hz, 1H), 6.69 (d, *J* = 8 Hz, 1H), 3.98 (t, *J* = 6.5 Hz, 2H), 3.76 (s, 4H), 3.72 (t, *J* = 6.5 Hz, 2H), 2.48 (s, 3H), 1.92 (m, 2H), 1.74 (m, 2H), 1.41 (s, 18H), 0.93 (s, 9H), 0.09 (s, 6H). ^{13}C NMR (126 MHz, $CDCl_3$) δ = 170.8, 157.1, 139.4, 137.9, 126.0, 122.7, 109.6, 80.4, 67.9, 63.0, 57.8, 29.8, 28.2, 26.3, 26.1, 18.8, 18.5, -5.1. MS (ESI-positive) *m/z* Calcd for (M + H^+): 537.4, Found 538.4; Calcd for (M + Na^+): 560.3, Found: 560.4.

{*tert*-Butoxycarbonylmethyl-[2-(4-hydroxy-butoxy)-6-methyl-phenyl]-amino}-acetic acid *tert*-butyl ester (12). **12** was synthesized following the same procedure used for **5** in 93% yield. ^{1}H NMR (500 MHz, $CDCl_3$) δ = 6.99 (t, *J* = 8 Hz, 1H), 6.79 (d, *J* = 7.5 Hz, 1H), 6.70 (d, *J* = 8.5 Hz, 1H), 3.99 (t, *J* = 6 Hz, 2H), 3.78 (s, 4H), 3.74 (t, *J* = 6.5 Hz, 2H), 2.46 (s, 3H), 1.95 (m, 2H), 1.81 (m, 2H), 1.40 (s, 18H). ^{13}C NMR (126 MHz, $CDCl_3$) δ = 171.1, 156.9, 139.2, 137.8, 126.0, 122.9, 109.8, 80.7, 67.9, 62.7, 57.5, 29.7, 28.3, 26.2, 19.0. MS (ESI-positive) *m/z* Calcd for (M + H^+): 423.3, Found: 424.2; Calcd for (M + Na^+): 446.3, Found: 446.2.

{[2-(4-Bromo-butoxy)-6-methyl-phenyl]-*tert*-butoxycarbonylmethyl-amino}-acetic acid *tert*-butyl ester (13). **13** was synthesized following the same procedure used for **6** in 40% yield.

^{1}H NMR (500 MHz, $CDCl_3$) δ = 6.99 (t, *J* = 8 Hz, 1H), 6.79 (d, *J* = 8 Hz, 1H), 6.68 (d, *J* = 7.5 Hz, 1H), 3.98 (t, *J* = 5.5 Hz, 2H), 3.76 (s, 4H), 3.52 (t, *J* = 6 Hz, 2H), 2.46 (s, 3H), 2.12 (m, 2H), 1.99 (m, 2H), 1.40 (s, 18H). ^{13}C NMR (126 MHz, $CDCl_3$) δ = 170.9, 156.8, 139.4, 137.9, 126.0, 123.1, 109.7, 80.6, 67.0, 57.6, 33.8, 29.7, 28.3, 21.3, 18.9. MS (ESI-positive) *m/z* Calcd for (M + H^+): 485.2, Found: 486.1; Calcd for (M + Na^+): 508.2, Found: 510.1.

(tert-Butoxycarbonylmethyl-{2-methyl-6-[4-(4,7,10-tris-tert-butoxycarbonylmethyl-1,4,7,10-tetraaza-cyclododec-1-yl)-butoxy]-phenyl}-amino)-acetic acid tert-butyl ester (14). **14** was synthesized following the same procedure used for **7** in 53% yield. ^{1}H NMR (500 MHz, $CDCl_3$) δ = 6.97 (t, *J* = 8 Hz, 1H), 6.79 (d, *J* = 7.5 Hz, 1H), 6.68 (d, *J* = 8 Hz, 0.5H) 6.62 (d, *J* = 8 Hz, 0.5H), 4.01 (t, *J* = 5.5 Hz, 2H), 3.91 (t, *J* = 6 Hz, 2H), 3.76 (s, 2H), 3.72 (s, 4H), 3.54 (s, 2H), 3.32 (s, 2H), 3.17-2.80 (broad, 16H), 2.44 (s, 3H), 1.98 (m, 2H), 1.81 (m, 2H), 1.45 (s, 27H), 1.39 (s, 18H). MS (ESI-positive) *m/z* Calcd for (M + H^+): 919.6, Found: 920.7; Calcd for (M + Na^+): 942.6, Found: 942.7.

General metallation procedure. A TFA solution, 95 : 2.5 : 2.5 (TFA : H_2O : triisopropylsilane) was added to the protected ligands **7** and **14** for several hours. After the TFA was removed by purging the solution with air, about 15 mL of diethyl ether was added. The precipitate was centrifuged and decanted. The diethyl ether wash was repeated two more times with the final pellet being brought up in H_2O and the pH adjusted to 6.5 with 1 M NaOH. 1.1 equivalents of $GdCl_3 \cdot 6H_2O$ was then added and stirred at RT for several days. Unreacted Gd(III) precipitated as $Gd(OH)_3$ after the addition of 1 M NaOH and the crude mixture was purified by semi-preprative HPLC on a reverse phase column eluting with acetonitrile and water using an isocratic

ramp from 0% to 35% acetonitrile over 35 minutes. Analytical HPLC-MS was used to confirm the purity and identity of the collected fractions. Pure fractions were then freeze-dried and stored in a dessicator. The same procedure is followed with $EuCl_3 \cdot 6H_2O$ and $TbCl_3 \cdot 6H_2O$ to obtain the Eu(III) and Tb(III) metal complexes.

Gd-daa2 (1). Gadolinium(III)-(Carboxymethyl-{2-methyl-6-[2-(4,7,10-tris-carboxymethyl-1,4,7,10-tetraaza-cyclododec-1-yl)-ethoxy]-phenyl}-amino)-acetic acid. Analytical LC-MS showed a single peak with *m/z* (ESI-positive) Calcd for ($M + H^+$): 764.2, Found: 763.3. Anal. Calc. for $C_{27}H_{38}GdN_5O_{11} \cdot 2H_2O \cdot Na$: C 39.31, H 5.13, N 8.49. Found: C 38.95, H 5.29, N 8.31.

Tb-daa2. Analytical LC-MS showed a single peak with *m/z* (ESI-positive) Calcd for ($M + H^+$): 765.2, Found: 760.2.

Eu-daa2. Analytical LC-MS showed a single peak with *m/z* (ESI-positive) Calcd for ($M + H^+$): 759.2, Found: 758.3.

Gd-daa4 (3). Gadolinium(III)-(Carboxymethyl-{2-methyl-6-[4-(4,7,10-tris-carboxymethyl-1,4,7,10-tetraaza-cyclododec-1-yl)-butoxy]-phenyl}-amino)-acetic acid. Analytical LC-MS showed a single peak with *m/z* (ESI-positive) Calcd for ($M + H^+$): 792.2, Found: 791.2. Anal. Calc. for $C_{29}H_{42}GdN_5O_{11} \cdot H_2O \cdot 2Na$: C 40.60, H 5.17, N 8.16. Found: C 40.91, H 5.23, N 7.78.

Tb-daa4. Analytical LC-MS showed a single peak with *m/z* (ESI-positive) Calcd for ($M + H^+$): 793.2, Found: 790.1.

Eu-daa4. Analytical LC-MS showed a single peak with *m/z* (ESI-positive) Calcd for ($M + H^+$): 787.2, Found: 788.3.

Relaxivity measurements. A 1 mM solution of the gadolinium complex was made up in buffer containing 100 mM KCl/100 mM HEPES at pH = 7.4 or in human blood serum. These solutions were serially diluted four times to give 500 μL of five different sample concentrations at a [Gd]:[Zn] ratio of 1:0. Aliquots of a 5.0 mM $ZnCl_2$ solution in HEPES was added to each of the samples to give a [Gd]:[Zn] ratio of 1 : 0.5. After 30 minutes of incubation at 37 °C, T_1 measurements were performed on a Bruker mq60 Minispec relaxometer with an inversion recovery pulse sequence with the appropriate recycle delays. This titration was repeated until a 1:3 ([Gd]:[Zn]) ratio was reached.

Luminescence Lifetime Measurements. The fluorescence decay rates of the terbium analogs of **1** and **2** in buffered H_2O and D_2O were measured on a Hitachi F4500 fluorometer monitoring the emission at 544 nm with an excitation of 254 nm. Aliquots of HEPES buffer and $ZnCl_2$ in HEPES were freeze dried before bringing up in D_2O to assure there was no water present. A 200 μM solution of the terbium complex in HEPES buffer was measured in the presence of 300 μM $ZnCl_2$ and without $ZnCl_2$. Twenty-five scans were averaged and fit to a mono-exponential decay with an r^2 value of 0.99.

Calculation of Zinc-Dissociation Constants. To a 10 μM sample of $ZnCl_2$ in HEPES buffer are titrated 100 μL aliquots of 0.1 mM FluoZin-1 until saturation of fluorescence was reached. Between aliquots, 30 minutes was allowed for the reaction to reach equilibrium. Solutions of **1** and **2** at various concentrations in 10 μM $ZnCl_2$ were then titrated with FluoZin-1 in the same manner. After each aliquot of fluorophore was added, the percent saturation of fluorescence ($f = (F - F_0)/(F - F_{max})$ where F_0 is the minimum fluorescence without zinc and F_{max} is the

fluorescence when saturated with zinc, was calculated to determine the amount of Zn(II) bound to the dye. With known amounts of Zn(II), FluoZin-1, and contrast agent, the equilibrium constant was determined.

Inductively coupled plasma – atomic emission spectrometry (ICP-AES). The concentration of each sample for relaxivity and ^{17}O NMR measurements was determined by ICP-AES (Varian). A 10 µL aliquot of each sample was digested in 90 µL nitric acid. Each sample was then diluted with water to the appropriate concentration for ICP-AES analysis. Gadolinium concentrations were determined from a standardized curve of six standards ranging from 0 – 500 ppb Gd(III) measuring the emission of Gd(III) at 335.048, 336.224, and 342.246 nm.

^{17}O Transverse Relaxation Rate Measurements. Samples of each complex in water with and without Zn(II) were enriched with 1 % $^{17}OH_2$ and the ^{17}O spectra were obtained at 54 MHz at temperatures ranging from 5 °C to 75 °C in 5 °C increments. The ^{17}O transverse relaxation rate was determined by obtaining the line width at half of the peak height, $\Delta\nu_{1/2}$, of the ^{17}O water signal. The plots of R_{2p} versus temperature were fit according to the Swift-Connick theory using the calculated hydration numbers and concentration of Gd(III) as determined by ICP-AES.[17]

Chapter 4

Investigating the Mechanism of Activation of Zn(II)-Responsive Contrast Agents

Adapted from:

Major, J. L., Boiteau, R. M., Meade, T. J. "Investigation into the Mechanism of Zn(II)-Activated MRI Contrast Agents." *Inorg. Chem.* to be submitted.

4.1 Introduction

Lanthanide ions can adopt a coordination number of up to nine due to their available *f*-orbitals. The Gd(III) aqua ion is often considered to have a coordination of eight.[1] The safe administration of Gd(III) for MRI requires chelation to mask the cytotoxic effects of the Gd(III) ion. Most often, the poly(amino-carboxylate) ligands used for chelation provide eight coordinating oxygen and nitrogen atoms leaving the ninth coordination open for water access. Gd-DOTA and Gd-DTPA fall into this category (**Figure 4.1 A** and **B**). The Gd-DO3A complex, a commonly used chelate for the development of activated contrast agents such as the ones described in this thesis, only contains seven coordinating atoms and a hydration number of two (**Figure 4.1 C**). However, the increase in hydration number reduces the log K_d from 25 for Gd-DOTA to 21 for Gd-DO3A.[2] Each of these ligands results in a total coordination number of nine. However, there are examples of contrast agents with a coordination number eight. An example of this type of coordination is represented by Gd-TREN-1-Me-3,2-HOPO that binds Gd(III) through six oxygen atoms with two open coordination sites for water.[3] In this case, the ninth coordination site is blocked by the capping amine of the ligand (**Figure 4.1 D**).

The contrast agents discussed in Chapters 2 and 3 have only seven coordinating atoms available from the macrocyclic chelate and two available Zn(II)-binding aminoacetates. Based on relaxivity and fluorescence luminescence studies previously discussed, when there is no Zn(II) present, the agent exists in a closed $q = 0$ complex. In the presence of Zn(II), the hydration was determined to be one. This result brought into question the total coordination number of the complexes and the role of the coordinating acetate groups in the mechanism of activation.

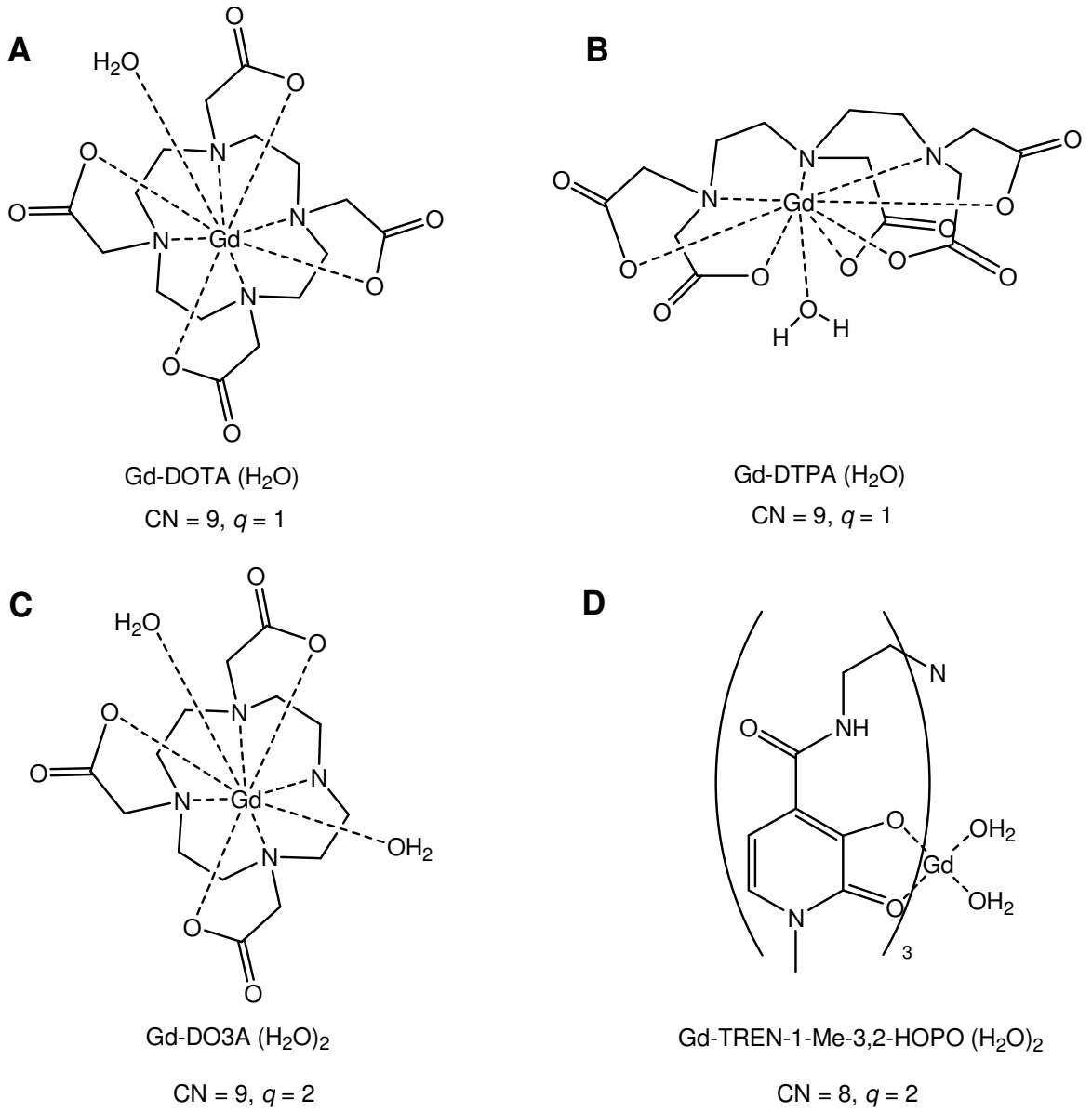

Figure 4.1 Gd(III) complexes used as MRI contrast agents with a total coordination number of eight or nine.

There are three possible scenarios that can be envisioned to support the previous findings that are outlined in **Figure 4.2**. The first (**A**) is the proposed mechanism presented in Chapter 2, in which the closed structure has a coordination of nine with both Zn(II)-binding aminoacetates contributing to the chelation of Gd(III). In the open state, both aminoacetates bind Zn(II) leaving seven coordinating arms from the chelate and allowing the access of one water molecule creating a complex with a coordination number of eight. The second possibility (**B**) would have the same closed coordination structure as described in the first example but will only have one aminoacetate participating in the binding of Zn(II). This scenario would provide a complex with a total coordination of nine in both the closed and open state. The final possibility (**C**) would be with both the closed and open complex having a total coordination of eight. In this case, only one aminoacetate would participate in the binding to Gd(III) to create a closed structure.

To study the role of the aminoacetates in the blocking of water from Gd(III), a series of agents with varying Zn(II)-binding groups are introduced. The four agents investigated in this chapter provide evidence of the mechanism of activation for Zn(II)-responsive contrast agents. The original Zn(II)-responsive contrast agent, **Gd-daa3**, has two aminoacetate arms that are proposed to change metal-binding coordination upon the addition of Zn(II). Three new agents are introduced in which the proposed Zn(II)-binding groups are modified with one or two pyridyl groups (**Gd-apa3** and **Gd-dpa3**, respectively) or with the complete removal of one of the coordinating aminoacetate arms (**Gd-aa3**) (**Figure 4.3**). Through investigation of their relaxivities, hydration numbers, and zinc-dissociation constants it was determined that two coordinating arms are necessary for the binding of Zn(II) while only one acetate arm is required to provide a coordinatively saturated Gd(III) metal center. This suggests that through variation of the second coordinating arm, a series of ion-responsive agents can be designed for future

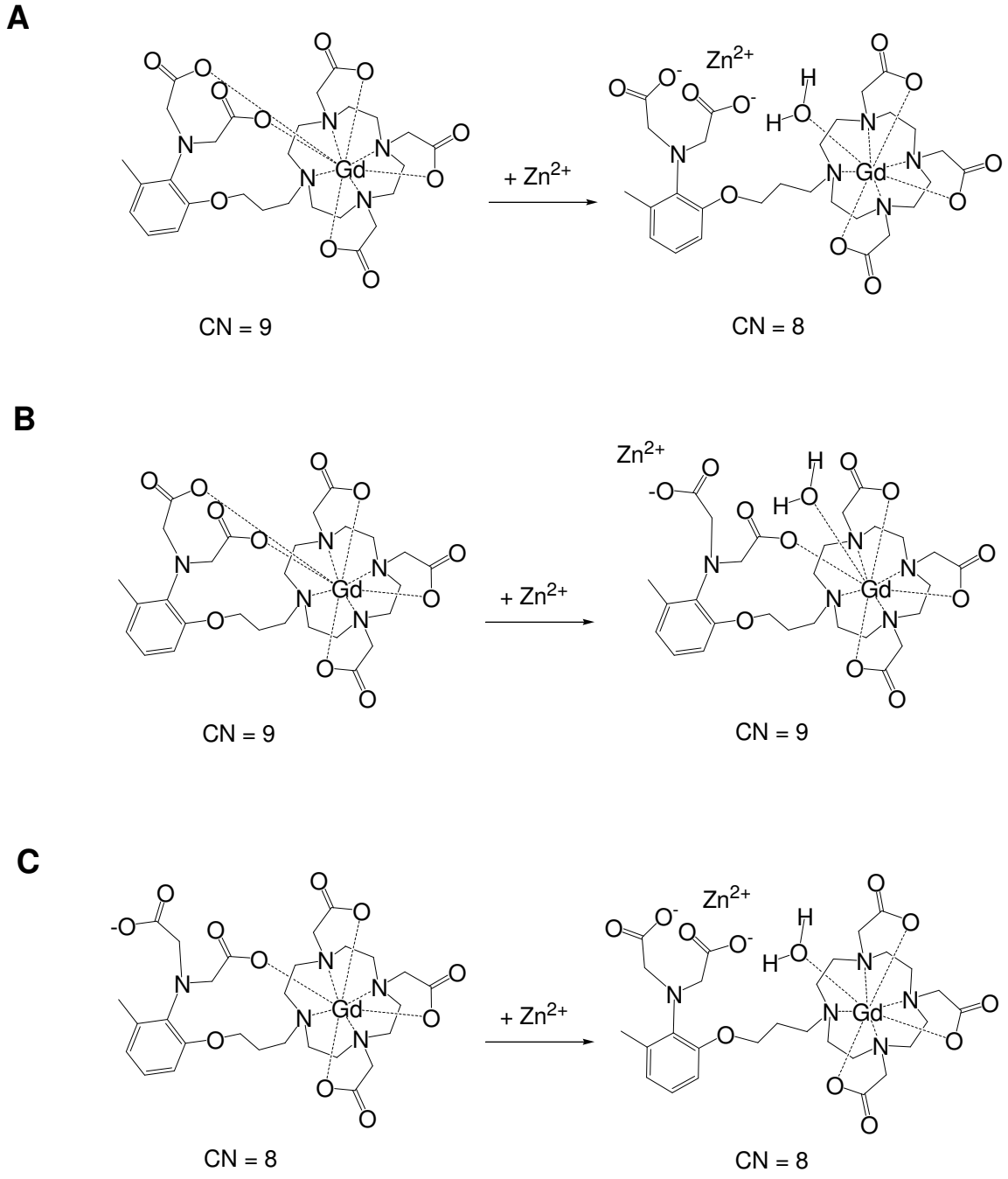

Figure 4.2. Three possible mechanisms for activation of the Zn(II)-responsive MRI contrast agent **Gd-daa3** and the resulting coordination environments. **A**. Closed structure has a coordination number of 9 and changes to a coordination number of 8 in the open structure. **B**. Both closed and open structures have a coordination number of 9. **C**. Both closed and open structures have a coordination number of 8.

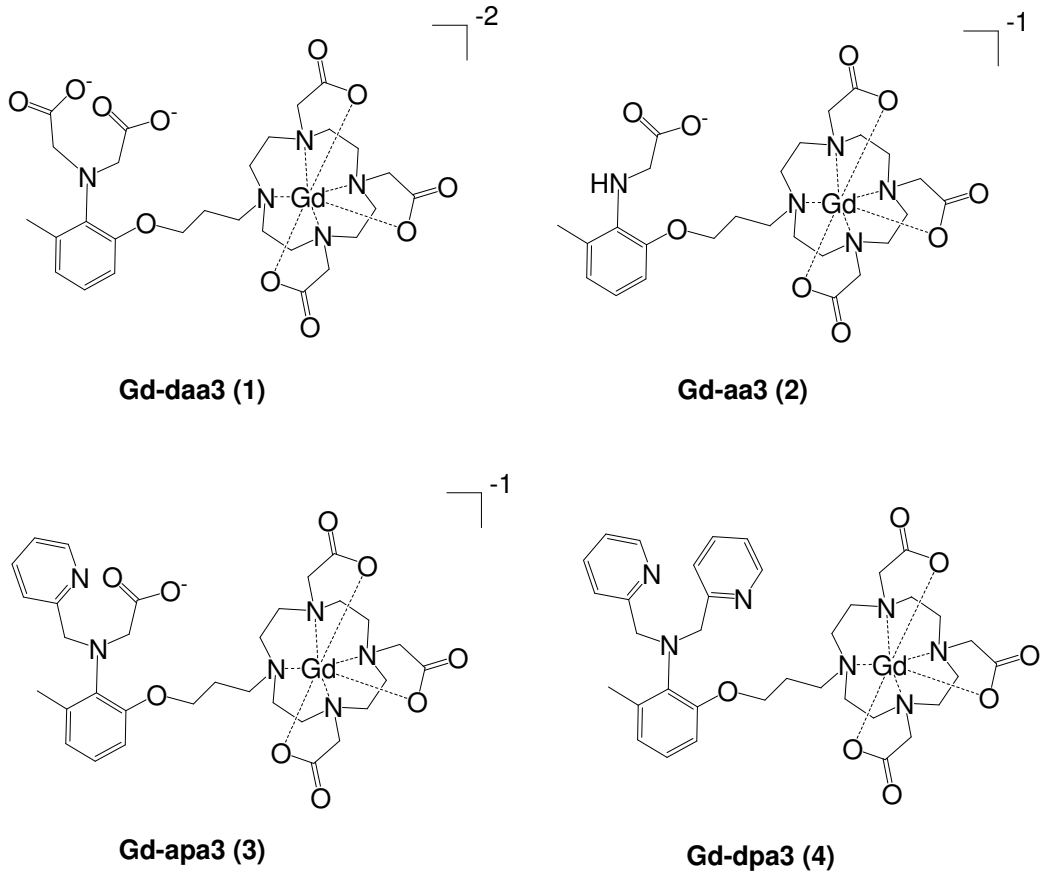

Figure 4.3. A series of Zn(II)-responsive contrast agents with varying Zn(II)-binding groups.

contrast agents. In addition, ^{13}C isotopic labeling of the europium version of **Gd-daa3** was synthesized. NMR spectroscopy studies in the absence and presence of Zn(II) confirm the binding event of Zn(II) takes place through the two aminoacetate arms as proposed.

4.2 Results and Discussion

4.2.1 Synthesis and Characterization

To study the role of aminoacetates in the binding of Gd(III) and Zn(III) a series of contrast agents with varying Zn(II)-binding groups was designed. The first new agent provides only one aminoacetate arm (**Gd-aa3** (aa = **a**mino**a**cetate)) to determine if a coordination number of eight will allow the complete blocking of water from Gd(III). Zn(II) displays characteristics of both hard and soft Lewis acids allowing it to form bonds with hard oxygen ligands as well as with softer nitrogen ligands.[4] With this in mind, complexes incorporating pyridyl rings as Zn(II)-binding groups were designed. The DTPA-based Zn(II)-responsive agents created by Nagano and coworkers discussed in Chapter 1, show the pyridyl groups exhibit little binding affinity towards Gd(III) yet still have the ability to bind Zn(II).[5, 6] The replacement of one aminoacetate arm of the original Zn(II)-responsive agent **Gd-daa3** with a pyridyl group to make **Gd-apa3** (apa = **a**cetate and **p**icoly**a**mine) is expected to provide a coordination of eight in the non-active state due to the binding of the aminoacetate to Gd(III). It is expected to be able to bind Zn(II) as well as to create an open complex for access of water. Replacement of both aminoacetates with two pyridyl groups provides **Gd-dpa3** (dpa = **d**i**p**icoyl**a**mine). This agent is not likely to create a closed complex but is expected to provide evidence of Zn(II) binding.

The synthesis and characterization of **Gd-daa3 (1)** was accomplished as previously described in Chapter 2. **Gd-aa3 (2)**, having only one aminoacetate binding arm, is an impurity

from the synthesis of **1** that is collected during HPLC purification. Elemental analysis of the final gadolinium complex was used to confirm purity.

The synthesis of **Gd-apa3 (3)** and **Gd-dpa3 (4)** is outlined in **Scheme 4.1**. Starting with the commercially available 3-methyl-2-nitrophenol, 1,3-dibromopropane was added using potassium carbonate in dry acetonitrile to give **5**. DO3A-tris-*tert*-butyl ester was synthesized following literature procedure[7] and combined with **5** with potassium carbonate as a base to yield **6**. For the synthesis of **Gd-apa3** the nitro group of **6** was reduced under standard palladium-catalyzed hydrogenation conditions and reacted with one equivalence of *tert*-butylbromoacetate. The formation of **7** with the addition of only one acetate arm is carefully monitored by thin layer chromatography to avoid formation of the product with two acetate arms. After purification of **7**, the final Zn(II) binding group was added with one equivalent of the commercially available 2-methylbromopyridine hydrobromide salt to yield the protected ligand **8**. To synthesize **Gd-dpa3**, after reduction of the nitro group, two equivalents of 2-picoyl chloride are added in the presence of potassium carbonate in acetonitrile under refluxing conditions to yield **9**.

To create the final metal complexes, the *tert*-butyl protecting groups of both **7** and **9** were removed with trifluoroacetic acid in the presence of triisopropylsilane and water. After precipitation of the deprotected ligands with diethylether they were reacted with $GdCl_3$ at a pH of 6.5 for two days. The final compounds **Gd-apa3** and **Gd-dpa3** were then purified by semi-preparatory HPLC and characterized by LC-MS and elemental analysis.

In addition to the synthesis of complexes **1-4**, ^{13}C isotopic labeling of the aminocarboxylates of **Eu-daa3** was synthesized following the procedures outlined in **Scheme**

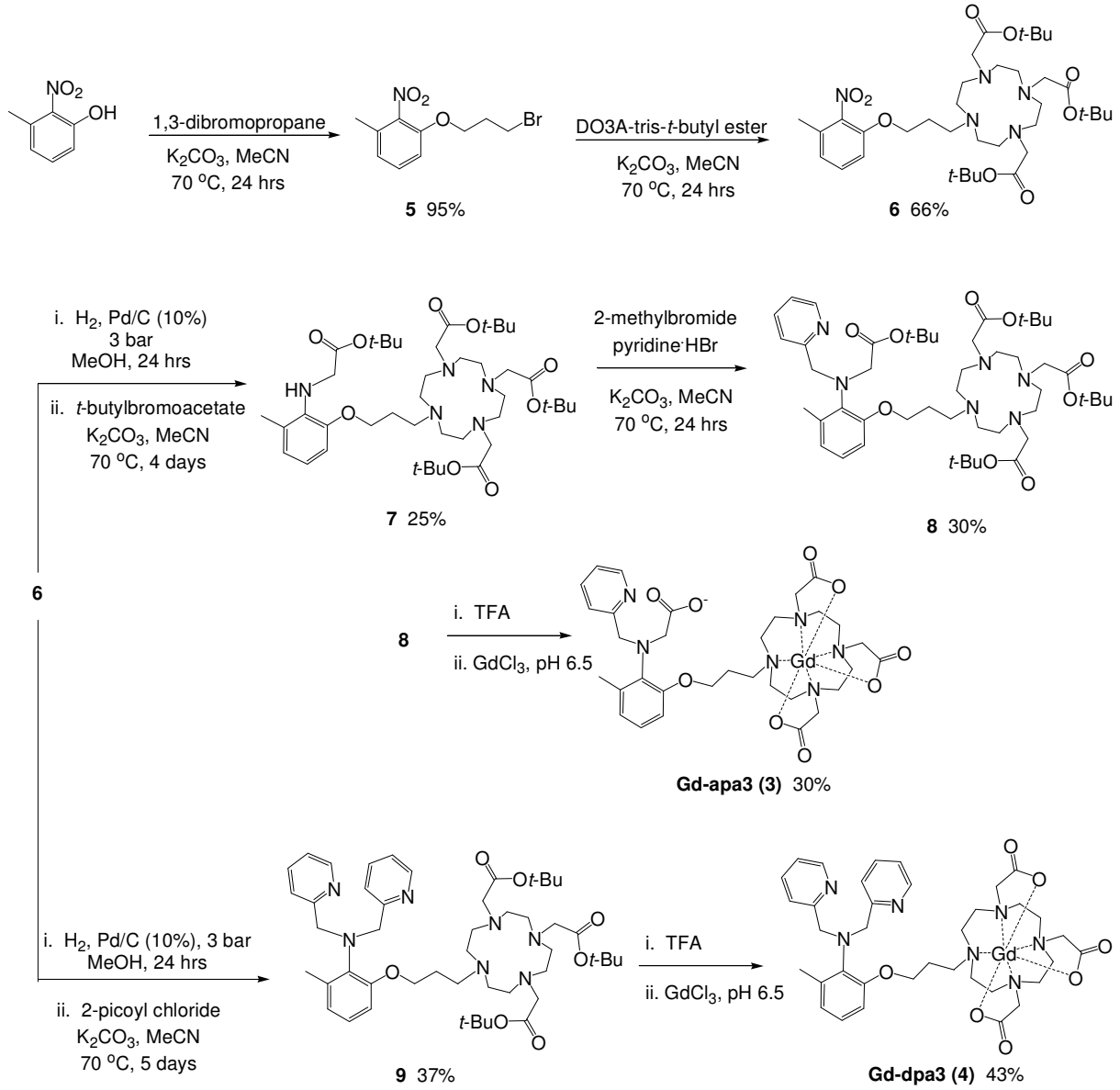

Scheme 4.1. The synthesis of **Gd-apa3 (3)** and **Gd-dpa3 (4)**.

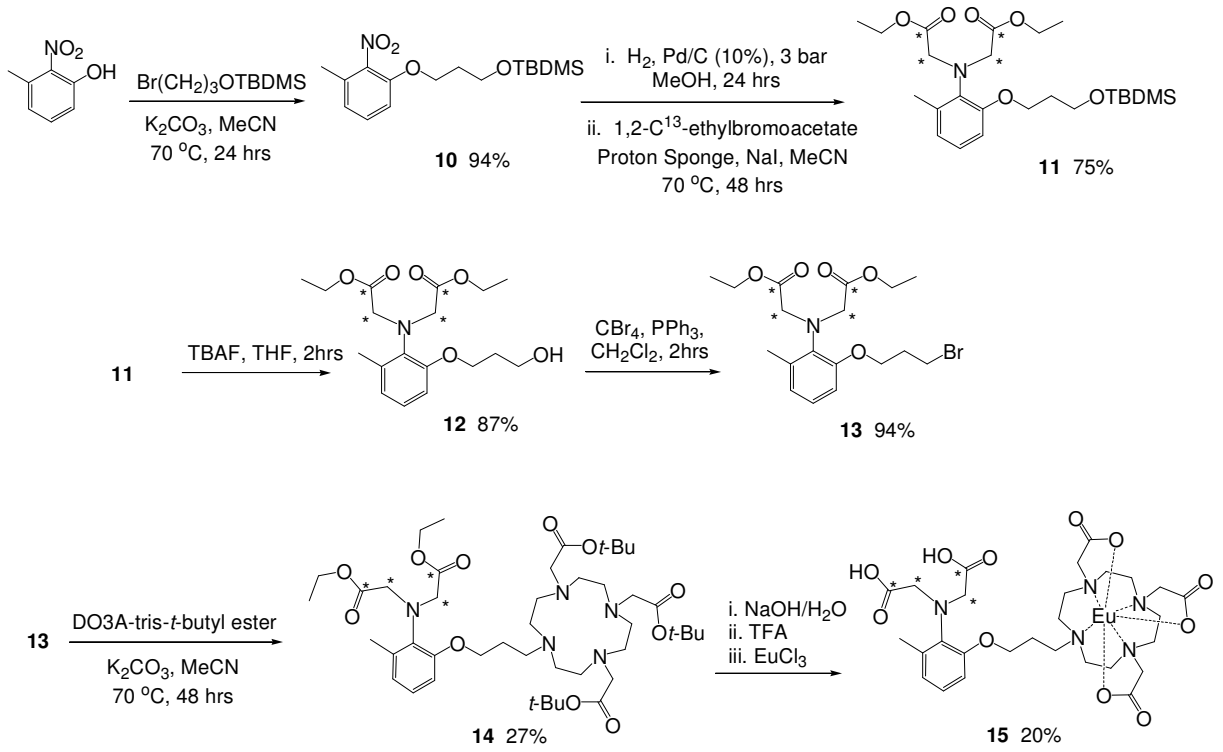

Scheme 4.2. The synthesis of the ^{13}C isotopically labeled **Eu-daa3** (* = ^{13}C).

4.2 to study the binding properties of the aminoacetates using NMR spectroscopy. The synthesis began with alkylation of the commercially available 3-methyl-2-nitrophenol with the *tert*-butyldimethylsilyl protected alcohol to give **10**. After standard palladium-catalyzed hydrogenation conditions the two aminoacetate arms were added using 1,2-^{13}C-ethyl bromoacetate in the presence of proton sponge and sodium iodide. Deprotection of the TBDMS protecting group was achieved with tetrabutylammonium fluoride to yield **12** that was brominated with carbon tetrabromide in the presence of triphenylphosphine to give **13**. Addition of DO3A-tris-*tert*-butyl ester was achieved with potassium carbonate in acetonitrile under refluxing conditions to give the fully protected ligand **14**. The ethyl groups were deprotected through the addition of 1 M NaOH at room temperature. After neutralization, the *tert*-butyl groups were deprotected with trifluoroacetic acid before addition of the metal with $EuCl_3$. The final compound was purified by semi-preparatory HPLC and characterized by analytical LC-MS.

4.2.2 Relaxivity

To evaluate the binding properties of the aminoacetate and pyridyl groups employed in complexes **1-4**, their relaxivity was first measured in the absence of Zn(II) at 60 MHz and 37 °C in HEPES buffer to measure their effectiveness in binding Gd(III). As seen in **Figure 4.4**, with the exception of **Gd-dpa3** containing two pyridyl groups, the complexes with one or two aminoacetates were able to bind Gd(III) and thus create a low relaxivity closed complex. The high relaxivity of **Gd-dpa3**, 7.5 $mM^{-1}s^{-1}$, illustrates the inability of the pyridyl nitrogens to bind the Gd(III) and therefore cannot effectively block water access to Gd(III). The lowest relaxivity observed is for **Gd-daa3**, suggesting that both carboxylic acids participate in the binding of Gd(III) as depicted in **Figure 4.2 A** and **B**. The two complexes containing only one

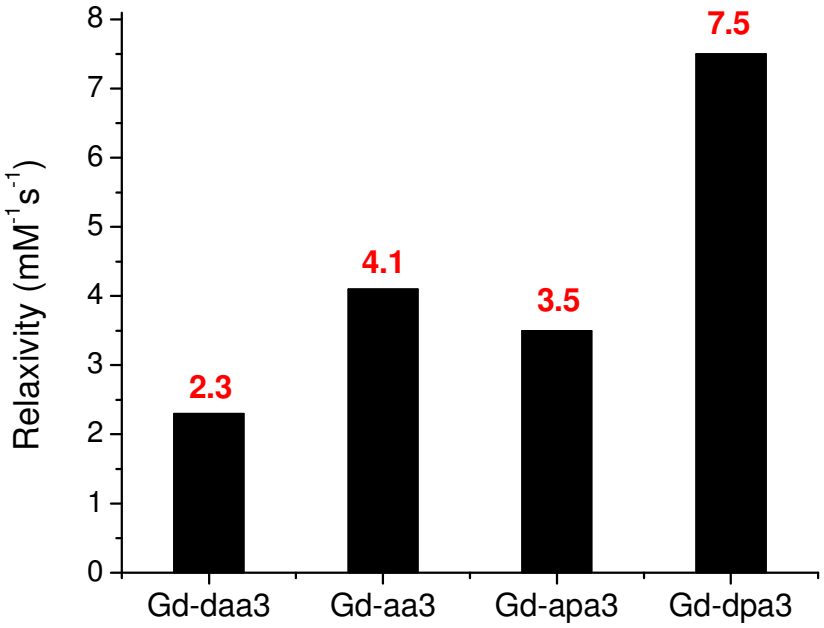

Figure 4.4. Relaxivities of **1-4** at 60 MHz and 37 °C in the absence of Zn(II) in HEPES buffer.

aminoacetate do not have as low of a relaxivity as observed for **Gd-daa3** but still have the ability to bind Gd(III) and effectively block the access of water. This result suggests that a coordination number of eight can provide a closed complex as shown in **Figure 4.2 C**. The slightly lower relaxivity for **Gd-apa3** compared to **Gd-aa3** may likely be due to the added steric effects in blocking water from the second arm even though it is not coordinating to the Gd(III).

In the presence of one equivalent of $ZnCl_2$, the relaxivity of both **Gd-daa3** and **Gd-apa3** increase by 114% and 99%, respectively, while there was no significant change in relaxivity for **Gd-aa3** (**Figure 4.5**). What is most striking about these results is that **Gd-aa3** remains in a closed structure when Zn(II) is added to the solution. This is the only complex with only one available binding group suggesting that two binding groups are necessary for binding Zn(II). Therefore, the mechanism proposed in **Figure 4.2 B** would not be plausible as Zn(II) must be coordinated to two arms to create an open sturcutre.

Since **Gd-dpa3** was not able to create a closed structure when no Zn(II) was present, it was expected that there would be no change in its relaxivity with the addition of Zn(II), as was observed. These studies support the theory that pyridyl nitrogens do not provide enough nucleophilicity to coordinate Gd(III). However, while there was no observable change in relaxivity, fluorescent binding assays (Section 4.2.4) show that the pyridyl groups can bind Zn(II).

Relaxivity studies done in male human serum showed a similar trend as seen in HEPES buffer (**Figure 4.6**). Both **Gd-daa3** and **Gd-apa3** display a 20% increase in relaxivity in the presence of $ZnCl_2$ while **Gd-aa3** and **Gd-dpa3** show slight decreases. As discussed in previous chapters, the relaxivity values are much higher in serum due to interactions with the protein human serum albumin.

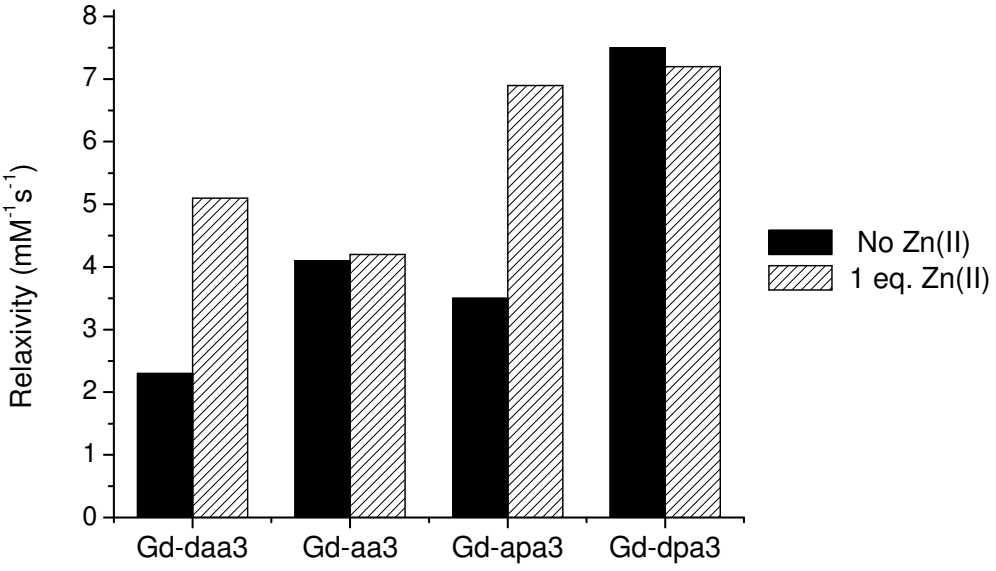

Figure 4.5. Relaxivities of **1-4** at 60 MHz and 37 °C before and after addition of $ZnCl_2$ in HEPES buffer.

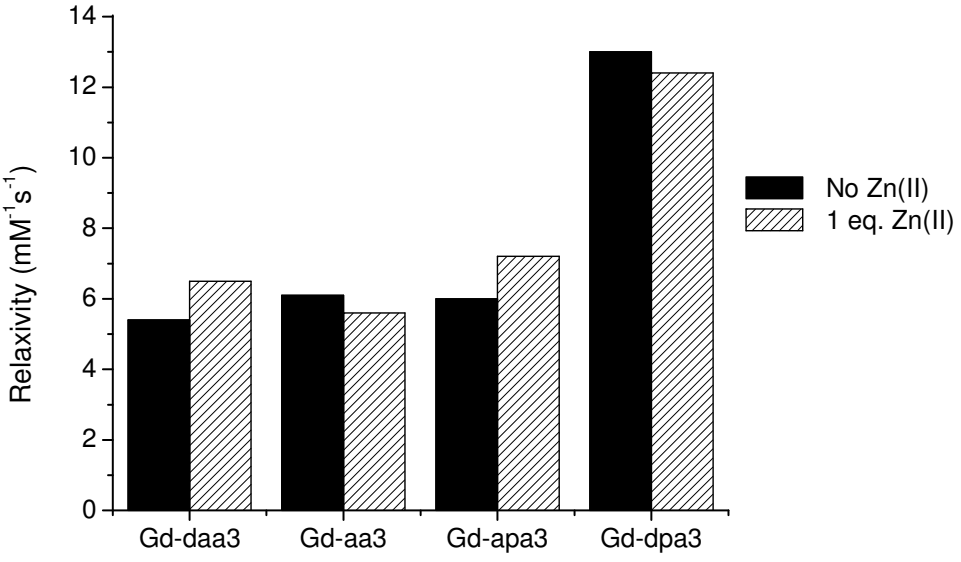

Figure 4.6. Relaxivities of **1-4** at 60 MHz and 37 °C in male human serum before and after addition of Zn(II).

4.2.3 Hydration Number (q)

The relaxivity studies presented above show that in the absence of Zn(II), compounds with at least one available aminoacetate arm to bind Gd(III) have low relaxivity values as would be expected for a q = 0 complex. To determine if in fact an eight-coordinate complex could provide a coordinatively saturated complex, the hydration numbers (q) of the terbium analogs of **Gd-daa3**, **Gd-apa3**, and **Gd-dpa3** were determined using time-based fluorescence microscopy measurements. The fluorescence decay rates of the Tb(III) analogs in water and D_2O both with and without Zn(II) were measured to calculate q. Due to more efficient vibronic coupling of the Tb(III) excited state to the O-H oscillators than to the O-D oscillators, a shorter luminescence lifetime is observed in H_2O than in D_2O.[8, 9] The number of coordinated water molecules is then calculated using equation **4.1**.[10]

$$q = 4.2 \text{ ms}\left[\left(\frac{1}{\tau_{H2O}}\right) - \left(\frac{1}{\tau_{D2O}}\right) - 0.06\right] \qquad \textbf{Equation 4.1}$$

The fluorescence lifetimes and calculated q values are summarized in **Table 4.1**. These measurements confirm that a saturated Gd(III) complex with a hydration number of zero can be accomplished with only eight coordinating atoms. Additonally, a hydration number of one is seen for both **Tb-daa3** and **Tb-apa3** as expected after binding Zn(II). The hydration numbers calculated for **Gd-dpa3** confirm that in the absence of Zn(II) the lone pair on the nitrogen of the pyridyl groups do not provide enough nucleophilicity to bind Gd(III) and effectively create a closed structure. Therefore, the hydration number in the absence and presence of Zn(II) remains unchanged.

Table 4.1. Fluorescence decay lifetimes of **Tb-daa3, Tb-apa3,** and **Tb-dpa3** in H_2O and D_2O and their calculated *q* values with an error of +/- 0.1.

	τ H_2O (ms)	**τ D_2O (ms)**	***q*** **Zn(II)**	**τ H_2O (ms) + Zn(II)**	**τ H_2O (ms) + Zn(II)**	***q*** **+ Zn(II)**
Tb-daa3	1.97	2.71	0.3	1.46	2.65	1.0
Tb-apa3	1.76	2.21	0.2	1.63	2.67	0.8
Tb-dpa3	1.21	2.33	1.4	1.18	2.33	1.5

4.2.4 Zinc Dissociation Constants

The ability of these agents to bind Zn(II) was investigated by a competition assay with the Zn(II)-binding fluorophore FluoZin-1 that binds Zn(II) through two aminoacetate arms. The fluorescent titration curves for **Gd-aa3**, **Gd-apa3**, and **Gd-dpa3** are shown in **Figures 4.7-4.9** respectively. The Zn(II)-dissociation constants presented in **Table 4.2** were determined following procedures outlined in Chapter 2. Dissociation constants in the hundreds of micromolar range are found for **Gd-daa3**, **Gd-apa3**, and **Gd-dpa3**, all of which contain two Zn(II)-binding groups. Conversely, **Gd-aa3**, having only one available Zn(II)-binding group, shows a dissociation constant in the millimolar range. This result is consistent with our previous findings in that a change in the coordination geometry around Gd(III) is only possible when there are two available Zn(II)-binding groups. Another important discovery is that **Gd-dpa3** shows a Zn(II)-dissociation constant on the same order of magnitude as that seen for **Gd-daa3** and **Gd-apa3**. While there was no observable change in relaxivity or hydration number for **Gd-dpa3**, these studies suggest that with the two available pyridyl groups, Zn(II) binding is still possible.

4.2.5 Mean Residence Lifetime of Water Protons (τ_m)

The water exchange rate can be determined directly from variable temperature ^{17}O NMR measurements. The line width of the ^{17}O NMR signal were measured both with and without zinc for variable temperature (VT), proton-decoupled ^{17}O NMR. R_{2p} at each temperature is then calculated using $R_{2p} = \Delta\nu_{1/2}*\pi$ and plotted against temperature. The experimental data was fit to the Swift-Connick theory (outlined in Chapter 3) to determine τ_m.[11, 12] Plots of R_{2p} for **Gd-apa3** and **Gd-dpa3** are presented in **Figures 4.10** and **4.11** respectively. The plots for **Gd-apa3** and

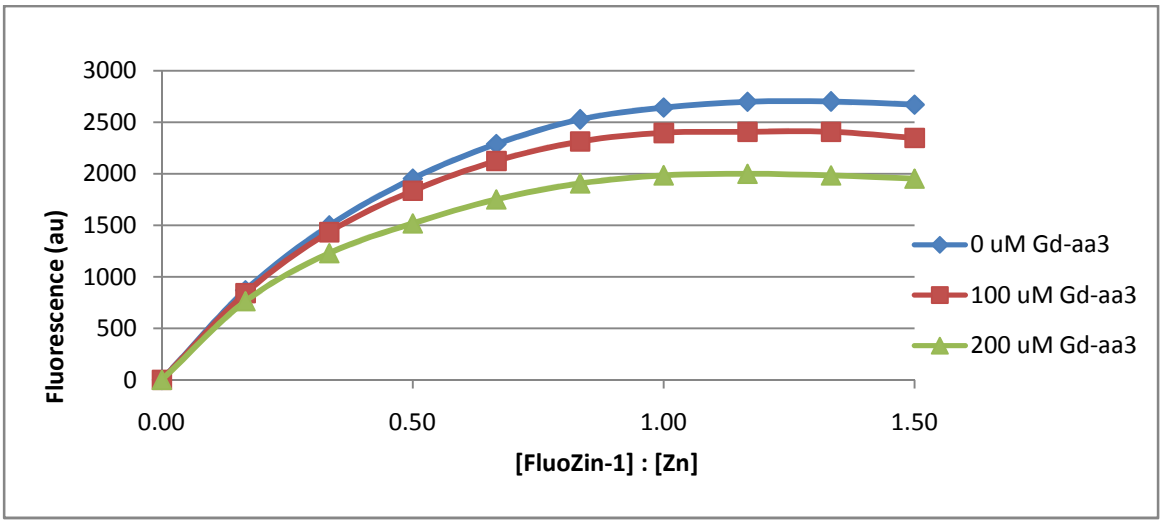

Figure 4.7. Observed titration curves of FluoZin-1 with Zn(II) at varying concentrations of **Gd-aa3** measuring the fluorescence at λ_{em} = 515 nm in HEPES buffer at a pH of 7.4.

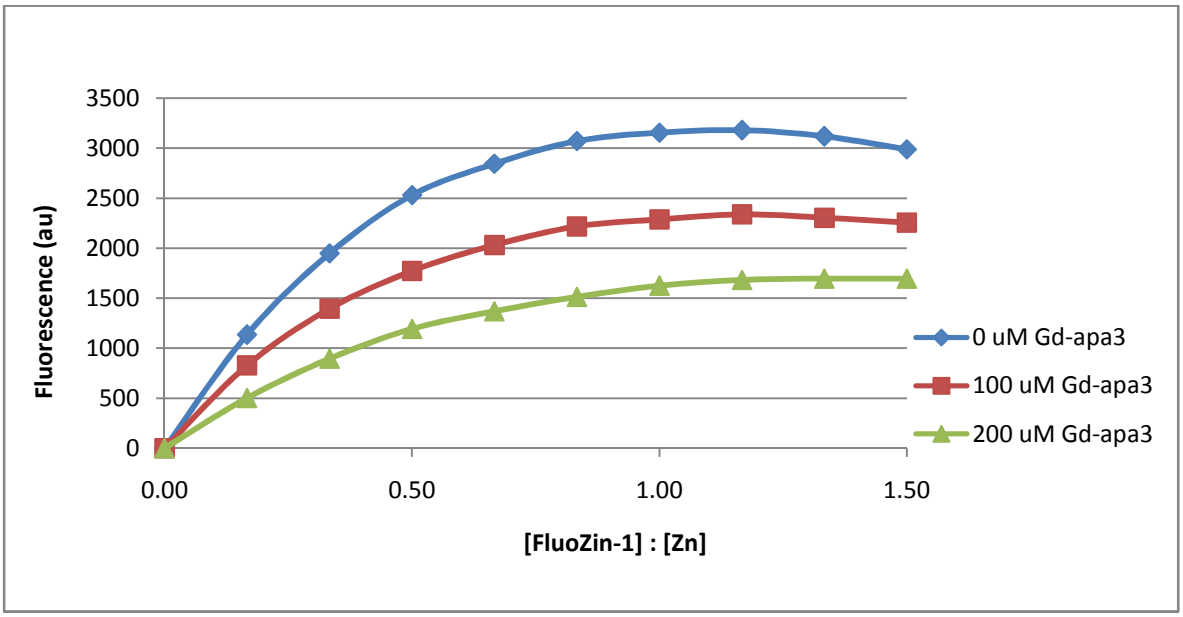

Figure 4.8. Observed titration curves of FluoZin-1 with Zn(II) at varying concentrations of **Gd-apa3** measuring the fluorescence at λ_{em} = 515 nm in HEPES buffer at a pH of 7.4.

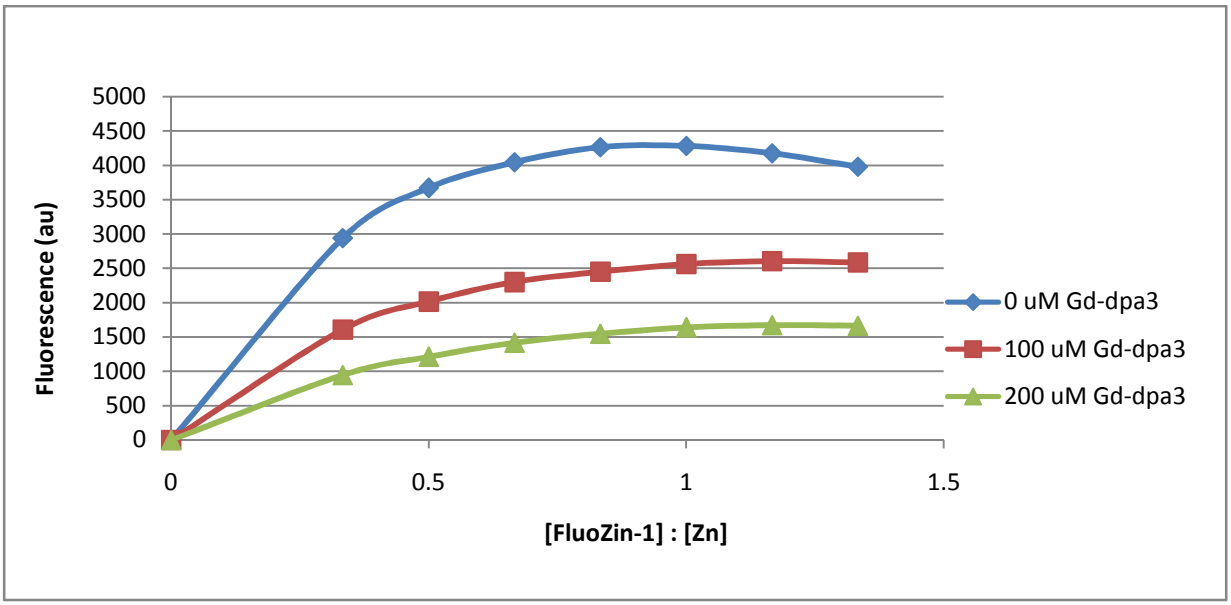

Figure 4.9. Observed titration curves of FluoZin-1 with Zn(II) at varying concentrations of **Gd-dpa3** measuring the fluorescence at λ_{em} = 515 nm in HEPES buffer at a pH of 7.4.

Table 4.2. Zn(II)-dissociation constants calculated for **1-4**.

	Zn(II) K_d (M)
Gd-daa3	2×10^{-4}
Gd-aa3	4×10^{-3}
Gd-apa3	4×10^{-4}
Gd-dpa3	1×10^{-4}

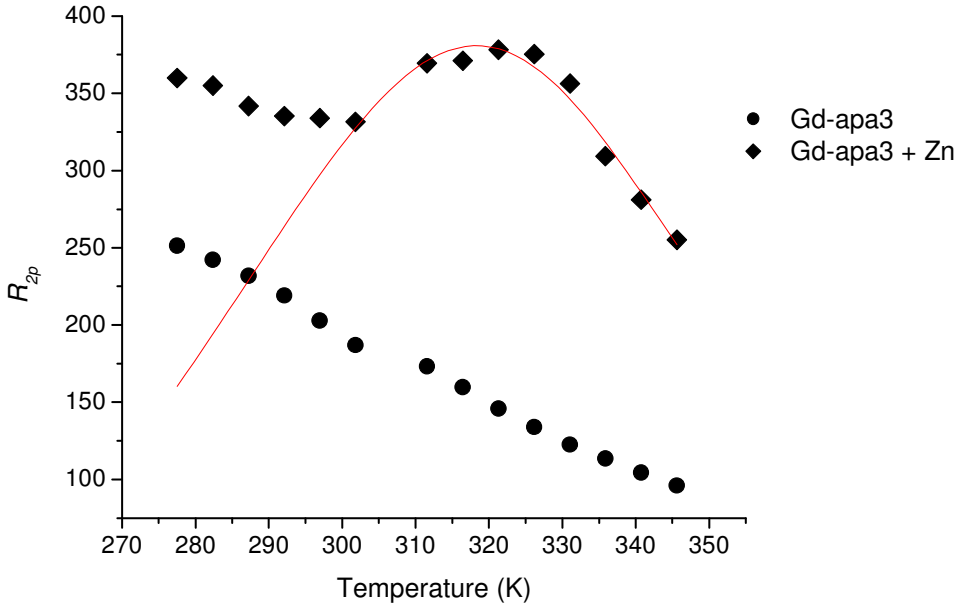

Figure 4.10. ^{17}O transverse relaxation rates with variable temperature for **Gd-apa3** at 54 MHz with and without Zn(II) showing the fit to the experimental data for **Gd-apa3 + Zn** (red line). The least-squares fitting procedure[11] gave [Gd] = 0.02 mM, τ_m = 197 ns, ΔH_M = 45.5 kJ mol^{-1}, T_{1e} = 14.4 ns, and q = 1. The hyperfine coupling constant was taken to be A/h = -3.8 × 10^6 rad s^{-1}.

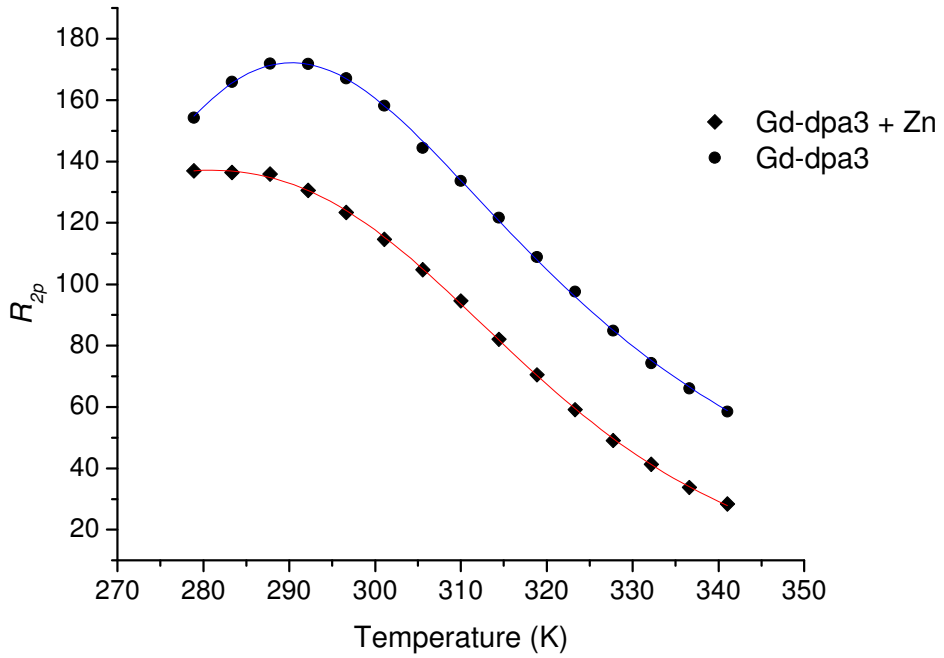

Figure 4.11. ^{17}O transverse relaxation rates with variable temperature for **Gd-dpa3** at 54 MHz with and without Zn(II) showing the fit to the experimental data for both plots. For **Gd-dpa3 + Zn** the least-squares fitting procedure[11] gave [Gd] = 0.018 mM, τ_m = 10.8 ns, ΔH_M = 47.2 kJ mol^{-1}, T_{1e} = 4.7 ns, and q = 1.5 (red line). For **Gd-dpa3** without Zn(II) the fitting parameters gave [Gd] = 0.02 mM, τ_m = 6.2 ns, ΔH_M = 25.5 kJ mol^{-1}, T_{1e} = 11.5 ns, and q = 1.5 (blue line). The hyperfine coupling constant was taken to be $A/h = -3.8 \times 10^6$ rad s^{-1} for both plots.

Gd-dpa3 in the presence of Zn(II) exhibit characteristic R_{2p} dependencies on temperature that are expected.[13] There are slight deviations from the curve at low temperature for **Zn-Gd-apa3** most likely due to the presence of the twisted square-antiprism isomer which provides a faster water exchange rate.[14] The plots for **Gd-apa3** and **Gd-dpa3** in the absence of Zn(II) could not produce a best-fit curve due to the limited access of water to Gd(III) in the closed structure. This was the case for **Gd-aa3** as well both with and without Zn(II) (data not shown).

The water residence lifetimes calculated from these curves provide a τ_m equal to 197 ns for **Gd-apa3** and 7.5 ns for **Gd-dpa3**. These are within the range of 10-1000 ns commonly seen for DOTA derivatives.[13] The low τ_m found for **Gd-dpa3** is expected due to the high hydration number of 1.5. The seven coordinating atoms from the ligand allows the possibility of two water molecules to bind Gd(III). A hydration number of 1.5 and a low τ_m suggests that the mechanism of water exchange in **Gd-dpa3** is associative. However, comparison of the residence lifetime calculated for **Gd-apa3** and that calculated for **Gd-daa3** in Chapter 3 (112 ns) suggests that the replacement of an amine with a pyridyl group results in reduction of the water exchange rate. This finding can most likely be explained by the hydrophobic character of the pyridyl groups causing repulsion of the water molecules. Further investigation with variable pressure NMR spectroscopy to determine the volume of activation of the water binding site would help determine if this was the case.

4.2.6 Europium NMR

In order to investigate the Zn(II)-binding event of the diaminoacetate arms the europium(III) analog of **Gd-daa3** was synthesized with carbon-13 isotopic labeling of the aminoacetate groups. In the closed structure with no Zn(II) present there is no visible carbon

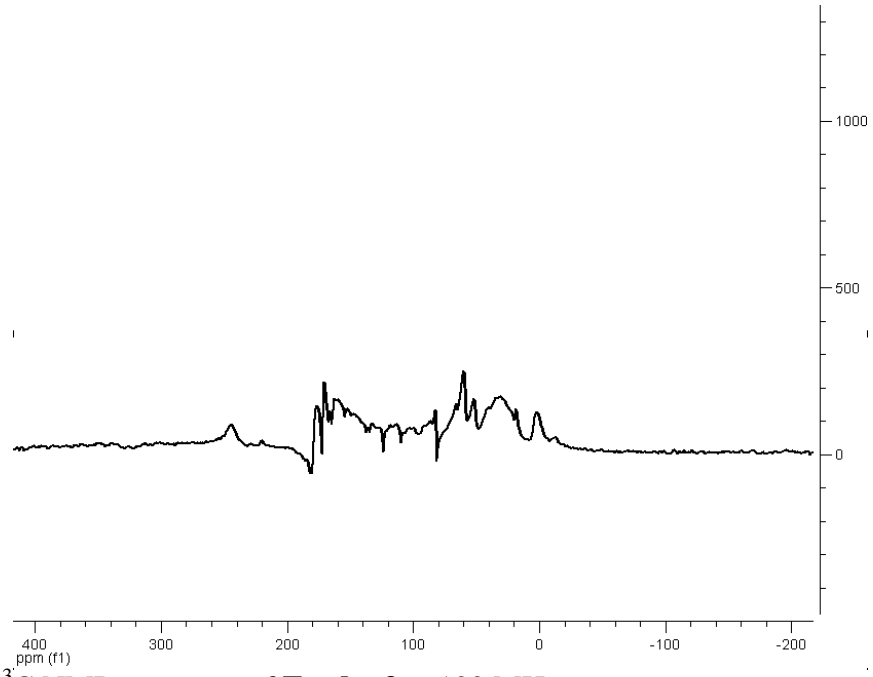

Figure 4.12. ^{13}C NMR spectrum of **Eu-daa3** at 100 MHz.

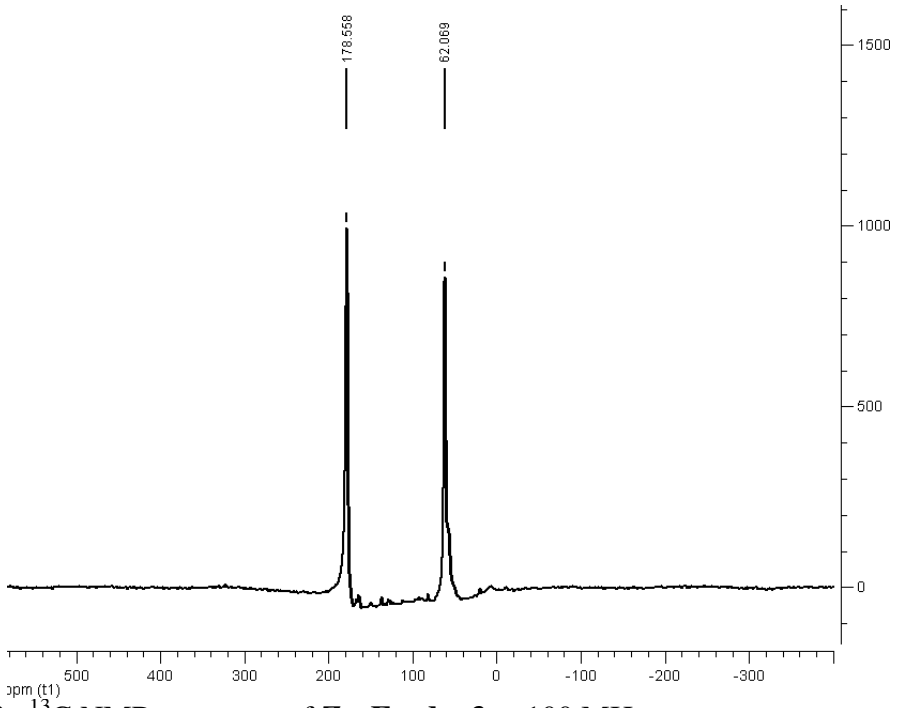

Figure 4.13. ^{13}C NMR spectrum of **Zn-Eu-daa3** at 100 MHz.

shifts due to the line-broadening effects of the paramagnetic Eu(III) metal center when the acetate arms are bound to Eu(III) (**Figure 4.12**) even after a 12 hour scan. Upon the addition of Zn(II) to the same sample, two peaks are immediately observed in the carbon NMR spectrum corresponding to the two isotopically labeled carbons on the aminocetates with shifts at 178 ppm for the carbonyl and 62 ppm for the methylene (**Figure 4.13**). When bound to Zn(II) and not bound directly to the Eu(III) metal, the line broadening due to the paramagnetism is greatly reduced resulting in two clear carbon shifts that were not previously observed. These studies provide direct evidence of the interaction of the aminoacetates with the two different metal ions. If only one aminoacetate arm was bound to Zn(II) in the closed structure as for the mechanism proposed in **Figure 4.2 C**, two carbon peaks would be seen before the addition of Zn(II). As this is not the case, **Figure 4.2 C** can be ruled out as a possible mechanism.

4.3 Conclusions and Future Perspectives

Investigation of the four agents described in this chapter provide evidence of the mechanism of activation for Zn(II)-responsive contrast agents. The original Zn(II)-responsive contrast agent, **Gd-daa3**, has two aminoacetate arms that are proposed to change metal-binding coordination upon the addition of Zn(II). Three new agents are introduced in which the proposed Zn(II)-binding groups are modified with one or two pyridyl groups (**Gd-apa3** and **Gd-dpa3**, respectively) or with the complete removal of one of the coordinating aminoacetate arms (**Gd-aa3**). Through investigation of their relaxivities, hydration numbers and zinc-dissociation constants it was determined that the mechanism depicted in **Figure 4.2 A** most closely resembles the experimental data.

Relaxivity values of **1-3** in the absence of Zn(II) represent closed conformations in which the access of water to Gd(III) is blocked. Addition of Zn(II) increases the relaxivity by more than 100% for **Gd-daa3** and **Gd-apa3** while no increase is observed for compound **Gd-aa3**. This result suggests two important factors for the development of Zn(II)-responsive contrast agents. The first criteria is that efficient blocking of water can occur with only one carboxylate coordinating arm present to bind to Gd(III). **Gd-aa3** shows a low relaxivity value, similar to **Gd-daa3** and **Gd-apa3**, in the absence of Zn(II) indicating the ability of the one available carboxylate arm to effectively coordinate Gd(III) and block the access of water. However, the high relaxivity value of **Gd-dpa3** in the absence of Zn(II) is indicative of an open structure in which water can easily access the Gd(III) metal center as there is no available carboxylic acid for coordination. The second criterion is that Zn(II)-binding can only occur if there are at least two Zn(II) coordinating arms present. In the case of compound **Gd-aa3**, only one arm is available for Zn(II)-binding and can therefore not coordinate Zn(II). NMR spectroscopy of ^{13}C labeled aminoacetates of **Eu-daa3** provides evidence of the Zn(II)-binding event with the aminoacetates to support the mechanism of activation presented in this thesis.

The mechanism described in this work is crucial for the development of future responsive MR contrast agents. With this work, it has been determined that one of the aminoacetate arms can be modified with a variety of functional groups while still maintaining the ability of *q*-modulation necessary for activation of the contrast agent. Future work will focus on the variation of one of the aminoacetate arms to improve Zn(II)-binding capabilities for imaging Zn(II) or to create new responsive agents that are sensitive to other ions such as Pb(II) or Cu(II).

4.4 Experimentals

General Methods. $GdCl_3 \cdot 6H_2O$, $EuCl_3 \cdot 6H_2O$, $TbCl_3 \cdot 6H_2O$, and 1,4,7,10-tetraazacyclododecane (cyclen) were purchased and used as is from Strem Chemicals (Newburyport, MA). FluoZin-1 was purchased from Invitrogen. Isotopically labeled 1,2-^{13}C-ethyl bromoacetate and $^{17}OH_2$ was purchased from Cambridge Isotope Laboratories, Inc. (Andover, MA). Male human blood serum was obtained from Sigma (St. Louis, MO) (catalog no. H1388). All other chemicals were purchased and used as is from Sigma-Aldrich. CH_2Cl_2, THF, and MeCN were dried using a solvent system purchased from Glass Contour, San Diego, CA. Water was purified using a Millipore Milli-Q synthesis water system. NMR spectra were recorded on either Varian Inova 400-MHz or Varian Inova-500 MHz instruments with deuterated chloroform or water as the solvent. All spectra were referenced to an internal TMS standard. Electrospray mass spectra were obtained on a Varian 1200L single-quadrupole mass spectrometer. Elemental analysis was performed by Desert Analytics Laboratory (Tucson, AZ). All samples were prepared in a 100 mM KCl/100 mM HEPES buffer at a pH of 7.4 unless otherwise noted.

Synthesis. The synthesis and characterization of **Gd-daa3** was accomplished as previously described.[15] **Gd-aa3** is an impurity from the synthesis of **Gd-daa3** that is collected from the semi-preparatory HPLC. The synthetic procedure and characterization for **Gd-dpa3** and **Gd-apa3** are described. DO3A-tris-*tert*-butyl ester was synthesized following literature procedures[7] in a 40% yield.

1-(3-Bromo-propoxy)-3-methyl-2-nitro-benzene (5). To a solution of 3-methyl-2-nitrophenol (3.0 g, 19.6 mmol) in 200 mL of dry acetonitrile under nitrogen was added 9.12 g (58.7 mmol) of anhydrous potassium carbonate. After the reaction turned bright red due to the deprotonation of the phenol (about ten minutes), 5.96 mL (58.7 mmol) of 1,3-dibromopropane was added. The reaction was refluxed overnight and returned to a light yellow color when complete. After cooling to room temperature, the reaction was filtered, and the filtrate was washed with ethyl acetate and concentrated via rotary evaporation. The oil product was then brought up in 100 mL ethyl acetate and washed once with water then brine. The organic layer was dried over Na_2SO_4, filtered and concentrated. The crude product was purified on a silica gel column eluting with 5% ethyl acetate in hexanes to yield **5** as a light yellow oil (5.1 g, 95% yield). ^{1}H NMR (400 MHz, $CDCl_3$) δ = 7.23 (t, *J* = 8 Hz, 1 H), 6.85 (d, *J* = 8 Hz, 1H), 6.81 (d, *J* = 7.6 Hz, 1H), 4.12 (t, *J* = 5.6 Hz, 2H), 3.48 (t, *J* = 6.8 Hz, 2H), 2.22 (s, 3H), 2.21 (m, 2H). ^{13}C NMR (100 MHz, $CDCl_3$) δ = 149.9, 142.3, 130.9, 130.8, 123.1, 111.2, 66.8, 32.1, 29.0, 17.1. MS (ESI-positive) *m/z* Calcd for (M + H^+): 273.0, Found: 273.9.

{4,7-Bis-*tert*-butoxycarbonylmethyl-10-[3-(3-methyl-2-ntiro-phenoxy)-propyl]-1,4,7-10-tetraaza-cyclododec-1-yl}-acetic acid tert-butyl ester (6). In a 250 mL round bottom flask, 2.0 g (7.3 mmol) of **5** was dissolved in 50 mL of dry acetonitrile. DO3A-tris-*tert*-butyl ester (2.5 g, 4.9 mmol) and anhydrous potassium carbonate (3.4 g, 24.3 mmol) were then added and refluxed for two days. The reaction was cooled to room temperature and filtered. The crude product was absorbed onto silica and purified on a silica gel column eluting with a slow ramp from 2% methanol in dichloromethane to 5%. A 66% yield (2.3 g, 3.2 mmol) of **6** was obtained as a light yellow oil. ^{1}H NMR (500 MHz, $CDCl_3$) δ = 7.24 (t, *J* = 8 Hz, 1H), 6.83 (d, *J* = 8 Hz, 1H), 6.81

(d, J = 8 Hz, 1H), 4.01 (t, J = 6 Hz, 2H), 3.58-2.32 (broad, 24H), 2.23 (s, 3H), 1.92 (m, 2H), 1.38 (s, 27H). ^{13}C NMR (126 MHz, $CDCl_3$) δ = 170.6, 170.3, 149.6, 142.0, 131.2, 130.9, 123.2, 111.5, 82.0, 81.8, 66.4, 56.8, 55.5, 53.8, 53.4, 52.6, 50.0, 49.8, 48.0, 28.1, 22.9, 17.0. MS (ESI-positive) *m/z* Calcd for (M + H^+): 707.5, Found: 708.5; Calcd for (M + Na^+): 730.4, Found: 730.5.

{2-Methyl-6-[3-(4,7,10-tris-tert-butoxycarbonylmethyl-1,4,7,10-tetraaza-cyclododec-1-yl)-propoxy]-phenylamino}-acetic acid tert-butyl ester (7). Product **6** (1.5g, 2.1 mmol) was dissolved in methanol and added to a flask preloaded with 10% palladium on carbon (wet) in catalytic amounts. The reaction was shaken under a hydrogen pressure of 3.0 bar. After 48 hours the reaction mixture was filtered through celite rinsing several times with methanol. Reduction of the nitro group to the amine was confirmed with MS (ESI-positive *m/z* = 678.5 (M + H^+)) before continuing on. The resulting orange oil was then dissolved in 25 mL dry acetonitrile. To this solution was added anhydrous potassium carbonate (0.85 g, 6.2 mmol) followed by 0.7 mL (4.5 mmol) *tert*-butylbromoacetate. The reaction was refluxed for four days and monitored closely by TLC. When a new spot was observed on the TLC due to the addition of the second acetate arm the reaction was cooled to room temperature and filtered. The crude product was adsorbed onto silica and purified on a silica gel column eluting with 2% methanol in dichloromethane. **7** was obtained as an orange oil in 25% yield (0.42 g, 0.5 mmol). ^{1}H NMR (400 MHz, $CDCl_3$) δ = 6.66 (Ar, 3H), 3.89 (t, J = 6 Hz, 2H), 3.71 (s, 2H), 3.66 (s, 1H, N*H*), 3.39-2.26 (broad, 24H), 2.22 (s, 3H), 1.91 (m, 2H), 1.38 (s, 27H), 1.32 (s, 9H). ^{13}C NMR (100 MHz, $CDCl_3$) δ = 173.8, 172.8, 171.4, 170.7, 149.4, 137.1, 128.0, 124.0, 120.7, 109.8, 82.9,

82.6, 81.7, 80.6, 67.1, 57.3, 56.7, 53.9, 51.9, 50.5, 28.1, 26.6, 18.9. MS (ESI-positive) *m/z* Calcd for (M + H^+): 791.5, Found: 792.5; Calcd for (M + Na^+): 814.5, Found: 814.5.

({2-Methyl-6-[3-(4,7,10-tris-tert-butoxycarbonylmethyl-1,4,7,10-tetraaza-cyclododec-1-yl)-propoxy]-phenyl}-pyridin-2-ylmethyl-amino)-acetic acid tert-butyl ester (8). To 50 ml of dry acetonitrile was added 0.4 g (0.5 mmol) of **8** followed by anhydrous potassium carbonate (0.28 g, 2.0 mmol) and 2-(bromomethyl)pyridine hydrobromide (0.26 g, 1.0 mmol). The reaction was refluxed overnight, cooled to room temperature, filtered, and concentrated via rotary evaporation. The crude product was adsorbed onto silica and purified on a silica gel column eluting with 3% methanol in dichloromethane. **8** was collected in 30% yield (0.13 g, 0.15 mmol) as an orange oil. MS (ESI-positive) *m/z* Calcd for (M + H^+): 882.6, Found: 883.2; Calcd for (M + Na^+): 905.6, Found: 905.1.

(4-{3-[2-(Bis-pyridin-2-ylmethyl-amino)-3-methyl-phenoxy]-propyl}-7,10-bis-tert-butoxycarbonylmethyl-1,4,7,10-tetraaza-cyclododec-1-yl)-acetic acid tert-butyl ester (9). Product **6** (0.35 g, 0.5 mmol) was dissolved in methanol and added to a flask preloaded with 10% palladium on carbon (wet) in catalytic amounts. The reaction was set up on a hydrogen reactor at 3.0 bar. After 48 hours the reaction mixture was filtered through celite rinsing several times with methanol. Reduction of the nitro group to the amine was confirmed with MS (ESI-positive *m/z* = 678.5 (M + H^+)) before continuing on. The product was concentrated via rotary evaporations and brought up in 30 mL of dry acetonitrile. To this solution was added anhydrous potassium carbonate (0.17 g, 1.3 mmol) followed by 2-picoyl chloride (0.15 g, 0.9 mmol). The reaction was refluxed for five days to ensure that both picoyl groups were added. After filtering

and rinsing with ethyl acetate and methanol the crude product was adsorbed onto silica for column purification eluting with 5% methanol in dichloromethane. **9** was obtained as a pale orange oil (0.15 g, 37% yield). ^{1}H NMR (500 MHz, $CDCl_3$) δ = 8.44 (d, *J* = 4.5 Hz, 2H), 7.54 (t, *J* = 7.5 Hz, 2H), 7.33 (d, *J* = 7.5 Hz, 2H), 7.08 (t, *J* = 7 Hz, 2H), 6.95 (t, *J* = 8 Hz, 1H), 6.68 (overlapping doublets, *J* = 8 Hz, 2H), 4.35 (s, 2H), 4.30 (s, 2H), 3.91 (t, *J* = 6 Hz, 2H), 3.2-2.2 (broad, 24H), 2.17 (s, 3H), 1.95 (m, 2H), 1.42 (s, 27H). ^{13}C NMR (126 MHz, $CDCl_3$) δ = 172.8, 160.0, 157.7, 148.9, 138.8, 137.6, 136.2, 126.2, 123.4, 123.0, 121.9, 109.8, 82.8, 82.5, 66.3, 60.2, 55.9, 51.6, 51.1-50.0 (overlapping cyclen peaks), 28.0, 25.6, 19.0. MS (ESI-positive) Calcd for ($M + H^+$): 859.6, Found: 860.6; Calcd for ($M + Na^+$): 882.5, Found: 882.6.

General metallation procedure. A TFA solution, 95 : 2.5 : 2.5 (TFA : H_2O : triisopropylsilane) was added to the protected ligands **8** and **9** for twelve hours. After the TFA was removed by purging the solution with air, ~15 mL of diethyl ether was added. The precipitate was centrifuged and decanted. The diethyl ether wash was repeated two more times. The final pellet was brought up in H_2O and the pH adjusted to 6.5 with 1 M NaOH. 1.1 equivalents of $GdCl_3 \cdot 6H_2O$ was then added and stirred at room temperature for several days. Unreacted Gd(III) was precipitated as $Gd(OH)_3$ after the addition of 1 M NaOH to a pH of ~10 and the crude mixture was purified by semi-preprative HPLC on a reverse phase column eluting with acetonitrile and water using an isocratic ramp from 0% to 100% acetonitrile over 35 minutes. Analytical HPLC-MS was used to confirm the purity and identity of the collected fractions. Pure fractions were then freeze-dried and stored in a dessicator. The same procedure is followed with $TbCl_3.6H_2O$ to obtain the Tb(III) metal complexes.

Gd-daa3. Gadolinium(III)-Carboxymethyl-{2-methyl-6-[3-(4,7,10-tris-carboxymethyl-1,4,7,10-tetraaza-cyclosdodec-1-yl)-propoxy]-phenyl}-amino)-acetic acid (1). Analytical LC-MS showed a single peak with *m/z* (ESI-positive) Calcd for (M + H^+): 778.2, Found: 781.2. Anal. Calcd for $C_{28}H_{38}GdN_5O_{11}\cdot 2H_2O\cdot 2Na$: C 39.11, H 4.93, N 8.14. Found: C 39.33, H 4.93, N 7.84.

Tb-daa3. Analytical LC-MS showed a single peak with *m/z* (ESI-positive) Calcd for (M + H^+): 779.2, Found: 779.2; Calcd for and (M + Na^+): 802.2, Found: 801.2.

Gd-aa3. Gadolinium(III)- {2-Methyl-6-[3-(4,7,10-tris-carboxymethyl-1,4,7,10-tetraaza-cyclododec-1-yl)-propoxy]-phenylamino}-acetic acid (2). Analytical LC-MS showed a single peak with *m/z* (ESI-positive) Calcd for (M + H^+): 721.1, Found: 720.2. Anal. Calculated for $C_{26}H_{38}GdN_5O_9\cdot H_2O\cdot Na$: C 40.94, H 5.29, N 9.18. Found: C 40.81, 5.27, 9.02.

Gd-apa3. Gadolinium(III)- ({2-Methyl-6-[3-(4,7,10-tris-carboxymethyl-1,4,7,10-tetraaza-cyclododec-1-yl)-propoxy]-phenyl}-pyridin-2-ylmethyl-amino)-acetic acid (3). Analytical LC-MS showed a single peak with *m/z* (ESI-positive) Calcd for (M + H^+): 812.2, Found: 813.0. Anal Calculated for $C_{32}H_{42}GdN_6O_9\cdot 2H_2O$: C 45.32, H 5.47, N 9.91. Found: C 45.37, H 5.79, N 10.32.

Tb-apa3. Analytical LC-MS showed a single peak with *m/z* (ESI-positive) Calcd for (M + H^+): 813.2, Found: 814.2.

Gd-dpa3. Gadolinium(III)-(4-{3-[2-(Bis-pyridin-2-ylmethyl-amino)-3-methyl-phenoxy]-propyl}-7,10-bis-carboxymethyl-1,4,7,10-tetraaza$_2$-cyclododec-1-yl)-acetic acid (4).

Analytical LC-MS showed a single peak with *m/z* (ESI-positive) Calcd for (M + H^+): 846.3, Found: 847.2. Anal. Calculated for $C_{36}H_{47}GdN_7O_7$: C 51.05, H 5.59, N 11.58. Found: C 51.15, H 5.61, N 11.22.

Tb-dpa3. Analytical LC-MS showed a single peak with *m/z* (ESI-positive) Calcd for (M + H^+): 847.3, Found: 848.3.

tert-Butyl-dimethyl-[3-(3-methyl-2-nitro-phenoxy)-propoxy]-silane (10). To a solution of 3-methyl-2-nitrophenol (5.0 g, 32.6 mmol) in dry acetonitrile (300 mL) under nitrogen was added K_2CO_3 (11.26 g, 81.5 mmol). After the reaction had turned a bright red color due to the deprotonated state of the phenol (~10 minutes), (3-bromopropoxy)-*tert*-buytldimethyl silane (9.04 mL, 39.2 mmol) was added. The reaction was refluxed at 70 °C until it was a pale yellow color (several days), cooled to room temperature and filtered. After rotary evaporation of the solvent, the mixture was brought up in 100 mL ethyl acetate and washed once with an aqueous saturated sodium bicarbonate solution and once with brine. The organic layer was dried over Na_2SO_4 and concentrated in vacuo. The residue was purified on a silica gel column eluting with 1% ethyl acetate in hexanes, yielding **10** as light yellow crystals after drying (10.11 g, 94% yield). ^{1}H NMR (500 MHz, $CDCl_3$) δ = 7.27 (t, J = 8 Hz, 1H), 6.89 (d, J = 8.5 Hz, 1H), 6.84 (d, J = 8 Hz, 1H), 4.15 (t, J = 6 Hz, 2H), 3.75 (t, J = 6 Hz, 2H), 2.30 (s, 3H), 1.96 (m, 2H), 0.88 (s, 9H), 0.04 (s, 6H); ^{13}C NMR (126 MHz, $CDCl_3$) δ = 150.44, 142.43, 131.06, 130.76, 122.54, 111.01, 65.89, 59.15, 32.23, 26.11, 18.49, 17.17, -5.13, -5.41; MS (ESI-positive) m/z Calcd for (M + H^+): 325.2, Found: 326.2; Calcd for (M + Na^+): 348.2, Found: 348.1.

({2-[3-(tert-Butyl-dimethyl-silanyloxy)-propoxy]-6-methyl-phenyl}-ethoxycarbonylmethyl-amino)-acetic acid ethyl ester (11). In 30 mL of methanol, **10** (1 g, 3.07 mmol) was dissolved and added to a flask preloaded with 10% Pd on carbon in catalytic amounts. The reaction was set up on a hydrogen reactor at 3 bar for 24 hours. Upon completion of reduction, the reaction was filtered over celite and rinsed several times with 50 mL methanol and concentrated via rotary evaporation of the solvent. The resulting oil was transferred to a 100 mL round bottom flask and dissolved in dry acetonitrile (30 mL). Proton sponge (2.79g, 13.0 mmol) was added to the reaction before adding 1g (5.92 mmol) of 1,2-^{13}C-ethyl bromoacetate followed by NaI (1.95 g, 13.0 mmol). After two days at refluxing temperatures, the reaction was cooled, then filtered, rinsing with ethyl acetate, and concentrated via rotary evaporation. The crude product was absorbed onto silica and purified on a silica gel column eluting with a slow gradient of 2% ethyl acetate in hexanes to 5% to separate any product with only the addition of on acetate arm. The desired product **11** was collected in 75% yield (1.1 g, 2.3 mmol) as a light yellow oil. ^{1}H NMR (500 MHz, $CDCl_3$) δ = 7.00 (t, *J* = 8 Hz, 1H), 6.79 (d, *J* = 7.5 Hz, 1H), 6.72 (d, *J* = 7.5 Hz, 1H), 4.12 (m, 4H), 4.05 (t, *J* = 6.5 Hz, 2H), 3.91 (s, *broad*, 2H), 3.85 (t, *J* = 6 Hz, 2H), 3.74 (s, *broad*, 2H), 2.47 (s, 3H), 2.04 (m, 2H), 1.24 (t, *J* = 7 Hz, 6H), 0.91 (s, 9H), 0.07 (s, 6H). ^{13}C NMR (126 MHz, $CDCl_3$) δ = 172.5, 157.0, 139.3, 137.7, 126.4, 122.9, 109.7, 64.8, 60.5, 56.6, 49.8, 32.9, 26.2, 21.3, 18.6, 14.4, -5.1. MS (ESI-positive) *m/z* Calcd for (M + H^+) 469.3, Found: 472.3; Calcd for (M + Na^+): 492.2, Found: 494.3.

{Ethoxycarbonylmethyl-[2-(3-hydroxy-propoxy)-6-methyl-phenyl]-amino}-acetic acid ethyl ester (12). To a solution of **11** (1.1 g, 2.3 mmol) in THF (25 mL) was added tetrabutylammonium fluoride (1.5 g, 5.8 mmol). After two hours at room temperature the

deprotection was completed as observed by TLC (1:3 EtOAc:hexanes). THF was removed via rotary evaporation. The crude product was brought up in ethyl acetate and washed once with water and then brine. The organic layer was dried over sodium sulfate, filtered, concentrated, and purified through a silica plug eluting with 25% ethyl acetate in hexanes yielding the desired product in 83% yield (0.68 g, 1.9 mmol). ^{1}H NMR (500 MHz, $CDCl_3$) δ = 7.00 (t, *J* = 8 Hz, 1H), 6.80 (d, *J* = 8 Hz, 1H), 6.74 (d, *J* = 8.5 Hz, 1H), 4.14 (m, 6H, overlapping O*CH*$_2$CH3 and O*CH*$_2$CH$_2$CH$_2$OH), 4.06 (s, *broad*, 2H), 3.90 (t, *J* = 5.5 Hz, 2H), 3.79 (s, *broad*, 2H), 2.45 (s, 3H), 2.08 (m, 2H), 1.23 (t, *J* = 7Hz, 6H). ^{13}C NMR (126 MHz, $CDCl_3$) δ = 172.5, 156.4, 138.5, 137.3, 126.1, 123.4, 110.1, 65.7, 60.2, 49.6, 32.4, 18.7, 14.4. MS (ESI-positive) *m/z* Calcd for (M + H$^+$): 355.2, Found: 358.2; Calcd for (M + Na$^+$): 378.2, Found: 380.1.

{[2-(3-Bromo-propoxy)-6-methyl-phenyl]-ethoxycarbonylmethyl-amino}-acetic acid ethyl ester (13). To a solution of **12** (0.5 g, 1.4 mmol) in dry methylene chloride (15 mL) was added carbon tetrabromide (0.7 g, 2.1 mmol) followed by slow addition of triphenylphosphine (0.7 g, 2.8 mmol) After two hours at room termperature the reaction was washed with water and brine. The organic layer was then dried over sodium sulfate, filtered and concentrated. The crude product was purified on a silica gel column eluting with 5% ethyl acetate in hexanes giving **13** in 94% yield (0.55 g, 1.3 mmol) as an orange oil. ^{1}H NMR (500 MHz, $CDCl_3$) δ = 7.01 (t, *J* = 8 Hz, 1H), 6.81 (d, *J* = 7 Hz, 1H), 6.73 (d, *J* = 8.5 Hz, 1H), 4.11 (m, 6H, overlapping O*CH*$_2$CH3 and O*CH*$_2$CH$_2$CH$_2$Br), 4.00 (s, *broad*, 2H), 3.73 (s, *broad*, 2H), 3.67 (t, *J* = 6.5 Hz, 2H), 2.46 (s, 3H), 2.37 (m, 2H), 1.23 (t, *J* = 6.5 Hz, 6H). ^{13}C NMR (126 MHz, $CDCl_3$) δ = 172.0, 156.5, 139.2, 137.6, 126.3, 123.5, 109.9, 65.7, 60.6, 56.3, 49.6, 32.7, 18.6, 14.5. MS (ESI-positive) *m/z* Calcd for (M + H$^+$): 417.1, Found: 420.0; Calcd for (M + Na$^+$): 440.1, Found: 442.0.

(Ethoxycarbonylmethyl-{2-methyl-6-[3-(4,7,10-tris-tert-butoxycarbonylmethyl-1,4,7,10-tetraaza-cyclododec-1-yl)-propoxy]-phenyl}-amino)-acetic acid ethyl ester (14). To a solution of DO3A-tris-*t*-butyl ester (0.55 g, 1.1 mmol) in 15 mL of dry acetonitrile was added anhydrous potassium carbonate (0.44 g, 3.2 mmol). After five minutes, a solution of **13** (0.55 g, 1.3 mmol) in 5 mL of dry acetonitrile was added to the reaction and the mixture was refluxed overnight. The reaction was cooled and filtered rinsing with acetonitrile and methanol. After the solvents were removed by rotary evaporation, the crude product was purified on a silica gel column eluting with 3% MeOH in dichloromethane to yield **14** in 27% yield (0.26 g, 0.3 mmol). After trituration with diethyl ether several times a pale yellow solid was obtained. ^{1}H NMR (400 MHz, $CDCl_3$) δ = 6.91 (t, *J* = 8 Hz, 1H), 6.72 (d, *J* = 7.6 Hz, 1H), 6.62 (d, *J* = 8.4 Hz, 1H), 3.95 – 2.30 (*broad*, 36H), 2.35 (s, 3H), 1.27 (s, 27H), 1.17 (m, 6H). ^{13}C NMR (126 MHz, $CDCl_3$) δ = 172.6, 164.2, 156.4, 139.0,126.3, 123.3, 109.7, 82.9, 82.6, 66.5, 60.5, 55.8, 51.7, 50.7, 50.0, 49.8, 49.4, 49.2, 47.9, 28.1, 18.4, 14.4. MS (ESI-positive) *m/z* Calcd for (M + Na^+): 874.5, Found: 876.6.

Eu-daa3. Europium(III)-Carboxymethyl-{2-methyl-6-[3-(4,7,10-tris-carboxymethyl-1,4,7,10-tetraaza-cyclosdodec-1-yl)-propoxy]-phenyl}-amino)-acetic acid (15). The protected ligand **14** was first reacted with 1.0 M NaOH for 20 hr to deprotect the ethyl groups. After neutralization to a pH of 7 the crude product was freeze-dried then brought up in a solution of TFA for 20 hr. After the TFA was removed by purging the solution with air, ~15 mL of diethyl ether was added. The precipitate was centrifuged and decanted. The diethyl ether wash was repeated two more times. The final pellet was brought up in H_2O and the pH adjusted to 6.5

with 1 M NaOH. 1.1 equivalents of $EuCl_3 \cdot 6H_2O$ was then added and stirred at room temperature for several days. Unreacted Eu(III) precipitated as $Eu(OH)_3$ after the addition of 1 M NaOH to a pH of 10 and the crude mixture was purified by semi-preprative HPLC on a reverse phase column eluting with acetonitrile and water using an isocratic ramp from 0% to 100% acetonitrile in 35 minutes. Analytical HPLC-MS was used to confirm the purity and identity of the collected fractions and showed a single peak with *m/z* (ESI-positive) Calcd for ($M + H^+$): 777.2, Found: 772.5.

Relaxivity measurements. A 1 mM solution of the gadolinium complex was made up in buffer containing 100 mM KCl/100 mM HEPES at pH = 7.4 or in human blood serum. These solutions were serially diluted four times to give 500 μL of five different sample concentrations at a [Gd]:[Zn] ratio of 1:0. Aliquots of a 5.0 mM $ZnCl_2$ solution in HEPES was added to each of the samples to give a [Gd]:[Zn] ratio of 1:0.5. After 30 minutes of incubation at 37 ^oC, T_1 measurements were performed on a Bruker mq60 Minispec relaxometer with an inversion recovery pulse sequence with the appropriate recycle delays. This titration was repeated until a 1:3 ([Gd]:[Zn]) ratio was reached.

Luminescence Lifetime Measurements. The fluorescence decay rates of the terbium analogs of **1**, **3**, and **4** in buffered H_2O and D_2O were measured on a Hitachi F4500 fluorometer monitoring the emission at 544 nm with an excitation of 254 nm. Aliquots of HEPES buffer and $ZnCl_2$ in HEPES were freeze-dried before bringing up in D_2O to assure there was no water present. A 200 μM solution of the terbium complex in HEPES buffer was measured in the

presence of 300 μM $ZnCl_2$ and without $ZnCl_2$. Twenty-five scans were averaged and fit to a monoexponential decay with an r^2 value of 0.99.

Calculation of Zinc-Dissociation Constants. To a 10 μM sample of $ZnCl_2$ in HEPES buffer is titrated 100 μL aliquots of 0.1 mM FluoZin-1 until saturation of fluorescence was reached. Between aliquots, 30 minutes was allowed for the reaction to reach equilibrium. A series of **1-4** at various concentrations in 10 μM $ZnCl_2$ were then titrated with FluoZin-1 in the same manner. After each aliquot of fluorophore was added, the percent saturation of fluorescence ($f = (F - F_0)/(F - F_{max})$ where F_0 is the minimum fluorescence without zinc and F_{max} is the fluorescence when saturated with zinc, was calculated to determine the amount of Zn(II) bound to the dye. With known amounts of Zn(II), FluoZin-1, and contrast agent, the equilibrium constant was determined.

Inductively coupled plasma – atomic emission spectrometry (ICP-AES). The concentration of each sample for relaxivity was determined by ICP-AES (Varian). A 10 μL aliquot of each sample was digested in 90 μL nitric acid. Each sample was then diluted with water to the appropriate concentration for ICP-AES analysis. Gadolinium concentrations were determined from a standardized curve of six standards ranging from 0 – 500 ppb Gd(III) measuring the emission of Gd(III) at 335.048, 336.224, and 342.246 nm.

^{17}O Transverse Relaxation Rate Measurements. Samples of each complex in water with and without Zn(II) were enriched with 1 % $^{17}OH_2$ and the ^{17}O spectra were obtained at 54 MHz at temperatures ranging from 5 °C to 75 °C in 5 °C increments. The ^{17}O transverse relaxation rate

was determined by obtaining the line width at half of the peak height, $\Delta\nu_{1/2}$, of the ^{17}O water signal. The plots of R_{2p} versus temperature were fit according to the Swift-Connick theory using the calculated hydration numbers and concentration of Gd(III) as determined by ICP-AES.[11]

Appendix

Zn(II)-Responsive MRI Contrast Agents for Attachment to Nanoparticles

A.1 Introduction

The development of MRI contrast agents has been progressively moving toward the use of polymer and dendrimer scaffolds to increase their efficiency in relaxivity.[1-3] This design to increase relaxivity is twofold. First, it provides a means to increase the number of gadolinium chelates and secondly it provides a way to effectively slow down the tumbling rate and increase the relaxation enhancement per Gd(III) ion. However, many of these approaches have had limited success because the entrapped chelates have a slower bulk water exchange rate which adversely affects relaxivity. An alternative approach to increase τ_R that has been studied to a lesser extent is through the use of nanoparticle scaffolds. Appendage of Gd(III) chelates to the periphery of nanoparticles will provide a method to amplify the MR signal from the large increase in Gd(III) ions and still allow for fast water exchange by not burying the chelate in a protein or a micelle. The use of SiO_2 nanoparticles (SiNPs) as a scaffold for Gd(III) chelates has been previously demonstrated with Gd-DTPA complexes.[4-6] SiNPs have been shown to have increased vascular retention time and can be taken up into cells via pynocytosis or phagocytosis.[7] In addition, SiNPs are non toxic and relatively hydrophilic from the presence of silanol groups.

Attachment of activated contrast agents to nanoparticles would provide a novel means of amplifying the signal upon activation. To date, there has been no investigation of the use of activated contrast agents attached to particles. The work presented in this Appendix aims to investigate the use of SiNPs as a scaffold for Zn(II)-responsive MRI contrast agents for signal amplification. The first part of this study investigates the use of Gd-DO3A complexes conjugated to SiNPs. Preliminary results indicate that a T_1 relaxation enhancement of 11.3 $mM^{-1}s^{-1}$ per Gd(III) ion is observed at 60 MHz and 37 °C. This is a vast improvement over Gd-DOTA which has a relaxivity of 3.1 $mM^{-1}s^{-1}$ per Gd(III) at 60 MHz and 37 °C. This increase in

relaxivity is most likely caused by the large increase in molecular weight and hence a slowing down of the rotational correlation time. The second part of this study focuses on the synthesis of a modified version of the Zn(II)-responsive agent **Gd-daa3** for covalent attachment to nanoparticles. Several strategic routes are discussed.

A.2 Results and Discussion

A.2.1 Synthesis, Characterization, and Relaxivity of Gd-DO3A SiNPs

Covalent attachment of Gd-DO3A to silica nanoparticles can be accomplished using a peptide coupling reaction with amine-coated particles and a carboxylic acid available from the Gd(III) chelate (**Scheme A.1**). To make the amine-coated particles, commercially available SiNPs with a hydrodynamic diameter of 20 nm are modified with 3-aminopropyltrimethoxy-silane (APS) following literature procedures.[5] The synthesis of the carboxylic acid derivative of DO3A (**2**) began with DO3A-tris-*tert*-butyl ester which was first synthesized following literature procedures.[8] To this was added benzyl bromoacetate using potassium carbonate in acetonitrile to produce **1**. Deprotection of the benzyl group under standard palladium hydrogenation conditions afforded **2**.

Using the coupling reagent EDC in the presence of *N*-hydroxysuccinimide (NHS) in DMF, **2** was covalently attached to the SiNPs to produce **DO3A-SiNP**. Deprotection of the *tert*-butyl acetates was achieved through vigorous shaking with 100% formic acid for twenty hours. After several washes of the particles with water, 1.1 equivalents of $GdCl_3$ was added and stirred at room temperature for five days at a pH of 6. Purification of the **Gd-DO3A-SiNPs** was

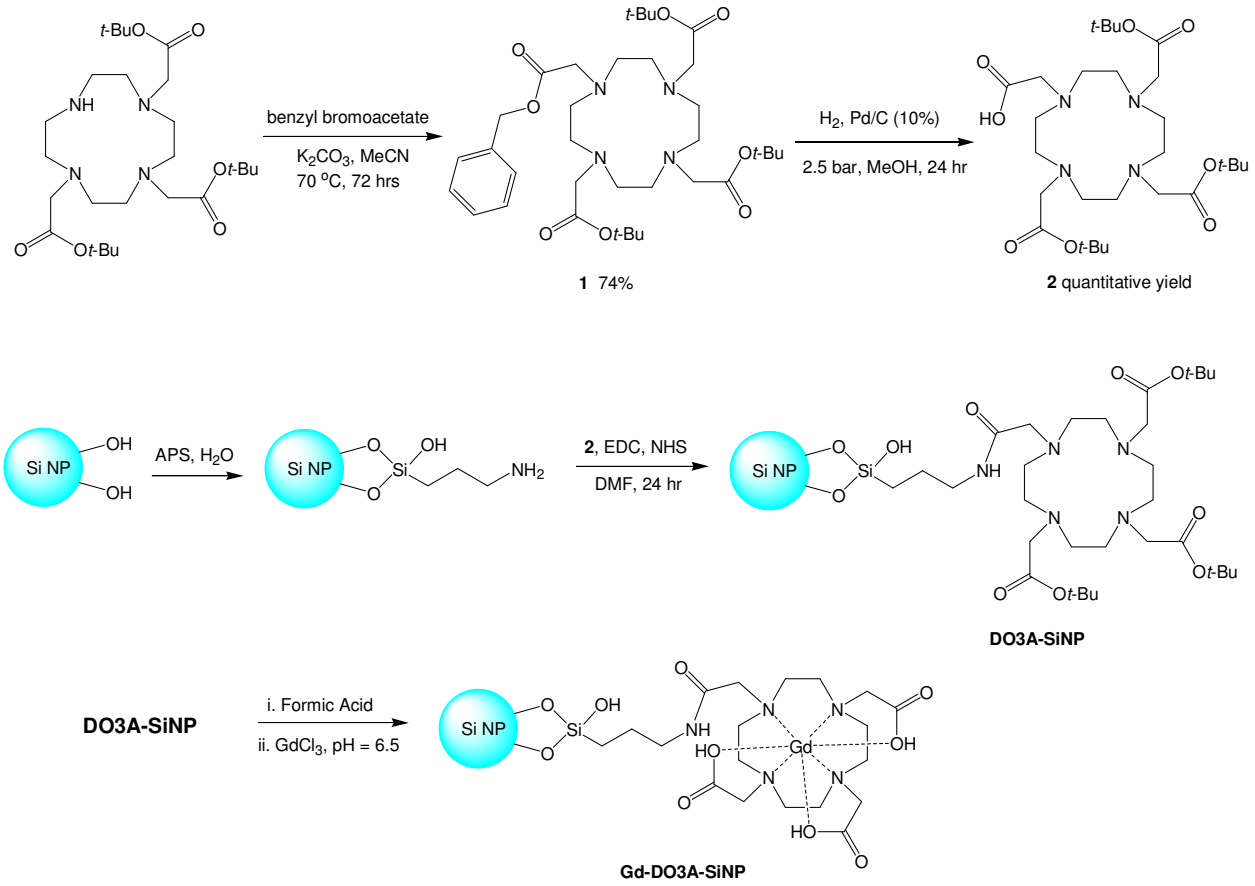

Scheme A.1. Synthetic scheme for conjugation of DO3A to silica nanoparticles.

accomplished with dialysis and filtration to remove any unreacted Gd(III). Transmission electron microscopy (TEM) images were obtained to verify that both particle size and morphology were maintained throughout the synthesis (**Figure A.1**). Energy dispersive X-ray spectroscopy (EDX) was used to confirm the presence of gadolinium in the final modified SiNPs (**Figure A.2**). A control reaction of amine-modified silica nanoparticles with $GdCl_3$ following the same reaction conditions was performed as well.

Assuming the density of the SiNPs to be 1.96 g/mL,[7, 9] the concentration of the particles could be determined by measuring the mass of SiNPs per volume. Gd(III) concentrations were measured via ICP-AES then divided by the concentration of particles to determine the number of Gd(III) ions per particle. For **Gd-DO3A-SiNPs**, it was found that there were about 9,200 Gd(III) ions per particle, consistent with results from similar studies.[4, 10] On the other hand, the control particles subjected to $GdCl_3$ measured over 72,000 Gd(III) ions per particle. In this case, it is likely that because Gd(III) has a high affinity for the exposed amines on the surface of the SiNPs, a large number of ions are able to associate with the particles. Modification of the surface with the DO3A chelate prevents the Gd(III) from being able to interact with the amine surface and therefore the only Gd(III) remaining is speculated to be bound to the chelate.

To determine the efficacy of these particles as contrast agents, their T_1 relaxation times were measured at 37 °C and 60 MHz. Results of these studies are summarized in **Table A.1**. The relaxivity per Gd(III) for the **Gd-DO3A-SiNPs** was found to be 11.3 $mM^{-1}s^{-1}$. This is greater than a 3-fold improvement compared to Gd-DOTA alone. The large increase in molecular weight and subsequent change in τ_R is most likely the reason for such a high relaxation enhancement. The control particles subjected to Gd(III) only measured a relaxivity of

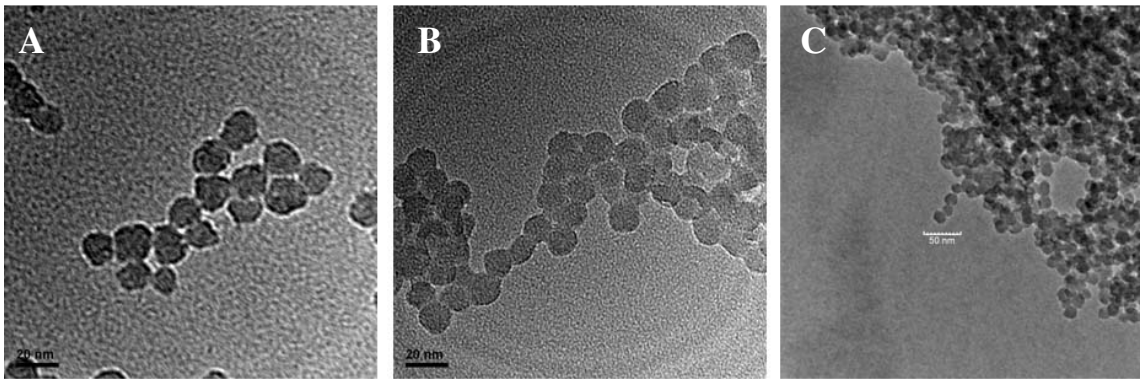

Figure A.1. TEM images of (**A**) Si nanoparticles; (**B**) amine coated nanoparticles; and (**C**) **Gd-DO3A-SiNPs**. The images show that particle size and morphology is maintained throughout the synthesis of the nanoparticles, indicating that the particles are not affected by the reaction conditions. Scale bars for **A** and **B** are 20 nm and for **C** is 50 nm.

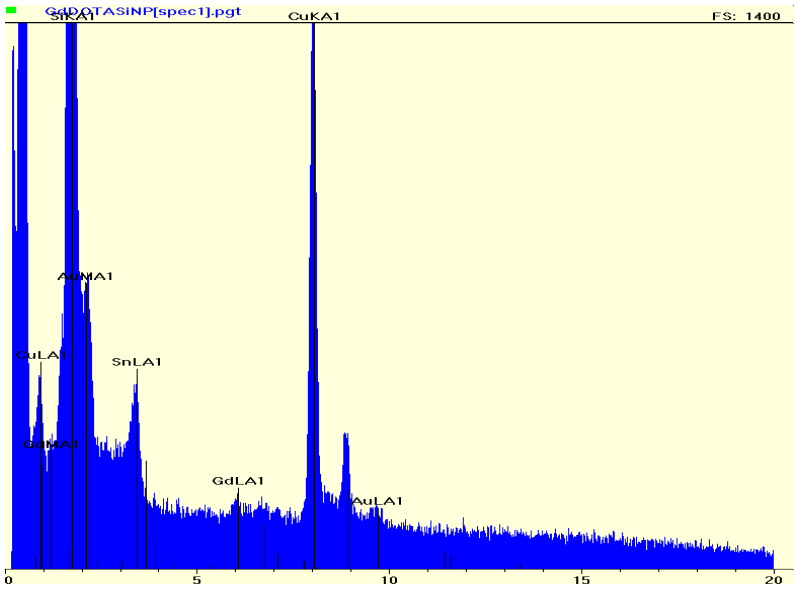

Figure A.2. EDX spectra of final **Gd-DO3A-SiNPs**.

Table A.1. Relaxivity values (60 MHz and 37 °C) and number of Gd(III) ions per particle.

	Gd-DOTA	**Gd-DO3A-SiNPs**	**Gd-SiNPs**
R_1 **per Gd (mM^{-1}s^{-1})**	3.2	11.3	1.9
Gd(III)/particle	1	9,287	72,105

1.9 $mM^{-1}s^{-1}$. With such a large number of Gd(III) ions per particle as discussed previously, a possible reason for the low relaxivity is that the Gd(III) ions are buried within the SiNP core and therefore have limited water exchange.

The advantage to this synthetic method is that purification of the nanoparticles is simply achieved by washing and centrifugation. In addition, the amination of the particles with APS and the peptide coupling reaction are well characterized and high yielding reactions.[4, 5, 11] A major drawback to this method is that characterization of the SiNPs after each modification is difficult. Although the EDX data confirms the presence of Gd(III) in the final **Gd-DO3A-SiNPs**, it is difficult to know for sure if all of the Gd(III) ions are chelated or if there are some that are non-specifically bound to the particle surface. A method to overcome this would be to synthesize and purify the Gd(III) chelate before attachment to the particle. This would ensure that any Gd(III) present would be of the chelated form.

Scheme A.2 presents a future method to modify DO3A with a triethoxysilane group for conjugation to SiNPs. Beginning with the ethylacetate protected DO3A derivative, allyl bromide is added using potassium carbonate in acetonitrile to make **3**. The deprotection of the ethyl groups can then be achieved with sodium hydroxide while keeping the alkene moiety intact. After reaction with $GdCl_3$, the final metal complex (**4**) can be purified and characterized by HPLC. Further modification of **4** to the triethoxysilyl derivative (**5**) can be achieved with triethoxysilane in the presence of the Pt(0) Karstedt's catalyst.[12]

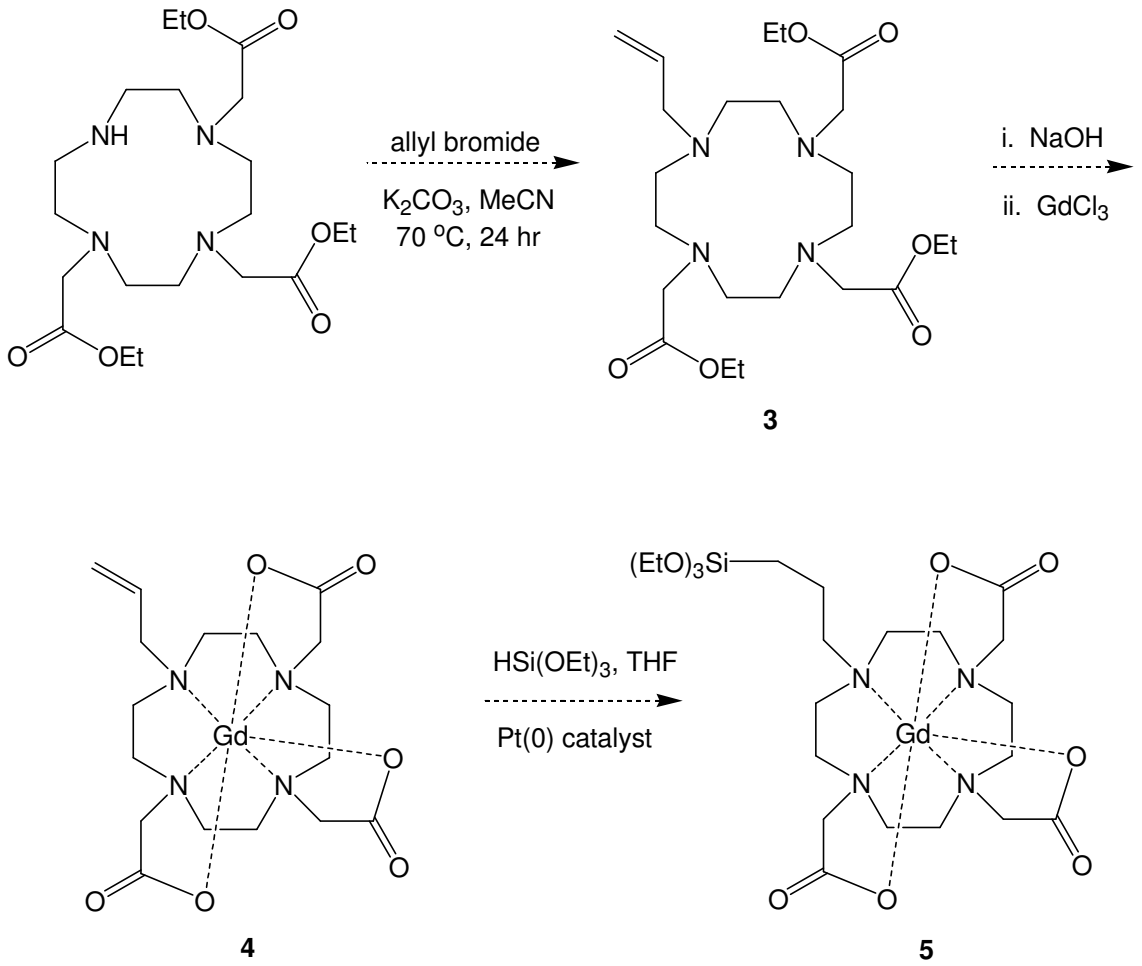

Scheme A.2. Synthesis of Gd-DO3A modified with triethyoxysilane.

A.2.2 Synthetic Approach to Modification of Gd-daa3 for Conjugation to SiNPs

Synthetic modification of **Gd-daa3** to create an available carboxylic acid for coupling to SiNPs was looked at using several different synthetic routes. To maintain the Zn(II)-binding ability without affecting the mechanism of activation of the agent, there were two positions that were looked at for synthetic modification (**Figure A.3**). Position A, *para* to the phenolic oxygen, was presumed to have the least affect on **Gd-daa3** and its activity because of it being the furthest away from the Zn(II)-binding group and the Gd(III)-chelate. Modification to position B, *meta* to the phenolic oxygen, should also present little interference of the Zn(II)-binding activity of the agent. Because the methyl group at position B is highly inert, any modifications at this position would require the use of 2-nitroresorcinol as a starting material rather than the original 3-methyl-2-nitrophenol starting material. This is synthetically more challenging therefore making position A a more attractive choice for modification.

Attempts were first made to add a protected carboxylic acid at position A to make the final metal complex **10**. This would provide a benzyl protected carboxylic acid that could be easily removed under standard palladium catalyzed hydrogenation conditions after the full metal complex was purified. Following **Scheme A.3**, bromination of the aromatic ring at this position could be accomplished with acetic acid and bromine at room temperature to produce **6**. Addition of the *tert*-butyldimethylsilyl protected alcohol was accomplished with potassium carbonate to yield **7**. Efforts to produce **8** following synthetic procedures used to make **Gd-daa3**, proved to be unfruitful and resulted in compound **2.8** (from Chapter 2). It is likely that the bromine was eliminated during hydrogenation, producing HBr, which then deprotected the TBDMS protecting group. The addition of benzyl glycolate before reduction of the nitro group may be possible if a

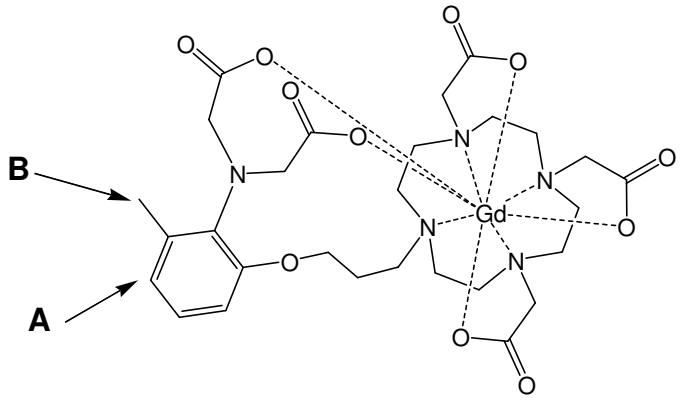

Figure A.3. Possible sites for modification to **Gd-daa3** for attachment to SiNPs.

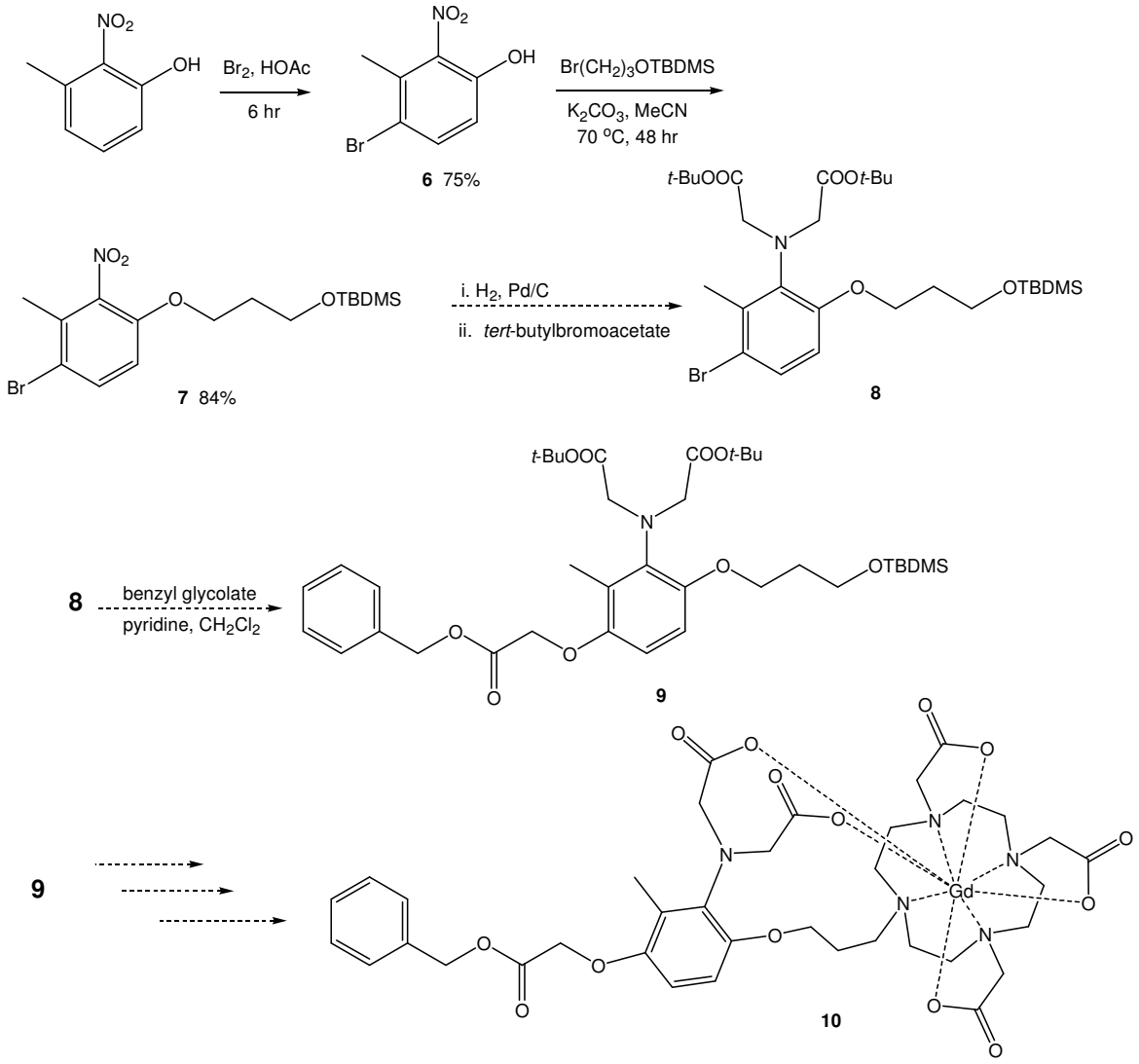

Scheme A.3. Synthesis of **Gd-daa3** with modifications to position A.

new method of reduction is used to produce the amine. One such method may be the use of $SnCl_2$ which should leave the benzyl protecting group intact.

After attempts at modification of position A were unsuccessful, efforts were focused on modifications at position B. Following **Scheme A.4**, it may be possible to make the final metal complex, **14**, with an ethyl protected carboxylic acid that would be able to be cleaved under basic conditions. In this reaction scheme, 2-nitroresorcinol is used as the starting material and is alkylated asymmetrically with arms providing orthogonal protecting groups. After several attempts, reaction of 2-nitroresorcinol with 3-bromopropoxy-*tert*-butyldimethl silane was successful in producing compound **11**. Although the yields of this reaction were very low, efforts to change the base and reaction conditions to increase the yield of compound **11** proved to have no effect. Attempts at the addition of ethylbromoacetate to 2-nitroresorcinol as the first step yielded only product with both phenolic positions being alkylated. This is most likely because the addition of an electron donating group to one phenolic oxygen probably led to the activation of the second oxygen, therefore making it hard to control the addition of just one ethylbromoacetate.

Addition of the second arm to **11** with ethyl bromoacetate in potassium carbonate was successful in producing compound **12** in high yields. The design of compound **12** provided two protecting groups that are stable to hydrogenation conditions and anhydrous base conditions which would allow for the addition of the aminoacetate arms to give **13**. Once **13** is produced, the reaction scheme follows the same procedures as described earlier in this thesis for making **Gd-daa3** and the other derivatives. Deprotection of the TBDMS group with a fluoride source followed by bromination should not affect the ethyl and *tert*-butyl acetate protecting groups.

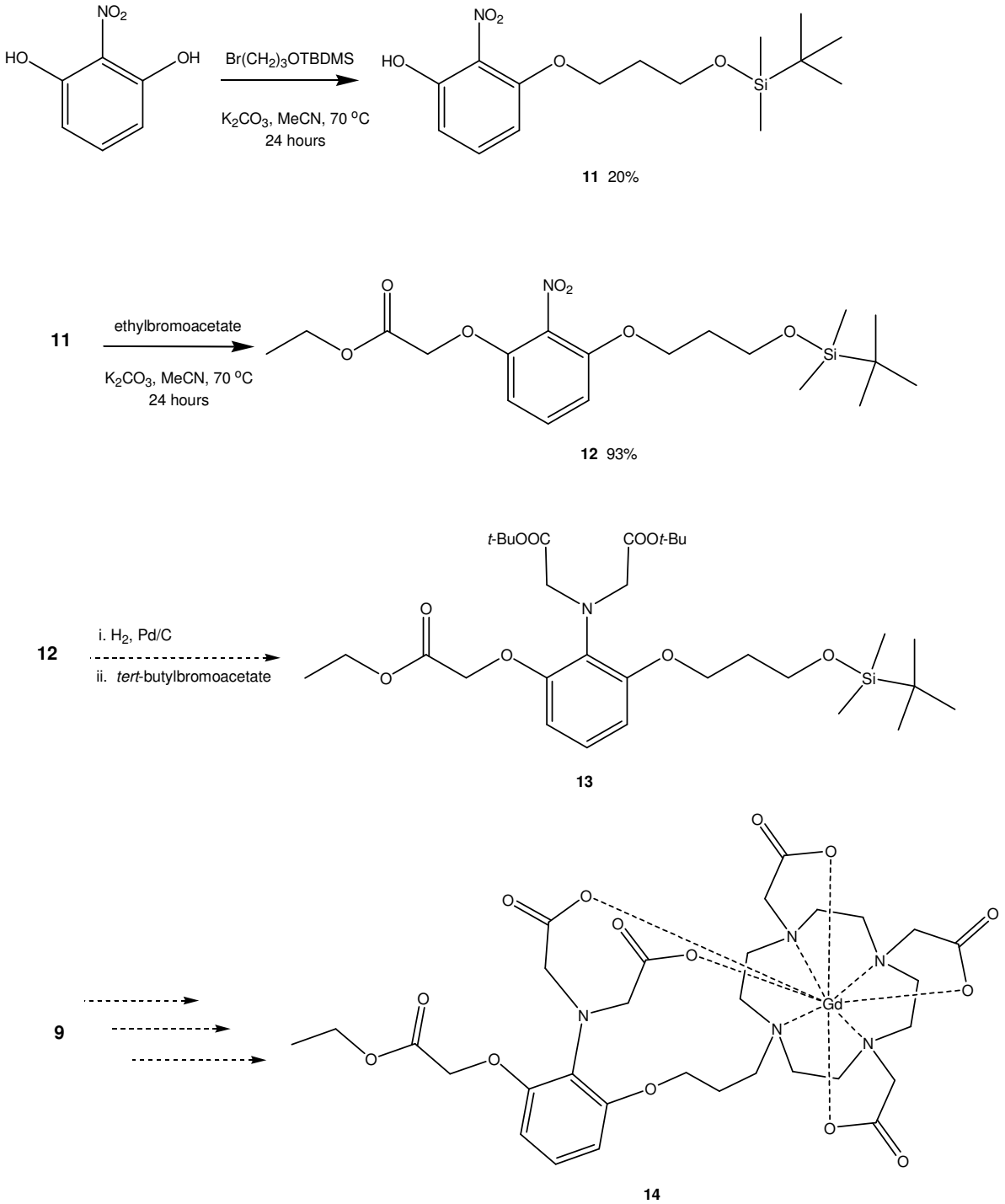

Scheme A.4. Synthesis of **Gd-daa3** with modifications at position B.

This would allow facile attachment of DO3A-tris-*tert*-butyl ester. From this point, deprotection of the *tert*-butyl acetates followed by metallation would produce **14**. The only protecting group remaining on **14** is the ethyl acetate which can be removed with a sodium hydroxide solution before attachment of the agent to SiNPs. Work on this synthetic scheme is still in progress.

A.3 Conclusions and Future Aspects

In this work, the concept of covalent attachment of biologically activated MRI contrast agents to nanoparticle scaffolds is presented. Currently, there have been no reported research efforts in this area despite the promising results it may hold. The first focus of this research is to study the T_1 relaxation enhancement from attachment of Gd-DO3A chelates to SiNPs. This research will provide a method to create high relaxivity MRI contrast agents to lower the current dosage amounts of contrast agents while providing a greater contrast enhancement as well. The second aim of this research is to synthetically modify **Gd-daa3** for attachment to nanoparticles. This would be the first example of a biologically active MRI contrast agent conjugated to a large molecular weight scaffold. It is expected that this method will provide a way to amplify the MRI signal upon activation by Zn(II) due to the large number of Gd(III) chelates present.

Preliminary results with attachment of DO3A to SiNPs shows a greater than 3-fold increase in relaxivity per Gd(III) as compared to the clinically approved Gd-DOTA complex. Additionally, **Gd-DO3A-SiNPs** exhibits the attachment of about 9,000 Gd(III) chelates yielding a high density contrast agent with a high relaxivity per Gd(III). Although the control samples provide evidence that the relaxation enhancement observed is from the binding of Gd(III) to DO3A chelates on the surface of the nanoparticles, future work will require synthesis and

purification of the Gd(III) chelate before appendage to the SiNPs. This will ensure that there is no nonspecific binding of Gd(III) to the particles.

The development of a Zn(II)-responsive contrast agent for covalent attachment to nanoparticles is still underway. Several synthetic strategies were discussed for the modification of **Gd-daa3**. Although it may be synthetically difficult to modify the agent, **Scheme A.4** presents a feasible method in which to achieve attachment of **Gd-daa3** to SiNPs. Work is continuing on this effort.

Though the research presented in this Appendix has focused on the use of SiNPs as a scaffold, it should be noted that the strategies presented can be used with iron-oxide nanoparticles, common T_2 MRI contrast agents. Ongoing research in the Meade group focuses on the investigation of T_1-T_2 bimodal contrast agents in which Gd(III) chelates are conjugated to iron-oxide nanoparticles. Preliminary results have shown that covalent attachment of a T_1 contrast agent to T_2 particles significantly enhances the T_2 effect producing a dark T_2-weighted MR image.[13] Attachment of a T_1-activated MRI contrast agent to iron-oxide nanoparticles should produce a dark T_2-weighted MR image and a bright T_1-weighted image after activation to provide a method of co-validation.

A.4 Experimentals

General Methods. $GdCl_3 \cdot 6H_2O$ and 1,4,7,10-tetraazacyclododecane (cyclen) were purchased from Strem Chemicals. SiO_2 (negatively charged silica sol Ludox HS-40 (Dupont) (composition: 40% SiO_2, 60% H_2O, < 1% Na_2O, average diameter of 20 nm)) was purchased from Aldrich. Low melting temperature agarose was purchased from Fisher Scientific. All other chemicals were purchased and used as is from Sigma Aldrich. CH_2Cl_2, THF, DMF and MeCN

were dried using a solvent system purchased from Glass Contour, San Diego, CA. Water was purified using a Millipore Milli-Q synthesis water system. Nuclear magnetic resonance spectra were recorded on either Varian Mercury 400 MHz or Varian Inova 500 MHz using deuterated chloroform as the solvent. All spectra were referenced to an internal TMS standard. Electrospray mass spectra were obtained on a Varian 1200L single quadrupole mass spectrometer. TEM images were obtained on a Hitachi HF-2000 instrument operated at 200 kV using standard copper grids coated with carbon. EDX was performed on an Oxford EDX System attached to HF-2000 TEM instrument. DO3A-tris-*tert*-butyl ester was prepared following literature procedures.[8]

(4-Benzyloxycarbonylmethyl-7,10-bis-tert-butoxycarbonylmethyl-1,4,7,10-tetraaza-cyclododec-1-yl)-acetic acid tert-butyl ester (1). To a solution of DO3A-tris-*tert*-butyl ester (2.0 g, 3.8 mmol) dissolved in 100 mL acetonitrile was added potassium carbonate (1.07 g, 7.7 mmol). Benzyl bromoacetate (0.92 mL, 5.8 mmol) was added to the stirring solution, and the reaction was heated under refluxing conditions for three days before being cooled to room temperature. After filtration, the filtrate was concentrated via rotary evaporation and purified on a silica gel column eluting with a gradient of 1-5% methanol in dichloromethane. **1** was collected in 74% yield (1.9 g, 2.9 mmol) as a yellow oil. ^{1}H NMR (500 MHz, $CDCl_3$) δ = 7.35 (m, 5H), 5.17 (s, 2H), 3.48-2.17 (*broad*, 24H). 1.45 (s, 27H). ^{13}C NMR (126 MHz, $CDCl_3$) δ = 173.8, 173.3, 135.4, 128.9, 128.8, 82.2, 67.1, 56.0, 55.8, 55.2, 53.7, 28.2. MS (ESI-positive) *m/z* = 663.5 ($M + H^+$), 685.5 ($M + Na^+$).

(4,7,10-Tris-tert-butoxycarbonylmethyl-1,4,7,10-tetraaza-cyclododec-1-yl)-acetic acid (2). 1 (1.9 g, 2.9 mmol) was dissolved in 30 mL methanol and added to a flask preloaded with 10% Pd on carbon in catalytic amounts. The reaction was set up on a hydrogen reactor at 2.5 bar for 24 hours. Upon completion of hydrogenation, the reaction mixture was filtered over celite and concentrated via rotary evaporation to produce **2** in quantitative yield. MS (ESI-positive) *m/z* = 573.4 ($M + H^+$), 595.4 ($M + Na^+$).

APS-grafted SiO_2 nanoparticles. A 40% solution of silica nanoparticles in water (5.0 g) was diluted into 100 mL H_2O and dispersed by sonication. 3-aminopropyltrimethoxy-silane (APS) (2.0 mL) was added. The reaction was left stirring at room temperature for 36 hrs, then heated under reflux for 2 hours to push the reaction to completion. The resulting nanoparticles were washed five times with water by centrifugation and redispersion to remove any unreacted APS. The final amine-modified SiNPs were brought up in 15 mL of water.

DO3A-SiNPs. APS-grafted SiNPs were coupled to **2** (0.3 g, 0.5 mmol) using a peptide coupling reaction with 1-ethyl-3-(3-dimethylaminopropyl)carbodiimide (EDC) (0.2 g, 1.3 mmol) and N-hydroxysuccinimide (NHS) (0.2 g, 1.7 mmol) in DMF (10 mL). The reaction was left shaking overnight, and then the nanoparticles were washed five times with water by centrifugation and redispersion to remove any unreacted reagents. The final conjugated particles were resuspended in 10 mL DMF.

Gd-DO3A-SiNPs. A sample of **DOTA-SiNPs** in DMF were centrifuged down and the DMF was decanted. Particles were then brought up in 10 mL of 100% formic acid and stirred

overnight at room temperature to deprotect the *tert*-butyl esters before addition of Gd(III). The deprotected particles were washed with water, centrifuged, and decanted. This was repeated four more times and then the final product was brought up in 5 mL of water and reacted with 0.06 g $GdCl_3 \cdot 6H_2O$ at a pH of ~6. The particles were left shaking at room temperature for five days and were then washed five times with water by centrifugation and redispersion to remove excess gadolinium. Further purification was achieved by dialysis using a 12 – 14 K molecular weight cutoff (MWCO) regenerated cellulose membrane for 48 hours in water. Finally, the nanoparticles were purified via Amicon Ultra-4 1 K MWCO centrifugal filter unit to remove any excess gadolinium that was not covalently coordinated to the grafted DOTA chelates. As a control, $GdCl_3$ was added to APS-grafted nanoparticles under the same conditions and taken through the same purification steps.

4-Bromo-3-methyl-2-nitro-phenol (6). 3-methyl-2-nitrophenol (0.5 g, 3.26 mmol) was dissolved in 50 mL acetic acid. To the yellow solution, bromine (0.08 mL, 1.63 mmol) was added and the reaction immediately turned red. After three hours, when the reaction had returned to a yellow color, another 0.08 mL of bromine was added and left reacting at room temperature for three more hours. The reaction was quenched with 20 mL of a 20% $Na_2S_2O_4$ aqueous solution. The organic layer was separated and dried over sodium sulfate. After filtration, the filtrate was concentrated via rotary evaporation and dried overnight under vacuum to produce **6** in 75% yield (0.56 g, 2.44 mmol) as yellow crystals. ^{1}H NMR (400 MHz, $CDCl_3$) δ = 7.62 (d, J = 9.6 Hz, 1H), 6.88 (d, J = 8.8 Hz, 1H), 2.57 (s, 3H). MS (ESI-negative) m/z = 231.7 ($M - H^+$).

[3-(4-Bromo-3-methyl-2-nitro-phenoxy)-propoxy]-tert-butyl-dimethyl-silane (7). In 10 mL of acetonitrile was dissolved **6** (0.25 g, 1.1 mmol). Anhydrous potassium carbonate (0.45 g, 3.2 mmol) was added followed by 3-bromopropoxy-*tert*-butyldimethyl silane (0.27 mL, 1.1 mmol). The reaction was left refluxing for 48 hours then cooled to room temperature. The crude reaction was filtered and concentrated via rotary evaporation then brought up in ethyl actate. The organic layer was washed with water and brine, then dried over sodium sulfate, filtered, and concentrated. Product **7**, an orange oil, was purified through a silica gel plug eluting with 5% ethyl acetate in hexanes in 84% yield (0.37 g, 0.91 mmol). ^{1}H NMR (400 MHz, $CDCl_3$) δ = 7.51 (d, *J* = 8.8 Hz, 1H), 6.78 (d, *J* = 8.4 Hz, 1H), 4.10 (t, *J* = 5.6 Hz, 2H), 3.68 (t, *J* = 6 Hz, 2H), 2.28 (s, 3H), 1.90 (m, 2H), 0.89 (s, 9H), 0.02 (s, 6H). ^{13}C NMR (100 MHz, $CDCl_3$) δ = 149.5, 134.2, 130.7, 122.5, 115.6, 112.4, 66.2, 59.1, 58.9, 32.1, 26.2, 18.1, -5.4. MS (ESI-positive) *m/z* = 404.1 ($M + H^+$).

3-[3-(tert-Butyl-dimethyl-silanyloxy)-propoxy]-2-nitro-phenol (11). 2-nitroresorcinol (1.0 g, 6.44 mmol) was dissolved in 20 mL acetonitrile. Anhydrous potassium carbonate (0.3 g, 2.15 mmol) was added followed by 3-bromopropoxytrimethyl silane (0.5 mL, 2.15 mmol). The reaction was left refluxing for several days then cooled to room temperature and filtered. The filtrate was concentrated via rotary evaporation then purified by silica gel chromatography. Product was eluted with 5% ethyl acetate in hexanes. **11** was collected as a red solid in 20% yield (0.13 g, 0.4 mmol). ^{1}H NMR (500 MHz, $CDCl_3$) δ = 10.22 (s, O*H*, 1H), 7.39 (t, *J* = 8.5 Hz, 1H), 6.70 (d, *J* = 8.5 Hz, 1H), 6.57 (d, *J* = 8.5 Hz, 1H), 4.19 (t, *J* = 6 Hz, 2H), 3.87 (t, *J* = 6 Hz, 2H), 2.05 (m, 2H), 0.89 (s, 9H), 0.05 (s, 6H). ^{13}C NMR (126 MHz, $CDCl_3$) δ = 155.9, 155.6,

135.9, 128.3, 110.6, 104.6, 66.5, 59.3, 32.2, 26.1, 18.5, -5.2. MS (ESI-negative) *m/z* = 326.1 (M – H^+).

{3-[3-(tert-Butyl-dimethyl-silanyloxy)-propoxy]-2-nitro-phenoxy}-acetic acid ethyl ester (12). To a solution of **11** (0.13 g, 0.4 mmol) in 7 mL acetonitrile was added potassium carbonate (0.2 g, 1.2 mmol) and ethyl bromoacetate (0.09 mL, 0.8 mmol). The reaction was left refluxing for two hours, then cooled to room temperature and filtered. The filtrate was concentrated via rotary evaporation of the solvent then brought up in 20 mL ethyl acetate and washed with a solution of saturated sodium bicarbonate, water, and brine. The organic layer was dried over sodium sulfate, filtered, and concentrated. Purification on a silica gel column eluting with 5% ethyl acetate in hexanes gave **12** in 93% yield (0.15 g, 0.36 mmol). ^{1}H NMR (400 MHz, $CDCl_3$) δ = 7.24 (t, *J* = 8.4 Hz, 1H), 6.66 (d, *J* = 8.8 Hz, 1H), 6.46 (d, *J* = 8.4 Hz, 1H), 4.6 (s, 2H), 4.21 (m, 2H), 4.12 (t, *J* = 6 Hz, 2H), 3.70 (t, 4.4 Hz, 2H), 1.91 (m, 2H), 1.23 (t, *J* = 6.4 Hz, 3H), 0.89 (s, 9H), -0.01 (s, 6H). ^{13}C NMR (100 MHz, $CDCl_3$) δ = 167.9, 151.7, 150.4, 131.1, 118.1, 106.7, 105.4, 66.4, 66.1, 61.8, 59.0, 32.2, 26.2, 18.4, 14.3, -5.3. MS (ESI-positive) *m/z* = 414.2 (M + H^+), 436.2 (M + Na^+).

Relaxivity measurements. A solution of **Gd-DO3A-SiNPs** was serially diluted four times to give 300 μL of five different sample concentrations. To each sample was added 300 μL of a 2% agarose solution in water. After the agarose solution solidified, they were incubated for 30 minutes at 37 °C and T_1 measurements were performed on a Bruker mq60 Minispec relaxometer with an inversion recovery pulse sequence with the appropriate recycle delays. Gd(III) concentrations were determined using ICP-AES.

Inductively coupled plasma – atomic emission spectroscopy (ICP-AES). The concentration of each sample used for relaxivity was determined by ICP-AES (Varian). A 10 μL aliquot of each sample was digested in 90 μL nitric acid. Each sample was then diluted with water to the appropriate concentration for ICP-AES analysis. Gadolinium concentrations were determined from a standardized curve of six standards ranging from 0 – 500 ppb Gd(III) measuring the emission of Gd(III) at 335.048, 336.224, and 342.246 nm.

REFERENCES

Chapter 1

1. Raymond, K. N.; Pierre, V. C., Next Generation, High Relaxivity Gadolinium MRI Agents. *Bioconj. Chem.* **2005,** *16,* 3-8.

2. Aime, S.; Botta, M.; Fasano, M.; Terreno, E., Lanthanide(III) Chelates for NMR Biomedical Applications. *Chem. Soc. Rev.* **1998,** *27,* 19-29.

3. Lauffer, R. B., Paramagnetic Metal Complexes as Water Proton Relaxation Agents for NMR Imaging: Theory and Design. *Chem. Rev.* **1987,** *87,* 901-927.

4. Lauterbur, P. C., Image Formation by Induced Local Interactions: Examples Employing Nuclear Magnetic Resonance. *Nature* **1973,** *242,* 190-191.

5. Merbach, A.; Toth, E., *The Chemistry of Contrast Agents in Medical Magnetic Resonance Imaging*. John Wiley & Sons, Ltd.: New York, 2001.

6. Caravan, P.; Ellison, J. J.; McMurry, T. J.; Laufer, R. B., Gadolinium(III) Chelates as MRI Contrast Agents: Structure, Dynamics, and Applications. *Chem. Rev.* **1999,** *99,* 2293-2352.

7. Solomon, I., Relaxation Processes in a System of Two Spins. *Phys. Rev.* **1955,** *99,* 559-565.

8. Bloembergen, N.; Morgan, L. O., Proton Relaxation Times in Paramagnetic Solutions. Effects of Electron Spin Relaxation. *J. Chem. Phys.* **1961,** *34,* 842-850.

9. Caravan, P., Strategies for Increasing the Sensitivity of Gadolinium Based MRI Contrast Agents. *Chem. Soc. Rev.* **2006,** *35,* 512-523.

10. Cohen, S. M.; Xu, J.; Radkov, E.; Raymond, K. N.; Botta, M.; Barge, A.; Aime, S., Synthesis and Relaxation Properties of Mixed Gadolinium Hydroxypyridinonate MRI Contrast Agents. *Inorg. Chem.* **2000,** *39,* 5747-5756.

11. Xu, J.; Churchill, D. G.; Botta, M.; Raymond, K. N., Gadolinium(III) 1,2-Hydroxypyridonate-Based Complexes: Toward MRI Contrast Agents of High Relaxivity. *Inorg. Chem.* **2004,** *43,* 5492-5494.

12. Xu, J.; Franklin, S. J.; Whisenhunt, D. W.; Raymond, K. N., Gadolinium Complex of Tris[(3-Hyrdroxy-1-Methyl-2-Oxo-1,2-Didehydropyridine-4-Carboamido)Ethyl]-Amine: A New Class of Gadolinium Magnetic Resonance Relaxation Agents. *J. Am. Chem. Soc.* **1995,** *117,* 7245-7246.

13. Laus, S.; Ruloff, R.; Toth, E.; Merbach, A. E., Gd(III) Complexes with Fast Water Exchange and High Thermodynamic Stability: Potential Building Blocks for High-Relaxivity MRI Contrast Agents. *Chem. Eur. J.* **2003,** *9,* 3555-3566.

14. Cheng, T.-H.; Wang, Y.-M.; Lin, K.-T.; Liu, G.-C., Synthesis of Four Derivatives of 3,6,10-Tri(Carboxymethyl)-3,6,10-Triazadodecanedioic Acid, the Stabilities of Their Complexes with Ca(II), Cu(II), Zn(II) and Lanthanide(III) and Water-Exchange Investigations of Gd(III) Chelates. *J. Chem. Soc., Dalt. Trans.* **2001***,* 3357-3366.

15. Ruloff, R.; Toth, E.; Scopelliti, R.; Tripier, R.; Handel, H.; Merbach, A. E., Accelerating Water Exchange for Gd(III) Chelates by Steric Compression around the Water Binding Site. *Chem. Comm.* **2002***,* 2630-2631.

16. Wiener, E.; Brechbiel, M. W.; Brothers, H.; Magin, R. L.; Gansow, O. A.; Tomalia, D. A.; Lauterbur, P. C., Dendrimer-Based Metal Chelates: A New Class of Magnetic Resonance Imaging Contrast Agents. *Mag. Res. Med.* **1994,** *31,* 1-8.

17. Huber, M. M.; Staubi, A. B.; Kustedjo, K.; Gray, M. H.; Shih, J.; Fraser, S. E.; Meade, T. J., Fluorescently Detectable Magnetic Resonance Imaging Agents. *Bioconj. Chem.* **1998,** *9,* 242-249.

18. Casali, C.; Janier, M.; Canet, E.; Obadia, J. F.; Benderbous, S.; Corot, C.; Revel, D., Evaluation of Gd-DOTA-Labeled Dextran Polymer as an Intravascular MR Contrast Agent for Myocardial Perfusion. *Acad. Rad.* **1998,** *5,* S214-S218.

19. Langereis, S.; Dirksen, A.; Hackeng, T. M.; van Genderen, M. H. P.; Meijer, E. W., Dendrimers and Magnetic Resonance Imaging. *New J. Chem.* **2007,** *31,* 1152-1160.

20. Bull, S. R.; Guler, M. O.; Bras, R. E.; Venkatasubramanian, P. N.; Stupp, S. I.; Meade, T. J., Magnetic Resonance Imaging of Self-Assembled Biomaterial Scaffolds. *Bioconj. Chem.* **2005,** *16,* 1343-1348.

21. Mulder, W. J. M.; Strijkers, G. J.; van Tilborg, G. A. F.; Griffioen, A. W.; Nicolay, K., Lipid-Based Nanoparticles for Contrast-Enhanced MRI and Molecular Imaging. *NMR in Biomed.* **2006,** *19,* 142-164.

22. Li, K. C. P.; Bednarski, M. D., Vascular-Targeted Molecular Imaging Using Functionalized Polymerized Vesicles. *J. Mag. Res. Imaging* **2002,** *16,* 388-393.

23. Zhang, Z.; Greenfield, M. T.; Spiller, M.; McMurry, T. J.; Lauffer, R. B.; Caravan, P., Multilocus Binding Increases the Relaxivity of Protein-Bound MRI Contrast Agents. *Angew. Chem. Int. Ed. Engl.* **2005,** *44,* 6766-6769.

24. Aime, S.; Chiaussa, M.; Digilio, G.; Gianolio, E.; Terreno, E., Contrast Agents for Magnetic Resonance Angiographic Applications: ^{1}H and ^{17}O NMR Relaxometric Investigations on Two Gadolinium(III) DTPA-Like Chelates Endowed with High Binding Affinity to Human Serum Albumin. *J. Biol. Inorg. Chem.* **1999,** *4,* 766-774.

25. Jacques, V.; Desreux, J. F., New Classes of MRI Contrast Agents. *Top. Curr. Chem.* **2002,** *221,* 123-164.

26. Livramento, J. B.; Toth, E.; Sour, A.; Borel, A.; Merbach, A. E.; Ruloff, R., High Relaxivity Confined to a Small Molecular Space: A Metallostar-Based, Potential MRI Contrast Agent. *Angew. Chem. Int. Ed. Engl.* **2005,** *44,* 1480-1484.

27. Allen, M. J.; Meade, T. J., Magnetic Resonance Contrast Agents for Medical and Molecular Imaging. *Metal Ions in Biological Systems* **2004,** *42,* 1-38.

28. Meade, T. J.; Taylor, A. K.; Bull, S. R., New Magnetic Resonance Contrast Agents as Biochemical Reporters. *Curr. Opin. Neurobiol.* **2003,** *13,* 597-602.

29. Lowe, M. P., Activated MR Contrast Agents. *Curr. Pharm. Biotech.* **2004,** *5,* 519-528.

30. Li, W.-H.; Fraser, S. E.; Meade, T. J., A Calcium-Sensitive Magnetic Resonance Imaging Contrast Agent. *J. Am. Chem. Soc.* **1999,** *121,* 1413-1414.

31. Li, W.-H.; Parigi, G.; Fragai, M.; Luchinat, C.; Meade, T. J., Mechanistic Studies of a Calcium-Dependent MRI Contrast Agent. *Inorg. Chem.* **2002,** *41,* 4018-4024.

32. Dhingra, K.; Fouskova, P.; Angelovski, G.; Maier, M. E.; Logothetis, N. K.; Toth, E., Towards Extracellular Ca^{2+} Sensing by MRI: Synthesis and Calcium-Dependent ^{1}H and ^{17}O Relaxation Studies of Two Novel Bismacrocyclic Gd^{3+} Complexes. *J. Biol. Inorg. Chem.* **2007**.

33. Mishra, A.; Fouskova, P.; Angelovski, G.; Balogn, E.; Mishra, A. K.; Logothetis, N. K.; Toth, E., Facile Synthesis and Relaxation Properties of Novel Bispolyazamacrocyclic Gd^{3+} Complexes: An Attempt Towards Calcium-Sensitive MRI Contrast Agents. *Inorg. Chem.* **2008,** *47,* 1370-1381.

34. Hanaoka, K.; Kikuchi, K.; Urano, Y.; Nagano, T., Selective Sensing of Zinc Ions with a Novel Magnetic Resonance Imaging Contrast Agent. *J. Chem. Soc., Perkin Trans. 2* **2001**, 1840-1843.

35. Hanaoka, K.; Kikuchi, K.; Urano, Y.; Narazaki, M.; Yokawa, T.; Sakamoto, S.; Yamaguchi, K.; Nagano, T., Design and Synthesis of a Novel Magnetic Resonance Imaging Contrast Agent for Selective Sensing of Zinc Ion. *Chem. Biol.* **2002,** *9,* 1027-1032.

36. Zhang, X.-a.; Lovejoy, K. S.; Jasanoff, A.; Lippard, S. J., Water-Soluble Porphyrins as a Dual-Function Molecular Imaging Platform for MRI and Fluorescence Zinc Sensing. *Proc. Natl. Acad. Sci. USA* **2007,** *104,* 10780-10785.

37. Moats, R. A.; Fraser, S. E.; Meade, T. J., A "Smart" Magnetic Resonance Imaging Agent That Reports on Specific Enzymatic Activity. *Angew. Chem. Int. Ed. Engl.* **1997,** *36,* 726-728.

38. Louie, A. Y.; Huber, M. M.; Ahrens, E. T.; Rothbacher, U.; Moats, R.; Jacobs, R. E.; Fraser, S. E.; Meade, T. J., In Vivo Visualization of Gene Expression Using Magnetic Resonance Imaging. *Nat. Biotechnol.* **2000,** *18,* 321-325.

39. Urbanczyk-Pearson, L. M.; Femia, F. J.; Smith, J.; Parigi, G.; Duimstra, J. A.; Eckermann, A. L.; Luchinat, C.; Meade, T. J., Mechanistic Investigation of Beta-Galactosidase-Activated MR Contrast Agents. *Inorg. Chem.* **2008,** *47,* 56-68.

40. Duimstra, J. A.; Femia, F. J.; Meade, T. J., A Gadolinium Chelate for Detection of Beta-Glucuronidase: A Self-Immolative Approach. *J. Am. Chem. Soc.* **2005,** *127,* 12847-12855.

41. Nivorozhkin, A. L.; Kolodziej, A. F.; Caravan, P.; Greenfield, M. T.; Lauffer, R. B.; McMurry, T. J., Enzyme-Activated Gd^{3+} Magnetic Resonance Imaging Contrast Agents with a Prominent Receptor-Induced Magnetization Enhancement. *Angew. Chem. Int. Ed. Engl.* **2001,** *40,* 2903-2906.

42. Aime, S.; Barge, A.; Botta, M.; Howard, J. A. K.; Kataky, R.; Lowe, M. P.; Moloney, J. M.; Parker, D.; deSousa, A. S., Dependence of the Relaxivity and Luminescence of Gadolinium and Europium Amino-Acid Complexes on Hydrogencarbonate and pH. *Chem. Comm.* **1999***,* 1047-1048.

43. Lowe, M. P.; Parker, D.; Reany, O.; Aime, S.; Botta, M.; Castellano, G.; Gianolio, E.; Pagliarin, R., pH-Dependent Modulation of Relaxivity and Luminescence in Macrocyclic Gadolinium and Europium Complexes Based on Reversible Intramolecular Sulfonamide Ligation. *J. Am. Chem. Soc.* **2001,** *123,* 7601-7609.

44. Zhang, S.; Wu, K.; Sherry, A. D., A Novel pH-Sensitive MRI Contrast Agent. *Angew. Chem. Int. Ed. Engl.* **1999,** *38,* 3192-3194.

45. Bhorade, R.; Weissleder, R.; Nakakoshi, T.; Moore, A.; Tung, C.-H., Macrocyclic Chelators with Paramagnetic Cations Are Internalized into Mammalian Cells Via a HIV-Tat Derived Membrane Translocation Peptide. *Bioconj. Chem.* **2000,** *11,* 301-305.

46. Josephson, L.; Tung, C.-H.; Moore, A.; Weissleder, R., High-Efficiency Intracellular Magnetic Labeling with Novel Superparamagnetic-Tat Peptide Conjugates. *Bioconj. Chem.* **1999,** *10,* 186-191.

47. Futaki, S.; Suzuki, T.; Ohashi, W.; Yagami, T.; Tanaka, S.; Ueda, K.; Sugiura, Y., Arginine-Rich Peptides: An Abundant Source of Membrane-Permeable Peptides Having Potential as Carriers Fro Intracellular Protein Delivery. *J. Biol. Chem.* **2001,** *276,* 5836-5840.

48. Futaki, S.; Goto, S.; Sugiura, Y., Membrane Permeability Commonly Shared among Arginine-Rich Peptides. *J. Molec. Recog.* **2003,** *16,* 260-264.

49. Allen, M. J.; Meade, T. J., Synthesis and Visualization of a Membrane-Permeable MRI Contrast Agent. *J. Biol. Inorg. Chem.* **2003,** *8,* 746-750.

50. Allen, M. J.; MacRenaris, K. W.; Venkatasubramanian, P. N.; Meade, T. J., Cellular Delivery of MRI Contrast Agents. *Chem. & Biol.* **2004,** *11,* 301-307.

51. Endres, P. J.; MacRenaris, K. W.; Vogt, S.; Allen, M. J.; Meade, T. J., Quantitative Imaging of Cell-Permeable Magnetic Resonance Contrast Agents Using X-Ray Fluorescence. *Mol. Imag.* **2006,** *5,* 485-497.

52. Artemov, D.; Mori, N.; Ravi, R.; Bhujwalla, Z. M., Magnetic Resonance Molecular Imaging of the Her-2/*Neu* Receptor. *Cancer Res.* **2003,** *63,* 2723-2727.

53. Gustafsson, B.; Youens, S.; Louie, A. Y., Development of Contrast Agents to Macrophage Scavenger Receptors for MRI of Vascular Inflammation. *Bioconj. Chem.* **2006,** *17,* 538-547.

54. Zigelboim, I.; Offen, D.; Melamed, E.; Panet, H.; Rehavi, M.; Cohen, Y., Synthesis, Binding Affinity, and Relaxivity of Target-Specific MRI Contrast Agents. *Journal of Inclusion Phenomena and Macrocyclic Chemistry* **2007,** *59,* 323-329.

55. Saborowski, O.; Simon, G. H.; Raatschen, H.-J.; Wendland, M. F.; Fu, Y.; Henning, T.; Baehner, R.; Corot, C.; Chen, M.-H.; Daldrup-Link, H. E., MR Imaging of Antigen-Induced Arthritis with a New, Folate Receptor-Targeted Contrast Agent. *Cont. Med. & Mol. Imag.* **2007,** *2,* 72-81.

56. Kayyem, J. F.; Kumar, R. M.; Fraser, S. E.; Meade, T. J., Receptor-Targeted Co-Transport of DNA and Magnetic Resonance Contrast Agents. *Chem. & Biol.* **1995,** *2,* 615-620.

57. Lee, J.; Zylka, M. J.; Anderson, D. J.; Burdette, J. E.; Woodruff, T. K.; Meade, T. J., A Steroid-Conjugated Contrast Agent for Magnetic Resonance Imaging of Cell Signaling. *J. Am. Chem. Soc.* **2005,** *127,* 13164-13166.

58. Lee, J.; Burdette, J. E.; MacRenaris, K. W.; Mustafi, D.; Woodruff, T. K.; Meade, T. J., Rational Design, Synthesis, and Biological Evaluation of Progesterone-Modified MRI Contrast Agents. *Chem. & Biol.* **2007,** *14,* 824-834.

Chapter 2

1. Stefanidou, M.; Maravelias, C.; Dona, A.; Spiliopoulou, C., Zinc: A Multipurpose Trace Element. *Arch. Toxicol.* **2006,** *80,* 1-9.

2. Frederickson, C. J.; Koh, J.-Y.; Bush, A. I., The Neurobiology of Zinc in Health and Disease. *Nat. Rev. Neurosci.* **2005,** *6,* 449-462.

3. Takeda, A., Movement of Zinc and Its Functional Significance in the Brain. *Brain Res Brain Res Rev* **2000,** *34,* 137-148.

4. Vallee, B. L.; Falchuk, K. H., The Biochemical Basis of Zinc Physiology. *Physiol Rev* **1993,** *73,* 79-118.

5. Frederickson, C. J.; Suh, S. W.; Silva, D.; Frederickson, C. J.; Thompson, R. B., Importance of Zinc in the Central Nervous System: The Zinc-Containing Neuron. *The Journal of Nutrition* **2000,** *130,* 1471S-1483S.

6. Frederickson, C. J.; Cuajungco, M. P.; Frederickson, C. J., Is Zinc the Link between Compromises of Brain Perfusion (Excitotoxicity) and Alzheimer's Disease? *J. Alzheimer's Dis.* **2005,** *8,* 155-160.

7. Bush, A. I., The Metallobiology of Alzheimer's Disease. *TRENDS in Neurosciences* **2003,** *26,* 207-214.

8. Noy, D.; Solomonov, I.; Sinkevich, O.; Arad, T.; Kjaer, K.; Sagi, I., Zinc-Amyloid Beta Interactions on a Millisecond Time-Scale Stabilize Non-Fibrillar Alzheimer-Related Species. *J. Am. Chem. Soc.* **2008,** *130,* 1376-1383.

9. Lim, N. C.; Freake, H. C.; Bruckner, C., Illuminating Zinc in Biological System. *Chem. Eur. J.* **2005,** *11,* 38-49.

10. Jiang, P.; Guo, Z., Fluorescent Detection of Zinc in Biological Systems: Recent Development on the Design of Chemosensors and Biosensors. *Coord. Chem. Rev.* **2004,** *248,* 205-229.

11. Kikuchi, K.; Komatsu, K.; Nagano, T., Zinc Sensing for Cellular Application. *Curr. Op. Chem. Bio.* **2004,** *8,* 182-191.

12. Zhang, X.-a.; Lovejoy, K. S.; Jasanoff, A.; Lippard, S. J., Water-Soluble Porphyrins as a Dual-Function Molecular Imaging Platform for MRI and Fluorescence Zinc Sensing. *Proc. Natl. Acad. Sci. USA* **2007,** *104,* 10780-10785.

13. Hanaoka, K.; Kikuchi, K.; Urano, Y.; Nagano, T., Selective Sensing of Zinc Ions with a Novel Magnetic Resonance Imaging Contrast Agent. *J. Chem. Soc., Perkin Trans. 2* **2001**, 1840-1843.

14. Hanaoka, K.; Kikuchi, K.; Urano, Y.; Narazaki, M.; Yokawa, T.; Sakamoto, S.; Yamaguchi, K.; Nagano, T., Design and Synthesis of a Novel Magnetic Resonance

Imaging Contrast Agent for Selective Sensing of Zinc Ion. *Chem. Biol.* **2002,** *9,* 1027-1032.

15. Li, W.-H.; Fraser, S. E.; Meade, T. J., A Calcium-Sensitive Magnetic Resonance Imaging Contrast Agent. *J. Am. Chem. Soc.* **1999,** *121,* 1413-1414.

16. Li, W. H.; Parigi, G.; Fragai, M.; Luchinat, C.; Meade, T. J., Mechanistic Studies of a Calcium-Dependent MRI Contrast Agent. *Inorg. Chem.* **2002,** *41,* 4018-4024.

17. Raheul-Clermont, S.; Dunn, M. F., The Biological Chemsitry of Zinc. In *Copper and Zinc in Inflammatory and Degenerative Diseases*, Rainsford, K. D., Ed. Kluwer Academic Publishers: Dordrecht, Great Britain, 1998; pp 47-59.

18. Dadabhoy, A.; Faulkner, S.; Sammes, P. G., Long Wavelength Sensitizers for Europium(III) Luminescence Based on Acridone Derivatives. *J. Chem. Soc., Perkin Trans. 2* **2002***,* 348-357.

19. Caravan, P.; Ellison, J. J.; McMurry, T. J.; Laufer, R. B., Gadolinium(III) Chelates as MRI Contrast Agents: Structure, Dynamics, and Applications. *Chem. Rev.* **1999,** *99,* 2293-2352.

20. Gee, K. R.; Zhou, Z.-L.; Ton-That, D.; Sensi, S. L.; Weiss, J. H., Measuring Zinc in Living Cells. A New Generation of Sensitive and Selective Fluorescent Probes. *Cell Calcium* **2002,** *31,* 245.

21. Barnham, K. J.; Masters, C. L.; Bush, A. I., Neurodegenerative Diseases and Oxidative Stress. *Nat. Rev. Drug Discovery* **2004,** *3,* 205-214.

22. Henrotte, V.; Elst, L. V.; Laurent, S.; Muller, R., Comprehensize Investigation of the Non-Covalent Binding of MRI Contrast Agents with Human Serum Albumin. *J. Biol. Inorg. Chem.* **2007,** *12,* 929-937.

23. Kropp, J. L.; Windsor, M. W., Luminescence and Energy Transfer in Solutions of Rare-Earth Complexes. I. Enhancement of Fluorescence by Deuterium Substitution. *J. Chem. Phys.* **1965,** *42,* 1599-1608.

24. Kropp, J. L.; Windsor, M. W., Luminescence and Energy Transfer in Solutions of Rare Earth Complexes. II. Studies of the Solvation Shell in Europium(III) and Terbium(III) as a Function of Acetate Concentration. *J. Phys. Chem.* **1967,** *71,* 477-482.

25. Horrocks, W. D.; Sudnick, D. R., Lanthanide Ion Luminescence Probes of the Structure of Biological Macromolecules. *Acc. Chem. Res.* **1981,** *14,* 384-392.

26. Quici, S.; Cavazzini, M.; Marzanni, G.; Accorsi, G.; Armaroli, N.; Ventura, B.; Barigelletti, F., Visible and near-Infrared Intense Luminescence from Water-Soluble Lanthanide [Tb(III), Eu(III), Sm(III), Dy(III), Pr(III), Ho(III), Yb(III), Nd(III), Er(III)] Complexes. *Inorg. Chem.* **2005,** *44,* 529-537.

27. Powell, D. H.; Dhubhghaill, O. M. N.; Pubanz, D.; Helm, L.; Lebedev, Y. S.; Schlaepfer, W.; Merbach, A. E., Structural and Dynamic Parameters Obtained from ^{17}O NMR, EPR, and NMRD Studies of Monomeric and Dimeric Gd^{3+} Complexes of Interest in Magnetic Resonance Imaging: An Intergrated and Theoretically Self-Consistent Approach. *J. Am. Chem. Soc.* **1996,** *118,* 9333-9346.

28. Hwang, L. P.; Freed, J. H., Dynamic Effects of Pair Correlation Functions on Spin Relaxation by Transitional Diffusion in Liquids. *J. Chem. Phys.* **1975,** *63,* 4017-4025.

29. Bloembergen, N.; Morgan, L. O., Proton Relaxation Times in Paramagnetic Solutions. Effects of Electron Spin Relaxation. *J. Chem. Phys.* **1961,** *34,* 842-850.

30. Bertini, I.; Kowalewsi, J.; Luchinat, C.; Nilsson, T.; Parigi, G., Nuclear Spin Relaxation in Paramagnetic Complexes of S=1: Electron Spin Relaxation Effects. *J. Chem. Phys.* **1999,** *111,* 5795-5807.

31. Bertini, I.; Luchinat, C.; Parigi, G., "1H NMRD Profiles of Paramagnetic Aquo-Complexes and Metalloproteins". In *Relaxometry of Water-Metal Ion Interactions*, Bertini, I.; van Eldik, R., Eds. 2005; Vol. 57, pp 105-172.

32. Kruk, D.; Nilsson, T.; Kowalewsi, J., Nuclear Spin Relaxation in Paramagnetic Systems with Zero-Field Splitting and Arbitrary Electron Spin. *Phys. Chem. Chem. Phys.* **2001,** *3,* 4907-4917.

33. Tweedle, M. F.; Hagan, J. J.; Kumar, K.; Mantha, S.; Chang, C. A., Reaction of Gadolinium Chelates with Endogenously Available Ions. *Mag. Res. Imaging* **1991,** *9,* 409-415.

34. Que, E. L.; Chang, C. J., A Smart Magnetic Resonance Contrast Agent for Selective Copper Sensing. *J. Am. Chem. Soc.* **2006,** *128,* 15942-15943.

Chapter 3

1. Frederickson, C. J.; Koh, J.-Y.; Bush, A. I., The Neurobiology of Zinc in Health and Disease. *Nat. Rev. Neurosci.* **2005,** *6,* 449-462.

2. Frederickson, C. J.; Suh, S. W.; Silva, D.; Frederickson, C. J.; Thompson, R. B., Importance of Zinc in the Central Nervous System: The Zinc-Containing Neuron. *The Journal of Nutrition* **2000,** *130,* 1471S-1483S.

3. Frederickson, C. J.; Cuajungco, M. P.; Frederickson, C. J., Is Zinc the Link between Compromises of Brain Perfusion (Excitotoxicity) and Alzheimer's Disease? *J. Alzheimer's Dis.* **2005,** *8,* 155-160.

4. Bush, A. I., The Metallobiology of Alzheimer's Disease. *TRENDS in Neurosciences* **2003,** *26,* 207-214.

5. Noy, D.; Solomonov, I.; Sinkevich, O.; Arad, T.; Kjaer, K.; Sagi, I., Zinc-Amyloid Beta Interactions on a Millisecond Time-Scale Stabilize Non-Fibrillar Alzheimer-Related Species. *J. Am. Chem. Soc.* **2008,** *130,* 1376-1383.

6. Lim, N. C.; Freake, H. C.; Bruckner, C., Illuminating Zinc in Biological System. *Chem. Eur. J.* **2005,** *11,* 38-49.

7. Jiang, P.; Guo, Z., Fluorescent Detection of Zinc in Biological Systems: Recent Development on the Design of Chemosensors and Biosensors. *Coord. Chem. Rev.* **2004,** *248,* 205-229.

8. Takeda, A., Movement of Zinc and Its Functional Significance in the Brain. *Brain Res Brain Res Rev* **2000,** *34,* 137-148.

9. Vallee, B. L.; Falchuk, K. H., The Biochemical Basis of Zinc Physiology. *Physiol Rev* **1993,** *73,* 79-118.

10. Dadabhoy, A.; Faulkner, S.; Sammes, P. G., Long Wavelength Sensitizers for Europium(III) Luminescence Based on Acridone Derivatives. *J. Chem. Soc., Perkin Trans. 2* **2002**, 348-357.

11. Corey, E. J.; Venkateswarlu, A., Protection of Hydroxyl Groups as Tert-Butyldimethylsilyl Derivatives. *J. Am. Chem. Soc.* **1972,** *94,* 6190-6191.

12. Barnham, K. J.; Masters, C. L.; Bush, A. I., Neurodegenerative Diseases and Oxidative Stress. *Nat. Rev. Drug Discovery* **2004,** *3,* 205-214.

13. Henrotte, V.; Elst, L. V.; Laurent, S.; Muller, R., Comprehensize Investigation of the Non-Covalent Binding of MRI Contrast Agents with Human Serum Albumin. *J. Biol. Inorg. Chem.* **2007,** *12,* 929-937.

14. Kropp, J. L.; Windsor, M. W., Luminescence and Energy Transfer in Solutions of Rare-Earth Complexes. I. Enhancement of Fluorescence by Deuterium Substitution. *J. Chem. Phys.* **1965,** *42,* 1599-1608.

15. Kropp, J. L.; Windsor, M. W., Luminescence and Energy Transfer in Solutions of Rare Earth Complexes. II. Studies of the Solvation Shell in Europium(III) and Terbium(III) as a Function of Acetate Concentration. *J. Phys. Chem.* **1967,** *71,* 477-482.

16. Quici, S.; Cavazzini, M.; Marzanni, G.; Accorsi, G.; Armaroli, N.; Ventura, B.; Barigelletti, F., Visible and near-Infrared Intense Luminescence from Water-Soluble Lanthanide [Tb(III), Eu(III), Sm(III), Dy(III), Pr(III), Ho(III), Yb(III), Nd(III), Er(III)] Complexes. *Inorg. Chem.* **2005,** *44,* 529-537.

17. Swift, T. J.; Connick, R. E., Nmr-Relaxation Mechanisms of O^{17} in Aqueous Solutions of Paramagnetic Cations and the Lifetime of Water Molecules in the First Coordination Sphere. *J. Chem. Phys.* **1962,** *37,* 307-320.

18. Merbach, A.; Toth, E., *The Chemistry of Contrast Agents in Medical Magnetic Resonance Imaging*. John Wiley & Sons, Ltd.: New York, 2001.

19. Caravan, P.; Ellison, J. J.; McMurry, T. J.; Laufer, R. B., Gadolinium(III) Chelates as MRI Contrast Agents: Structure, Dynamics, and Applications. *Chem. Rev.* **1999,** *99,* 2293-2352.

20. Gee, K. R.; Zhou, Z.-L.; Ton-That, D.; Sensi, S. L.; Weiss, J. H., Measuring Zinc in Living Cells. A New Generation of Sensitive and Selective Fluorescent Probes. *Cell Calcium* **2002,** *31,* 245.

21. Woods, M.; Kovacs, Z.; Kiraly, R.; Brucher, E.; Zhang, S.; Sherry, A. D., Solution Dynamics and Stability of Lanthanide(III) (*S*)-2-(P-Nitrobenzyl)Dota Complexes. *Inorg. Chem.* **2004,** *43,* 2845-2851.

22. Quici, S.; Marzanni, G.; Forni, A.; Accorsi, G.; Barigelletti, F., New Lanthanide Complexes for Sensitized Visible and near-IR Light Emission: Synthesis, ^{1}H NMR, and X-Ray Structural Investigation and Photophysical Properties. *Inorg. Chem.* **2004,** *43,* 1294-1301.

Chapter 4

1. Lauffer, R. B., Paramagnetic Metal Complexes as Water Proton Relaxation Agents for NMR Imaging: Theory and Design. *Chem. Rev.* **1987,** *87,* 901-927.

2. Kumar, K.; Chang, C. A.; Francesconi, L. C.; Dischino, D. D.; Malley, M. F.; Gougoutas, J. Z.; Tweedle, M. F., Synthesis, Stability, and Structure of Gadolinium(III) and Yttrium(III) Macrocyclic Poly(Amino Carboxylates). *Inorg. Chem.* **1994,** *33,* 3567-3575.

3. Raymond, K. N.; Pierre, V. C., Next Generation, High Relaxivity Gadolinium MRI Agents. *Bioconj. Chem.* **2005,** *16,* 3-8.

4. Raheul-Clermont, S.; Dunn, M. F., The Biological Chemsitry of Zinc. In *Copper and Zinc in Inflammatory and Degenerative Diseases*, Rainsford, K. D., Ed. Kluwer Academic Publishers: Dordrecht, Great Britain, 1998; pp 47-59.

5. Hanaoka, K.; Kikuchi, K.; Urano, Y.; Nagano, T., Selective Sensing of Zinc Ions with a Novel Magnetic Resonance Imaging Contrast Agent. *J. Chem. Soc., Perkin Trans. 2* **2001***,* 1840-1843.

6. Hanaoka, K.; Kikuchi, K.; Urano, Y.; Narazaki, M.; Yokawa, T.; Sakamoto, S.; Yamaguchi, K.; Nagano, T., Design and Synthesis of a Novel Magnetic Resonance Imaging Contrast Agent for Selective Sensing of Zinc Ion. *Chem. Biol.* **2002,** *9,* 1027-1032.

7. Dadabhoy, A.; Faulkner, S.; Sammes, P. G., Long Wavelength Sensitizers for Europium(III) Luminescence Based on Acridone Derivatives. *J. Chem. Soc., Perkin Trans. 2* **2002***,* 348-357.

8. Kropp, J. L.; Windsor, M. W., Luminescence and Energy Transfer in Solutions of Rare-Earth Complexes. I. Enhancement of Fluorescence by Deuterium Substitution. *J. Chem. Phys.* **1965,** *42,* 1599-1608.

9. Kropp, J. L.; Windsor, M. W., Luminescence and Energy Transfer in Solutions of Rare Earth Complexes. II. Studies of the Solvation Shell in Europium(III) and Terbium(III) as a Function of Acetate Concentration. *J. Phys. Chem.* **1967,** *71,* 477-482.

10. Quici, S.; Cavazzini, M.; Marzanni, G.; Accorsi, G.; Armaroli, N.; Ventura, B.; Barigelletti, F., Visible and near-Infrared Intense Luminescence from Water-Soluble Lanthanide [Tb(III), Eu(III), Sm(III), Dy(III), Pr(III), Ho(III), Yb(III), Nd(III), Er(III)] Complexes. *Inorg. Chem.* **2005,** *44,* 529-537.

11. Swift, T. J.; Connick, R. E., Nmr-Relaxation Mechanisms of O^{17} in Aqueous Solutions of Paramagnetic Cations and the Lifetime of Water Molecules in the First Coordination Sphere. *J. Chem. Phys.* **1962,** *37,* 307-320.

12. Bloembergen, N.; Morgan, L. O., Proton Relaxation Times in Paramagnetic Solutions. Effects of Electron Spin Relaxation. *J. Chem. Phys.* **1961,** *34,* 842-850.

13. Caravan, P.; Ellison, J. J.; McMurry, T. J.; Laufer, R. B., Gadolinium(III) Chelates as MRI Contrast Agents: Structure, Dynamics, and Applications. *Chem. Rev.* **1999,** *99,* 2293-2352.

14. Woods, M.; Kovacs, Z.; Zhang, S.; Sherry, A. D., Towards the Rational Design of Magnetic Resonance Imaging Contrast Agents: Isolation of the Two Coordination Isomers of Lanthanide DOTA-Type Complexes. *Angew. Chem. Int. Ed. Engl.* **2003,** *42,* 5889-5892.

15. Major, J. L.; Parigi, G.; Luchinat, C.; Meade, T. J., The Synthesis and in Vitro Testing of a Zinc-Activated MRI Contrast Agent. *Proc Natl Acad Sci U S A* **2007,** *104,* 13881-13886.

Appendix

1. Bull, S. R.; Guler, M. O.; Bras, R. E.; Venkatasubramanian, P. N.; Stupp, S. I.; Meade, T. J., Magnetic Resonance Imaging of Self-Assembled Biomaterial Scaffolds. *Bioconj. Chem.* **2005,** *16,* 1343-1348.

2. Karfeld, L. S.; Bull, S. R.; Davis, N. E.; Meade, T. J.; Barron, A. E., Use of a Genetically Engineered Protein for the Design of a Multivalent MRI Contrast Agent. *Bioconj. Chem.* **2007,** *18,* 1697-1700.

3. Langereis, S.; Dirksen, A.; Hackeng, T. M.; van Genderen, M. H. P.; Meijer, E. W., Dendrimers and Magnetic Resonance Imaging. *New J. Chem.* **2007,** *31,* 1152-1160.

4. Santra, S.; Bagwe, R. P.; Dutta, D.; Stanley, J. T.; Walter, G. A.; Tan, W.; Moudgill, B. M.; Mericle, R. A., Synthesis and Characterization of Fluorescent, Radio-Opaque, and Paramagnetic Silica Nanoparticles for Multimodal Bioimaging Applications. *Advanced Materials* **2005,** *17,* 2165-2169.

5. Voisin, P.; Ribot, E. J.; Miraux, S.; Bouzier-Sore, A.-K.; Lahitte, J.-F.; Bouchaud, V.; Mornet, S.; Thiaudiere, E.; Franconi, J.-M.; Raison, L.; Labrugere, C.; Delville, M.-H., Use of Lanthanide-Grafted Inorganic Nanoparticles as Effective Contrast Agents for Cellular Uptake Imaging. *Bioconj. Chem.* **2007,** *18,* 1053-1063.

6. Kim, J. S.; Rieter, W. J.; Taylor, K. M. L.; An, H.; Lin, W.; Lin, W., Self-Assembled Hybrid Nanoparticles for Cancer-Specific Multimodal Imaging. *J. Am. Chem. Soc.* **2007,** *129,* 8962-8963.

7. Santra, S.; Zhang, P.; Wang, K.; Tapec, R.; Tan, W., Conjugation of Biomolecules with Luminophore-Doped Silica Nanoparticles for Photostable Biomarkers. *Analytical Chemistry* **2001,** *73,* 4988-4993.

8. Dadabhoy, A.; Faulkner, S.; Sammes, P. G., Long Wavelength Sensitizers for Europium(III) Luminescence Based on Acridone Derivatives. *J. Chem. Soc., Perkin Trans. 2* **2002***,* 348-357.

9. Ye, Z.; Tan, M.; Wang, G.; Yuan, J., Preparation, Characterization, and Time-Resolved Fluorometric Application of Silica-Coated Terbium(III) Fluorescent Nanoparticles. *Analytical Chemistry* **2004,** *76,* 513-518.

10. Rieter, W. J.; Kim, J. S.; Taylor, K. M. L.; An, H.; Lin, W.; Tarrant, T.; Lin, W., Hybrid Silica Nanoparticles for Multimodal Imaging. *Angew. Chem. Int. Ed. Engl.* **2007,** *46,* 3680-3682.

11. Sehgal, D.; Vijay, I. K., A Method for the High Efficiency of Water-Soluble Carbodiimide-Mediated Amidation. *Analytical Biochemistry* **1994,** *218,* 87-91.

12. Martic, S.; Brennan, J. D.; Brook, M. A.; Ackloo, S.; Nagy, N., Towards the Development of a Covalently Tethered MALDI System - a Study of Allyl-Modified MALDI Matrixes. *Canadian Journal of Chemistry* **2007,** *85,* 66-76.

13. Sikma, E. A. S.; Aslam, M.; Endres, P. J.; Dravid, V. P.; Meade, T. J., Covalent Attachment of a Gd(III) Chelate to Cobalt Ferrite Nanoparticles as a Bimodal T_1-T_2 MRI Contrast Agent. *unpublished results*.

Jody L. Major

Northwestern University
Department of Chemistry
2145 Sheridan Road
Evanston, IL 60208-3113

Phone: (847) 491-4253 (lab)
Phone: (773) 412-4858 (home)
Email: j-major@northwestern.edu

Education

- **Ph.D.** Northwestern University, Evanston, IL – Chemistry – 3.70 GPA – May 2008
  Dissertation – "Coordination Complexes for the Development of Zn(II)-Activated MR Imaging Probes"

- **B.S.** University of California, Santa Barbara, CA – Biochemistry – 3.58 GPA – June 2001

Research Experience

Northwestern University - Graduate Student (August 2001 – March 2008)
Dissertation Advisor: Prof. Thomas Meade

- Design, synthesis, and characterization of a series of q-modulated zinc(II)-activated MRI contrast agents.
- Investigation of MR signal amplification of bioactivated contrast agents through conjugation to silica nanoparticles.
- Fours years of mentoring undergraduates from the sophomore to the senior thesis level.

University of California, Santa Barbara - Undergraduate Researcher (June 1999 – June 2001)
Advisor: Prof. Geoffrey Strouse

- Design, synthesis, and characterization of organic and biological polymers for assembly with quantum dots for use in nano-circuits and nano-sensing.

Honors and Awards

- Achievement Rewards for College Scientists (ARCS), Takeda Pharmaceuticals North American Scholar – Chicago Chapter (2004-present)
- Phi Lambda Upsilon, Alpha Gamma Chapter, Travel Award (February 2007)
- Society of Molecular Imaging Travel Grant (September 2006)
- The Graduate School and Office of Research Travel Award (September 2006)
- Preparing Future Faculty Fellow – University Award (2004-2005)
- American Institute of Chemists – Departmental Award (2001)
- Willard L. McRary Prize – Departmental Award (2001)
- Vice Chancellor for Research Award – University Award (2000)
- NSF-RISE Research Scholarship (September 1999 – December 2000)
- Dean's Honor Award (Winter 2000 and Spring 2000)
- University of California, Santa Barbara Regents Scholar (1997)

Professional Affiliations

- American Chemical Society
- Society for Molecular Imaging
- Phi Lambda Upsilon, The National Honorary Chemistry Society, Alpha Gamma Chapter
  Treasurer (2005 – 2006)
  Vice President (2004 – 2005)

Teaching Experience

Preparing Future Faculty Fellow, Professor Pratibha Varma-Nelson, Northeastern University, September 2004 – May 2005

- One on one interaction with a mentor at a four-year university to experience all elements of academia including teaching and faculty obligations.
- Invited lecturer for three classes in Chemistry 348 – Advanced Organic Chemistry: Bio-Organic Compounds.

Teaching Assistant, Chemistry 103, Professor Thomas O'Halloran, Northwestern University, Spring 2002 and Spring 2003

Laboratory Teaching Assistant, Chemistry 101 and 102, Professor Patricia Todebush, Northwestern University, Fall 2001 and Winter 2002.

Publications

- **Major, J. L**., Parigi, G., Luchinat, C., Meade, T. J. "The synthesis and *in vitro* testing of a zinc-activated MRI Contrast Agent" *Proc. Nat. Acad. Sci. USA.*, **2007**, *104 (35)*, 13881-13886.
- **Major, J. L.**, Boiteau, R. M., Meade, T. J. "Investigation into the Mechanism of Zn(II)-Activated MR Imaging Contrast Agents" *Inorg. Chem.* **2008** *Manuscript in preparation..*
- **Major, J. L.**, Meade, T. J. "Bio-Activated MR Imaging Probes" *Acct. Chem. Res.* **2008** *Manuscript in preparation..*
- Yun, C. S., **Major, J. L**., Strouse, G. F. "Assembly of Nanomaterials Using Bio-Scaffolding" *Mat. Res. Soc. Symp. Proc.*, **2001**, *642*, J2.3-J2.6.

Patents

- **Major, J. L.**, Meade, T. J. "Zinc Activated Contrast Agents" U. S. Provisional Patent Application, NU 26103.

Presentations

- **Jody L. Major** and Thomas J. Meade. "Zinc-Activated MRI Contrast Agents: Investigation into the Mechanism of Activations." Invited Talk and Poster Presentation. Gordon Research Conference, Graduate Research Seminar: Bioinorganic Chemistry. February 2008.
- **Jody L. Major** and Thomas J. Meade. "A Zn-Activated MRI Contrast Agent." Poster Presentation. American Chemical Society National Conference, Chicago. March 2007.
- **Jody L. Major** and Thomas J. Meade. "The Synthesis and Testing of a Zn-Activated MRI Contrast Agent." Poster Presentation. Gordon Research Conference, Graduate Research Seminar: Bioinorganic Chemistry. February 2007.
- **Jody L. Major** and Thomas J. Meade. "Modulating water access to lanthanide chelates: The synthesis and testing of a zinc-activated MRI contrast agent." Poster presentation. The Society of Molecular Imaging Conference, Hawaii. September 2006.
- **Jody L. Major**. "Modulating water access to lanthanide chelates: The synthesis of a coordinatively saturated macrocycle." Invited Seminar. Northeastern Illinois University. September 2005.
- Rene Boiteau, **Jody L. Major** and Thomas J. Meade. "Synthesis of Chelated Gadolinium as MR Contrast Agents for Zinc Detection." Poster Presentation. American Chemical Society National Conference, Boston. August 2007.